


1995

# Spectral hole burning studies of Photosystem II

Hai-Chou Chang  
*Iowa State University*

Follow this and additional works at: <https://lib.dr.iastate.edu/rtd>

 Part of the [Biophysics Commons](#), [Physical Chemistry Commons](#), and the [Plant Sciences Commons](#)

## Recommended Citation

Chang, Hai-Chou, "Spectral hole burning studies of Photosystem II " (1995). *Retrospective Theses and Dissertations*. 10766.  
<https://lib.dr.iastate.edu/rtd/10766>

This Dissertation is brought to you for free and open access by the Iowa State University Capstones, Theses and Dissertations at Iowa State University Digital Repository. It has been accepted for inclusion in Retrospective Theses and Dissertations by an authorized administrator of Iowa State University Digital Repository. For more information, please contact [digirep@iastate.edu](mailto:digirep@iastate.edu).

## **INFORMATION TO USERS**

**This manuscript has been reproduced from the microfilm master. UMI films the text directly from the original or copy submitted. Thus, some thesis and dissertation copies are in typewriter face, while others may be from any type of computer printer.**

**The quality of this reproduction is dependent upon the quality of the copy submitted. Broken or indistinct print, colored or poor quality illustrations and photographs, print bleedthrough, substandard margins, and improper alignment can adversely affect reproduction.**

**In the unlikely event that the author did not send UMI a complete manuscript and there are missing pages, these will be noted. Also, if unauthorized copyright material had to be removed, a note will indicate the deletion.**

**Oversize materials (e.g., maps, drawings, charts) are reproduced by sectioning the original, beginning at the upper left-hand corner and continuing from left to right in equal sections with small overlaps. Each original is also photographed in one exposure and is included in reduced form at the back of the book.**

**Photographs included in the original manuscript have been reproduced xerographically in this copy. Higher quality 6" x 9" black and white photographic prints are available for any photographs or illustrations appearing in this copy for an additional charge. Contact UMI directly to order.**

# **UMI**

A Bell & Howell Information Company  
300 North Zeeb Road, Ann Arbor, MI 48106-1346 USA  
313/761-4700 800/521-0600



**Spectral hole burning studies of Photosystem II**

by

**Hai-Chou Chang**

**A Dissertation Submitted to the  
Graduate Faculty in Partial Fulfillment of the  
Requirements for the Degree of  
DOCTOR OF PHILOSOPHY**

**Department: Chemistry  
Major: Physical chemistry**

**Approved:**

Signature was redacted for privacy.

Signature was redacted for privacy.

**In Charge of Major Work**

Signature was redacted for privacy.

**For the Major Department**

Signature was redacted for privacy.

**For the Graduate College**

**Iowa State University  
Ames, Iowa**

**1995**

**UMI Number: 9540880**

---

**UMI Microform 9540880**  
**Copyright 1995, by UMI Company. All rights reserved.**

**This microform edition is protected against unauthorized  
copying under Title 17, United States Code.**

---

**UMI**  
**300 North Zeeb Road**  
**Ann Arbor, MI 48103**

**TABLE OF CONTENTS**

CHAPTER 1.	GENERAL REMARKS ON PHOTOSYNTHESIS	1
CHAPTER 2.	SPECTRAL HOLE BURNING SPECTROSCOPIES	15
CHAPTER 3.	THEORETICAL BACKGROUND	29
CHAPTER 4.	EXCITON LEVEL STRUCTURE AND DYNAMICS IN THE CP47 ANTENNA COMPLEX OF PHOTOSYSTEM II	55
CHAPTER 5.	ON THE QUESTION OF THE CHLOROPHYLL A CONTENT OF THE PSII REACTION CENTER	89
CHAPTER 6.	TEMPERATURE DEPENDENT HOLE BURNING OF THE 684 NM CHLOROPHYLL A OF THE ISOLATED REACTION CENTER OF PHOTOSYSTEM II: CONFIRMATION OF THE LINKER MODEL	144
CHAPTER 7.	PRESSURE DEPENDENCE OF PRIMARY CHARGE SEPARATION IN A PHOTOSYNTHETIC REACTION CENTER	175
CHAPTER 8	GENERAL CONCLUSIONS	216
ACKNOWLEDGEMENTS		218
APPENDIX A.	A HOLE BURNING STUDY OF THE CP43 COMPLEX	219
APPENDIX B.	COMPARISON OF THE ABSORPTION SPECTRA OF THE PHOTOSYSTEM II D1-D2-CYT B <sub>559</sub> REACTION CENTER FROM TWO DIFFERENT PREPARATIONS	235

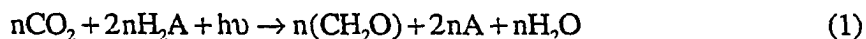
## CHAPTER 1 GENERAL REMARKS ON PHOTOSYNTHESIS

### 1.1 Dissertation Organization

This dissertation contains the candidate's original work on spectral hole burning of Photosystem II. General introduction is divided into three chapters (chapters 1-3). Photosynthesis, spectral hole burning spectroscopies, and theoretical background are described in chapter 1, 2, and 3, respectively. Chapter 4 contains one published paper which report hole burning experiments performed on the CP47 complex. Chapters 5, 6 and 7 are published papers which report experiments performed on the Photosystem II reaction center. Each of these published works contains a description of the experimental apparatus as it was used for the specific experiment. Additional results of the CP43 complex and Photosystem II reaction center are described in the appendix. The references for each chapter are found at the end of that chapter.

### 1.2 Introduction

Most of the energy which is available on earth comes from photosynthesis. Every year  $3 \times 10^{21}$  joules of energy are stored by photosynthesis [1]. Therefore, as our reserves of energy diminish, it becomes important to understand how photosynthesis works. The whole process of photosynthesis can be resolved into numerous reaction steps [1-3]. An overall equation of the process that occurs is [1-3]



where  $(\text{CH}_2\text{O})$  represents part of a carbohydrate molecule and  $\text{H}_2\text{A}$  is the oxidizable substrate, such as  $\text{H}_2\text{O}$  or  $\text{H}_2\text{S}$ . Photosynthesis can be regarded as a process of converting radiant energy of the sun into chemical energy.

Photosynthesis in green plants takes place inside of the chloroplasts. The apparatus used by plants to perform photosynthesis is both complex and highly efficient. As shown in Figure 1, three different membranes (outer, inner, and thylakoid membranes) divide the chloroplast into three separate spaces (intermembrane, stroma, and thylakoid spaces or lumen) [1-3]. The stroma that surrounds the thylakoid membrane contains the enzymes responsible for the actual fixation of CO<sub>2</sub> and the synthesis of carbohydrates. The thylakoid membranes are very important to the primary steps of photosynthesis. The photosynthetic proteins, such as the light-harvesting proteins, and reaction centers are buried inside the thylakoid membranes [1-3]. The pigment molecules are specifically bound to proteins which determine the positions, environments, orientations and spacings of the pigment molecules. Chlorophyll *a* and *b* are the primary photoreceptors of green plants. The absorption spectra of chlorophyll *a* (Chl *a*) and chlorophyll *b* (Chl *b*) are different [1-3]. Thus, coexistence of these two kinds of chlorophyll is important to the absorption of a wide range of solar wavelengths. The incorporation of different pigments (e.g., Chl *a*, Chl *b*, and carotenoids), absorbing at different wavelengths, allows the photosynthetic unit to use a greater portion of the solar spectrum.

Functionally, pigmented proteins are divided into two classes: antenna and reaction center complexes (RC). The initial event in photosynthesis is the capture of light by antenna. Light absorbed by antenna pigments leads to singlet excitons. The funneling of these excitons to the reaction centers induces electron transfer. Finally the energy of electron flow is stored in chemical forms.

Antenna only absorb light and cannot transform the energy of light into chemical energy. The antenna systems are generally characterized by different absorption maxima and form "ladder" systems for heterogeneous and directed excited energy transfer (EET)



[4,5]. Antenna chromophores nearer to the reaction center absorb at longer wavelengths, leading to an energy funneling effect. This downhill transfer has been shown to increase trapping rates by as much as a factor of ten [5].

Photosynthesis by oxygen-evolving organisms is comprised of two photosystem mechanisms: Photosystem I (PSI) and Photosystem II (PSII). The excitation energy is

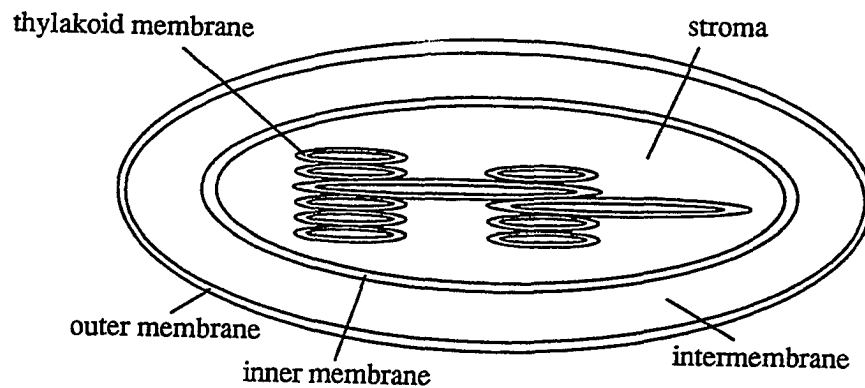


Figure 1. Diagram of chloroplast structure. Chloroplasts have three different membranes (outer, inner, and thylakoid membranes) and three separate space (intermembrane, stroma, and lumen). The thylakoid membranes contain the energy-transducing machinery.

transferred to the reaction centers: P680 in PSII, and P700 in PSI. Photosystem I leads to the formation of NADPH. Photosystem II generates a strong oxidant  $P680^+$  which extracts electrons from water and leads to the formation of  $O_2$ .

The mechanism of electron transport of green plants is called the Z-scheme (Figure 2). The primary charge separation of Photosystem II leads to the formation of  $P680^+$  and  $Pheo^-$ .  $P680^+$  is reduced via various steps (indicated as S) by an electron which is

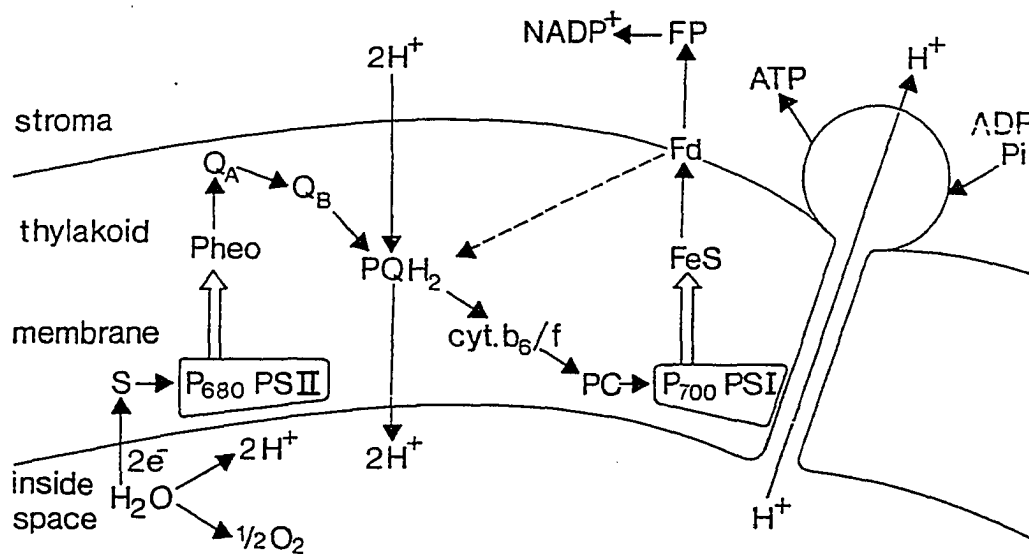


Figure 2. Pathway of electron and proton flow in photosynthesis of green plants.

ultimately derived from water [1-3]. From Pheo<sup>-</sup>, the electron is transported to the first quinone Q<sub>A</sub> and then to the secondary quinone Q<sub>B</sub>. Q<sub>B</sub> accumulates two electrons and becomes protonated with two protons from the stroma and exchanges with the plastoquinone pool (PQH<sub>2</sub>). From PQH<sub>2</sub>, electrons are transferred to the cytochrome b<sub>6</sub>/cytochrome f (cyt b<sub>6</sub>/f) complex and two protons are liberated into the internal lumen of the thylakoid. Plastocyanin (PC) transfers a electron to P700<sup>+</sup> to fill the electron hole produced by the primary separation of Photosystem I. The electron is transferred to FeS centers. Eventually the high energy electron flow leads to the formation of NADPH and ATP.

### 1.3 Photosystem II And The Similarity To Bacteria

As shown in Figure 3, the main portion of the light-harvesting antenna of Photosystem II is made up of several chlorophyll *a/b*-proteins, mainly LHCII. LHCII is the most abundant pigment protein of the thylakoid membrane. Based on the analysis of the crystal structure of LHCII complex, a trimeric structure of triangular shape has been resolved and also believed to be the native form [6,7]. All chlorophylls are arranged in two levels near the upper and lower surfaces of the thylakoid membrane [6,7]. The shortest center-to-center distances between Chls were estimated to be less than 15 Å [6,7]. The densely-packed structure of LHCII demonstrates that excitonic interactions can play an important role in antenna systems. LHCII is connected with the reaction center complex via other chlorophyll proteins referred to as CP24, CP26, and CP29. There are also two more major chlorophyll *a* proteins (CP47 and CP43) which are more tightly associated with the reaction center. CP47 and CP43 are called inner antenna which serve as the intermediary between LHCII and Photosystem II reaction center. Additional discussion of CP47 and CP43 can be found in Chapter 5 and the appendix A, respectively.

Consequently the light energy captured by the antenna is transferred to the primary electron donor P680 of Photosystem II reaction center where the electron transport starts.

It is particularly interesting to ask whether or not the structures and functions of Photosystem II RC are similar to those of bacterial RCs. As resolved by an X-ray

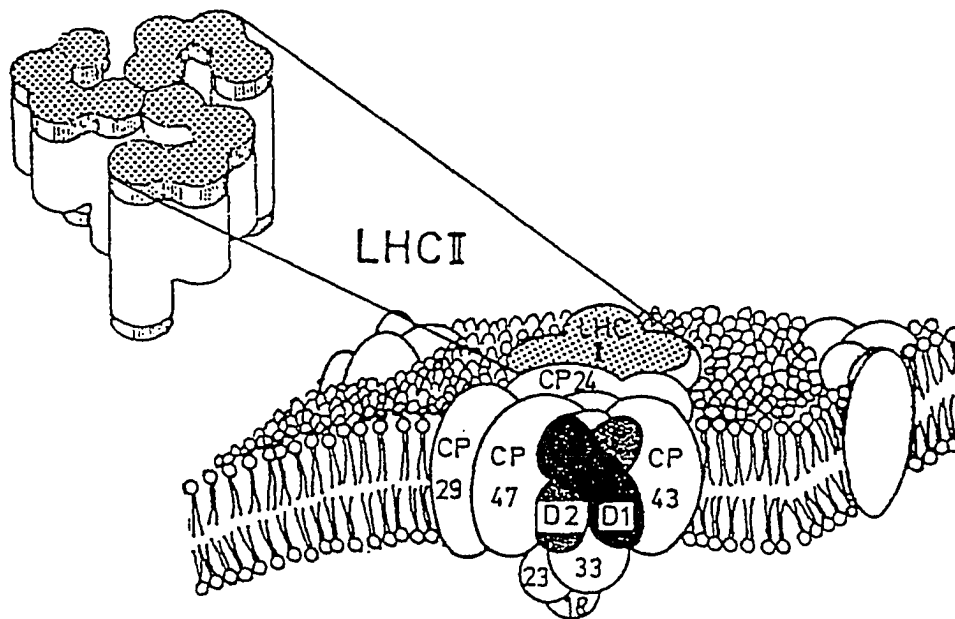


Figure 3. Simplified scheme of the incorporation of antenna-pigment protein complexes into the thylakoid membrane of green plants. The light-harvesting complex II is explicitly shown. CP= chlorophyll-protein complexes, numbers refer to the approximate molecular weight of the polypeptides. The cytochrome complex and PSI are not explicitly shown in the membrane section.

crystallograph [8,9] (see Figure 4), the purple bacterial reaction center from *Rps. viridis* carries four BChl, two BPheo, and two menaquinone ( $Q_A$ ,  $Q_B$ ). Two closely-coupled BChl molecules ( $P_L$ ,  $P_M$ ) comprise a "special pair" that functions as the primary electron donor. One BPheo ( $H_L$ ) is the proximal acceptor, receiving an electron from a special pair in 3 ps [14]. The electron moves in 200 ps to a quinone acceptor ( $Q_A$ ) and subsequently, in 60  $\mu$ s, to a secondary quinone ( $Q_B$ ). These pigments are organized in two almost identical branches by the L and M proteins. With the availability of the X-ray structure of *Rps. viridis* [8,9] significant homologies between the amino acid sequences of the L and M subunits of the bacterial RC and D1 and D2 proteins of PSII were realized [10]. This discovery led several groups [9,11,12] to predict that the D1 and D2 proteins were homologous to the L and M subunits in both structure and function.

In 1987 Nanba and Satoh announced the method which can extract the reaction center of PSII from green plants [13]. As predicted, the isolated PSII reaction center contained D1, D2, and cyt b<sub>559</sub>. The homologies of the amino acid sequences between bacterial and PSII reaction centers suggest that the structure of both may be similar, although there is no crystallographic proof yet. Photosystem II RC, i.e., D1-D2-cytb<sub>559</sub> complex, contains 4-6 Chl *a*, 2 Pheo *a*, 1 or 2  $\beta$ -carotenes, 1 cytochrome b<sub>559</sub> and no plastoquinones (see chapter 5). The pigment cofactor composition of D1-D2-cytb<sub>559</sub> complex also resembles that of bacterial RCs. As a consequence, it was suggested that P680 is most likely a dimer [14]. Certain optical properties suggest a dimeric structure for P680 as well [14-17]. For example, spectral hole burning studies of the PSII RC yielded data which strongly indicate that P680 is a special pair with a dimer splitting of only 300  $\text{cm}^{-1}$  [16,17]. The  $Q_y$  transition moments of two monomers are nearly anti-parallel. This geometry results in nearly all transition probability being found in one of the two exciton

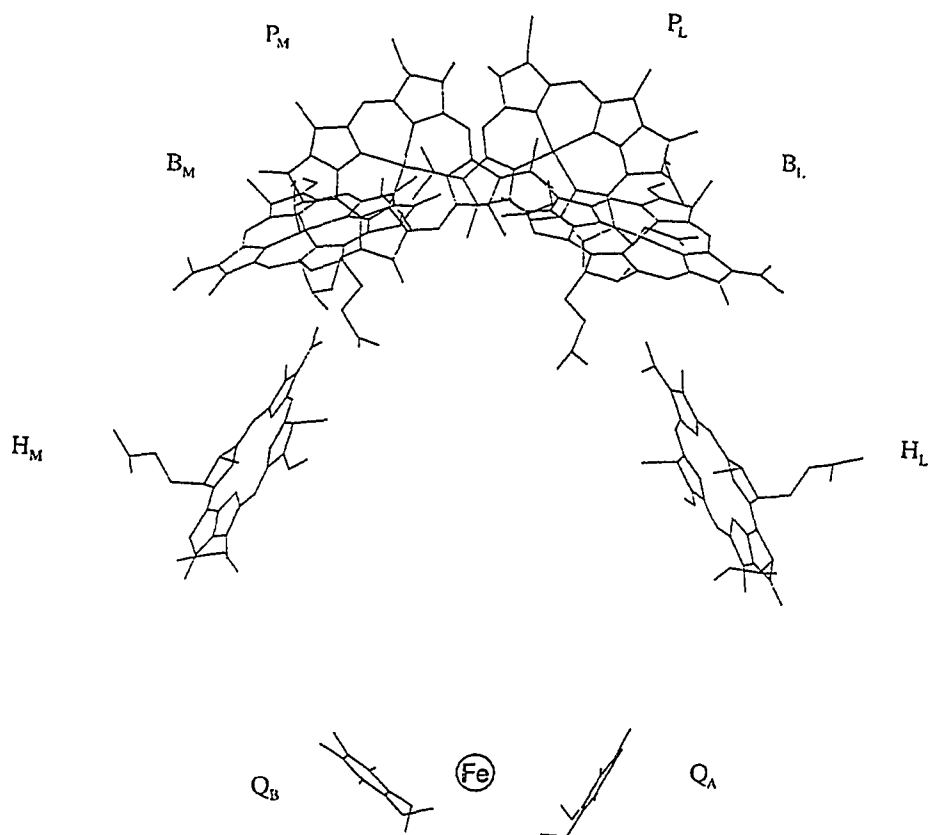


Figure 4. Structure of the reaction center of purple bacteria. Four bacteriochlorophylls ( $P_L$ ,  $P_M$ ,  $B_L$ ,  $B_M$ ), two bacteriopheophytin ( $H_L$ ,  $H_M$ ) and two menaquinone ( $Q_A$ ,  $Q_B$ ) are shown. The molecules are arranged in two branches, L and M forming an approximate  $C_2$ -symmetry.

bands. On the basis of the  $300\text{ cm}^{-1}$  splitting, Kwa et al. [17] deduce that the separation ( $\text{Mg}^{\bullet\bullet}\text{Mg}$ ) between the monomers of P680 is  $\sim 11\text{ \AA}$ . Therefore, P680 is a relatively weak coupled special pair, but may be disguised as a monomer by the geometry of two monomers.

As indicated in Figure 5, the kinetics scheme of PSII RC shows the similarity with that of bacterial RC. The primary charge separation in PSII ( $\text{P680}^* + \text{Pheo} \rightarrow \text{P680}^+ + \text{Pheo}^-$ ) takes place in a few picoseconds in the isolated D1-D2-cyt  $b_{559}$  complex (3.0 ps at 277K [18] and 1.9 ps at 4.2K [16], respectively). The rate of the process of the electron transfer from  $\text{Pheo}^-$  to  $\text{Q}_A$  was determined from PSII membrane fragment or PSII core complex instead of D1-D2-cyt  $b_{559}$  complex which does not have  $\text{Q}_A$ . The rate of  $\text{Q}_A^-$  formation exhibits a half-rise time of about 300 ps [19,20]. The reduction kinetics of  $\text{Q}_A$  in PSII are slightly slower than those of the corresponding reaction in bacteria (200 ps).  $\text{Q}_A^-$  transfers the electron to the secondary quinone  $\text{Q}_B$ , which is a two-electron carrier. The rate of electron transfer from  $\text{Q}_A^-$  depends on the reduced state of the secondary quinone. A value of 100-200  $\mu\text{s}$  is observed for the first reduction, but is increased to 300-500  $\mu\text{s}$  for the second reduction [19,20].

#### 1.4 Superexchange Or Two-Step

The basic arguments involved in the understanding of the bacterial reaction center are not settled even though the crystal structure has been solved. One of the major reasons is that the information required for excited-state dynamics can not be obtained directly from the X-ray structure in the ground state. Whether or not  $\text{P}^+\text{B}_L^-$  serves as a real or virtual state in the primary charge separation process is one of the long-standing questions [21,22]. Three mechanisms have been proposed: (i) one-step superexchange mechanisms in which  $\text{P}^+\text{B}_L^-\text{H}_L$  is simply a virtual state and  $\text{P}^+\text{B}_L\text{H}_L^-$  serves as the acceptor state.

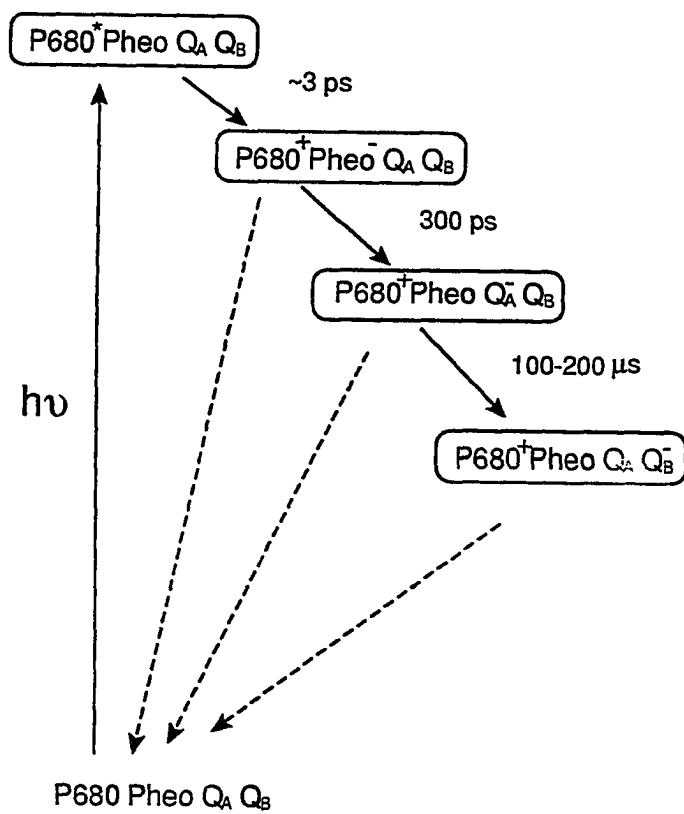


Figure 5. Reaction scheme of primary processes in the reaction center of Photosystem II at room temperature. P680, Pheo,  $Q_A$ , and  $Q_B$  represent the primary donor, pheophytin, first and secondary quinone, respectively. The rate of the second reduction of  $Q_B$  (300-500  $\mu\text{s}$ ) is not shown.



(ii) two-step mechanism; here  $P^+B_L^-H_L$  is a real state and serves as the acceptor state. The electron is subsequently transferred to the second state, i.e.,  $P^+B_L H_L^-$ . (iii) the parallel sequential-superexchange mechanism; this mechanism includes both superexchange and two-step mechanisms as limiting cases.

In order to illustrate the major differences between the superexchange and the two-step mechanisms, we consider the general multilevel multimode system of the excited states [23,24]. The Hamiltonian can be written as

$$H = \sum_{i=1}^N \epsilon_i |i\rangle\langle i| + \sum_{i<j} J_{ij} |i\rangle\langle j| + \sum_{n=1}^M \omega_n b_n^\dagger b_n + \sum_{ij} \sum_n \theta_{ij}^n |i\rangle\langle j| (b_n + b_n^\dagger) \quad (2)$$

where  $N$  is the number of excited states involved and  $M$  is the number of vibrational modes.  $|i\rangle$  is the excited state with electronic energy  $\epsilon_i$ .  $J_{ij}$  is the electronic coupling element between states  $|i\rangle$  and  $|j\rangle$  and  $\omega_n$  is the vibrational frequency of mode  $n$ .  $\theta_{ij}^n$  corresponds to vibronic coupling parameter. Assume a dipole allowed excited state  $D$  to interact with a dipole forbidden excited state  $A$ . Note that, in the case of bacterial RC,  $D$  is the lowest energy state ( $P_-$ ) of the special pair and  $A$  corresponds to  $P^+B_L^-$ . Then

$$\langle 0|\mu|D\rangle \neq 0 \quad (3)$$

and  $\langle 0|\mu|A\rangle = 0 \quad (4)$

where  $|0\rangle$  represents the ground electronic state. Eq.2 is rewritten as

$$H = \sum_{i=D,A} \epsilon_i |i\rangle\langle i| + \sum_{i,j=D,A} J_{ij} |i\rangle\langle j| + \omega b^\dagger b + \sum_{i,j=D,A} \theta_{ij} |i\rangle\langle j| (b^\dagger + b) \quad (5)$$

For simplicity, we consider only one vibrational mode with frequency  $\omega$  and define  $|\Delta E| = |\epsilon_D - \epsilon_A|$ . The calculations of Friesner et al. [23] reveal how, for a fixed  $|\Delta E|$  and  $J$ , the extent to which the  $|D\rangle$  state steals  $S$  from the  $|A\rangle$  state increases in passing from  $\theta/\omega < 1$  to  $\theta/\omega > 1$  where the adiabatic limit is in effect. That is, Huang-Rhys factor of  $P_-$  state ( $|D\rangle$  state) is not affected by  $P^+B_L^-$  ( $|A\rangle$  state) in the weak coupling limit.

It is known from the data of spectral hole burning that a zero-order  $P^*$  state, with weak electron-phonon coupling, receives the Huang-Rhys factor ( $S$ ) from a charge transfer state through the coupling (or electronic state mixing) between these two states. (The key observation is that the electron-phonon coupling for  $P_+$  is weak, but strong for  $P_-$  of *Rb. sphaeroides* RC [24].) To explain this observation, one must consider the coupling between the lowest energy excited electronic state ( $P_-$ ) of the special pair with weak electron-phonon coupling and a nearby external charge transfer state ( $P^+B_L^-$ ) with strong electron-phonon coupling (see Small [24] for detail). In order to explain the effect of the "stealing" of  $S$  from the dark charge transfer state, the case of a strong coupling limit needs to be addressed.

The strong coupling between  $P_-$  and  $P^+B_L^-$  results in an adiabatic energy surface associated with two wells, as indicated in Figure 1 of Chapter 3. These two wells originate from the nonadiabatic  $P_-$  and  $P^+B_L^-$  surfaces, respectively. Therefore, the question of whether or not  $P^+B_L^-$  serves as a real or virtual state in the primary charge separation process becomes irrelevant in the strong coupling limit.

## References

1. Hall, D.O.; Rao, K.K. in *Photosynthesis*; Cambridge Press: Cambridge, 1994
2. Zubay, G. in *Biochemistry*; Addison-Wesley: Reading, 1983
3. Stryer, L. in *Biochemistry*; Freeman: New York, 1988

4. Zuber,H.; Brunisholz,R.; Sidler,W. in *Photosynthesis*; Amesz,J., Ed.; Elsevier: The Netherland, 1987
5. Borisov,A.Y.; Fetisova,Z.G. *Mol. Biol.* 1971, 5, 509
6. Kühlbrandt,W.; Wang,D.N. *Nature* 1991, 350, 130
7. Kühlbrandt,W.; Wang,D.N.; Fujiyoshi,Y. *Nature* 1994, 367, 614
8. Deisenhofer,J.; Epp,O.; Miki,K.; Huber,R.; Michel,H. *J. Mol. Biol.* 1984, 180, 385
9. Deisenhofer,J.; Epp,O.; Miki,K.; Huber,R.; Michel,H. *Nature* 1985, 318, 618
10. Rochaix,J.D.; Dron,M.; Rahire,M.; Malnoe,P. *Plant Mol. Biol.* 1984, 3, 363
11. Cramer,W.A.; Widger,W.R.; Herrmann,R.G.; Trebst,A. *Trends Biochem. Sci.* 1985, 10, 125
12. Kyle,D.J. *Photochem. Photobiol.* 1985, 41, 107
13. Nanba,O.; Satoh,K. *Proc. Natl. Acad. Sci. USA* 1987, 84, 109
14. Seibert,M. in *The Photosynthetic Reaction Center*, Vol.I; Deisenhofer,J., Norris,J., Eds.; Academic Press: New York, 1993, p.319
15. Braun,P.; Greenberg,B.M.; Scherz,A. *Biochem.* 1990, 29, 10376
16. Chang,H.-C.; Jankowiak,R.; Reddy,N.R.S.; Yocum,C.F.; Picorel,R.; Seibert,M.; Small,G.J. *J. Phys. Chem.* 1994, 98, 7725
17. Kwa,S.L.S.; Eijkelhoff,C.; van Grondelle,R.; Dekker,J.P. *J. Phys. Chem.* 1994, 98, 7702
18. Wasielewski,M.R.; Johnson,D.G.; Seibert,M.; Govindjee *Proc. Natl. Acad. Sci.* 1989, 86, 524
19. Evans,M.C.W.; Nugent,J.H.A. in *The Photosynthetic Reaction Center*, Vol.I, Deisenhofer,J., Norris,J., Eds.; Academic Press: New York, 1993, p.391
20. Renger,G. in *Topics in Photosynthesis*, Vol.11; Barber,J., Ed.; Elsevier: The Netherland, 1992, p.45

21. Bixon,M.; Jortner,J.; Michel-Beyerle,M.E. in *The Photosynthetic Bacterial Reaction Center II*; Breton,J., Vermeglio,A., Eds.; NATO-ASI series A, Vol.237; Plenum Press: New York, 1992, p.291
22. Bixon,M.; Jortner,J.; Michel-Beyerle,M.E. *Chem. Phys.* (in press) and references therein.
23. Lathrop,E.J.P.; Friesner,R.A. *J. Phys. Chem.* 1994, 98, 3050
24. Small,G.J. *Chem. Phys.* in press

## CHAPTER 2 SPECTRAL HOLE BURNING SPECTROSCOPIES

### 2.1 Introduction

Fundamentally amorphous systems are not in thermodynamic equilibrium. Various local structures make dominant contributions to the properties of amorphous systems, and, as indicated in Figure 1, the absorbing centers are surrounded by different local environments [1]. The distribution of these local environments results in inhomogeneous broadening ( $\Gamma_{inh}$ ). In order to observe a homogeneous line width and obtain useful information about the dynamics of an amorphous system, spectral hole burning can be effective. It removes the inhomogeneous broadening. Proteins, like glass, possess many conformational substates which may transform from one state to another state by virtue of thermal energies [2]. As the temperature goes down to the temperature of liquid helium, the transformations among the substates are frozen and the distribution of these substates results in inhomogeneity. To put proteins in perspective, the intrinsic glass-like character of proteins needs to be adequately addressed. Therefore, spectral hole burning serves as a useful tool in the studies of proteins [3-5].

The invention of the narrowband laser provided a suitable excitation source for spectral hole burning. This provided an improvement in the resolution of the optical spectra by 2-3 orders of magnitude [6]. Typically these holes, burned at very low temperatures, are narrow and sensitive to the microscopic environment. A zero-phonon hole is the one with no net change in the number of phonons which accompany the electronic transition. The width of the zero-phonon line (ZPL) is mainly determined by homogeneous broadening which originates with the effective decay time of excited molecules. The effective decay time is described [7] as

$$\frac{2}{T_2} = \frac{1}{T_1} + \frac{2}{T_2^*} \quad (1)$$

where  $T_1$  is the lifetime of the excited state and  $T_2^*$  is the pure dephasing time of the molecules. Eq.1 is not symmetric in  $T_1$  and  $T_2^*$ , because the scattering processes with characteristic time  $T_2^*$  can occur in both the ground and excited state [1]. That is why the

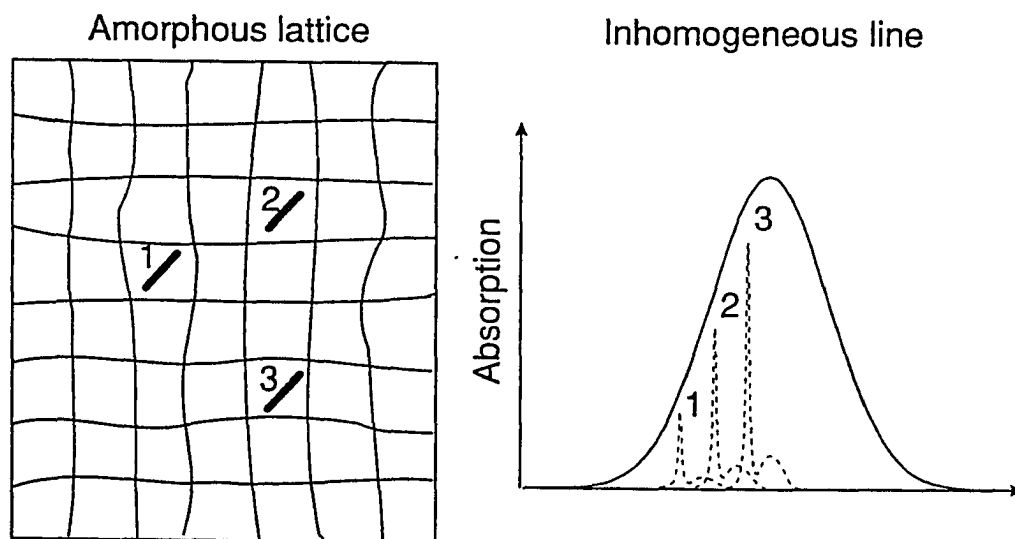


Figure 1. Schematic view of the optical absorption of three identical guest molecules in an amorphous host. In contrast to the situation in a crystalline lattice, the lines appear at different transition frequencies. The broad sidebands represent the phonon spectra of molecules 1, 2, and 3, respectively.

term of  $T_2^*$  owns a factor of two. Glass or proteins provide a high density of very low-frequency lattice states (due to the presence of two-level systems) which cause broadening via dephasing [6]. Due to the disappearance of thermal-excited lattice modes, the dephasing time is increased with decreasing temperature. As the temperature approaches zero, the zero-phonon hole width approaches its limiting value determined by  $T_1$ . Eq.1 is rewritten as

$$\frac{2}{T_2} = \frac{1}{T_1} \quad \text{or} \quad T_2 = 2T_1 \quad (2)$$

The absorption spectrum after a burn for time  $\tau$  at a frequency of  $\omega_b$  in the low temperature limit is written as (see section 3.3)

$$\begin{aligned} A_\tau(\Omega) &= \int d\nu N_\tau(\nu - \nu_m) L(\Omega - \nu) \\ &= \sum_{p=0}^{\infty} \frac{e^{-S} S^p}{p!} \int d\nu N_0(\nu - \nu_m) \exp[-\sigma I \phi \tau L(\omega_b - \nu)] \\ &\quad \times I_p(\Omega - \nu - p\omega_m) \end{aligned} \quad (3)$$

Consider the case of the short burn time limit [8] which we are interested in. Then

$$\exp[-\sigma I \phi \tau L(\omega_b - \nu)] = 1 - \sigma I \phi \tau L(\omega_b - \nu) \quad (4)$$

Substitution Eq.4 into Eq.3 leads to

$$\begin{aligned} A_\tau(\Omega) &= \sum_{p=0}^{\infty} \frac{e^{-S} S^p}{p!} \int d\nu N_0(\nu - \nu_m) (1 - \sigma I \phi \tau L(\omega_b - \nu)) \\ &\quad \times I_p(\Omega - \nu - p\omega_m) \end{aligned} \quad (5)$$

The hole profile is given by

$$A_r(\Omega) - A_0(\Omega) = - \sum_{p=0}^{\infty} \frac{e^{-S} S^p}{p!} \int dv N_0(v - v_m) \times \sigma I \phi \tau L(\omega_B - v) l_p(\Omega - v - p\omega_B) \quad (6)$$

Thus the hole profile is the convolution of two Lorentzians. Assuming  $\Delta v_h$  is the full width at half-maximum of the Lorentzians, we have

$$\Gamma_{hole} = 2\Delta v_h \quad (7)$$

where  $\Gamma_{hole}$  is the full width at half-maximum of the hole measured. The uncertainty principle leads to

$$\Delta v_h = \frac{1}{2\pi T_1} \quad (8)$$

By substituting Eq.2 and Eq.8 into Eq.7, the relationship between measured hole-width and total dephasing time is written as

$$\Gamma_{hole} = \frac{2}{\pi T_2} \quad (9)$$

## 2.2 NPHB, PHB vs Bottleneck HB: Mechanistic Aspects

Three basic hole-burning mechanisms can be described [3]. These are referred to as photochemical hole burning (PHB), nonphotochemical hole burning (NPHB), and transient hole burning. Photochemical hole burning [1] means the absorbing center (the guest) is involved in some internal change, such as tautomerization, bond-breaking,



isomerization, and so on. If the absorbing center is photoreactive, selective photobleaching of absorption spectrum can be engineered. What is required for PHB is the photoreactivity of the absorbing chromophore. Therefore, PHB can be observed for both amorphous and crystalline hosts. Photochemical hole burning was first observed [9] for free base phthalocyanine in n-octane where the PHB is caused by an intramolecular hydrogen tautomerization. In PHB the antihole is usually not near the zero-phonon hole as shown in Figure 2. The antihole is usually much broader than its parent hole because of the inhomogeneous broadening of the zero phonon lines of the photoproducts.

In the case of nonphotochemical hole burning, photoreactivity of the absorbing centers is not required. Nonphotochemical processes result from the change of the environment (the host) around the absorbing center. As indicated in Figure 2, absorption positions of the products (antihole) for nonphotochemical processes are not moved very far from the original absorption position. Since the host configurations need to be changed in the case of NPHB, NPHB has only been observed with glasses and polymers, with a few exceptions [8]. Nonphotochemical hole burning was first observed [10] for perylene and for 9-aminoacridine in the ethanol glass. The nonphotochemical holes often irreversibly disappear after increasing the temperature. In 1972, Anderson et al. [11] and, independently, Phillips [12] proposed that in any glass system there should be a certain number of atoms or groups of atoms which may occupy, with nearly equal probability, two equilibrium positions separated by an energy barrier, the so-called two-level system (TLS) (see Figure 3). At very low temperatures, atoms or groups of atoms cannot be thermally activated over the barrier, but can tunnel through it. As indicated in Figure 3, the excited molecules are produced by the excitation light ( $\omega_B$ ). At the burn temperature, relaxation between the minima of ground state  $TLS_\alpha$  is slow on the time scale of the experiment,

while it is competitive with the excited state lifetime at  $\text{TLS}_\beta$  ( $\beta$  denotes the impurity excited state). The degree of competitiveness determines the hole burning efficiency.

In 1978 the two-level system (TLS) model, based on the coupling of the electronic transition to the glass  $\text{TLS}_{\text{ext}}$ , was utilized for the NPHB mechanism [13]. Extrinsic TLSs ( $\text{TLS}_{\text{ext}}$ ) are suggested to be strongly associated with the absorbing center and are

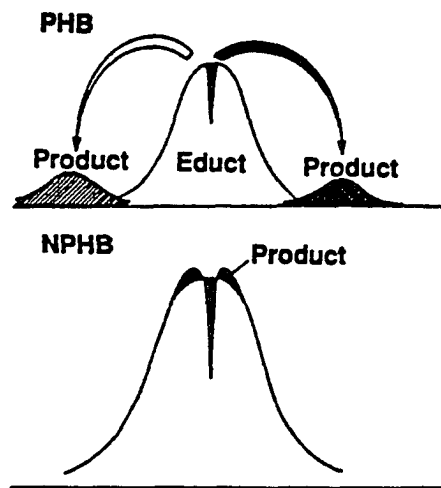


Figure 2. Spectral distribution of the photoproducts after photochemical (PHB) and nonphotochemical (NPHB) hole burning.

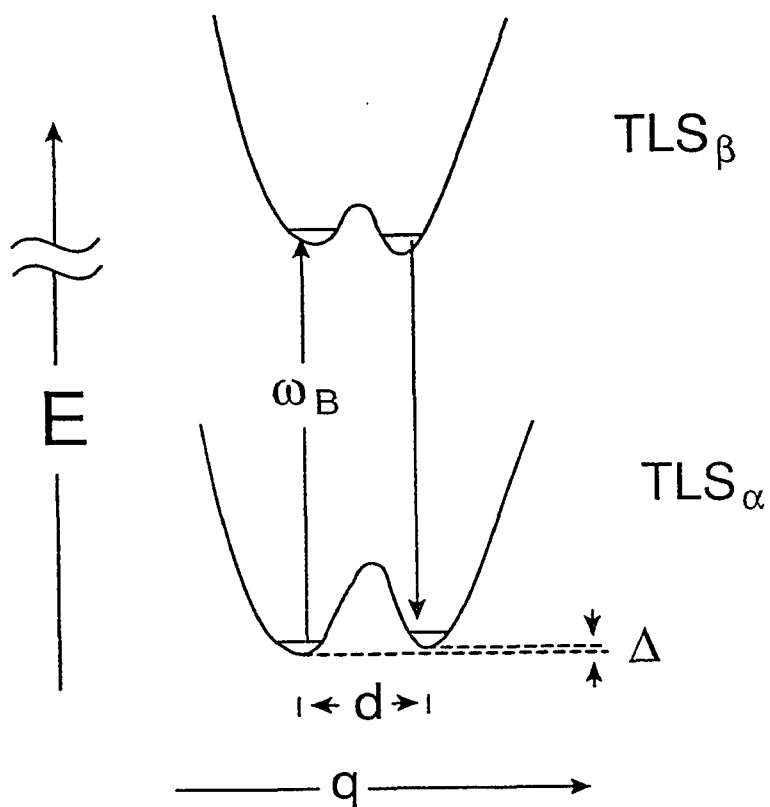


Figure 3. The two-level system (TLS) model for nonphotochemical hole burning. The subscripts  $\alpha$  and  $\beta$  label the TLS that interact with the impurity in its ground and excited electronic states. Asymmetries, displacements, intermolecular coordinates are labeled as  $\Delta$ ,  $d$ , and  $q$ , respectively.

responsible for the initiation of hole burning. NPHB occurs primarily in amorphous (glassy) matrices due to a rearrangement of the host environment, triggered by the electron-TLS<sub>ext</sub> coupling. The rate-determining step for hole formation is phonon-assisted tunneling of TLS<sub>ext</sub>. The intrinsic bistable configuration of the host itself is denoted by TLS<sub>int</sub>. The intrinsic TLSs (TLS<sub>int</sub>) was proposed to cause optical dephasing [8,13]. The mechanistic model for persistent NPHB was further developed by Shu et al. [14]. NPHB is triggered by electronic excitation and results in an increase in the free volume of the probe. An increase in the free volume for the probe in its inner shell of host molecules successfully explained the blue-shift of the antihole since  $^1\pi\pi^*$  states typically undergo a red-shift in going from the gas to the condensed phase. From the above we know that NPHB is the result of phonon-assisted tunneling of TLSs and provides a physical observance of TLS relaxation.

In NPHB only two electronic states of the guest molecules are involved (the ground and excited states). Population bottleneck hole burning utilizes a third, long-lived state to store the population depleted from the ground state [3,4]. The triplet state is usually the suitable candidate to serve as a population reservoir. In transient hole burning of bacterial reaction center, however, the analogous state is a product of the charge separation state of the primary electron donor, P<sup>\*</sup>. Although photoexcitation of P results in electron transfer on a picosecond timescales, return of the electron to the primary donor requires milliseconds [4,5].

### 2.3 Remarks On The Application Of Hole-Burning

During the past decade, spectral hole-burning has been generally applied to photosynthetic protein-pigment complexes [3-5]. The width of the ZPH, which coincides with the burn frequency, was used to determine the lifetimes of the excited states which

correspond to rapid electronic energy transfer or the primary charge separation. As indicated in Figure 4, a zero-phonon line is accompanied by a phonon side band (PSB). Therefore, the zero-phonon hole (ZPH) is normally associated with phonon sideband holes (PSBH). The PSBH in the high energy side of the ZPH is referred to as real-PSBH. In contrast to real-PSBH, the pseudo-PSBH lies to lower energy of  $\lambda_B$  (burning wavelength). The pseudo-PSBH are comprised of the bleached zero-phonon lines which absorb the laser light by virtue of the PSB.

Importantly, hole burning reveals the frequencies and coupling strengths (Huang-Rhys factors, i.e.,  $S$ ) of the phonons that couple to the electronic transition [3-5]. Weak electron-phonon coupling ( $S < 1$ ) is the main condition for observing intense zero-phonon lines. As discussed in the previous section, weak phonon coupling corresponds to a small change of the equilibrium configuration of the lattice due to the transition from the ground state to the excited state. Up to now all hole burning studies of the photosynthetic complexes showed weak electron-coupling for antenna [3-5] in contrast to strong coupling for reaction centers. Studies of the neutral excitonic  $\pi\pi^*$  dimer states of organic crystals such as anthracene [15] and naphthalene [16], had shown that the exciton-phonon coupling is weak and charge-transfer states of 1:1 donor-acceptor complexes are characterized by very strong electron-phonon coupling [17]. Therefore an excited primary donor ( $P^*$ ) may possess a significant amount of charge transfer character. Besides the character of strong electron-phonon coupling, the primary donors of bacterial RCs also showed a Franck-Condon progression of low-frequency vibrational mode(s), the so called marker mode(s) [3-5]. The marker mode can be viewed as a pseudolocalized or resonant phonon whose lengthy Franck-Condon progression signals a significant geometry change for the special pair in its excited state. One should notice that the marker mode is not observed in the

system of monomeric chlorophylls. In contrast to bacterial RC, the hole spectra of P680 show a weak contribution from the marker mode ( $S_{sp} < 0.3$ ). This observation reflects the fact that P680 is a monomer-like dimer, as indicated by a longer intra-dimer distance (11Å) of P680 than those of bacterial RCs [18]. The marker mode may originate from the intermolecular vibration of the special pair. Such special properties of the reaction centers

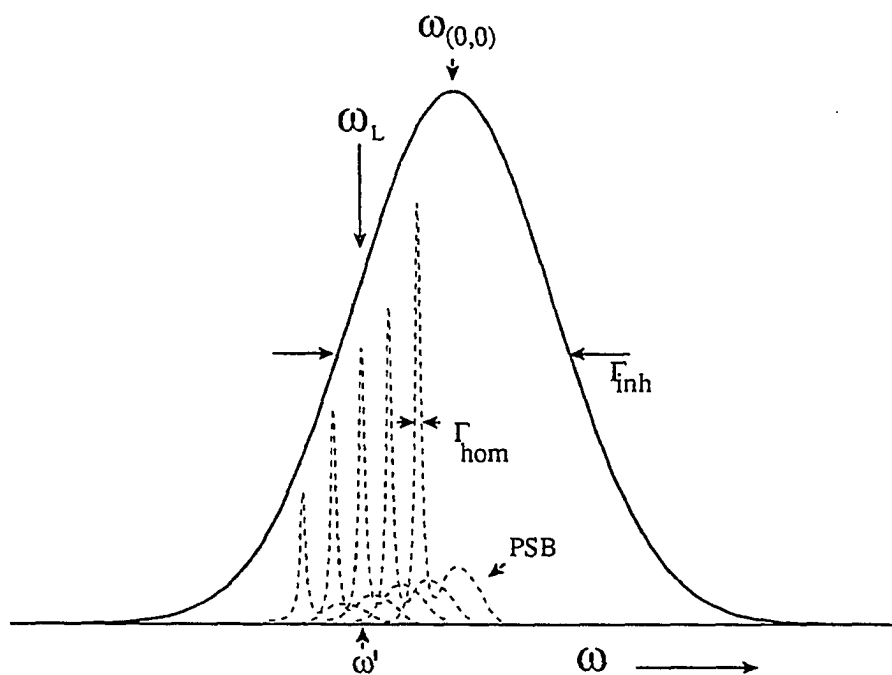


Figure 4. Schematic representation of homogeneous and inhomogeneous broadening. Profiles of the zero-phonon lines (ZPL) and their associated sidebands (PSB) at different frequencies are shown.

have stimulated several works of ultrafast studies [19-21]. The time evolution of the stimulated emission of the primary donor showed a modulation on a picosecond timescale. This phenomenon confirms the existence of the low-frequency nuclear vibrations and implicates the coherent nuclear motion in the primary electron transfer reaction in functional reaction centers.

Spectral hole burning also provides information about inhomogeneous broadening. In the action spectrum the ZPHs were burned under constant burn fluence conditions [22,23]. Assuming that NPHB efficiency is independent of burning frequency, the envelopes of the ZPHs represent the inhomogeneously broadened absorption bands. Nonphotochemical ZPH action spectroscopy has been used to probe weakly-absorbing components of photosynthetic systems (see chapter 4). Due to the inherent "glass-like" structural disorder of proteins, the action spectrum reveals a heterogeneity which is responsible for site inhomogeneous broadening ( $\Gamma_{inh}$ ) of the individual absorption bands.  $\Gamma_{inh}$  for chlorophylls and pheophytins of antenna protein-pigment complexes and reaction centers is in the range  $\approx 50\text{-}200\text{ cm}^{-1}$  and is comparable to that observed for chromophores in glasses and polymers [3-5]. Due to the glass-like structure of protein, it is known that the kinetics of electronic energy or electron transfer can be dispersive [24]. To illustrate the relationship between the inhomogeneous broadening and the dispersive kinetics, assume the decay time for a single system to be a single exponential and described as

$$f(t, \omega) = A_{\omega} e^{-\frac{t}{\tau(\omega)}} \quad (10)$$

where  $\tau(\omega)$  is the lifetime of the system which is isoenergetic with frequency  $\omega$ . Consider the distribution of heterogeneity to be a Gaussian with a variance  $\sigma_{inh}^2$ . Then

$$g(\omega) = \frac{1}{\sqrt{2\pi}\sigma_{inh}} \exp[-(\omega - \omega_0)^2 / 2\sigma_{inh}^2] \quad (11)$$

where  $\omega_0$  corresponds to the position of the maximum. The full-width at half maximum of the Gaussian, i.e.,  $\Gamma_{inh}$  is written as

$$\Gamma_{inh} = 2.354\sigma_{inh} \quad (12)$$

The measured kinetic decay is expressed as

$$F(t) = \int f(t, \omega) g(\omega) d\omega \quad (13)$$

Substitution of Eq.10 and Eq.11 into Eq.13 leads to

$$F(t) = \int A_0 e^{-\frac{t}{\tau(\omega)}} \frac{1}{\sqrt{2\pi}\sigma_{inh}} \exp[-(\omega - \omega_0)^2 / 2\sigma_{inh}^2] d\omega \quad (14)$$

As indicated in Eq.14, the measured kinetic decay may be non-single exponential or dispersive due to the inhomogeneous broadening. Whether the system is dispersive or not depends on the magnitudes of inhomogeneous broadening and homogeneous broadening. As discussed by Small et al. [24] (see chapter 3), the average value of rate constant is written as

$$\langle k_{DA} \rangle =$$

$$2\pi V^2 [2\pi(\Gamma^2 + \hat{S}(\sigma^2 + \omega_m^2))]^{-1/2} \exp[-(\Delta E_0 - S\omega_m)^2 / 2[\Gamma^2 + \hat{S}(\sigma^2 + \omega_m^2)]] \quad (15)$$

In the case of



$$S(\sigma^2 + \omega_m^2) \ll \Gamma_{inh}^2, \quad (16)$$

the system is dispersive.

Whether or not the energy gaps between the  $Q_y$  states of different pigments of a particular complex are perfectly correlated (remain the same) between different minimal subunits is particularly interesting. In a highly correlated system the appearance of a sharp ZPH, instead of the whole absorption profile of a acceptor state, represents the presence of a correlation between the donor and acceptor states. Recently, spectral hole burning was used to prove that there is an absence of such correlation for the accessory Chl *a*, active pheophytin *a* and primary electron donor (P680) of the reaction center complex of Photosystem II [25,26].

#### References

1. Friedrich, J.; Haarer, D. *Angew. Chem. Int. Ed. Engl.* 1984, 23, 113
2. Frauenfelder, H. et al. *J. Phys. Chem.* 1990, 94, 1024
3. Jankowiak, R.; Hayes, J.M.; Small, G.J. *Chem. Rev.* 1993, 93, 1471
4. Jankowiak, R.; Small, G.J. in *The Photosynthetic Reaction Center*, Vol.2, Deisenhofer, J.; Norris, J., Eds.; Academic Press: New York, 1993, p.133
5. Reddy, N.R.S.; Lyle, P.A.; Small, G.J. *Photosyn. Res.* 1992, 31, 167
6. Moerner, W.E., Ed. in *Persistent Spectra Hole-Burning: Science and Applications*; Springer-Verlag: Berlin, 1988
7. Völker, S. in *Relaxation Processes in Molecular Excited States*, Fünfschilling, J., Ed.; Kluwer: Dordrecht, 1989, p.113
8. Jankowiak, R.; Small, G.J. *Science* 1987, 237, 618
9. Gorokhovskii, A.A.; Kaarli, R.K.; Rebane, L.A. *JETP Lett.* 1974, 20, 216

10. Kharlamov, B.M.; Personov, R.I.; Bykovskaya, L.A. *Opt. Commun.* 1974, 12, 191
11. Anderson, P.W.; Halperin, B.J.; Varma, C.M. *Philos. Mag.* 1972, 25, 1
12. Philips, W.A. *J. Low Temp. Phys.* 1972, 7, 351
13. Hayes, J.M.; Small, G.J. *Chem. Phys.* 1978, 27, 151
14. Shu, L.; Small, G.J. *Chem. Phys.* 1990, 141, 447
15. Port, H.; Rund, D.; Small, G.J.; Yakhot, V. *Chem. Phys.* 1979, 39, 175
16. Robinette, S.C.; Small, G.J.; Stevenson, S.H. *J. Chem. Phys.* 1978, 68, 4790
17. Haarer, D. *Chem. Phys. Lett.* 1974, 27, 91
18. Kwa, S.L.S.; Eijkelhoff, C.; van Grondelle, R.; Dekker, J.P. *J. Phys. Chem.* 1994, 98, 7702
19. Vos, M.H.; Rappaport, F.; Lambry, J.-C.; Breton, J.; Martin, J.-L. *Nature* 1993, 363, 320
20. Vos, M.H.; Jones, M.R.; Hunter, C.N.; Breton, J.; Lambry, J.-C.; Martin, J.-L. *Biochemistry* 1994, 33, 6750
21. Vos, M.H.; Jones, M.R.; McGlynn, P.; Hunter, C.N.; Breton, J.; Martin, J.-L. *Biochim. Biophys. Acta* 1994, 1186, 117
22. Reddy, N.R.S.; Picorel, R.; Small, G.J. *J. Phys. Chem.* 1992, 96, 6458
23. Reddy, N.R.S.; Cogdell, R.J.; Zhao, L.; Small, G.J. *Photochem. Photobiol.* 1993, 57, 35
24. Small, G.J.; Hayes, J.M.; Silbey, R.J. *J. Phys. Chem.* 1992, 96, 7499
25. Tang, D.; Jankowiak, R.; Seibert, M.; Yocum, C.F.; Small, G.J. *J. Phys. Chem.* 1990, 94, 6519
26. Jankowiak, R.; Tang, D.; Small, G.J.; Seibert, M. *J. Phys. Chem.* 1989, 93, 1649

## CHAPTER 3 THEORETICAL BACKGROUND

### 3.1 Nonadiabatic Electron Transfer Theory

In the application of weak coupling, a nonadiabatic electron transfer theory has been developed by Marcus [1-3], Hopfield [4], Jortner [5] et al., and employed routinely. To illustrate the difference between adiabatic and nonadiabatic cases, the potential energy for nuclear motion for the whole system of donor, acceptor, and surroundings of both cases are plotted against the nuclear configuration (Figure 1). Initial and final equilibrium configurations are labeled as A and B, respectively. In the adiabatic case, the interaction between R and P is so strong that appreciable splitting into curve 1 and 2 is seen at C. In contrast to the adiabatic case, while the nuclear vibrates about the equilibrium position in curve R, passage through C does not usually cause transition from R to P. It is well known that the rate of a transition in the nonadiabatic case from an initial state R to P follows Fermi's golden rule [6]:

$$W_{R \rightarrow P} = \frac{2\pi}{\hbar} V^2 (\text{FC}), \quad (1)$$

where  $V$  is the interaction matrix element between R and P and FC represents the effective Franck-Condon density of states.

To simplify the situation, first consider two harmonic oscillators with the same frequency as shown in Figure 2. Assuming the nuclear vibrations follow Hook's law, the equations of R and P curves are :  $V_R = k_H(X - X_A)^2 / 2 + E_R$  and  $V_P = k_H(X - X_B)^2 / 2 + E_P$ , respectively. As indicated in Figure 2,  $\lambda$  (called the reorganization energy) is the amount of energy required to move the system from initial equilibrium system  $X_B$  to  $X_A$ .

$$\begin{aligned}\lambda &= V_P(X_A) - V_R(X_A) + \Delta E \\ &= (k_H/2)(X_A - X_B)^2\end{aligned}\quad (2)$$

Defining the Huang-Rhys factor ( $S$ ) as  $\lambda/\hbar\omega$ , then

$$S = \frac{k_H}{2\hbar\omega}(X_A - X_B)^2 \propto Q^2, \quad (3)$$

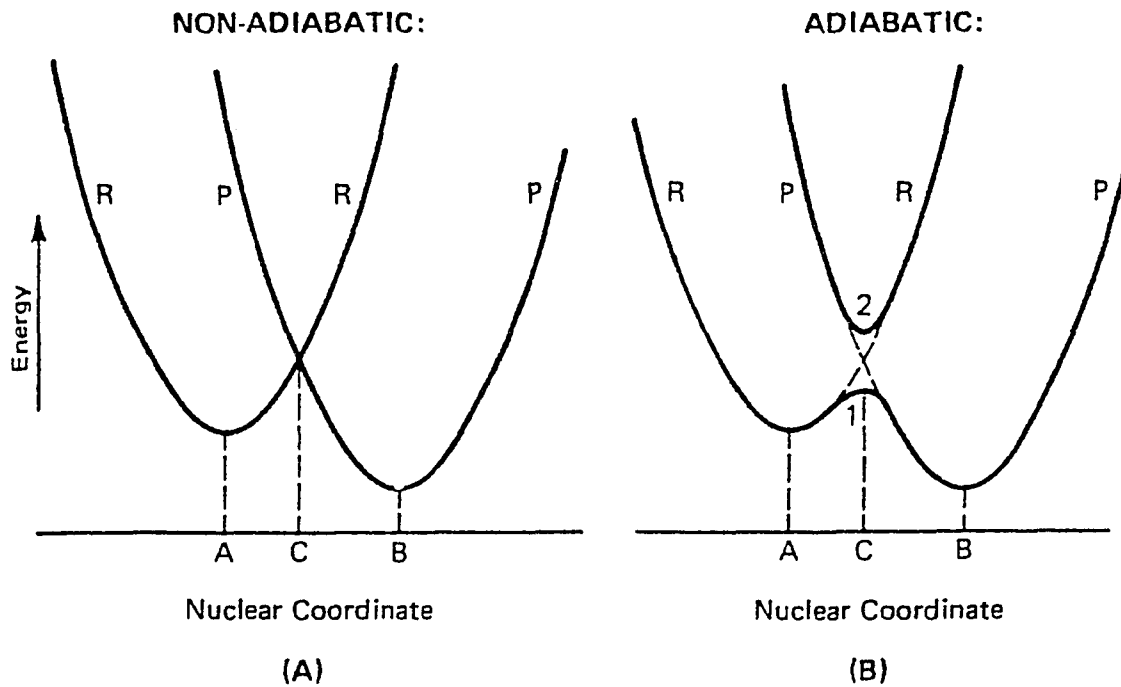


Figure 1. The role of nuclear motion in the cases of non-adiabatic (A) and adiabatic (B) transfer. The initial and final equilibrium configurations are labelled A and B, respectively. In the adiabatic case at the right, interaction between potential curves R and P is so strong that splitting into curves 1 and 2 is seen at C.

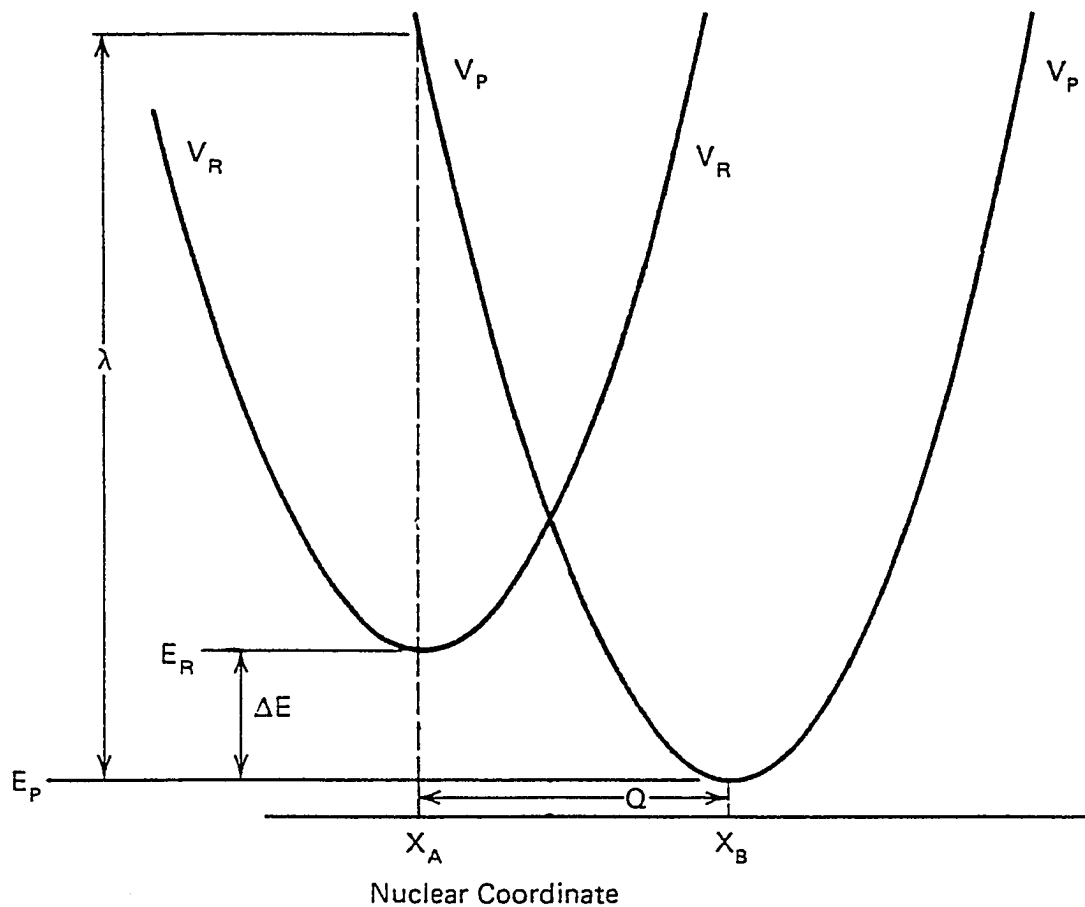


Figure 2. Nuclear motion accompanying non-adiabatic transfer.  $V_R$  and  $V_P$  represent the nuclear potential curves of the donor and acceptor, respectively.  $X_A$  and  $X_B$  are the initial and final equilibrium positions, respectively. The reorganization energy,  $\lambda$ , is the amount of energy required to displace the system from  $X_A$  to  $X_B$ .

where the angular frequency of oscillation,  $\omega$ , is given by  $\omega = \sqrt{\frac{k_H}{M}}$ . The Huang-Rhys factor (S) is a measure of the coupling of the nuclear vibrations to the system. If the system consists of a group of oscillators, S is a summation of values for each oscillator. The probability of the transition from R to P is proportional to the square of the 'overlap integral',  $C(n, n')$ , between the vibrational state  $n'$  in P and the corresponding state  $n$  in R.  $C^2(n, n')$  is called the Franck-Condon factor given by

$$C^2(n, n') = \left[ \int \chi_n \chi_{n'} dx \right]^2, \quad (4)$$

where  $\chi_n$  is the vibrational wavefunction for state  $n$  in R, and  $\chi_{n'}$  is the wavefunction for state  $n'$  in P.  $x$  is the oscillator coordinate. At a given temperature, the fraction of systems expected to be in state  $n$  of R follows Boltzmann distribution under the assumption of thermal equilibrium. Then

$$B(n, T) = e^{-\beta \hbar \omega n} (1 - e^{-\beta \hbar \omega})^{-1}, \quad (5)$$

where  $B(n, T)$  is the fraction of systems at temperature  $T$ . By multiplying each  $C^2(n, n')$  by  $B(n, T)$  of various  $n$ , the FC term in Eq.1 is obtained.

$$FC = \sum_{n=0}^{\infty} C^2(n, n') B(n, T) \quad (6)$$

Substituting Eq.6 into Eq.1 leads to

$$W = A \sum_{n=0}^{\infty} C^2(n, n') B(n, T), \quad (7)$$

where  $A = 2\pi V^2 / \hbar^2 \omega$ . Manneback [7] derived the exact formula for  $C^2(n, n')$  with  $n' = n + p$  for the case where the frequency does not change.

$$C^2(n, n+p) = n!(n+p)! S^p e^{-S} \left[ \sum_{i=0}^n \frac{(-S)^i}{i!(n-i)!(p+i)!} \right]^2 \quad (8)$$

To get a more physical feeling for Eq.8, consider the situation as  $T \rightarrow 0$  K. At low temperature, almost all molecules occupy the lowest state ( $n=0$ ). Eq.8 then simplifies to

$$C^2(n=0, p) = \frac{S^p e^{-S}}{p!} \quad (9)$$

Substitution of Eq.9 and  $B(n=0, T \rightarrow 0 \text{ K}) = 1$  into Eq. 6, yields the reduced Franck-Condon factor

$$FC(p) = \frac{S^p e^{-S}}{p!}, \quad (10)$$

where  $p = n' - n = n'$  represents the number of vibrational quanta involved in the transition process. As indicated by Eq.10, the Franck-Condon factor of vibrational quanta (called phonon for the case of lattice vibration) follows the general formula for Poisson statistics [8].

$$P(x, \mu) = \frac{\mu^x e^{-\mu}}{x!} \quad (11)$$

and

$$\sum_{x=0}^{\infty} P(x, \mu) = e^{-\mu} \sum_{x=0}^{\infty} \frac{\mu^x}{x!} = e^{-\mu} e^{\mu} = 1 \quad (12)$$

As revealed by Eq.10, the Franck-Condon factor of zero and nonzero-vibrational quanta

processes ( $p=0$ ) are  $e^{-S}$  and  $1-e^{-S}$ , respectively. Eq.8 is suitable only for the case of two single oscillators with no frequency change. Kubo [9] and Lax [10] further developed the Franck-Condon factor for a system consisting of a group of oscillators which do not change frequency in the form of Eq.13. For a complete derivation, the reader is referred to Devault [11].

$$FC = \frac{1}{2\pi\hbar} \int_{-\infty}^{\infty} dt \exp\{-S[2\bar{n}+1-(\bar{n}+1)e^{i\omega t} - \bar{n}e^{-i\omega t}] - p i\omega t\}, \quad (13)$$

where  $S$  is a summation of values for each oscillator,  $\bar{n} = [\exp(\hbar\omega / kT) - 1]^{-1}$  is the average quantum number at thermal equilibrium (in analogy to  $B(n,T)$  in Eq.5), and  $t$  is a dummy variable. To explain the physical meaning of terms inside  $\exp(\ )$ , one starts with the delta function in intergral form

$$\delta(n' - n - p) = \frac{\omega}{2\pi} \int e^{i(n' - n - p)\omega t} dt \quad (14)$$

which satisfies conservation of energy, i.e.

$$p = n' - n. \quad (15)$$

As revealed by comparing Eq.13 and 14, the  $e^{i\omega t}$  and  $e^{-i\omega t}$  terms in Eq.13 correspond to  $\delta(1-p)$  and  $\delta(-1-p)$ , respectively. That is,  $e^{i\omega t}$  and  $e^{-i\omega t}$  terms describe the process of the absorption ( $p=n'-n=1$ ) and emission ( $p=-1$ ) of one vibrational quantum in a transition. Furthermore, the  $\exp$  term in Eq.13 describes all the vibrational quanta processes ( $n'-n=0,1,2,\dots$ ) as indicated by the Taylor expansion series in Eq.16.

$$e^z = 1 + z + \frac{z^2}{2!} + \dots \quad (16)$$



Each term of the right hand side of Eq. 16 can be further expanded,

$$z^R = (X + Y)^R = \sum_{T=0}^R \frac{X^{R-T} Y^T R!}{(R-T)! T!} . \quad (17)$$

With reference to Eq.13, a more general form of the Franck-Condon factor, modified from Eq.13 for multi-oscillators with different vibrational modes, is usually written as

$$FC = \frac{1}{2\pi\hbar} \int_{-\infty}^{\infty} f(t) e^{-i\Delta E t/\hbar} dt, \quad (18)$$

$$\text{where } f(t) = \exp\{-G + G_+(t) + G_-(t)\} \quad (19)$$

$$G_+(t) = \sum_{\alpha} S_{\alpha} (\bar{n}_{\alpha} + 1) e^{i\omega_{\alpha} t} \quad (20)$$

$$G_-(t) = \sum_{\alpha} S_{\alpha} \bar{n}_{\alpha} e^{-i\omega_{\alpha} t} \quad (21)$$

$$G = G_+(0) + G_-(0). \quad (22)$$

Again,  $G_+$  and  $G_-$  represent absorption and emission of one vibrational quantum, respectively.  $\alpha$  designates the different modes in a multi-oscillator system and the summations ( $\sum$ ) are over all modes. Substitution of Eq.18 into Eq.1, yields

$$W = \frac{2\pi}{\hbar} V^2 \frac{1}{2\pi\hbar} \int_{-\infty}^{\infty} f(t) e^{-i\Delta E t/\hbar} dt, \quad (23)$$

where  $W$  denotes the transition rate and  $V$  is the interaction matrix element. Eq.23 was the starting point for Small et al. [12] who obtained a simplified but accurate expression for the

rate constant for primary charge separation in the photosynthetic reaction center (RC). The summation terms ( $\Sigma$ ) carries the shape of one-vibration quantum (one-phonon) profile were approximated by a Gaussian function,  $g(\omega)$ , which carries a width of  $\sim 2\sigma$

$$g(\omega) = (\sqrt{2\pi}\sigma)^{-1} \exp[-(\omega - \omega_m)^2 / 2\sigma^2] \quad (24)$$

where  $\omega_m$  represents the mean phonon frequency. The substitution of the summations with a gaussian function,  $g(\omega)$ , is reasonable, since the hole-burning data [13] indicate that the one-phonon profile is smooth. That is,

$$\sum_{\alpha} S_{\alpha} \approx S \int g(\omega) d\omega \quad (25)$$

Substitution of Eq.25 into Eq.19 leads to

$$f(t) = \exp\left(-\int g(\omega) S \{(2\bar{n}_{\omega} + 1) - e^{i\omega t}(\bar{n}_{\omega} + 1) - e^{-i\omega t}(\bar{n}_{\omega})\} d\omega\right) . \quad (26)$$

After rearrangement one finds

$$f(t) = \exp\left[-\int g(\omega) S (2\bar{n}_{\omega} + 1) d\omega + \int g(\omega) S \bar{n}_{\omega} (e^{i\omega t} + e^{-i\omega t}) d\omega + \int g(\omega) S e^{i\omega t} d\omega\right]. \quad (27)$$

Substitution of the Gaussian function  $g(\omega)$ , i.e., Eq.24, into Eq.27 followed by integration yields

$$f(t) = \exp(-\hat{S}) \exp[Se^{-\sigma^2 t^2 / 2} \{(2\bar{n} + 1) \cos \omega_m t + i \sin \omega_m t\}], \quad (28)$$

where  $\hat{S}$  is defined as

$$\hat{S} = \int g(\omega) S(2\bar{n}_\omega + 1) d\omega \quad (29)$$

$\hat{S}$  is further simplified by employing the mean phonon frequency approximation

$$\begin{aligned} \hat{S} &= S(2\bar{n} + 1) \\ &= S \operatorname{ctnh}(\hbar\omega_m / 2kT) \end{aligned} \quad (30)$$

Eq.28 is further approximated by expanding the t-dependent functions in the argument of the exponential, sin and cos and neglecting terms of order higher than  $t^2$ .

$$f(t) \approx \exp[-S(2\bar{n} + 1)(\sigma^2 + \omega_m^2)t^2 / 2 + i\omega_m t] \quad (31)$$

Note that Eq.31 originates from Eq.19 which describes all of the phonon processes including the contribution from zero-phonon transition with Franck-Condon factor equal to  $\exp(-\hat{S})$ . To calculate the contribution of phonon side band mode ( $n'-n=1,2,\dots$ ) to energy or electron transfer rate, Eq.31 is multiplied by a factor of  $(1 - \exp(-\hat{S}))$ .

$$f(t) \approx (1 - e^{-\hat{S}}) \exp[-S(2\bar{n} + 1)(\sigma^2 + \omega_m^2)t^2 / 2 + i\omega_m t] \quad (32)$$

Substitution of Eq.32 into Eq.23 and taking the Fourier transform using

$$\frac{1}{\sqrt{2\pi}} \int e^{-Pt^2} e^{i\alpha t} dt = \frac{1}{\sqrt{2P}} e^{-\alpha^2/4P} \quad (33)$$

leads to

$$W = 2\pi V^2 (1 - e^{-\hat{S}}) [(2\pi \hat{S}(\sigma^2 + \omega_m^2))^{-1/2} e^{-\frac{(\Delta E - S\omega_m)^2}{2\hat{S}(\sigma^2 + \omega_m^2)}}] \quad (34)$$

Note that Eq.19 is the form suitable for harmonic oscillators with no frequency change between initial (donor) and final (acceptor) states. That is, Eq.34 assumes the phonons created by the energy or electron transfer process have no frequency change, and are shared entirely between donor and acceptor state. For delocalized phonon the assumption of no frequency change is an excellent one. Eq.34 was used to calculate the electron transfer rate constant for a single reaction center (RC).

$$k_{DA} = 2\pi V^2 (1 - e^{-\hat{S}}) [(2\pi \hat{S}(\sigma^2 + \omega_m^2))^{-1/2} e^{-\frac{(\Delta E - S\omega_m)^2}{2\hat{S}(\sigma^2 + \omega_m^2)}}] \quad (35)$$

In the strong electron-phonon coupling limit ( $\hat{S} > 1$ ), the rate constant for single RC can be approximated as

$$k_{DA} = 2\pi V^2 [(2\pi \hat{S}(\sigma^2 + \omega_m^2))^{-1/2} e^{-\frac{(\Delta E - S\omega_m)^2}{2\hat{S}(\sigma^2 + \omega_m^2)}}], \quad (36)$$

where  $\Delta E$  is the electronic energy gap and  $V$  is the electronic coupling matrix element between the donor and acceptor states. For a Gaussian distribution of  $\Delta E$  values centered at  $\Delta E_0$ , the average value for the rate is [14]

$\langle k_{DA} \rangle =$

$$2\pi V^2 [2\pi(\Gamma^2 + \hat{S}(\sigma^2 + \omega_m^2))]^{-1/2} \exp[-(\Delta E_0 - S\omega_m)^2 / 2[\Gamma^2 + \hat{S}(\sigma^2 + \omega_m^2)]], \quad (37)$$

where  $2\Gamma$  is the width of the normal distribution for  $\Delta E$ . As pointed out by Small et al. [12,14]  $\Gamma^2$  and  $\hat{S}(\sigma^2 + \omega_m^2)$  can be viewed as terms associated with inhomogeneous and

homogeneous broadening, respectively. In the case of

$$S(\sigma^2 + \omega_m^2) \gg \Gamma^2 \quad (38)$$

the average rate constant  $\langle k_{DA} \rangle$  is simplified to

$$\langle k_{DA} \rangle = 2\pi V^2 [(2\pi \hat{S}(\sigma^2 + \omega_m^2))^{-1/2} e^{-\frac{(\Delta E_0 - S\omega_m)^2}{2\hat{S}(\sigma^2 + \omega_m^2)}}] \quad (39)$$

That is, the kinetics are non-dispersive as indicated by  $\langle k_{DA} \rangle = k_{DA} (\Delta E = \Delta E_0)$ . Further application of Eq.37 in the high pressure studies of a Photosystem II reaction center will be discussed later in Chapter seven.

### 3.2 Theory Of Molecular Excitons

To illustrate the theory of molecular excitons, consider the case of a one-dimensional array of N identical molecules which are located at a distance r from each other. The energy states of an isolated molecule are determined by

$$(H - E^i)\phi^i = 0, \quad (40)$$

where i corresponds to the ground state (i=0) or excited state (i=e) of the molecule. For simplicity, non-degenerate levels of the molecule are assumed. In the case of N molecules, Eq.40 is rewritten as

$$\left( \sum_{n=1}^N H_n + \frac{1}{2} \sum_{n,m}' V_{nm} - E \right) \phi^i = 0, \quad (41)$$

where  $V_{nm}$  is the matrix element of interaction between molecules n and m.  $\sum_{n,m}'$  is the summation of all terms except n=m. The wavefunction of the ground state of the system of

N molecules can be written in the form of

$$\psi^0 = \prod_{n=1}^N \phi_n^0 . \quad (42)$$

From first-order perturbation theory [15], the energy of the ground state of the system of N identical molecules is equal to

$$E^0 = NE_u^0 + \frac{1}{2} \int \psi^{0*} \sum_{n,m} V_{nm} \psi^0 d\tau , \quad (43)$$

where  $E_u^0$  is the energy of the ground state of an unperturbed molecule. An excited state can be written in a similar manner if it is assumed that only one molecule is in an excited state. Then, for molecule at site n excited, one has

$$\phi_n^e = \phi_n^e \prod_{m(m \neq n)} \phi_m , \quad (44)$$

where e denotes the excited state and  $\phi_n^e$  is the excited state wavefunction with the excitation energy localized at nth molecule. It is clear from the perturbation theory that the wavefunctions of the excited states result in an N-fold degeneracy if the interactions among the states in which the excitation is at different sites are negligible. The first order energy correction of  $\phi_n^e$  is

$$D = \frac{1}{2} \int \phi_n^{e*} \sum_{n,m} V_{nm} \phi_n^e d\tau . \quad (45)$$

Eq.45 does not account for the interactions among the states. Furthermore, the states (Eq.44) are not stationary states of the system if there are nonvanishing matrix elements among these states. As shown in Eq.46, the interaction energy among states is

$$M = \frac{1}{2} \int \phi_n^{e*} \sum_{n,m} V_{nm} \phi_m^e d\tau . \quad (46)$$

To properly describe the coupling among states, the wavefunctions of the excited states are rewritten in the form of a linear combination of the states. Then

$$\psi^e = \frac{1}{\sqrt{N}} \sum_n b_n \phi_n^e , \quad (47)$$

where  $\psi^e$  represents the wavefunction of the delocalized excited state. In order to have a better understanding of the exciton theory, consider a model of two identical molecules coupled by an interaction  $V$ . The Hamiltonian of this system is simplified as

$$H = H_1 + H_2 + V , \quad (48)$$

where  $H_1$  and  $H_2$  are the Hamiltonians of the isolated molecules and  $V$  is the interaction operator between two molecules. As indicated by Eq.47, the wavefunction of the delocalized excited state is a linear combination of the localized wavefunctions with excitation energy localized at first and second molecules, respectively. Then

$$\psi_i^e = a_{1i} \phi_1^e \phi_2 + a_{2i} \phi_1 \phi_2^e , \quad (49)$$

where  $\psi_i^e$  represents the wavefunctions of the stationary excited states.  $i=1$  or  $2$  denotes the first or second stationary excited states of the system of two molecules. The wavefunctions of stationary states must be orthogonal to each other and normalized, i.e., they must satisfy the condition:

$$\int \psi_i^{e*} \psi_j^e d\tau = \delta_{ij} . \quad (50)$$

Substitution of Eq.49 into Eq.50 leads to the solutions:

$$\psi_1^e = \psi^+ = \frac{1}{\sqrt{2}}(\phi_1^e\phi_2 + \phi_1\phi_2^e) \quad (51)$$

and

$$\psi_2^e = \psi^- = \frac{1}{\sqrt{2}}(\phi_1^e\phi_2 - \phi_1\phi_2^e) , \quad (52)$$

where  $\psi^+$  and  $\psi^-$  are the wavefunctions of the excited dimer states. The first order energy correction of the excited states are

$$\langle \psi^\pm | V | \psi^\pm \rangle = \frac{1}{2} \{ [\int \phi_1^e\phi_2 V \phi_1^e\phi_2 d\tau + \int \phi_1\phi_2^e V \phi_1\phi_2^e d\tau] \pm [\int \phi_1^e\phi_2 V \phi_1\phi_2^e d\tau + \int \phi_1\phi_2^e V \phi_1^e\phi_2 d\tau] \} . \quad (53)$$

The physical meaning of Eq.53 is explained as follows. The first two terms of the right hand side of Eq.53 represent the interaction energy between the excited molecule and its neighboring molecule. The third and fourth terms mean the excitation transfer between two molecules induced by the coupling term  $V$  and cause the dimer splitting or exciton splitting in the excited states. The energy difference between  $\psi^+$  and  $\psi^-$  is

$$\Delta E = 2[\int \phi_1^e\phi_2 V \phi_1\phi_2^e d\tau + \int \phi_1\phi_2^e V \phi_1^e\phi_2 d\tau] . \quad (54)$$

With reference to Eq.45-47, the physical meaning of Eq.47 can be explained as the excitation energy which is no longer localized at  $n$ th molecules (delocalized exciton). As discussed above, Eq.46 determines the exchange of excitation between the  $n$ th and  $m$ th



molecules. That is,  $M$  of Eq.46 reflects the excitation transfer time  $\tau_t$  [16].  $D$  of Eq.45 represents the interaction of the excited  $n$ th molecule with all the other normal molecules [16]. The Hamiltonian for delocalized exciton is conveniently written as [16,17]

$$H_{EX} = \sum_n [(E_u + \sum'_m D_{nm}) B_n^+ B_n + \sum'_m M_{nm} B_m^+ B_n] , \quad (55)$$

where the operators  $B_n^+$  and  $B_n$  are the creation and annihilation operators for the  $n$ th site and  $E_u$  is the excitation energy of an isolated molecule. Again  $D$  represents the interaction between the excited  $n$ th molecule and all other ground state molecules and  $M$  represents the excitation transfer from the  $n$ th molecule to the  $m$ th molecule.  $H_{EX}$  is a function of the lattice configuration by virtue of the fact that the matrix element  $D_{nm}$  and  $M_{nm}$  are.  $D_{nm}$  and  $M_{nm}$  may be decomposed into a power series of the displacement  $R$  relative to the equilibrium positions of the molecules.

$$D_{nm}(R) = D_{nm}(0) + D_{nm}(1) + \dots \quad (56)$$

$$M_{nm}(R) = M_{nm}(0) + M_{nm}(1) + \dots \quad (57)$$

where

$$D_{nm}(1) = \sum_{\alpha} [R_{n\alpha} \left( \frac{\partial D_{nm}}{\partial R_{n\alpha}} \right)_0 + R_{m\alpha} \left( \frac{\partial D_{nm}}{\partial R_{m\alpha}} \right)_0] \quad (58)$$

$$M_{nm}(1) = \sum_{\alpha} [R_{n\alpha} \left( \frac{\partial M_{nm}}{\partial R_{n\alpha}} \right)_0 + R_{m\alpha} \left( \frac{\partial M_{nm}}{\partial R_{m\alpha}} \right)_0] \quad (59)$$

and  $\alpha$  represents the six degrees of freedom of the molecules (three for translation and

three for rotation). Obtained from Eq.57 and Eq.58, the Hamiltonian of exciton-phonon coupling is written as

$$H_{\text{EX-PH}}^{(1)} = \sum_n \sum_m B_m^+ B_n \sum_\alpha [(R_{n\alpha} (\frac{\partial M_{nm}}{\partial R_{n\alpha}})_0 + R_{m\alpha} (\frac{\partial M_{nm}}{\partial R_{m\alpha}})_0)] \quad (60)$$

$$H_{\text{EX-PH}}^{(2)} = \sum_n \sum_m B_n^+ B_n \sum_\alpha [(R_{n\alpha} (\frac{\partial D_{nm}}{\partial R_{n\alpha}})_0 + R_{m\alpha} (\frac{\partial D_{nm}}{\partial R_{m\alpha}})_0)] \quad (61)$$

To have a clearer understanding, consider the case of two identical molecules, i.e., D (donor) and A (acceptor). As indicated in Eq.55, the Hamiltonian of the dimer for the delocalized exciton is written as

$$H_{\text{EX}} = 2E_u + D_{\text{DA}}(B_D^+ B_D) + D_{\text{AD}}(B_A^+ B_A) + M_{\text{DA}} B_A^+ B_D + M_{\text{AD}} B_D^+ B_A . \quad (62)$$

D and A are identical molecules, so

$$D_{\text{DA}} = D_{\text{AD}} = D \quad (63)$$

and  $M_{\text{DA}} = M_{\text{AD}} = M . \quad (64)$

Substitution of Eq.63 and Eq.64 into Eq.62, we have

$$H_{\text{EX}} = 2E_u + D(B_D^+ B_D + B_A^+ B_A) + M(B_A^+ B_D + B_D^+ B_A) . \quad (65)$$

To illustrate the physical meaning of M, consider the operation of the creation and annihilation operators.

$$MB_A^+B_D|D^eA\rangle = MB_A^+|DA\rangle = M|DA^e\rangle \quad (66)$$

and 
$$MB_D^+B_A|DA^e\rangle = MB_D^+|DA\rangle = M|D^eA\rangle. \quad (67)$$

As revealed by Eq.66 and Eq.67, M represents the resonance-energy transfer matrix elements between two molecules, i.e., from  $D^eA$  to  $DA^e$ .

The matrix element D determines the extent of the lattice distortion which may occur at and around a given excitation site (donor or acceptor). The excited and normal molecules act with different forces upon their neighbors. A change in the force of interaction between neighboring molecules upon the excitation of one molecule in the system sometimes may cause a displacement of molecules to new equilibrium positions. The displacement of the molecules may involve the distortion of the lattice. The displacement time ( $\tau_d$ ) of molecules from the old equilibrium positions depends on the change in the force of the interaction of a molecule with neighboring ones upon excitation of the molecule. With reference to Eq.58, the distortion arises from the first order term of D, that is, from

$$D(1) = \sum_{\alpha} [R_{D\alpha} \left( \frac{\partial D_{DA}}{\partial R_{DA}} \right)_0 + R_{A\alpha} \left( \frac{\partial D_{DA}}{\partial R_{A\alpha}} \right)_0]. \quad (68)$$

The subscript 0 designates evaluation at the ground-state configuration. For simplicity, consider the case of a dimer system with strong dispersion coupling (D) which must be dealt with first before energy transfer (M) is considered. Note that the displacement of the molecules can be expressed as the ground-state phonon coordinate [17,18]. Then

$$D(1) = \sum_q Q_q \left( \frac{\partial D_{DA}}{\partial Q_q} \right)_0, \quad (69)$$

where  $Q_q$  is the phonon coordinate associated with mode  $q$ . To reach the thermal equilibrium among exciton levels, downward energy cascading between exciton levels ( $\psi^+$  and  $\psi^-$ ) is accompanied by emission of phonons (Davydov mechanism). To have a clear physical understanding, assume  $Q_p$  to be the promoting mode. It is convenient to express the phonon coordinate in terms of creation and annihilation operators [17]. Then

$$Q_p = \left(\frac{\hbar}{2\omega_p}\right)^{1/2}(b + b^+) \quad (70)$$

The interaction matrix element of downward energy cascading accompanied by the absorption of one phonon of the lattice takes the following form in the first order of perturbation:

$$\begin{aligned} & \left\langle \psi^- m_{n_p+1} \left| Q_p \left( \frac{\partial D_{DA}}{\partial Q_p} \right)_0 \right| \psi^+ m_{n_p} \right\rangle \\ &= \left\langle m_{n_p+1} \left| \left( \frac{\hbar}{2\omega_p} \right)^{1/2} (b + b^+) \right| m_{n_p} \right\rangle \left\langle \psi^- \left| \left( \frac{\partial D_{DA}}{\partial Q_p} \right)_0 \right| \psi^+ \right\rangle \\ &= \left( \frac{\hbar}{2\omega_p} \right)^{1/2} (n_p + 1)^{1/2} \left\langle \psi^- \left| \left( \frac{\partial D_{DA}}{\partial Q_p} \right)_0 \right| \psi^+ \right\rangle \end{aligned} \quad (71)$$

where  $m_{n_p}$  and  $m_{n_p+1}$  represent the phonon states before and after absorbing one phonon, respectively. The first term represents the absorption of one phonon of the promoting mode, and the second term represents the downward energy cascading from  $\psi^+$  to  $\psi^-$  state. In the case of a promoting mode of frequency  $\omega_p$  contributing to the process of the energy cascading, the energy gap left for the delocalized phonons to fulfill is equal to

$$\Delta E' = \Delta E - \hbar\omega_p . \quad (72)$$

With reference to Eq.35 of section 3.1, the rate constant with the summation of all phonon modes is rewritten as

$$k = 2\pi \left( \frac{\partial D_{DA}}{\partial Q_p} \right)_0^2 \left( \frac{\hbar}{2\omega_p} \right) (n_p + 1) (1 - e^{-\hat{S}}) \left[ (2\pi \hat{S} (\sigma^2 + \omega_m^2))^{-1/2} e^{-\frac{(\Delta E - \hbar\omega_p - S\omega_m)^2}{2\hat{S}(\sigma^2 + \omega_m^2)}} \right], \quad (73)$$

where  $\left( \frac{\hbar}{2\omega_p} \right) (n_p + 1)$  is the transition probability of the promoting mode, as indicated in

Eq.71. Further applications of Davydov mechanism in photosynthesis will be discussed in Chapter four.

### 3.3 Theory Of Hole Profile

Consider the absorption of light from the initial electronic state  $i$  leading to the final electronic state  $j$ . The absorption cross-section is written [19] as

$$\sigma(\Omega) = \frac{4\pi^2\Omega}{\hbar c} \sum_n \sum_{n'} |\langle j, n' | \mu | i, n \rangle|^2 \delta(\Omega - (E_{j,n'} - E_{i,n}) / \hbar), \quad (74)$$

where  $\mu$  is the dipole moment.  $n'$  and  $n$  denote the vibrational levels of the final and initial states, respectively. With the allowance for the homogeneous broadening, replace the delta function with a Lorentzian function  $l_{n'n}$ . Eq.74 is rewritten as

$$\sigma(\Omega) = \sum_{\alpha} \frac{4\pi^2\Omega}{\hbar c} \sum_n \sum_{n'} |\langle j, n' | \mu | i, n \rangle|^2 l_{n'n}(\Omega - (E_{j,n'} - E_{i,n}) / \hbar), \quad (75)$$

where  $\alpha$  denotes the phonon modes. With the Condon approximation, the matrix element in Eq.75 becomes

$$|\langle j, n' | \mu | i, n \rangle|^2 = |\langle j | \mu | i \rangle|^2 |\langle n' | n \rangle|^2 \quad (76)$$

Recall that  $|\langle n' | n \rangle|^2$  is the Franck-Condon factor,  $C^2(n, n')$ , discussed in section 3.1. With the benefit of the Condon approximation, the theory of nondiabatic transfer can be utilized for the development of the theory of hole profiles. Substitution of Eq.76 into Eq.75 leads to

$$\sigma(\Omega) \propto \sum_{\alpha} \sum_n \sum_{n'} |\langle n' | n \rangle|^2 I_{n,n'}(\Omega - (E_{j,n'} - E_{i,n}) / \hbar) \quad (77)$$

To have a better physical feeling, consider a low temperature case ( $T \rightarrow 0K$ ), in which only the  $n=0$  term is left. Eq.77 is rewritten as

$$\sigma(\Omega) \propto \sum_{\alpha} \sum_{n'} C^2(n=0, n') I_{n',0}(\Omega - (E_{j,n'} - E_{i,0}) / \hbar) \quad (78)$$

With reference to section 1.1, the Franck-Condon factor of the transition from  $n=0$  to  $n'$  is given by a Poisson distribution.

$$C^2(n=0, n') = C^2(p) = \frac{S^p e^{-S}}{p!}, \quad (79)$$

where  $p=n'-n$  is equal to  $n'$  at the low temperature limit. Substitution of Eq.79 into Eq.78 leads to

$$\sigma(\Omega) \propto \sum_{\alpha} \sum_{p=0}^{\infty} \frac{e^{-S} S^p}{p!} I_{n',0}(\Omega - (E_{j,n'} - E_{i,0}) / \hbar) \quad (80)$$

The zero-phonon line (ZPL) frequency is a Lorentzian centered at  $\nu$ .  $\nu$  is defined as

$$\nu = (E_{j,0} - E_{i,0}) / \hbar. \quad (81)$$

Substitution of Eq.81 into Eq.80 leads to

$$\sigma(\Omega) \propto \sum_{\alpha} \sum_{p=0}^{\infty} \frac{e^{-S} S^p}{p!} l_{n'0}(\Omega - \nu - n' \omega_{\alpha}) \quad (82)$$

Because the frequencies of the phonons are close together, the sum ( $\sum_{\alpha}$ ) of the Lorentzian functions becomes a smooth function of frequency with a one-phonon spectrum centered at  $\nu + \omega_m$  and the  $n'$ -phonon centered at  $\nu + n' \omega_m$ . Eq.82 is rewritten as

$$\sigma(\Omega) \propto \sum_{p=0}^{\infty} \frac{e^{-S} S^p}{p!} l_p(\Omega - \nu - p\omega_m), \quad (83)$$

where  $\omega_m$  is the mean phonon frequency. The  $p$  values of 0, 1, 2,... correspond to zero-, one-, two-, ... phonon transitions. The  $p$ -phonon lineshape ( $l_p$ ) is the result of convoluting one-phonon profile ( $l_1$ )  $p$ -times with itself. Note that the inhomogeneous distribution of various sites is not considered in Eq.83. Define the single site absorption profile in the low temperature limit [13] as

$$L(\Omega - \nu) = \sum_{p=0}^{\infty} \frac{e^{-S} S^p}{p!} l_p(\Omega - \nu - p\omega_m). \quad (84)$$

The absorption spectrum is the integral (or summation) of the single-site absorption profiles with a Gaussian distribution of ZPL frequencies. Then

$$A_0(\Omega) = \int d\nu N_0(\nu - \nu_m) L(\Omega - \nu), \quad (85)$$

where  $N_0(\nu - \nu_m)$  is the distribution of ZPL frequencies centered at frequency  $\nu_m$  and  $A_0(\Omega)$  is the absorption spectrum before burning. Substitution of Eq.84 into Eq.85 leads

to

$$A_0(\Omega) = \sum_{p=0}^{\infty} \frac{e^{-S} S^p}{p!} \int d\nu N_0(\nu - \nu_m) l_p(\Omega - \nu - p\omega_m). \quad (86)$$

Let the laser intensity and the quantum yield of hole burning equal to  $I$  and  $\phi$ , respectively. Then following a burn for time  $\tau$  [22]

$$N_\tau(\nu - \nu_m) = N_0(\nu - \nu_m) \exp[-\sigma I \phi \tau L(\omega_B - \nu)], \quad (87)$$

where  $\omega_B$  and  $\sigma$  are the laser burn frequency and the optical cross section, respectively. The absorption spectrum following hole burning at a frequency  $\omega_B$  for a time  $\tau$  is written as

$$A_\tau(\Omega) = \int d\nu N_\tau(\nu - \nu_m) L(\Omega - \nu). \quad (88)$$

Substitution Eq.87 into Eq.88 leads to

$$A_\tau(\Omega) = \sum_{p=0}^{\infty} \frac{e^{-S} S^p}{p!} \int d\nu N_0(\nu - \nu_m) \exp[-\sigma I \phi \tau L(\omega_B - \nu)] \times l_p(\Omega - \nu - p\omega_m). \quad (89)$$

The hole spectrum  $H(\Omega)$  is obtained as the difference between the absorption spectra of after-burn (Eq.89) and pre-burn (Eq.86).

$$H(\Omega) = A_\tau(\Omega) - A_0(\Omega) \quad (90)$$

Eq.84 is the expression of the single site absorption profile valid in the low temperature



limit. To extend the theory of hole profile to arbitrary temperatures [20], begin with the general form of Franck-Condon factor [11,21] mentioned in previous section (section 3.1).

$$FC = \frac{1}{2\pi\hbar} \int_{-\infty}^{\infty} f(t) e^{-i\Delta E t/\hbar} dt \quad (91)$$

where  $f(t) = \exp\{-G + G_+(t) + G_-(t)\}$  (92)

$$G_+(t) = \sum_{\alpha} S_{\alpha} (\bar{n}_{\alpha} + 1) e^{i\omega_{\alpha} t} \quad (93)$$

$$G_-(t) = \sum_{\alpha} S_{\alpha} \bar{n}_{\alpha} e^{-i\omega_{\alpha} t} \quad (94)$$

$$G = G_+(0) + G_-(0) \quad (95)$$

$G_+$  and  $G_-$  represent absorption and emission of one phonon [11], respectively. The parameter  $t$  is simply a dummy variable. As indicated in Eq.93 and 94,  $S_+ = (\bar{n} + 1)S$  and  $S_- = \bar{n} S$  correspond to absorption and emission of one phonon, respectively. At low temperature limit ( $\bar{n} \rightarrow 0$ ), only  $S_+$  (or  $G_+$ ) nonvanishes. The term of  $\exp$  in Eq.92 can be viewed as multi-phonon processes as revealed in the expansion of a Taylor series.

$$\begin{aligned} \exp[G_+ + G_-] &= \sum_{p=0}^{\infty} \frac{[G_+ + G_-]^p}{p!} \\ &= \sum_{p=0}^{\infty} \sum_{p'=0}^p \frac{[G_+]^{p-p'} [G_-]^{p'}}{(p-p')! p'!} \end{aligned} \quad (96)$$

Substituting Eq.96 into Eq.92 and Eq.91 and performing the integration gives

$$\begin{aligned}
\text{FC} = e^{-\sum_{\alpha} S_{\alpha}(2\bar{n}_{\alpha}+1)} & \sum_{p=0}^{\infty} \sum_{p'=0}^p \sum_{\alpha} \frac{[S_{\alpha}(\bar{n}_{\alpha}+1)]^{p-p'} [S_{\alpha} \bar{n}_{\alpha}]^{p'}}{(p-p')! p'!} \\
& \times \delta\left[-\frac{\Delta E}{\hbar} + \sum_{\alpha} \omega_{\alpha} [p-2p']\right]
\end{aligned} \quad (97)$$

In the case of low temperature ( $G_{-} \rightarrow 0$ ), Eq.96 is rewritten as

$$\begin{aligned}
& \exp[G_{+} + G_{-}] \\
& = \exp[G_{+}] = \sum_{p=0}^{\infty} \frac{G_{+}^p}{p!}
\end{aligned} \quad (98)$$

Substituting  $\bar{n} \rightarrow 0$  and Eq.98 into Eq.92 and Eq.91, we have

$$\begin{aligned}
\text{FC} = e^{-\sum_{\alpha} S_{\alpha}} & \sum_{p=0}^{\infty} \sum_{\alpha} \frac{S_{\alpha}^p}{p!} \delta\left[-\frac{\Delta E}{\hbar} + p\omega_{\alpha}\right] \\
& = e^{-S} \sum_{p=0}^{\infty} \frac{S^p}{p!} \delta\left[-\frac{\Delta E}{\hbar} + p\omega_m\right].
\end{aligned} \quad (99)$$

Eq.99 shows that Eq.97 is reduced to the Poisson distribution at low temperature limit.

That is, Eq.97 is the general form of Franck-Condon factor for arbitrary temperatures. In analogy to Eq.84, the delta function is replaced by a line shape function. The single site absorption profile for arbitrary temperature is written as

$$\begin{aligned}
L(\Omega - \nu) = e^{-\sum_{\alpha} S_{\alpha}(2\bar{n}_{\alpha}+1)} & \sum_{p=0}^{\infty} \sum_{p'=0}^p \sum_{\alpha} \frac{[S_{\alpha}(\bar{n}_{\alpha}+1)]^{p-p'} [S_{\alpha} \bar{n}_{\alpha}]^{p'}}{(p-p')! p'!} \\
& \times l_{pp'}(\Omega - \nu - (p-2p')\omega_{\alpha})
\end{aligned} \quad (100)$$

Consequently, following the same procedure as the case of low temperature (Eq.85-90), the equation of hole profile for arbitrary temperature is obtained. Applications of the theory of hole profile to photosynthesis will be discussed in later chapters (see chapter 5 to chapter 7)

### References

1. Marcus,R.A. *J Chem. Phys.* 1956, 24, 966
2. Marcus,R.A. *J. Chem. Phys.* 1965, 43, 679
3. Marcus,R.A.; Sutin,N. *Biochim. Biophys. Acta* 1985, 811, 265
4. Hopfield,J.J. *Proc. Natl. Acad. Sci. USA* 1974, 71, 3640
5. Jortner,J. *J. Chem. Phys.* 1976, 64, 4860
6. Atkins,P.W. in *Molecular Quantum Mechanics*; Oxford: London, 1983, p.198
7. Manneback,C. *Physica Grav.* 1951, 17, 1001
8. Bevington,P.R.; Robinson,D.K. in *Data Reduction and Error Analysis for the Physical Sciences*; McGraw-Hill: New York, 1992, p.24
9. Kubo,R. *Phys. Rev.* 1952, 86, 929
10. Lax,M. *J. Chem. Phys.* 1952, 20, 1752
11. DeVault,D. *Quart. Rev. of Biophys.* 1980, 13., 387
12. Small,G.J.; Hayes,J.M.; Silbey,R.J. *J. Phys. Chem.* 1992, 96, 7499
13. Hayes,J.M.; Gillie,J.K.; Tang,D.; Small,G.J. *Biochim. Biophys. Acta* 1988, 932, 287
14. Kolaczowski,S.V.; Hayes,J.M.; Small, G.J. *J. Phys. Chem.* 1994, 98, 13418
15. Davydov,A.S. in *Quantum Mechanics*; NEO Press: Ann Arbor, 1966, p.538

16. Davydov,A.S. in *Theory of Molecular Excitons*; Plenum: New York, 1971
17. Johnson,C.K.; Small,G.J. in *Excited States*, Vol.6; Lim,E.C.,Ed.; Academic Press: New York, 1982, p.97
18. Clark,M.; Craig,D.P.; Dissado,L.A. *Mol. Cryst. Liq. Cryst.* 1978, 44, 309
19. Pryce,M.H.L. in *Phonons in Perfect Lattices and Lattices with Point Defects*; Stenenson,R.W.H., Ed.; Oliver and Boyd: London, 1965, p.403
20. Hayes,J.M.; Lyle,P.A.; Small,G.J. *J. Phys. Chem.* 1994, 98, 7337
21. Englman,R. in *Non-Radiative Decay of Ions and Molecules in Solids*; North-Holland: Amsterdam, 1979
22. Friedrich,J.; Haarer,H. in *Optical Spectroscopy of Glasses*; Zschokke,I., Ed.; D. Reidel: Dordrecht, 1986, p.149

## CHAPTER 4 EXCITON LEVEL STRUCTURE AND DYNAMICS IN THE CP47 ANTENNA COMPLEX OF PHOTOSYSTEM II

A paper published in *J. Phys. Chem.* 1994, 98, 7717

H.-C. Chang, R. Jankowiak, C. F. Yocum, R. Picorel,  
M. Alfonso, M. Seibert, and G. J. Small

### Abstract

Persistent nonphotochemical and population bottleneck hole burning results obtained as a function of burn wavelength are reported for the CP47 proximal antenna protein complex of photosystem II. Attention is focused on the lower energy chlorophyll *a*  $Q_y$ -states. Results are presented for the CP47 complex from two preparations. The Chl *a* content per CP47 complex was determined, spectroscopically, to be  $14 \pm 2$ . On the basis of the analysis of the hole spectra and the 4.2 K static fluorescence spectrum, the lowest energy state of CP47 lies at 690 nm (fluorescence origin at 691 nm). The width of the weak 690 nm absorption band from inhomogeneous broadening is  $100 \text{ cm}^{-1}$ . The linear electron-phonon coupling of the 690 nm state is weak with a Huang-Rhys factor ( $S$ ) of about 0.2 and a mean phonon frequency ( $\omega_m$ ) of  $20 \text{ cm}^{-1}$ , which explains why the Stokes shift ( $2S \omega_m$ ) is so small. The 690 nm state is found to be excitonically correlated with a, hitherto, unobserved state at 687 nm. However, the combined absorption intensity of the 690 and 687 nm states was determined to be equivalent to only 1 Chl *a* molecule. Results are presented which illustrate that these two states are fragile (i.e. their associated chlorophyll *a* molecules are readily disrupted). Thus, it is possible that the correct number

of Chl *a* molecules is 2, not 1. Indeed, the simplest interpretation consistent with the hole burning data has the 687 and 690 nm states being associated with a Chl *a* dimer with the latter close to forbidden in absorption. The results indicate that the 687 nm state relaxes to the 690 nm state in about 70 fs. The zero-phonon holewidths for the higher integrity CP47 samples are used to determine the energy transfer times for the higher energy absorbing states at 4.2 K. The absorption intensity of a previously identified state at 684 nm is found to vary from preparation to preparation. Diminution of the intensity of the 684 nm band is accompanied by increased absorption at ~670 nm. This speaks to the fragility of the 684 nm absorbing Chl *a*. Consideration of the nature of the 684 nm absorbing Chl *a* of CP47 is mainly reserved for the accompanying paper (Chang et al., *J. Phys. Chem.* 1994, 98, 7725) on the D1-D2-cyt b<sub>559</sub> reaction center and CP47-D1-D2-cyt b<sub>559</sub> complexes.

## I. Introduction

Photosystem II (PS II), which encompasses the oxygen-evolving apparatus of photosynthesis, possesses two antenna protein-chlorophyll *a* (Chl *a*) complexes, CP47 and CP43, which are proximal to the D1-D2-cyt b<sub>559</sub> reaction center (RC) [1]. Both appear to serve as conduits for excitation energy transfer from the distal and major Chl *a/b* light-harvesting complex (LHC-II) to the RC. Other smaller proteins (CP24, CP26, CP29) [1,2] may also be instrumental in shuttling excitation energy from LHC-II to the RC. Along with D1, D2, the extrinsic manganese-stabilizing protein and the  $\alpha$  and  $\beta$  subunits of cyt b<sub>559</sub>, CP47 and CP43 and several low molecular weight proteins appear to be required for oxygen evolution (water splitting) within the PS II membrane [3].

During the past few years, we have been applying spectral hole burning spectroscopy [4,5] to a number of isolated complexes of PS II. They include the D1-D2-cyt b<sub>559</sub> RC [5b,6-8], LHC-II [9], CP47 and CP47-D1-D2-cyt b<sub>559</sub>. In this paper we

focus on CP47. The following paper is primarily concerned with the first and last of these complexes but relies on our new results for CP47.

An x-ray or electron diffraction structure for CP47 has not been determined. The reported values for the number of Chl *a* molecules bound to CP47 range from 9 to about 30 [10-14]. Hydropathy plots indicate that CP47 is comprised of six hydrophobic transmembrane spanning alpha helixes connected by five hydrophilic loops [1]. Of the total of 14 histidines, 12 belong to the transmembrane helixes. Histidine as well as other amino acids can provide ligands for binding Chl molecules. From the predicted membrane folding pattern of spinach CP47, it appears that the Chl *a* molecules bound to His residues are about equally divided into two layers near the stromal and luminal boundaries of the membrane [1].

There were three principal motivating factors for our studies of isolated CP47 complexes. The first was to use the line narrowing and other attributes of hole burning [4,5] to obtain more detailed information on the  $Q_y$ -exciton level structure and to study the energy cascading dynamics at liquid He temperature. (The lowest excited  $1\pi\pi^*$  state of chlorophylls is commonly referred to as the  $Q_y$ -state.) Such dynamics in CP47 appears to have received scant attention. Nor is there any information on the extent to which the  $Q_y$ -states are excitonically correlated, i.e., share common Chl *a* molecules. The second factor stems from our earlier suggestion that [5b] contamination of the D1-D2-cyt b559 RC complex by CP47 may be important to the solution of the problem of how many Chl *a* molecules the RC contains. Reported values range between 4 and 6, cf. Introduction to the accompanying paper [15]. The third factor was to characterize and determine the linear electron-phonon coupling and inhomogeneous broadening for as many of the  $Q_y$ -transitions as possible. Such information, along with  $Q_y$ -state wavefunctions and energies,

is important for understanding the temperature-dependence and dispersive kinetics of energy transfer [16-19].

Earlier absorption and fluorescence studies of the isolated CP47 complex at low temperatures will be discussed in sections III and IV. At this point we note only that the published low temperature absorption spectra shown some significant differences [20-23]. This motivated us to study CP47 samples from several preparations. The results for two are reported.

## II. Experimental

CP47 protein complex was isolated from sugar beet oxygen-evolving PS II core complex by a modification of the method described in Ghanotakis et al. [24]. Tris-washed core complex was suspended in 50 mM MES (pH 6.0), 150 mM NaCl, and 400 mM sucrose at 1.5 mg Chl/ml. The suspension was then mixed with an equal volume of 20 mM Tris-HCl (pH 6.0), 4 M LiClO<sub>4</sub>, and 15% lauryl maltoside for 10 min at 4° C in the dark. The suspension was then dialyzed against 20 mM Bis-Tris (pH 6.0) for 2 h, and the dialyzed material was loaded onto a 1.6 × 6 cm Fractogel TSK-DEAE 650S (Supelco, Bellefonte, PA) column equilibrated with 20 mM Bis-Tris (pH 6.0) and 0.05% lauryl maltoside. The column was then washed with two column volumes of the above buffer (flow rate, 3 ml/min), and the bound green material was eluted with a 0-175 mM LiClO<sub>4</sub> linear gradient (flow rate, 0.5 ml/min) in the same buffer. The green fractions with very low carotenoid absorption (i.e., fractions with similar absorbance at 490 and 630 nm) were pooled, dialyzed, concentrated using a 30 kDa cut-off membrane in a Diaflo ultrafiltration system (Amicon, Beverly, MA), and stored at -80° C until use. In one case (preparation II) the complex was further treated by loading it onto a 0.1-1.0 M sucrose density gradient in 20 mM Bis-Tris (pH 6.0) and 0.05% DM and centrifuging it at 185,000



× g in an SW 41 Ti swinging bucket rotor (Beckman, Palo Alto) for 23 h at 4° C. The single green band was recovered from the gradient and stored at −80° C until use. The samples from these two procedures will be referred to as CP47(I) and CP47(II), respectively.

The apparatus used for the absorption and hole burning measurements was the same as described elsewhere [7,8,25,26]. Briefly, hole burning employed a Coherent CR699-21 ring dye laser (linewidth of 0.05 cm<sup>-1</sup>) pumped by a 6 W Coherent Innova argon-ion laser. Hole and absorption spectra were read with a Bruker HR120 Fourier transform spectrometer. All reported results were obtained for a sample temperature of 4.2 K (convection cooling liquid helium cryostat). Hole burning conditions and read resolution are given in the figure captions.

### III. Results

In the first half of this section we present results for CP47(I) samples which differ from preparation II (CP47 II) only in that an additional processing step was implemented for the latter, cf. section II. The 4.2 K absorption of CP47(I) is shown as the solid curve in frame A of Fig. 1. The fourth derivative of this spectrum, dashed curve, clearly identifies bands near 683, 677, 669, 666 and 660 nm. On the basis of a Gaussian deconvolution, with variable FWHM (full-width at half-maximum), van Dorssen et al. concluded that bands at ~693, 682, 675, 668 and 661 nm contribute to their 4.2 K absorption spectrum of CP47 [20]. Using a similar procedure Kwa et al. [23] assigned bands at 690, 682, 676, 670 and 663 nm for CP47 at 77 K. In these works and ours, *vide infra*, the feature nearest 690 nm is by far the weakest. It is to be appreciated, however, that such a deconvolution procedure is suspect when used to identify weak features which are not even partially resolved. In addition, the derivative spectrum suggests that two

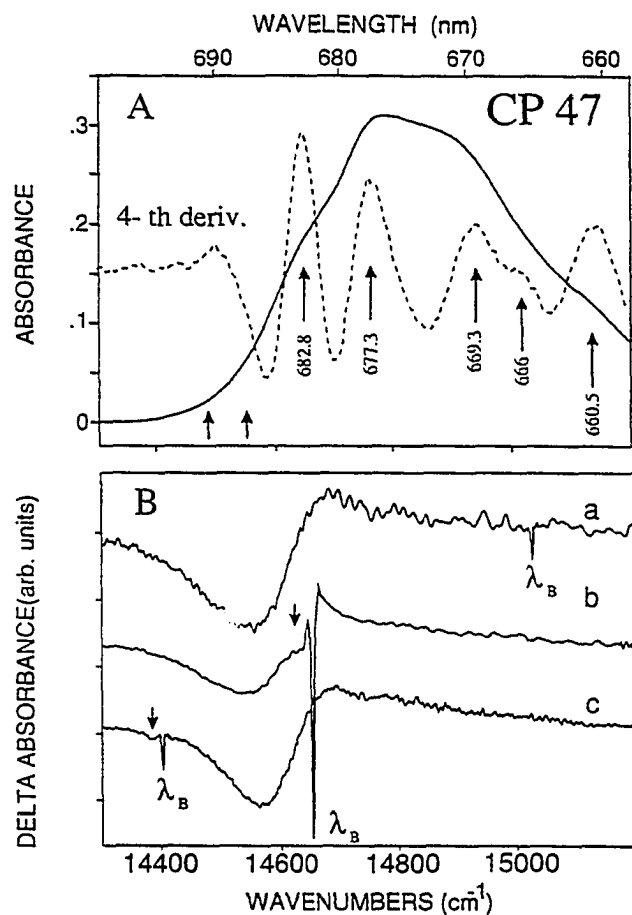


Figure 1. Absorption and persistent nonphotochemical hole burned (NPHB) spectra of CP47 from preparation I, CP47(I).  $T = 4.2$  K. Frame A: absorption (solid curve) plus fourth derivative (dashed curve). Frame B: NPHB spectra (read resolution of  $4 \text{ cm}^{-1}$ ) obtained with (a)  $\lambda_B = 665 \text{ nm}$  ( $I_B \sim 400 \text{ mW/cm}^2$ ,  $\tau_B = 4 \text{ min}$ ), (b)  $\lambda_B = 682.6 \text{ nm}$  ( $I_B \sim 400 \text{ mW/cm}^2$ ,  $\tau_B = 20 \text{ min}$ ) and (c)  $\lambda_B = 695.0 \text{ nm}$  ( $I_B \sim 250 \text{ mW/cm}^2$ ,  $\tau_B = 20 \text{ min}$ ). Percent absorbance changes at  $687 \text{ nm}$  in spectra a, b and c are 9, 15 and 7, respectively. Spectrum d represents the difference between spectra a and c.

relatively weak bands at 687 and 690 nm (short solid arrows) may exist. Our hole burned spectra, *vide infra*, prove that there are two  $Q_y$ -states of CP47 at 687 and 690 nm. The CP47 absorption spectrum of Fig. 1 is most similar to that of refs. [21,22]; the absorption shoulder at ~683 nm is about as pronounced while the absorption near 670 nm is less intense than the absorption at ~677 nm. The absorption spectrum reported in ref. 20 is quite similar to that shown later for preparation II (CP47(II)); in particular, the intensity of the ~683 nm is significantly diminished while the absorption near 670 nm is enhanced relative to the absorption near 677 nm. Thus, the low temperature absorption spectra of CP47 reported by different groups exhibit significant differences, differences that would be undetectable at room temperature.

Nonphotochemical hole burning (NPHB) can often provide a higher resolution analysis of the structure underlying inhomogeneously broadened and poorly resolved absorption spectra of antenna complexes [4,5]. NPHB spectra of CP47(I) were obtained for several burn wavelength ( $\lambda_B$ )-values between 695 and 665 nm. Three are shown in frame B of Fig. 1 for  $\lambda_B = 665.0, 682.8$  and  $695.0$  nm. For these, and all other spectra obtained, the broad hole at 687 nm is dominant in integrated intensity. The width of this hole is  $\sim 170 \text{ cm}^{-1}$  [27]. A key finding is that it is produced even when  $\lambda_B$  is much higher than 687 nm; see spectrum c where the ZPH (zero-phonon hole) at  $\lambda_B = 695$  nm is  $170 \text{ cm}^{-1}$  lower in energy than 687 nm. As argued in section IV, this spectrum is the result of hole burning in the lowest energy state at 690 nm which is excitonically correlated with the 687 nm state. Note that spectrum a of Fig. 1 (excited non-selectively at 665 nm) is much broader in the low energy range than spectrum c obtained with  $\lambda_B = 695$  nm. The difference between spectra a and c clearly accounts for the hole associated with the 690 nm state (see spectrum d). In each of the three hole spectra one can observe the blue-shifted,

broad and tailing anti-hole of the 687 nm hole which is the signature for NPHB of  $\pi\pi^*$  excited states [28]. The rising part of the anti-hole interferes with the high energy side of the hole to produce some asymmetry in the 687 nm hole profile, see spectra a and c. In spectrum b there is also an interference from the pseudo-phonon sideband hole [5a,5c] (located by the arrow) associated with the ZPH. This feature can also be seen in spectrum c, just to the left of the ZPH at  $\lambda_B$ . In spectrum b the real-phonon sideband hole [5a,5c] interferes with the anti-hole to yield the observed cusp-like feature just to the right of the ZPH. Such interference effects have been quite extensively studied in simpler systems [29]. Spectrum c and others obtained with  $\lambda_B > 687$  nm reveal that hole burning in the lowest energy state near 690 nm, vide infra, produces no pronounced satellite structure from the states responsible for absorption at wavelengths lower than 687 nm. Implications of this are considered in section IV. Important for what follows is a determination of the linear electron-phonon coupling of the 690 nm state. From spectrum c and others it was determined that the mean phonon frequency  $\omega_m = 20 \text{ cm}^{-1}$  with a one-phonon profile width of  $\sim 30 \text{ cm}^{-1}$ . Using standard theoretical analysis [30,31] based on the intensity of the ZPH relative to the phonon sideband holes, it was determined that the Huang-Rhys factor  $S \sim 0.2$ . Thus, as in all other antenna protein complexes studied [5a,5b,9,32-37], the coupling is weak ( $S < 1$ ), in sharp contrast to the primary donor state of the reaction centers of purple bacteria [38], PS I [39] and PS II [6].

Next, we consider the results of ZPH-action spectroscopy which has been successfully used to investigate the exciton level structure of B850 and B875 of *Rhodobacter sphaeroides* [36], B850 of *Rhodospseudomonas acidophila* [35] and the LHC-II peripheral antenna complex of PS II [9]. In this spectroscopy one determines the dependence of the ZPH-intensity on  $\lambda_B$  under constant burn fluence conditions. The

results for  $\lambda_B > 679$  nm are shown in frame A of Fig. 2. From the raw data one observes that the action spectrum has a maximum near 684 nm. The tailing of this spectrum at low burn frequencies indicates the existence of another contribution. The dashed curves are the result of a deconvolution of the data (for  $\lambda_B > 682$  nm) with two Gaussians, cf. figure caption. The maxima of the Gaussians are at 690 and 684 nm. Given that the results presented in Fig. 1 (frame B) establish that the 690 nm band is considerably weaker than the 687 nm band, the results of frame A in Fig. 2 indicate that the 687 nm state is, at best, a weak contributor to the observed ZPH. As mentioned, previous work had identified CP47 absorption bands near 690 and 684 nm. Discussion of additional prior work pertinent to these two states is presented in section IV. At this point, however, it is necessary to note that, on the basis of 77 K triplet-singlet absorption spectra (often referred to as population bottleneck hole burned spectra), van Kan et al. [21] observed a state at  $\sim 683$  nm which they associated with the shoulder in absorption at  $\sim 683$  nm, cf. Fig. 1. The transient triplet state bottleneck hole burned spectrum ( $\lambda_B = 665$  nm) shown in frame B of Fig. 2 is consistent with their result. Observed is a hole at 684 nm with an inhomogeneous width of  $120 \text{ cm}^{-1}$  (the observation of ZPHs, see frame A of Fig. 2, proves that the 684 nm band is inhomogeneously broadened). The work of van Kan et al. also reports an equally intense feature in the population bottleneck hole burned spectra at 670 nm. They concluded that it is most likely due to non-native Chl molecules produced by the isolation and/or sample handling procedures. We concur with this conclusion. In frame B of Fig. 2 a weak hole is observed near 670 nm (this hole is more pronounced for CP47(II), see frame B of Fig. 6). Its weakness establishes that the CP47(I) samples contain significantly less disrupted Chl than the samples used in ref. 21. (The samples of van Kan et al. also show enhanced absorption at 670 nm, the region where Chl monomers are expected to absorb, and

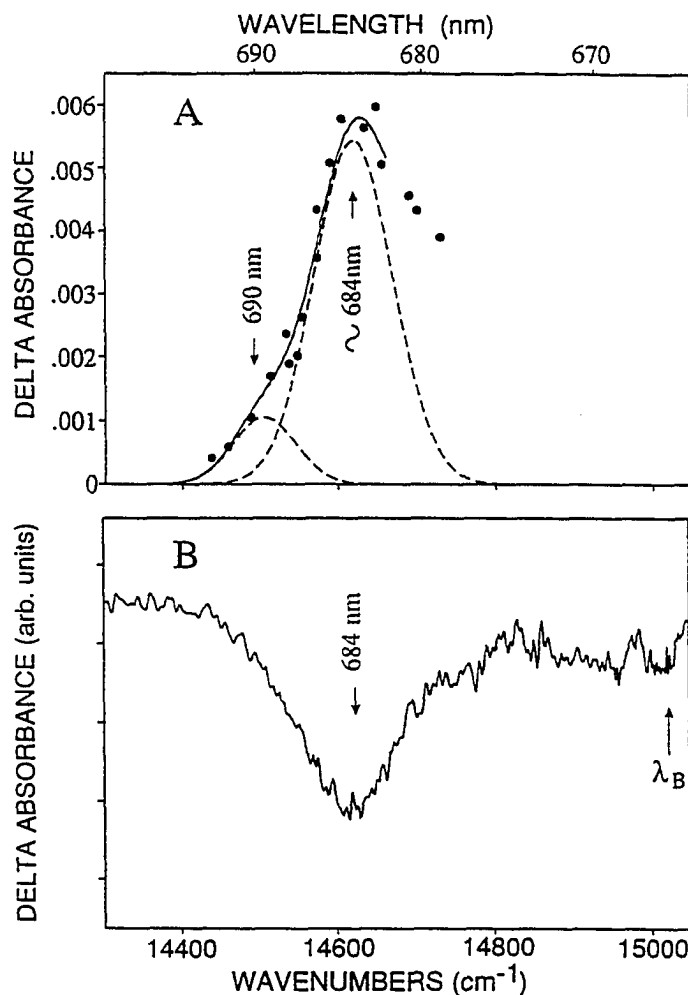


Figure 2. Zero-phonon hole (ZPH) action (frame A) and triplet bottleneck transient hole (frame B) hole spectra of CP47(I), 4.2 K. In frame A the data points are the ZPH intensities (for different  $\lambda_B$ -values) obtained under constant burn fluence conditions. The dashed curves are from a Gaussian deconvolution of the low energy part of the action spectrum. The widths of the 690 and 684 nm Gaussians are 95 and 120  $\text{cm}^{-1}$ . In frame B the hole spectrum is of the triplet population bottleneck type obtained with  $\lambda_B = 665$  nm,  $I_B \sim 500$   $\text{mW}/\text{cm}^2$ . The percent absorbance change at 684 nm is 4.

weaker absorption near 684 nm.)

The triplet bottleneck hole burned spectra presented in Fig. 3 for  $\lambda_B = 665, 684$  and 690 nm offer additional proof that the 684 nm band is inhomogeneously broadened. We note that the CP47 complexes in the glass are monodisperse, i.e., inter-complex energy transfer is negligible. This follows since the existence of a significant amount of CP47 aggregates would lead to fluorescence from the 690 nm state that is red-shifted from the absorption origin by more than  $2S\omega_m$ . This is not the case, *vide infra*. The first of the above  $\lambda_B$ -values provides excitation mainly of states higher in energy than the 684 nm state. Energy transfer from these states to the 684 nm state is expected to reveal the total inhomogeneous distribution of the 684 nm state given the spectral congestion at 665 nm and that the site excitation energy distributions of different states are largely uncorrelated [7]. Thus, the hole profile of curve c should be an accurate reflection of the 684 nm absorption band. For  $\lambda_B$ -values in the vicinity of 684 nm both a subset of the distribution of 684 nm states and a distribution from the intense absorption due to 677 nm states are excited. For the former, only 684 nm states of the inhomogeneous distribution whose zero-phonon lines (ZPLs) in absorption lie lower in energy than  $\lambda_B$  can be excited and, therefore, intersystem cross to the triplet population bottleneck state. Similarly, only 677 nm state(s) of the inhomogeneous distribution whose ZPLs lie lower in energy than  $\lambda_B$  can be excited. If energy transfer from the 677 nm to 684 nm state occurs, then energy conservation dictates that only 684 nm states with energy lower than  $\lambda_B$  can be excited and, therefore, be involved in intersystem crossing. Thus it is that in curve b for  $\lambda_B = 684$  nm the hole exhibits abrupt termination at 684 nm. In curve a ( $\lambda_B = 690$  nm) only a very small low energy portion of the inhomogeneously broadened 684 nm band is active in population bottleneck hole burning. In consideration of the above it should be kept in mind

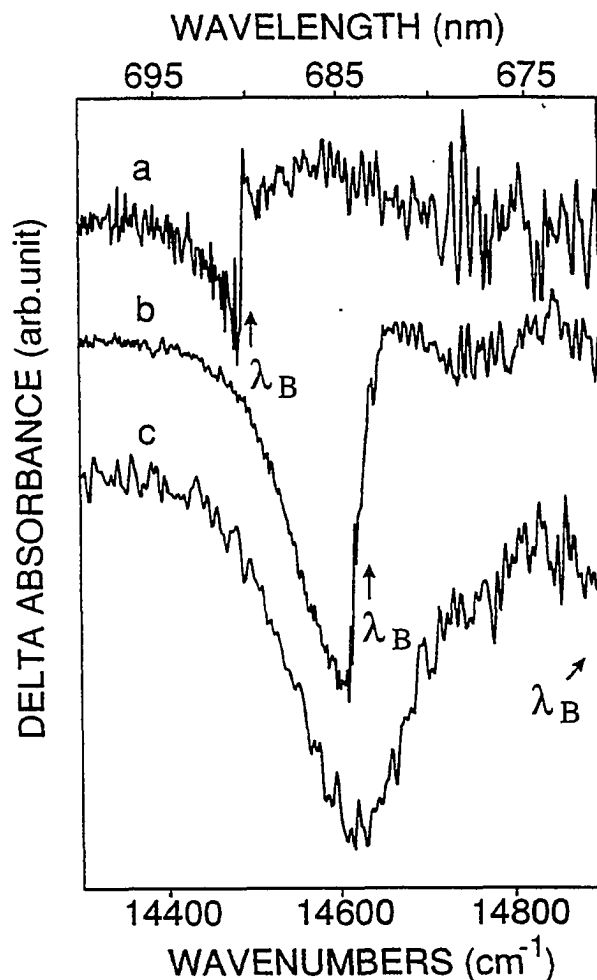


Figure 3. Transient triplet population bottleneck hole spectra of CP47(I) obtained for different burn wavelengths, 4.2 K. conditions: (a)  $I_B \sim 240 \text{ mW/cm}^2$ ,  $\lambda_B = 690 \text{ nm}$ ; (b)  $I_B \sim 360 \text{ mW/cm}^2$ ,  $\lambda_B = 684 \text{ nm}$ ; (c)  $I_B \sim 400 \text{ mW/cm}^2$ ,  $\lambda_B = 665 \text{ nm}$ . Percent absorbance changes are 3, 5 and 4 in spectra a, b and c at 691, 685 and 684 nm, respectively. Read resolution is  $4 \text{ cm}^{-1}$ .



that members of a distribution whose ZPLs lie lower in energy than  $\lambda_B$  are excited via the broad phonon sideband which builds on the ZPLs. This is the reason why pseudo-phonon sideband holes are observed, see Fig. 1 and refs. 5c, 30, 31 and 40 for detailed discussion. One last but important point is that triplet bottleneck hole burning of the 687 nm state is not observed, consistent with the 687 nm state having a very short lifetime, cf. section IV.

The results of high resolution measurements of the dependence of the ZPH width on  $\lambda_B$  are shown in Fig. 4 for CP47(I) (open circles). The widths (FWHM) given in Table I are for eight  $\lambda_B$ -values ranging between 670 and 692 nm. The total dephasing times ( $T_2$ ), which were calculated from  $\text{FWHM} (\text{cm}^{-1}) = 2(\pi c T_2)^{-1}$  [4], are also listed. The implied assumption that spectral diffusion makes a negligible contribution at 4.2 K to the holewidths is considered in section IV, as are the implications of the data for energy transfer dynamics and the rates of ZPH growth.

We present next results for CP47 from preparation II. The results, shown in Figs. 5 and 6, correspond to those in Figs. 1 and 2. The  $\lambda_B$ -dependence of the ZPH widths for CP47(II) are shown as the solid circles in Fig. 4. From a comparison of frames A of Figs. 1 and 5 it is immediately apparent that the amplitudes for absorption near 684 and 670 nm for CP47(II) are significantly diminished and enhanced, respectively, relative to those of CP47(I). Nevertheless, the NPHB spectra in frame B of Fig. 5 establish the existence of the 687 nm hole (state) identified for CP47(I). The 684 nm transient population bottleneck hole of Fig. 2 (frame B) is also observed, although with greater difficulty, see frame B of Fig. 6. Interesting is the comparison of the ZPH action spectrum of CP47(I), frame A of Fig. 2, with the corresponding spectrum of CP47(II), frame A of Fig. 6. This comparison, together with the absorption spectra of Figs. 1 and 5, strongly indicate that the significant reduction in the action spectrum of Fig. 6 near 684 nm

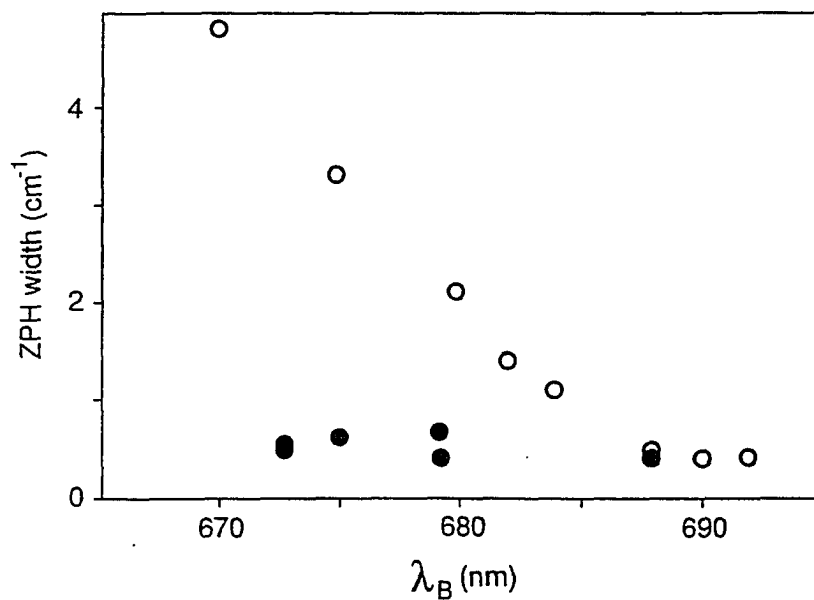


Figure 4. Homogeneous widths of the ZPHs of CP47(I), open circles, and CP47(II), solid circles at 4.2 K. Widths were obtained by fitting the ZPH profiles to a Lorentzian line shape. ZPH with a width of  $\lesssim 1 \text{ cm}^{-1}$  were read with a resolution of  $0.2 \text{ cm}^{-1}$ . For the broader holes a resolution of  $1.5 \text{ cm}^{-1}$  was used.

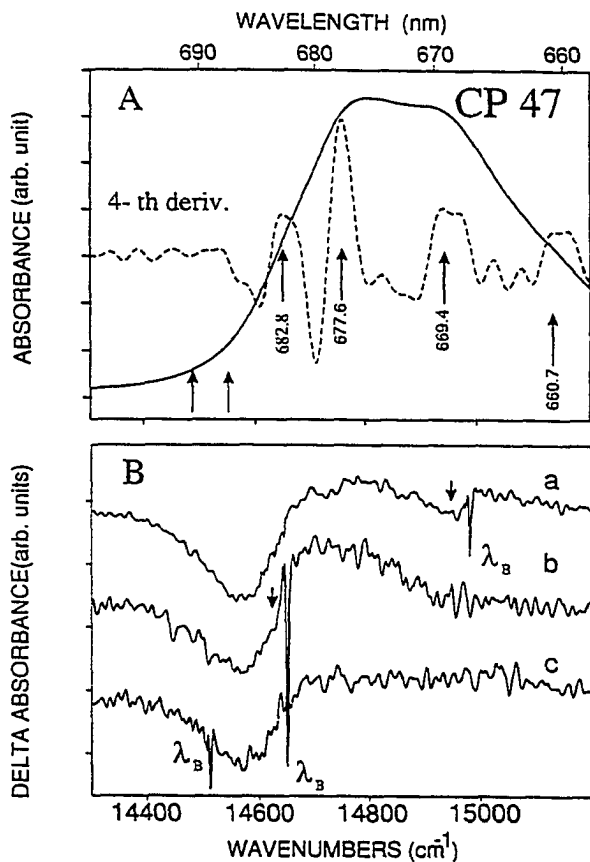


Figure 5. Absorption and persistent nonphotochemical hole burned spectra of CP47 from preparation II, CP47(II).  $T = 4.2$  K. Frame A: absorption (solid curve) plus fourth derivative (dashed curve). Frame B: NPHB spectra (read resolution of  $4 \text{ cm}^{-1}$ ) obtained with (a)  $\lambda_B = 667 \text{ nm}$  ( $I_B \sim 200 \text{ mW/cm}^2$ ,  $\tau_B = 2 \text{ min}$ ); (b)  $\lambda_B = 682.5 \text{ nm}$  ( $I_B \sim 280 \text{ mW/cm}^2$ ,  $\tau_B = 2 \text{ min}$ ); and (c)  $\lambda_B = 689.2 \text{ nm}$  ( $I_B \sim 80 \text{ mW/cm}^2$ ,  $\tau_B = 13 \text{ min}$ ). Percent absorbance changes at  $687 \text{ nm}$  in spectra a, b and c are 5, 4 and 3. In each spectrum the ZPH is coincident with  $\lambda_B$ .

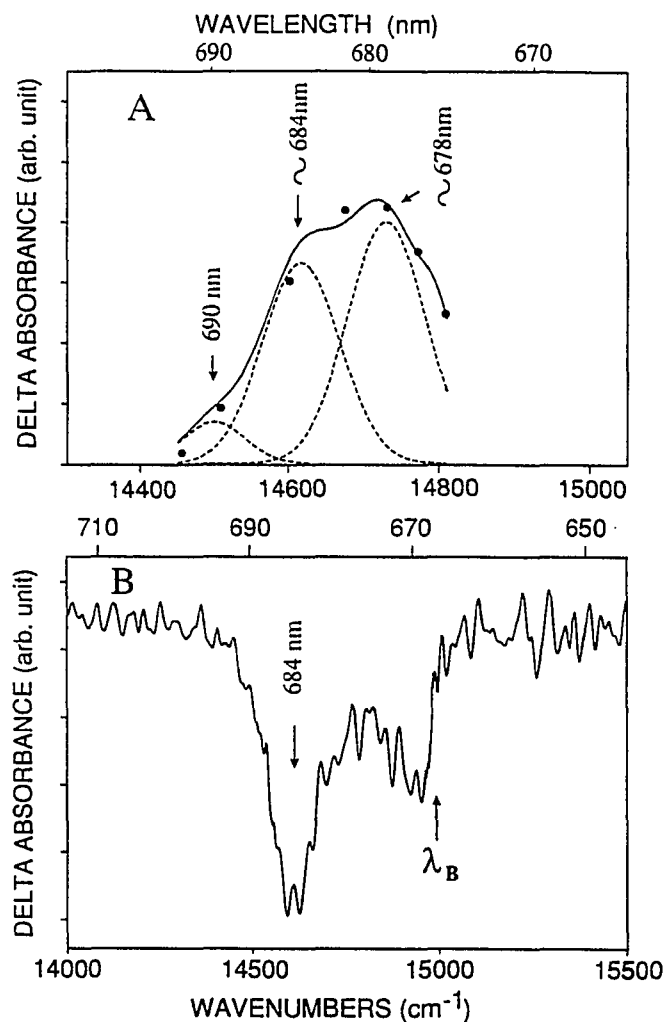


Figure 6. Zero-phonon hole (ZPH) action (frame A) and triplet bottleneck transient (frame B) hole spectra of CP47, 4.2 K. See Fig. 2 caption. The Gaussian profiles in frame A at  $\sim 690$ , 684 and 678 nm have widths of 95, 120 and 120  $\text{cm}^{-1}$ , respectively. Frame B:  $\lambda_B = 667$  nm ( $I_B \sim 800$   $\text{mW}/\text{cm}^2$ , read resolution = 4  $\text{cm}^{-1}$ ). Percent absorbance change at 684 nm is 1.4.

correlates with the diminution of the 684 nm band in the absorption spectrum of CP47(II). Also interesting is the  $\lambda_B$ -dependence of the ZPH width for CP47(II), Fig. 4 (solid circles), which is to be compared with the dependence for CP47(I) shown in the same figure. The rate of increase of the ZPH width with decreasing  $\lambda_B$  for CP47(II) is much slower than for CP47(I). For CP47(II) there is a much smaller contribution from the 684 nm band (state), as expected. Equally important is the observation that the hole widths for  $\lambda_B < \sim 680$  nm are significantly narrower for CP47(II) than CP47(I). For example, for  $\lambda_B \sim 670$  nm the holewidths for the former and latter are 0.6 and 4.8  $\text{cm}^{-1}$ , respectively. Moreover, the ZPH burning rate (for  $\lambda_B < \sim 678$  nm) of CP47(II) was observed to be greater than for CP47(I). This is illustrated by the two hole spectra in Fig. 7. Thus, it is apparent that the ZPH holewidths of CP47(II) for  $\lambda_B < \sim 680$  nm do not accurately reflect the dynamics of fully functional Chl molecules (states).

To conclude this section we present results which pertain to the Chl *a* content of CP47, the number of Chl *a* molecules per complex associated with the 690 and 687 nm states and contamination of the CP47(I) samples by the D1-D2-Cyt b559 RC complex of PS II. We consider these problems in reverse order.

The absorption spectrum of CP47 from Fig. 1 was compared with the absorption spectrum of a D1-D2-cyt-b559 RC complex containing 4 Chl *a* and 2 pheophytin *a* molecules [15]. Following the spectroscopic procedure described below for determination of the Chl *a* content of the CP47 complex, it was found that the contamination of CP47(I) by the RC complex is less than 10% on a complex basis. However, the absorption spectrum of CP47(I) corrected for 10% contamination by the 4 Chl *a*-RC was found to be essentially identical to the absorption spectrum shown in frame A of Fig. 1, and SDS-PAGE did not identify RC proteins in the CP47 sample (data not shown). Thus, we

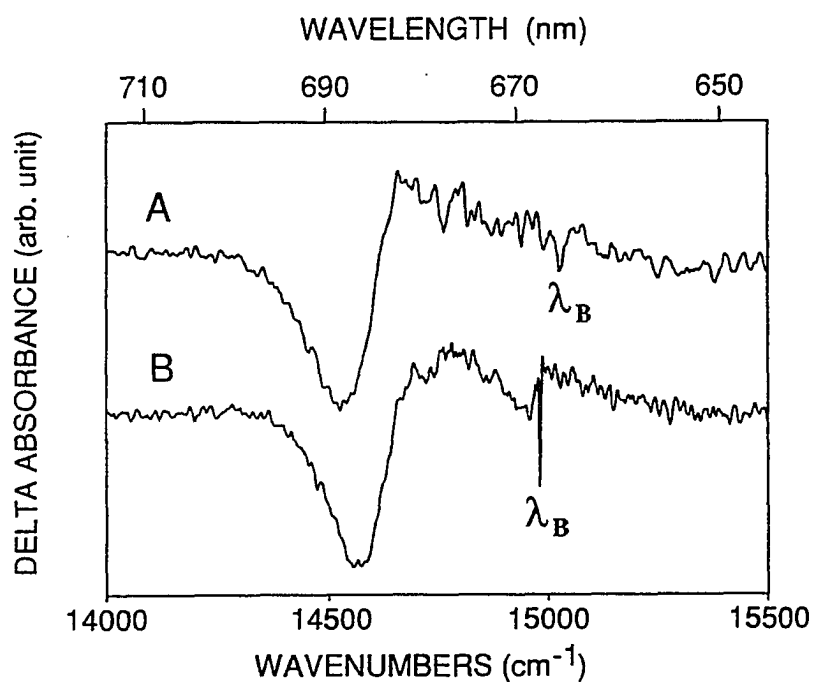


Figure 7. Persistent nonphotochemical hole burned spectra of CP47(I) (curve A) and CP47(II) (curve B), 4.2 K. Conditions: (A)  $\lambda_B = 665$  nm,  $I_B \sim 700$  mW/cm<sup>2</sup>,  $\tau_B = 2$  min; (B)  $\lambda_B = 667$  nm,  $I_B \sim 200$  mW/cm<sup>2</sup>,  $\tau_B = 3$  min. Absorbance change of ZPH in spectra A and B is 0.0008 and 0.002, respectively. Read resolution = 4 cm<sup>-1</sup>.

believe that there is very little RC contamination of our CP47 complex.

The hole burning results presented above confirm the existence of the 690 nm state and identify, for the first time, an excitonically correlated state at 687 nm. The 690 nm absorption band is inhomogeneously broadened with  $\Gamma_{inh} \sim 100 \text{ cm}^{-1}$ . Since ZPHs associated with the 687 nm state were not observed, a direct determination of  $\Gamma_{inh}$  for the 687 nm absorption band is not possible. However, the hole burning data for the B800-B850 and B875 antenna protein complexes of *Rb. sphaeroides* [35] indicate that  $\Gamma_{inh}$  for the 687 nm state should be similar to the value of  $\Gamma_{inh} \sim 100 \text{ cm}^{-1}$  for the 690 nm state since the two are excitonically correlated. In view of the results for the *Rb. sphaeroides* complexes and the FMO complex of *P. aestuarii* [33,41], the FWHM of the 687 nm band can be expected to be greater than  $100 \text{ cm}^{-1}$  due to ultra-fast relaxation from the 687 to 690 nm state. A relaxation time of 100 fs corresponds to a homogeneous broadening ( $\Gamma_{hom}$ ) of  $50 \text{ cm}^{-1}$ . It was also determined that the 684 nm band is inhomogeneously broadened with a  $\Gamma_{inh}$ -value of  $110 \text{ cm}^{-1}$ . Given the above results it was deemed justifiable to use them for a deconvolution of the low energy region of the CP47 absorption spectrum ( $\lambda > \sim 683 \text{ nm}$ ). For  $\lambda \geq 683 \text{ nm}$  the contribution from the intense band at 677 nm should be minimal. The only adjustable parameters used were the peak intensities of the 690, 687 and 684 nm bands and the aforementioned homogeneous broadening contribution to the FWHM of the 687 nm band. The results of this procedure, which yields a good fit to the low energy region, are shown in Fig. 8. Note the weakness of the 690 nm band relative to the 687 nm band which explains why the 690 nm state does not at all stand out in the non-line narrowed NPHB spectra (see, for example, spectrum a of frame B, Fig. 1). The FWHM of the 687 nm band is  $180 \text{ cm}^{-1}$  which, with  $\text{FWHM} \sim \Gamma_{inh} + \Gamma_{hom}$  and  $\Gamma_{inh} \sim 100 \text{ cm}^{-1}$ , leads to  $\Gamma_{hom} \sim 80 \text{ cm}^{-1}$ , corresponding to a  $T_1$  relaxation time for

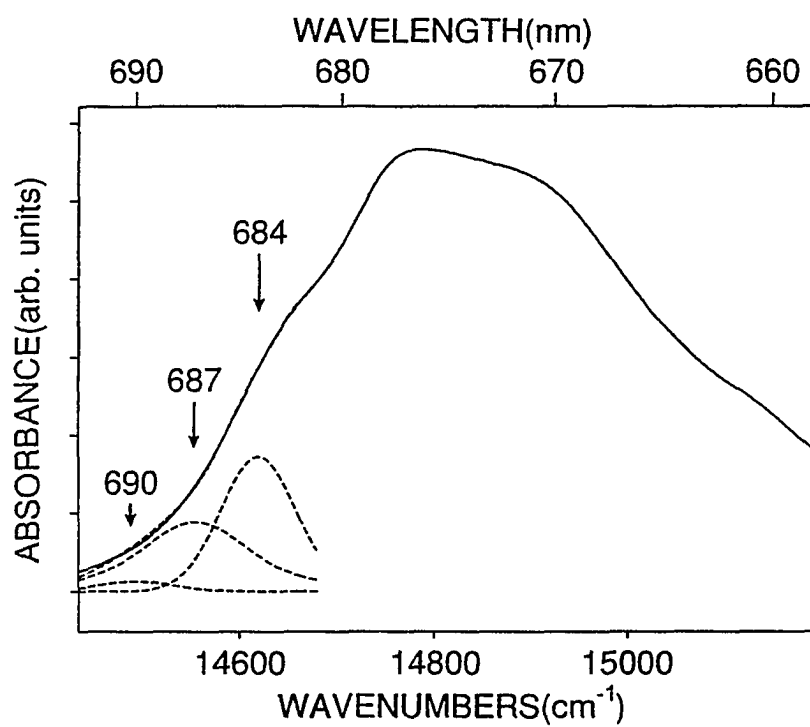


Figure 8. A deconvolution of the low energy region of the CP47(I) absorption spectrum based on hole burning results. See text for discussion.



the 687 nm state of 70 fs. The deconvolution also allows for a determination of the %-contribution from the 690 and 687 nm states to the total  $Q_y$ -absorption of CP47. The value determined is 7% (the CP47 absorption spectrum was terminated at  $\lambda = 657$  nm in order to exclude vibronic transitions which build on the intense 677 and 669 nm origin bands).

In order to convert this %-contribution into the number of Chl *a* molecules associated with the excitonically related 690 and 687 nm states it is necessary to know the number of Chl *a* molecules/CP47 complex. Literature estimates of this number range from 9 to 30 [10-14,23]. In view of the disparity in these numbers we determined a value on the basis of the low temperature absorption spectra of the D1-D2-cyt b559 RC and CP47-D1-D2-cyt b559 complexes. Experimental details concerning the isolation of these complexes are given in the following paper. These two spectra are presented in Fig. 9 with the lower being that for the D1-D2-cyt b559 RC. The relative intensities of the two spectra were determined by normalization of the  $Q_x$ -band of pheophytin *a* in both samples to the same intensity, see insert. We note again that CP47 is devoid of pheophytin *a*. The  $Q_y$ -spectrum of the RC is for a sample for which pigment analysis [15] yielded 4 Chl *a* molecules / RC. The  $Q_x$ -band of Pheo *a* for the 4 Chl *a*-RC is identical to those for preparations containing 5 and 6 Chl *a* molecules [15]. These Chls and the two pheophytin *a* molecules of the RC can, to a first approximation, be assumed to have the same  $Q_y$ -transition dipole strengths [23]. Subtraction of the lower from the upper spectrum yielded a CP47 spectrum in good agreement with that shown in Fig. 1. The integrated intensity of the difference spectrum relative to that of the D1-D2-cyt b559 RC led to a value of  $14 \pm 2$  Chl *a* molecules per CP47 complex, in good agreement with the value 13-15 recently reported by Kwa et al. [23]. The estimated uncertainty in our value

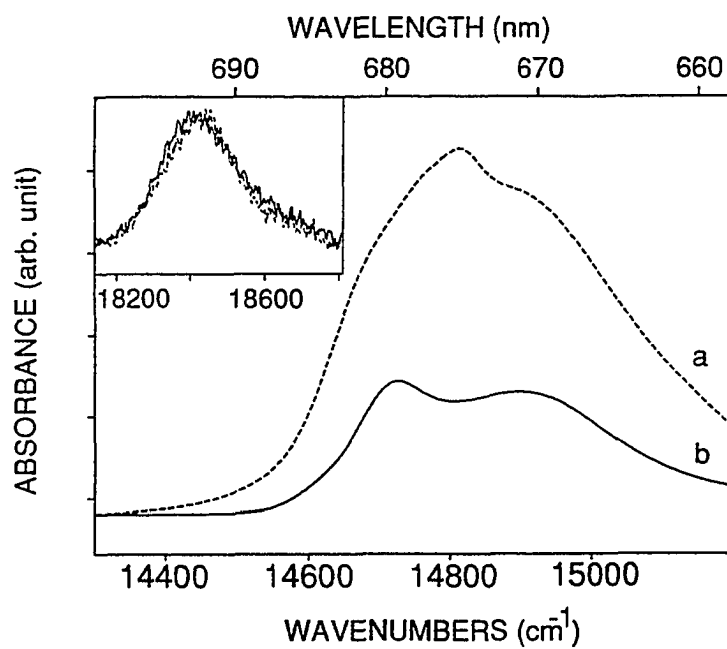


Figure 9. Absorption spectrum of CP47-D1-D2-cyt b<sub>559</sub> RC (curve a) and D1-D2-cyt b<sub>559</sub> RC complexes, 4.2 K (curve b). The inset shows the Q<sub>x</sub>-band of Pheo *a* at 543 nm for both complexes normalized to the same intensity. See text for discussion.

stems from the assumption that the  $Q_y$ -transition dipole strengths for Chl *a* and pheophytin *a* are equal. Given that the 690 and 687 nm states contribute 7% of the total CP47 absorption, *vide supra*, these two states have the equivalent of 1 Chl *a* molecule per complex associated with them.

## IV. Discussion

### A. The 690 And 687 nm States

The results presented here confirm the existence of a very weakly absorbing state of CP47 near 690 nm. Slight, ~1-2 nm, differences in the wavelength of this state reported may be due to the uncertainties in deconvolution procedures used and the fact that the isolation procedures and cooling rates employed are not identical. The low temperature fluorescence of CP47 complex has also been studied [20,22,42]. Vácha et al. and Carbonara et al. reported that the isolated fluorescence origin lies at ~691 nm while van Dorssen reported a value of 693 nm. However, the latter value is within 1 nm of the wavelength for their lowest energy absorption band. We determined that the lowest energy fluorescence origin for CP47 (preparation I) at 4.2 K lies at 691 nm (not shown but essentially identical to that given in the following paper for the CP47-D1-D2-cyt b559 complex). For the situation at hand, where inter-complex energy transfer in the cryomedium is negligible, and in the low temperature limit, the Stokes shift between the absorption and fluorescence origins is given by  $2S\omega_m$  [30], where  $\omega_m$  is the mean phonon frequency. In section III it was determined that  $\omega_m = 20 \text{ cm}^{-1}$  and  $S \sim 0.2$ . These values lead to a predicted Stokes shift of only 0.4 nm. Thus, one can quantitatively understand the very small Stokes shift for the 690 nm state in a manner previously done for the FMO complex of *P. aestuarii* [33,41] and the LHC-II Chl *a* / Chl *b* peripheral antenna complex of PS II [8]. We conclude that the weakly absorbing 690 nm state is the lowest energy

state of the CP47 complex.

The NPHB data, Fig. 1, establish the existence of a new state at 687 nm. The observation that hole burning with a  $\lambda_B$  as high as 695 nm, spectrum c of Fig. 1, produces a pronounced hole from the 687 nm state is important ( $\lambda_B = 695$  nm is in the low energy tail of the 690 nm state,  $170\text{ cm}^{-1}$  lower in energy than 687 nm). This behavior is very similar to that which has been observed from burning into the lowest energy state of the FMO antenna complex [33], and the B850 and B875 antenna bands of *Rb. sphaeroides* [36,37]. As discussed in greatest detail in ref. 33, this behavior is expected when the lowest energy state is excitonically correlated with one or more higher energy states of the complex. Most recently the upper dimer component of the special pair of the *Rps. viridis* was definitively assigned on this basis [25,38]. In the present case the excitonic relationship means that the 690 and 687 nm states are delocalized in the sense that they share at least two Chl *a* molecules. The question of how many Chl *a* molecules are needed to explain the relatively low integrated absorption intensity needs to be addressed. In the previous section we reported a value of  $14 \pm 2$  Chl *a* molecules per CP47 complex on the basis of comparison of a 4.2 K absorption spectrum of the CP47-D1-D2-cyt b559 complex with the 4.2 K absorption of a D1-D2-cyt b559 RC complex with 4 Chl *a* molecules. Kwa et al. [23] recently utilized low temperature absorption spectra of these two complexes to determine a value for the Chl *a* content of 13-15. Although their procedure is slightly different (they did not utilize the  $Q_X$ -band of pheophytin *a* as we do), a comparison of their  $Q_Y$ -absorption spectra with ours has led us to conclude that their analysis is consistent with ours. On the basis of this number and the results in Fig. 8, the number of Chl *a* molecules associated with the 690 and 687 nm state is 1 Chl *a* molecule per complex, *vide supra*. This poses a problem since one needs a minimum of a Chl *a*

dimer to explain the hole burning results. We consider, therefore, the possibility that the value of 1 Chl *a* is an underestimate. First, an unstated assumption in the determination of this number is that CP47(I) represents perfect CP47. This is highly questionable even though it was established in section III that CP47(I) contains less disrupted (or partially dysfunctional from an energy transfer point of view) Chl *a* absorbing near 670 nm than CP47(II). It was pointed out that CP47(II) has less 684 nm absorption than CP47(I) and that this reduction is accompanied by an increase in absorption near 670 nm. It was also found that CP47(II) has less absorption from the 690 and 687 nm states. For example, whereas the ZPH could be observed for the 690 nm state of CP47(I) for  $\lambda_B$  as high as 695 nm (cf. frame B of Fig. 1), it was not observed for CP47(II) for  $\lambda_B > \sim 690$  nm (for a sample whose maximal absorbance at 677 nm was nearly the same as for CP47(I)). In short, the intensities of the 690, 687 and 684 nm bands are easily perturbed as is the intensity of absorption near 670 nm. If only 5% of the absorption near 670 nm is due to disrupted Chl *a* molecules, which were originally associated with the 690/687 nm states, it follows that in perfect CP47 the number of Chl *a* molecules associated with these states could be as high as 2.

### B. Zero-Phonon Holewidths, Hole Growth Rates And Energy Transfer Dynamics

A quantitative theory for the overall hole profile (ZPH plus phonon sideband holes) was first developed in 1988 [30]. It has been successfully tested against the hole spectra of the primary donor state of bacterial and green plant RC [6,38,39]. The absorption at frequency  $\Omega$  following a burn at frequency  $\omega_B$  of duration  $\tau$  into an inhomogeneously broadened absorption band of an electronic state is given by

$$A_\tau(\Omega) = \int dv N_o(v - v_m) L(\Omega - v) \exp[-\sigma I \phi \tau L(\omega_B - v)], \quad (1)$$

where  $I$  is the burn laser spectral intensity,  $\nu$  is the ZPL absorption frequency of a single site of the inhomogeneous distribution described by a Gaussian,  $N_0$ , centered at  $\nu_m$ .  $L$  is the absorption lineshape function for a site with a ZPL frequency  $\nu$ . It describes the ZPL (a Lorentzian) plus its phonon sideband and has a precise mathematical form which need not concern us here since we focus only on the ZPH. For the ZPH one has  $\omega_B = \nu$  and it follows (for a suitably narrow burn laser) that the rate of ZPH growth is governed by  $\exp[-\sigma P \phi \tau]$ , where  $\sigma$  is the peak absorption cross-section of the ZPL,  $P$  the photon flux, and  $\phi$  the hole burning quantum yield. ( $\phi \approx k/(T_1)^{-1}$  with  $k$  the rate constant for hole burning and  $T_1$  is the lifetime of the excited electronic state.) For NPHB,  $k \ll (T_1)^{-1}$  even for  $T_1$  as long as a few nanoseconds [43]. To understand how the ZPH growth rate depends on  $T_1$  and pure dephasing one recalls that  $(T_2)^{-1} = (2T_1)^{-1} + (T_2^*)^{-1}$ , where  $T_2$  and  $T_2^*$  are the total and pure dephasing times respectively, and that  $\sigma$ , in the induced absorption rate  $P\sigma$ , is proportional to  $T_2$ . The pure dephasing is due to chromophore-bath interactions and is well known to vanish in the limit as  $T \rightarrow 0$  K. For simplicity we assume this limit ( $T_2 = 2T_1$ ) and consider the ZPH growth rates for two states, one that has a 1 ns lifetime and the other a lifetime of 1 ps. The assumption that the hole burning rate constants ( $k$ ) in a complex are about equal is also made. It follows that the growth rate for the 1 ps state is about six orders of magnitude slower than that for the 1 ns state. Put another way, for a fixed burn time  $\tau$  a six order of magnitude higher burn flux is required to burn a ZPH for the 1 ps state as deep as the ZPH for the 1 ns state. A less obvious lesson from this simple calculation is that one must beware of non-native or partially dysfunctional Chl molecules produced during complex isolation and handling. This is why in section III we concluded that the ZPH widths of CP47(II) for  $\lambda_B$  lower than the region encompassed by the 690 nm

state cannot be relied on to yield meaningful information on energy transfer dynamics of CP47, see Fig. 4. On the other hand, the ZPH widths for CP47(II) are probably too large to be attributed to totally dysfunctional (in energy transfer) Chl *a* molecules with a  $T_1$  of a few ns since, at 4.2 K, the pure dephasing contribution to the widths should be much smaller than  $1 \text{ cm}^{-1}$  [44,45]. Furthermore, we do not observe anything close to a six order of magnitude difference in the growth rates for CP47(I) and CP47(II) in the vicinity of 670 nm. Thus, the disrupted Chl *a* molecules are still associated with the complex and are quite active in energy transfer.

The remainder of the discussion will center around the results for CP47(I). We consider first the 687 nm state. The absence of ZPH for this state is consistent with (but does not prove) that its lifetime ( $T_1$ ) is ultra-short (relative, for example, to that of the 684 nm state for which ZPH are readily observed). Although the determination of 70 fs for  $T_1$  of the 687 nm state given in section III is rather crude, we consider such a  $T_1$ -value physically reasonable given that the 687 nm state lies only  $63 \text{ cm}^{-1}$  higher in energy than the 690 nm state with which it is excitonically correlated. In the FMO complex of *P. aestuarii* there is a dense manifold of exciton levels, involving 21 BChl *a* molecules, with adjacent level spacings of a few tens of  $\text{cm}^{-1}$ . NPHB data established that the higher energy exciton levels undergo downward energy cascading in  $\sim 100$  fs at 4.2 K [33]. Such ultra-fast relaxation has recently been confirmed by femtosecond spectroscopy [46]. As discussed in this reference, Förster theory is not applicable since, in the low temperature limit, the level spacings are larger than the pure dephasing frequencies of the exciton levels. Cascading occurs by the so-called Davydov mechanism [47] which involves emission of phonons, the most effective of which should be librational since modulation of the Chl-Chl dipole-dipole interactions is required [48]. Such ultra-fast exciton level relaxation by the

Davydov mechanism is known to occur in aromatic organic crystals at low temperatures [48-50]. The above physics was used to qualitatively explain why the B850 and B875 antenna bands of *Rb. sphaeroides* are predominantly homogeneously broadened at 4.2 K [35-37]. Thus, ultra-fast 687 nm  $\rightarrow$  690 nm inter-exciton level relaxation could be expected.

The production of ZPHs through the spectral regions of the 677 and 669 absorption bands, Figs. 1 and 4, indicates that these bands are largely inhomogeneously broadened. From Fig. 4 and Table I we see that the ZPH width increases significantly with decreasing  $\lambda_B$ . All observed widths are at least an order of magnitude greater than that expected from pure dephasing / spectral diffusion of an isolated chromophore in amorphous hosts at 4.2 K [4,5]. In addition, Boxer et al. [51] measured a ZPH width at 4.2 K of  $0.03 \text{ cm}^{-1}$  for zinc pyrochlorophyllide in apomyoglobin and Gillie et al. [52] measured widths of the same value for Chl *a* in PS I core antenna samples degraded by the harsh detergent Triton X-100. Thus, we believe that the larger ZPH widths in Table I probably reflect the dynamics of the initial phase of energy cascading in CP47(I). If the ZPH widths at 670 and 675 nm were to be assigned to downward cascading of the 677 and 669 nm states, the rate constants would be  $(2.2 \text{ ps})^{-1}$  and  $(3.2 \text{ ps})^{-1}$ , respectively.

Before turning our attention to the ZPH widths associated with the 690 and 684 nm bands, it should be noted that the weak shoulder at 661 nm in the absorption spectrum of CP47(I), Fig. 1 may be due to vibronic transitions building on the intense 677 and 669 nm origin bands, rather than another electronic state.

From Fig. 4 and Table I one observes that the ZPH width levels off at  $0.4 \text{ cm}^{-1}$  in the region of the 690 nm state. When viewed as homogeneous, this width corresponds to a total dephasing time ( $T_2$ ) of 50 ps, which is much shorter than the measured lifetime of



Table 1

Excitation Wavelength (nm)	ZPH Width ( $\text{cm}^{-1}$ )	$T_2$ (ps)
670	4.8	4.4
675	3.3	6.4
680	2.1	10
682	1.4	15
684	1.1	19
688	0.47	45
690	0.39	54
692	0.40	53

1 ns (77 K) for the long wavelength state [53]. By way of comparison, the 4.2 K holewidth for the lowest exciton levels of the FMO complex of *P. aestuarii* [38,39], the B800-B850 and B875 complexes of *Rb. sphaeroides* [35,36] and the LHC-II Chl *a*/Chl *b* complex of PS II [9] are also large (0.5 to 3.2 cm<sup>-1</sup>, depending on the complex). However, these complexes are a C<sub>3</sub>-trimer of chemically identical subunits which seems an unlikely possibility for CP47 [1]. (One interpretation offered in ref. 36 for large ZPH widths / fast dephasing is that they are associated with scattering/trapping of a subunit excitation with the other two subunits.) Thus, if the ZPH width of 0.4 cm<sup>-1</sup> is due to dephasing an alternative mechanism is required. To this end temperature-dependent studies may prove informative and are planned.

### C. The 684 nm State

The present work on CP47 establishes that the intensity of the relatively weak 684 nm absorption band is variable from one preparation to another. Diminution in its intensity by purification appears to be accompanied by an increase in absorption near 670 nm from disrupted Chl *a* molecules which can be dominant in zero-phonon hole burning, see Fig. 4. In the following paper [15], it is proven that a 684 nm band appears as a low energy shoulder of P680 which is the primary donor absorption band of the D1-D2-cyt b<sub>559</sub> RC complex. These results and those for the CP47-D1-D2-cyt b<sub>559</sub> [15] and CP47 complexes raise the possibility that the 684 nm state is due to linker chlorophyll [3] associated with the entire core complex of PS II. This possibility and other interpretations are considered in the accompanying paper [15].

From Fig. 4 and Table I the ZPH width at 684 nm corresponds to a T<sub>1</sub>-relaxation time of 10 ps at 4.2 K. For CP47 complexes that do possess the 684 nm Chl *a* a possible relaxation pathway for the 684 nm state is to the 687 nm state of CP47, which lies only

60 cm<sup>-1</sup> lower in energy.

### Acknowledgments

Research at the Ames Laboratory was supported by the Division of Chemical Sciences, Office of Basic Energy Sciences, U.S. Department of Energy. Ames Laboratory is operated for the U.S. Department of Energy by Iowa State University under Contract No. W-7405-Eng-82. Work at NREL was supported by the same division of USDOE under Contract No. DE-AC02-83 CH-10093. R. P. is grateful to DGICYT (Grant PB 92-0125) for partial financial support. The research of C.F.Y. was supported by NSF grant DCB 89-04075. We thank S. Toon at NREL for isolating the RC material used in this study.

### References

1. Bricker, T. M. *Photosynthesis Research* 1990, 24, 1.
2. Barbato, R.; Rigoni, F.; Giardi, M. T.; Giacometti, G. M. in *Current Research in Photosynthesis*; Baltscheffsky, M., Ed.; Kluwer Academic Publishers: Netherlands; 1990, Vol. 1, p. 339.
3. Seibert, M. in *The Photosynthesis Reaction Center*; Vol. I; Deisenhofer, J.; Norris, J., Eds.; Academic Press: New York, 1993; p. 319.
4. In *Persistent Spectral Hole-Burning: Science and Applications*, Moerner, W. E., Ed.; Springer-Verlag, 1988.
5. See
  - a. Jankowiak, R.; Hayes, J. M.; Small, G. J. *Chemical Reviews* 1993, 93(4), 1471,
  - b. Jankowiak, R.; Small, G. J. in *The Photosynthetic Reaction Center*; Deisenhofer, J., Norris, J., Eds.; Academic Press; 1993; Chapter 7, p. 133, and
  - c. Reddy, N. R. S.; Lyle, P. A.; Small, G. J. *Photosyn. Res.* 1992, 31, 167. for reviews of applications to photosynthetic complexes.
6. Jankowiak, R.; Tang, D.; Small, G. J.; Seibert, M. *J. Phys. Chem.* 1989, 93, 1649.

7. Tang, D.; Jankowiak, R.; Seibert, M.; Yocum, C. F.; Small, G. J. *J. Phys. Chem.* 1990, 94, 6519.
8. Tang, D.; Jankowiak, R.; Seibert, M.; Small, G. J. *Photosyn. Res.* 1991, 27, 19.
9. Reddy, N. R. S.; van Amerongen, H.; Kwa, S. L. S.; van Grondelle R.; Small, G. J. *J. Phys. Chem.*, submitted.
10. Rögner, M.; Chisholm, D. A.; Diner, B. A. *Biochemistry* 1991, 30, 5387.
11. Hansson, Ö.; Wydrzynski, T. *Photosyn. Res.* 1990, 23, 131.
12. de Vitry, C.; Wollmann, F. A.; Delepelaire, P. *Biochim. Biophys. Acta* 1984, 767, 415.
13. van Kan, P. J. M.; Groot, M. L.; Kwa, S. L. S.; Dekker, J. P.; van Grondelle, R. in *The Photosynthetic Bacterial Reaction Center II*; Breton, J., Vermeiglio, A., Eds.; Plenum Press: New York, 1992, p. 411.
14. Barbato, R. E.; Rigoni, F.; Giardi, M. T.; Giacometti, G. M. *FEBS Lett.* 1989, 251, 147.
15. Chang, H.-C.; Jankowiak, R.; Reddy, N. R. S.; Yocum, C. F.; Picorel, R.; Seibert, M.; Small, G. J. *J. Phys. Chem.* 1994, 98, 7725.
16. Jortner, J. *Biochim. Biophys. Acta* 1980, 594, 193.
17. Lyle, P. A.; Struve, W. S. *J. Phys. Chem.* 1991, 95, 4152.
18. Small, G. J.; Hayes, J. M.; Silbey, R. *J. Phys. Chem.* 1992, 96, 7499.
19. Gillie, J. K.; Small, G. J.; Golbeck, J. H. *J. Phys. Chem.* 1989, 93, 1620.
20. van Dorssen, R. J.; Breton, J.; Plijter, J. J.; Satoh, K.; van Gorkom, H. J.; Amesz, J. *Biochim. Biophys. Acta* 1987, 893, 267.
21. van Kan, P. J. M.; Groot, M. L.; van Stokkum, I. H. M.; Kwa, S. L. S.; van Grondelle, R. and Dekker, J. P. in *Research in Photosynthesis*, Vol. 1; Murata, N., Ed.; Kluwer Academic Publishers: Netherlands, 1992, 271.

22. Carbonera, D.; Giacometti, G.; Agostini, G.; Angerhofer, A.; Aust, V. *Chem. Phys. Lett.* 1992, 194, 275.
23. Kwa, S. L. S.; van Kan, P. J. M.; Groot, M. L.; van Grondelle, R.; Yocum, C. F. in *Research in Photosynthesis*, Vol. 1; Murata, N. Ed.; Kluwer Academic Publishers: Netherlands, 1992, 269.
24. Ghanotakis, D. F.; de Paula, J. C.; Demetriou, D. M.; Bowlby, N. R.; Petersen, J.; Babcock, G. T.; Yocum, C. F. *Biochim. Biophys. Acta* 1989, 974, 44.
25. Reddy, N. R. S.; Kolaczowski, S. V.; Small, G. J. *Science* 1993, 260, 68.
26. Lyle, P. A.; Kolaczowski, S. V.; Small, G. J. *J. Phys. Chem.* 1993, 97, 6926.
27. Determined as twice the half-width at half-maximum of the lower energy side since the rising edge of the anti-hole interferes with the higher energy side of the 687 nm hole.
28. Shu, L.; Small, G. J. *J. Chem. Phys.* 1990, 141, 441.
29. Shu, L.; Small, G. J. *J. Opt. Soc. Am. B.* 1992, 9, 724.
30. Hayes, J. M.; Gillie, J. K.; Tang, E.; Small, G. J. *Biochim. Biophys. Acta.* 1988, 932, 287.
31. Lee, I.-J.; Hayes, J. M.; Small, G. J. *J. Chem. Phys.* 1989, 91, 3463.
32. Gillie, J. K.; Hayes, J. M.; Small, G. J.; Golbeck, J. H. *J. Phys. Chem.* 1987, 91, 5524; *J. Phys. Chem.* 1989, 93, 1620.
33. Johnson, S. G.; Small, G. J. *J. Phys. Chem.* 1991, 95, 471.
34. Kohler, W.; Friedrich, J.; Fischer, R.; Scheer, H. *J. Chem. Phys.* 1988, 89, 871.
35. Reddy, N. R. S.; Cogdell, R. J.; Zhao, L.; Small, G. J. *Photochem. Photobiol.* 1993, 57(1), 35-39.
36. Reddy, N. R. S.; Picorel, R.; Small, G. J. *J. Phys. Chem.* 1992, 96, 6458.
37. Reddy, N. R. S.; Small, G. J.; Seibert, M.; Picorel, R. *Chem. Phys. Lett.* 1991, 181(5), 391.

38. See ref. 25 and Reddy, N. R. S.; Kolaczowski, S. V.; Small, G. J. *J. Phys. Chem.* 1993, 97, 6934 and references therein.
39. Gillie, J. K.; Lyle, P. A.; Small, G. J.; Golbeck, J. H. *Photosyn. Res.* 1989, 22, 333.
40. Friedrich, J.; Haarer, D. *Angew. Chem. Int. Ed. Engl.* 1984, 23, 113.
41. Johnson, S. G.; Small, G. J. *Chem. Phys. Lett.* 1989, 155, 371.
42. Vacha, M.; Adamec, F.; Ambroz, M.; Psencik, J.; Hala, J. *J. Mol. Struct.* 1993, 294, 131.
43. Kenney, M. J.; Jankowiak, R.; Small, G. J. *Chem. Phys.* 1990, 146, 47.
44. Völker, S. in: *Molecular Excited States: Optical Relaxation at Low Temperatures*; Fünfschilling, J., Ed.; Kluwer Academic Press, Dordrecht 1989, p. 113.
45. Narasimhan, L. R.; Littau, K. A.; Pack, D. W.; Bai, Y. S.; Elschner, A.; Fayer, M. D. *Chem. Rev.* 1990, 90, 439.
46. Savikhin, S.; Zhou, W.; Blankenship, R. E.; Struve, W. S. *Biophysical J.*, accepted.
47. Davydov, A. S. in *Theory of Molecular Excitons*; Plenum Press: New York, 1971.
48. See Dissado, L. A. *Chem. Phys.* 1975, 8, 289 and references therein.
49. Dissado, L. A.; Brillante, A. J. *J. Chem. Soc. Faraday Trans.* 1977, 9, 1262.
50. Dissado, L. A. *Chem. Phys. Lett.* 1975, 33, 57.
51. Boxer, S. G.; Gottfried, D. S.; Lockhart, D. J.; Middendorf, T. R. *J. Chem. Phys.* 1987, 86, 2439.
52. Gillie, J. K.; Hayes, J. M.; Small, G. J.; Golbeck, J. H. *J. Phys. Chem.* 1987, 91, 5524.
53. Mimuro, M. in *Research in Photosynthesis*, Vol. I; Murata, N., Ed.; Kluwer Academic Publishers, 1992, p. 259.

## CHAPTER 5 ON THE QUESTION OF THE CHLOROPHYLL *a* CONTENT OF THE PS II REACTION CENTER

A paper published in J. Phys. Chem. 1994, 98, 7725

H.-C. Chang, R. Jankowiak, N. R. S. Reddy, C. F. Yocum,  
R. Picorel, M. Seibert, and G. J. Small

### Abstract

Isolation procedures have led to chlorophyll *a* (Chl *a*) contents for the photosystem II reaction center that range between about 4 and 6. Since this content for the bacterial RC is 4, the nature of the "extra" Chl *a* in PS II RC preparations containing more than 4 Chl *a* molecules is of considerable interest. Absorption and triplet bottleneck hole spectra (4.2 K) are reported for RC preparations containing 4, 5 and 6 Chl *a* molecules. The results show that the extra Chl *a* are due to 684 nm absorbing Chl *a*, CP47 contamination and, probably, also non-native Chl *a* absorbing near 670 nm. Thus, RC preparations with higher Chl *a* content are heterogeneous, containing 4 Chl *a*-RC, 4 Chl *a*-RC with bound 684 nm Chl *a*, CP47-RC, etc. The lifetime of the primary electron-donor state (P680\*) of the 4 Chl *a* preparation, which contains very little 684 nm Chl *a* (~5% on a Chl *a* basis), was 1.9 ps at 4.2 K. This is identical to our previous determinations for higher Chl *a* content RC and CP47-RC samples. Thus, the 684 nm Chl *a* appear to play no role in primary charge separation. The 684 nm Chl *a* are extremely vulnerable to the ionic detergent TX-100 (much more so than P680) and, when denatured, absorb at ~670 nm. It can be concluded that the 684 nm band is not the dimer partner of

P680 or due to gross heterogeneity (i.e., the 684 nm band is not P684 of a distinctly different subset of the RC population). Interestingly, the intensities of the 684 nm band observed for the CP47 complex (Chang et al., *J. Phys. Chem.* 1994, 98, 7717) and the CP47-RC complex are also sensitive to the details of the isolation procedure. The hole burning characteristics and fragility of the 684 nm band appear to be quite similar for the three complexes. Two possibilities are considered: that the 684 nm Chl *a* are of the linker-type associated with the entire Chl *a* complex; or that both CP47 and the RC possess an intrinsic 684 nm state. A theoretical analysis of the burn wavelength dependence of the P680 hole spectra of the 4 Chl *a* preparation is given. In agreement with our previous work (Jankowiak et al. , *J. Phys. Chem.* 1989, 93, 1649), the linear electron-phonon (protein) coupling is as strong ( $S = 2$ ) as that observed for P870 and P960 of the bacterial RC. However, the special pair marker mode ( $125\text{-}145\text{ cm}^{-1}$ ) progression of P870 and P960 of the bacterial RC is essentially silent in P680. This, together with the observation that the weakly absorbing, upper dimer partner of P680 lies only  $300\text{ cm}^{-1}$  higher in energy, further establishes that the special pair of the PS II RC has a structure which is significantly different than in the bacterial RC. The question of which two Chl *a* molecules of the 4 Chl *a*-RC constitute the dimeric primary electron-donor is considered as are structural models for P680.

## I. Introduction

The isolation of the D1-D2-cyt *b*<sub>559</sub> reaction center (RC) complex of photosystem II (PS II) from higher plants by Nanba and Satoh [1] led to a substantial number of ultra-fast time domain and spectral hole burning studies of its primary charge separation and energy transfer properties (see Renger [2] and Seibert [3] for thorough reviews). The increased activity was also motivated by the availability of the x-ray



structure for the RC of *Rhodospseudomonas viridis* [4,5] since there is considerable homology between the L and M proteins of the bacterial RC and the D1 and D2 proteins [5,6]. The former bind the two bacteriochlorophyll (BChl) molecules of the special pair, two accessory BChl molecules, two bacteriopheophytin and two quinone molecules. It is the lowest excited  $Q_Y$ -state of the special pair ( $P^*$ ) which is the primary electron donor state of the bacterial RC [7]. The original preparation of the PS II RC was reported to contain 4-5 Chl *a* and 2 pheophytin *a* (Pheo *a*) molecules with the two quinone molecules of the RC lost during isolation [1].

Aside from the unavailability of an x-ray structure for the PS II RC, there are other reasons why an understanding of its electronic structure and transport properties is considerably more difficult than for the bacterial RC. The first is related to spectral congestion; the  $Q_Y$ -absorption spectrum of the PS II RC, Fig. 1, spans only about  $500\text{ cm}^{-1}$ , which is over a factor of 4 smaller than for the bacterial RC. Whereas all six  $Q_Y$ -state absorption bands of the RC of *Rps. viridis* have been resolved at 4.2 K [8], only two bands are apparent in the spectra of Fig. 1. Thus, in time-domain experiments on the PS II RC selective excitation of a particular state is far more difficult to achieve, especially at room temperature. The second reason has to do with material characterization. The PS II RC is considerably more fragile than the bacterial RC [3]. Recognizing that the RC isolated by the procedure of Nanba and Satoh (which relies heavily on the Triton X-100 (TX-100) detergent) is unstable, several groups developed procedures which led to significantly enhanced stability [3]. For example, in earlier work [9] we studied samples prepared by the procedures of McTavish et al. [10] and Dekker et al. [11]. Whereas the former includes modifications to the original Nanba/Satoh procedure designed to remove and replace excess TX-100 with the milder nonionic lauryl maltoside detergent, the latter

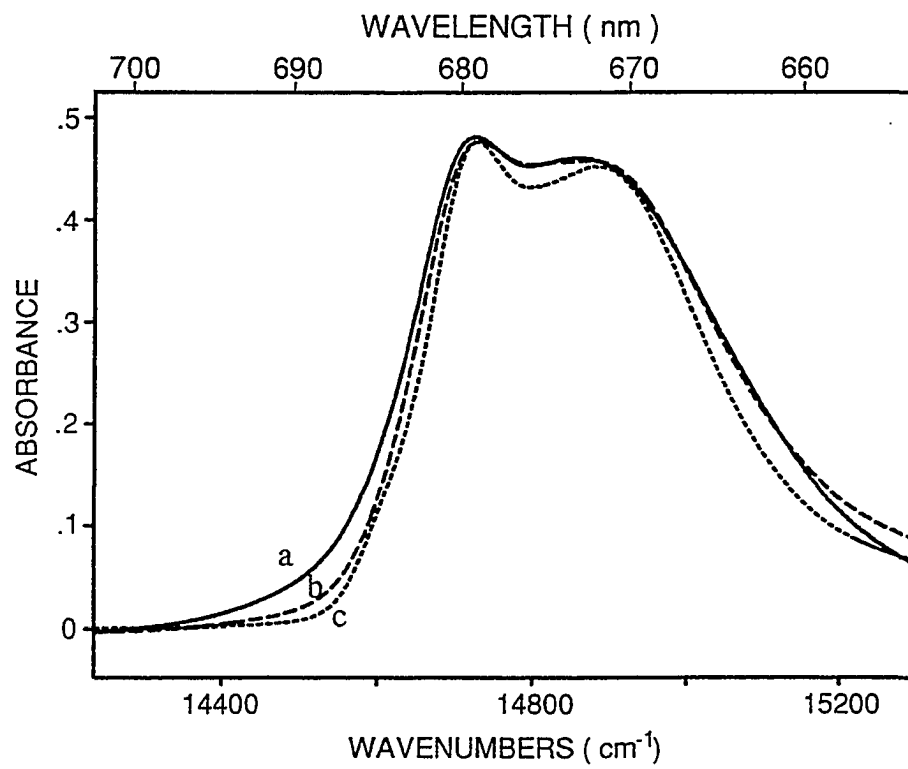


Figure 1. Low temperature (4.2 K) absorption spectra of three different PS II RC samples (see text for discussion).

avoids the use of TX-100 throughout the isolation procedure subsequent to the preparation of PS II-enriched membrane fragments. It was shown, by spectral hole burning, that the charge separation and energy transfer dynamics of the two preparations are very similar [9]. It was also shown that the addition of TX-100 to the glass-forming solvent markedly perturbs the low temperature absorption spectrum [12] and disrupts energy transfer within the RC [12]. Interestingly, the primary charge separation kinetics associated with P680\*, the primary donor state, were found to be unaffected by TX-100. The addition of the mild detergent lauryl maltoside to the solvent had no effect on the absorption spectrum or primary charge-separation kinetics of the RC.

While the lessons of the above and other [3] related works are important, they do not touch upon the important question of the correct number of Chl *a* molecules belonging to the PS II RC. As reviewed in ref. 3, biochemical analysis has shown that RC preparations with an average Chl *a* content between about 4 and 6 can be achieved. If it is assumed that the correct number is 4 (in analogy to the bacterial RC), then the additional 2 Chl *a* in a 6 Chl *a* preparation should be expected to affect the energy transfer dynamics. (Since the P680\* lifetime for the CP47-RC complex is the same [13] as that for the isolated RC complexes which have been studied, it seems unlikely that the additional 2 Chl *a* molecules have a significant effect on primary charge separation.) The additional Chl *a* molecules should also alter the low temperature absorption spectrum of the 4 Chl *a*-RC. It is the case that the published 4.2 K absorption spectra of the PS II RC exhibit some significant differences; e.g., the depth of the valley at 676 nm and the relative intensity of the ~680 and ~670 nm bands (see Fig. 1 for examples). However, the actual Chl *a* contents of the RC samples studied were not determined. Thus, the absorption characteristics and nature of the "extra" Chl *a* molecules could not be adequately assessed.

An additional complication is that the inhomogeneous broadenings of the  $Q_y$ -absorption bands may vary somewhat between samples due to the fragility of the RC. Non-native (dysfunctional to some degree) Chl *a* molecules may contaminate the spectrum at  $\sim 670$  nm as reported on in the preceding paper [14] for the CP47 core antenna complex.

In this paper we report the results of 4.2 K absorption and hole burning studies on PS II RC samples containing 4, 5 and 6 Chl *a* molecules. For an interpretation of the spectra it proved necessary to study different preparations of the CP47 complex (see accompanying paper [14]) and the CP47-RC complex. Results for the last complex are also presented here. Taken as a whole, the results allow for investigation of the suggestions that CP47 contamination [14] and linker Chl *a* molecules [3] are responsible, to a considerable extent, for the additional Chl *a* in RC preparations containing more than 4 Chl *a* molecules. The data also speak to the question of the correct number of Chl *a* molecules in the D1-D2-cyt b559 RC complex. The transient triplet-population bottleneck hole burned spectra reported here for the 4 Chl *a*-RC preparation are also used to address the question of whether or not the primary electron-donor is a special pair or a monomer. The literature on this question has been recently reviewed [2,3] and will be discussed in section IV. What is clear from these works is that, if P680 is a dimer, its monomers are much more weakly interacting than in the special pair of the bacterial RC. Hole burning experiments on the RC of *Rps. viridis* [8,16] and *Rb. sphaeroides* [17] led to a zero-point level dimer splitting of 1900 and 1300  $\text{cm}^{-1}$  at 4.2 K, respectively. At room temperature these splittings are slightly reduced due to the temperature-dependence of the P960 and P870 lower dimer component energies of *Rps. viridis* and *Rb. sphaeroides* [18]. Nevertheless, the dimer state splittings are still much larger than the entire width of the  $Q_y$ -absorption spectrum of the PS II RC.

To conclude this section we review some results of frequency domain experiments on the excited electronic state ( $Q_y$ ) structure of the PS II RC and those of hole burning and time domain studies on the transport properties. It is generally accepted that [2,3] the absorption of the primary donor, P680, contributes significantly to the  $Q_y$ -band near 680 nm, Fig. 1. The white light plus dithionite reduction experiments of Breton [19] provided evidence for the  $Q_y$ -state of a Pheo *a* molecule being essentially degenerate with P680\*, the  $Q_y$ -state of the primary donor. This result was proven by hole burning [9] and absorbance-detected magnetic resonance [20] experiments. The results of the hole burning also showed that the  $Q_y$ -state of this Pheo *a* undergoes persistent nonphotochemical hole burning (NPHB [21]). The primary donor state, P680\*, was found not to exhibit NPHB but could be probed by population bottleneck hole burning via the metastable  $^3P680^*$  state [22,23]. Burn frequency-dependent hole spectra established that the electron-phonon coupling for the Pheo *a*  $Q_y$ -state (band) is weak with a Huang-Rhys factor  $S$  of 0.7 and mean phonon frequency ( $\omega_m$ ) of  $\sim 20 \text{ cm}^{-1}$ . In sharp contrast, the coupling for P680\* was found to be strong with  $S \sim 2$  and  $\omega_m \sim 20 \text{ cm}^{-1}$ . Thus, while the Pheo *a* state exhibits the weak coupling characteristic of the Chl- $Q_y$  states of antenna protein complexes [13,24], P680\* exhibits the strong coupling to low frequency protein phonons characteristic of the primary donor state P870\* and P960\* of *Rb. sphaeroides* [17,18,25,26] and *Rps. viridis* [16,18,25,26], respectively. The strong coupling for P870\* and P960\* was attributed to the fact that, as dimer states of the RC, they possess significant charge-transfer character, as also indicated by experimental Stark data [27-29] and some electronic structure calculations [30,31]. Strong coupling also characterizes the primary electron-donor state, P700\*, of the RC of PS I [32]. As a consequence it was concluded that P700\* is most likely a dimer state [32]. That it is a dimer state was subsequently indicated by the x-ray

diffraction structure of Krauss et al. [33]. By the same reasoning it was suggested that P680\* is probably a dimer state even though P680 did not appear to exhibit the special pair marker mode progression [9,12] of P870 and P960, cf. section IV.C.

Several groups [13,34-36] have reported low temperature spectra which identify a low energy absorbing Chl *a* band of PS II RC samples near ~684 nm. Discussion of these works, which are very relevant to the present paper, is reserved for section IV. Suffice it to say at this point that the interpretations offered for this state include it being a dimer component of the special pair, a second P680 pool due to gross heterogeneity, and it being due to linker Chl *a* molecules and/or CP47 contamination. By linker it is meant that the Chl *a* molecules are associated with the core complex of PS II rather than any complex of the core.

Moving next to the higher energy region of the Q<sub>y</sub>-absorption spectrum of the PS II RC, we note that the absorption maximum near 670 nm, cf. Fig. 1, is generally taken to be mainly due to the accessory Chl *a* molecules of the RC. However, a contribution from one of the two Pheo *a* molecules of the RC cannot be excluded. (The two bacteriopheophytin transitions of the bacterial RC are split by about 200-300 cm<sup>-1</sup>.) Spectral hole burning experiments [12,37] established that the electron-phonon coupling for the states probed in the vicinity of 670 nm is weak.

In 1989 persistent NPHB and transient population bottleneck hole burning were used to study the transport properties of the isolated PS II RC at 4.2 K [38]. A lifetime of  $1.9 \pm 0.2$  ps for P680\* was determined and attributed to primary charge separation. At the same time the results of pump-probe experiments on samples from the same batch led to a time constant of  $3.0 \pm 0.6$  ps for primary charge separation at 277 K [39]. Similar time-domain experiments later led to a time constant of  $1.4 \pm 0.2$  ps at 15 K [40]. Thus, the rate

of charge separation and its temperature dependence in the PS II RC appeared to be very similar to those of the bacterial RC [41]. Shortly thereafter, picosecond fluorescence data obtained at room temperature revealed a dominant 1-6 ps decaying component which was attributed to primary charge separation [42]. Other fluorescence studies [43,44] have confirmed the existence of a dominant ~3 ps decay component of P680\* at 77 and 277 K. Hole burning data also led to energy transfer decay times (4.2 K) for the accessory Chl *a* and the active Pheo *a* of the RC of 12 and 50 ps, respectively [9,12]. It was noted in these works that these decay times are remarkably slow in comparison to the corresponding  $\leq 100$  fs relaxation times of the bacterial RC [26,45,46]. Time domain data obtained at 15 K were reported [40] that are consistent with such slow energy transfer dynamics. The data of refs. 43 and 44 also identify a ~30 ps energy transfer process. However, femtosecond pump-probe data have been reported [47] which indicate the existence of subpicosecond energy transfer processes. It appears that further studies on PS II RC preparations, of defined Chl *a* content, with a wider variety of pump-excitation wavelengths are necessary in order to understand the complex energy transfer dynamics. However, it now seems certain that P680\* decays in ~3 ps at ambient temperature (see also ref. 48) and that the primary charge separation kinetics of the PS II RC are essentially identical to those of the bacterial RC.

## II. Experimental

Lauryl maltoside-stabilized [3] PS II RC complex was isolated from spinach according to the procedure of Nanba and Satoh [1] as modified by Chumanov et al. [50]. PS II-enriched membrane fragments [51] were solubilized with 4% Triton X-100 in 50 mM Tris-HCl for 1 hr at 4° C. In all cases solubilization started out with membranes containing 120 mg Chl at 1 mg Chl/ml, and the suspension was centrifuged at 32,000  $\times$  g for 1 hr.

The resultant green supernatant was carefully loaded onto a Fractogel TSK-DEAE 650S anionic exchange column pre-equilibrated with 50 mM Tris-HCl (pH 7.2), 30 mM NaCl, and 0.05% Triton X-100. The sample was washed with the same buffer using an FPLC (Pharmacia) until the absorption of the eluent at 670 nm was equal to or less than 0.03. The number of Chl/RC in the final material was dependent on when the wash step was stopped. An absorption of about 0.03 led to preparations with about 6 Chls/RC while lower values led to preparations with 4-5 Chls/RC. Intermediary absorption values resulted in preparations with intermediary numbers of Chls/RC. Following the wash step, the buffer was exchanged with 50 mM Tris-HCl (pH 7.2), 30 mM NaCl, and 0.03% lauryl maltoside, and the column was washed with 150 ml of this buffer. The RCs were then eluted from the column with a 30-200 mM NaCl linear gradient in the same buffer, and the green fractions at around 125 mM NaCl were pooled, desalted and concentrated with an Amicon ultrafiltration system, and stored at  $-80^{\circ}$  C until use. The Chl stoichiometry of the RC preparations was assayed as in Montoya et al. [52]. Concentrated RC material was extracted with 80% acetone (final concentration) in a microfuge tube placed in a sonication bath for 30 s. The sample was centrifuged briefly in a microfuge to remove cell debris, and the supernatant was transferred to a 1-cm cuvette. Spectra (room temperature) from 350-750 nm were taken with an HP8450A UV-vis spectrophotometer and stored. The sample was then pheophytinized by bringing the sample to 1.5 mM HCl in the cuvette and a second spectrum obtained. The Chl to Pheo ratio was determined by assuming that (a) the native RCs contain 2 pheos, (b) the 665.5 and 535 nm peaks in HCl-treated material represents the total Chl plus Pheo in the sample, and (c) the 535 nm peak in the non-pheophytinized extract represents the amount of Pheo in the material. Note that a broad baseline absorption must be subtracted to obtain data for the relatively sharp 535 nm band,



and extinction coefficients of  $49.3$  and  $6.504 \text{ mM}^{-1} \text{ cm}^{-1}$  were used at  $665.5$  and  $535$  nm, respectively [52]. It is possible that a very weak Chl *a* vibronic band may underlie the  $535$  nm Pheo *a* band, i.e. the analysis procedure may systematically underestimate the Chl *a* content by several percent. Samples from four separate preparations were studied.

Results for samples with  $3.7 \pm 0.2$ ,  $5.0 \pm 0.2$  and  $6.3 \pm 0.2$  Chl *a*/RC are presented. In section III the  $4.2$  K absorption spectra of these RC preparations are shown to be consistent with the relative Chl *a* contents deduced from the above Chl *a*/RC ratios. Hereafter, we will refer to the above RC-preparations as 4, 5 and 6 Chl *a*-RC preparations (samples).

CP47-RC complexes from spinach were prepared according to the procedure of Dekker et al. [11] as described in the accompanying paper. Low temperature spectroscopic results are presented for samples from three separate isolations. The Chl *a* and Pheo *a* contents per complex for these samples were not determined by biochemical analysis. However in section III a novel procedure, which is based on low temperature absorption spectroscopy, is shown to provide values for the relative Chl *a* contents of the complexes from the three isolations. In the accompanying paper [14] of the CP47 complex, the Chl *a* content was determined to be  $14 \pm 2$  on the basis of the  $4.2$  K absorption spectrum of one of the above three isolated CP47-RC complexes and the  $4.2$  K absorption spectrum of the 4 Chl *a*-RC sample. Thus, values for the Chl *a* contents of the other two CP47-RC samples could be determined, cf. section III.

Towards the end of the low temperature absorption and hole burning experiments it became apparent that the 5 and 6 Chl *a*-RC samples suffered from some contamination by the CP47 complex, cf. sections III and IV. At this point it was only possible to perform SDS-gel electrophoresis on the 6 Chl *a*-RC sample. CP47 and CP43-CP47-RC samples

were run simultaneously. The 6 Chl *a*-RC sample exhibited a weak CP47 band. Analysis of the densitometer tracing (not shown) showed that CP47 contributes 2.5% of the total staining with the D1, D2, D1/D2 heterodimer and  $\alpha$  (*psbE* gene product) subunits contributing 92.7%. By assuming that CP47 stains only as well as the other subunits, one can arrive at an upper limit for Chl *a* contamination from CP47 to the RC sample. It is 4% of the number of Chl *a* molecules per CP47.

The apparatus used for the low temperature absorption and hole burning experiments is described in the accompanying paper [14]. The apparatus used for the 4.2 K static (non-line narrowed) fluorescence experiments is the same as that used for our laser-induced fluorescence studies of DNA-carcinogen adducts [53].

### III. Results And Discussion

The published low temperature absorption spectra of the D1-D2-cyt *b*<sub>559</sub> RC complex (referred to hereafter as the RC complex) from our laboratory and others exhibit some significant differences in the  $Q_y$ -region. The spectra of Tang et al. [9] shown in Fig. 1 serve to illustrate, quite well, the extent of these differences. Spectra a and c are for RC complexes isolated according to the procedure of McTavish et al. [10] while spectrum b is from a sample prepared according to the procedure of Dekker et al. [11]. Although the Chl *a* contents per RC of the three samples were not determined, one expects that they lie between about 4 and 6 and that the RC of each sample contains 2 Pheo *a* molecules. All three spectra in Fig. 1 exhibit band maxima at ~680 and ~670 nm which are characteristic of the RC. The band at 680 nm is mainly contributed to by P680, the absorption of the primary electron donor. However, persistent nonphotochemical and triplet population bottleneck hole burning data have established that the zero-point level of the  $Q_y$ -state of a Pheo *a* molecule lies about  $20\text{ cm}^{-1}$  above that of P680\* at 4.2 K [9,38].

That these two states are nearly degenerate at low temperature is also the conclusion reached by Breton [19] and van der Vos et al. [20].

The three spectra in Fig. 1 differ in the depth of the valley at  $\sim 676$  nm, the intensity at  $\sim 670$  nm and the extent of tailing to lower energy of the 680 nm maximum. That the upper two spectra (a,b) are nearly identical for wavelength shorter than 680 nm but different for wavelengths longer than 680 nm suggests that there is more than one cause for the spectral differences. It was concluded in ref. 13 that contamination of the RC by the proximal antenna complex CP47 is one cause. With reference to Fig. 1 of the accompanying paper [12] it is clear that CP47 contamination would, for example, diminish the depth of the valley at 676 nm.

The absorption spectrum of the 4 Chl *a* per RC preparation is shown in frame A of Fig. 2. The inset spectrum, which extends out to the  $Q_x$ -band of Pheo *a*, is shown for comparison against published spectra. The  $Q_x$ -bands at 16900/17300 and 18405  $\text{cm}^{-1}$  (591.7/578.0 and 543.3 nm) can be assigned to Chl *a* and Pheo *a*, respectively. The barely resolved doublet at 16,000  $\text{cm}^{-1}$  is due to vibronic bands which build on the  $Q_y$ -origins at 680 and 670 nm. We have compared the  $Q_y$ -absorption spectrum in frame A of Fig. 2 with those of Fig. 1 and other published spectra as well as those of the 5 and 6 Chl *a* / RC preparations (Fig. 3). The spectrum of Fig. 2 exhibits the deepest valley at 676 nm and the red edge of P680 is as sharp as observed in any other spectrum. Nevertheless, inspection of the low energy side of P680 in Fig. 2 reveals a weak band at  $\sim 684$  nm.

The 684 nm band of the 4 Chl *a*-RC is more apparent in the two transient triplet-bottleneck hole burned spectra of frame B in Fig. 2. Following the procedure of refs. 9 and 38 it was confirmed that these spectra are not contributed to by the Pheo *a*  $Q_y$ -state near 680 nm. The weak zero-phonon hole (ZPH) in spectrum a (due to P680 [9,38]) is

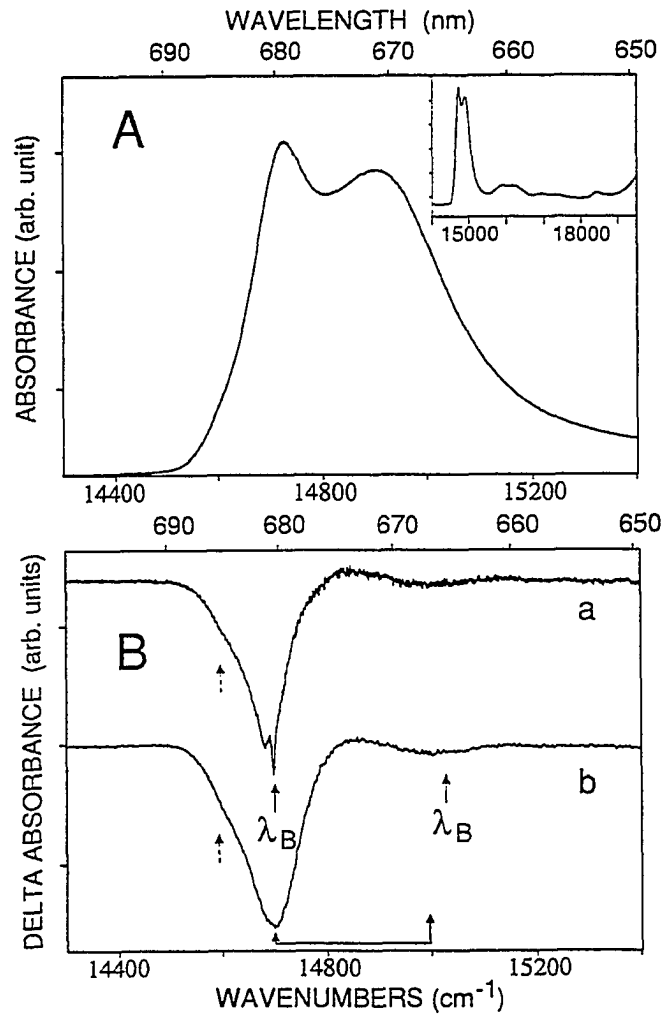


Figure 2. Low temperature absorption spectrum (A) and transient hole-burned spectra (B) of 4 Chl *a*-RC sample obtained at  $T = 4.2$  K. Spectra a ( $\lambda_B = 680.5$  nm,  $I_B = 400$  mW/cm<sup>2</sup>,  $\Delta OD$  change at ZPH  $\sim 20\%$ ) and b ( $\lambda_B = 665$  nm,  $I_B \sim 200$  mW/cm<sup>2</sup>,  $\Delta OD$  change  $\sim 10\%$ ) (frame B) were obtained under line narrowing and non-line narrowing conditions, respectively. The exciton splitting is indicated by the lower solid arrows. Note the low energy shoulder at  $\sim 684$  nm (dashed arrows).

coincident with the burn wavelength ( $\lambda_B$ ) at 680.5 nm. The width of the ZPH is  $5.5 \text{ cm}^{-1}$  (see inset of Fig. 11) which corresponds to a P680\* lifetime of 1.9 ps, in agreement with our previous determinations. The broader feature just to the left of the ZPH is the pseudo-phonon sideband hole with a mean phonon frequency ( $\omega_m$ ) of  $\sim 20 \text{ cm}^{-1}$ . Spectrum b is the transient hole burned spectrum obtained under non-line narrowing conditions with  $\lambda_B = 665.7 \text{ nm}$ . In both spectra the hole profile centered near 681 nm is predominantly due to P680. However, both have a distinct shoulder at  $\sim 684 \text{ nm}$  (dashed arrow). The positive increase in absorption with an apparent maximum near 675 nm and the broad and relatively weak hole near 668 nm (to the blue of the absorption maximum at 670 nm in frame A) will be discussed in section IV.C.

Spectrum a of frame B in Fig. 2 is of the type reported in our earlier work for  $\lambda_B$  in the near vicinity of 680 nm. Preliminary theoretical calculations of the  $\lambda_B$ -dependence of the P680 hole profile [38] led to a value for the phonon Huang-Rhys factor ( $S$ ) of  $\sim 2$  for P680 which is equal to that determined for P870 of *Rb. sphaeroides* [17] and P960 of *Rps. viridis* [16]. The intensity of the ZPH relative to the intensity of the overall profile in a spectrum such as spectrum a of frame B in Fig. 2 is given approximately by  $\exp(-2S)$  [18]. The results of our analysis of the  $\lambda_B$ -dependence of the P680 hole profile for the 4 Chl *a*-RC preparation still indicate that  $S \sim 2$  and that the inhomogeneous broadening of P680 of the RC is  $\sim 100 \text{ cm}^{-1}$ , cf. section IV.C. This broadening is similar to that observed for P870 [17] and P960 [18].

As indicated in ref. 13, an understanding of the observed differences in the low temperature absorption spectra of the PS II RC and the nature of the 684 nm band requires spectroscopic studies of samples with different and known Chl *a* content. The 4.2 K absorption spectra of the RC containing 4, 5 and 6 Chl *a* are shown as curves a, b and c in

Fig. 3. The relative intensities of the spectra shown were determined by requiring that the intensities of the  $Q_x$ -band of Pheo *a* at 543 nm be equal, see inset. It is important to note that the 543 nm absorption profiles are identical and the same as that shown in the preceding paper for the CP47-RC complex. The extent to which the Pheo *a*  $Q_x$ -band is resolved is illustrated by the inset spectrum of Fig. 2A. From this spectrum it is obvious that the very weak vibronic bands which build on the  $Q_y$ - and  $Q_x$ - Chl *a* origin bands would be diffuse and only contribute to the broad background absorption which underlies the sharp Pheo *a* band at 543 nm. Therefore, subtraction of the baseline absorption, which yielded the inset spectra of Fig. 3, renders the interference of the 543 nm band by Chl *a* absorption negligible. Taking the Chl *a* content of the sample from which spectrum c was obtained to be 4 and integrating the three spectra out to 660 nm led [54] to Chl *a* contents for spectra a and b of close to 6 and 5, i.e., values which are, within experimental uncertainty, the same as those determined by the biochemical procedure described in section II.

As will become apparent, it is informative to examine the difference between the absorption spectrum of the 4 Chl *a*-RC and those of the 6 Chl *a*-RC and 5 Chl *a*-RC. They are shown, respectively, as curves b and c in Fig. 4. Curve a is the absorption spectrum of the 4 Chl *a*-RC. The features and intensity distributions for the two difference spectra are quite similar. They are to be compared with spectrum b of Fig. 5, which is the difference between the absorption spectrum of a sample from one of the three CP47-RC preparations studied and that of the 4 Chl *a*-RC. The CP47-RC preparation chosen is characterized by a spectrum with the least amount of absorption at ~684 nm and ~670 nm (due to non-native Chl *a*), *vide infra*. Spectrum b of Fig. 5, like spectra b and c of Fig. 4, exhibits bands near 683 and 677 nm as well as a more pronounced shoulder at ~670 nm. Spectrum a of Fig. 5

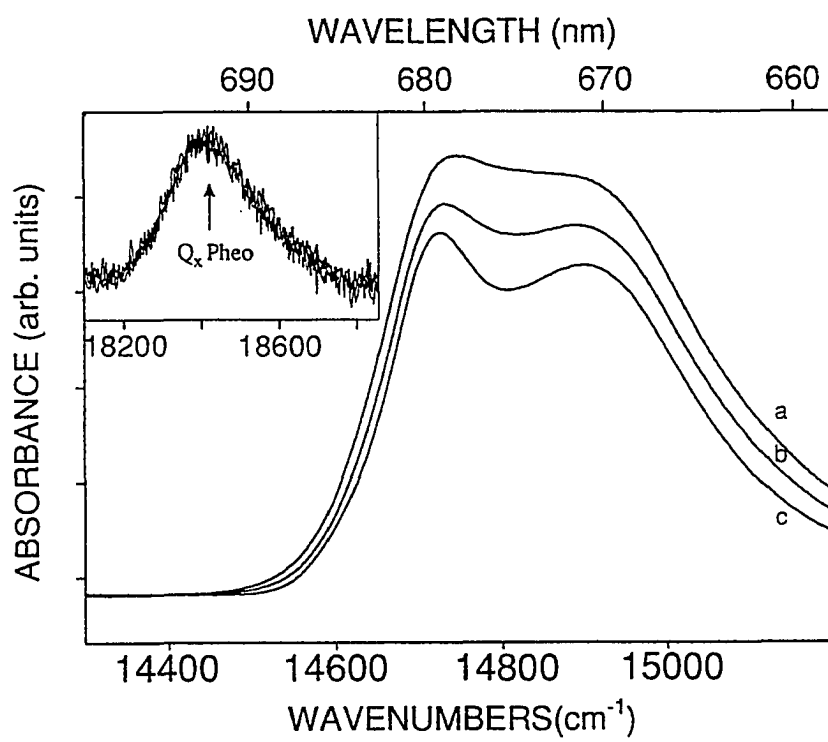


Figure 3. Low temperature (4.2 K) Q<sub>y</sub>-absorption spectra of 6 Chl *a*-RC (a) 5 Chl *a*-RC (b) and 4 Chl *a*-RC (c) complexes. The spectra were normalized to the same intensity of the Q<sub>x</sub> band of Pheo *a* (see insert).

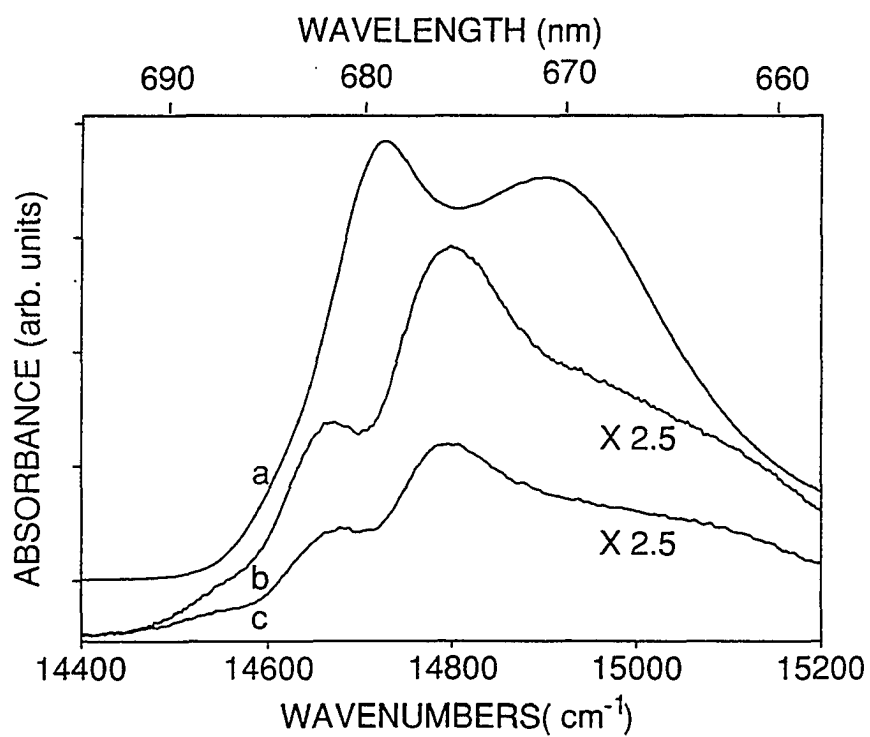


Figure 4. Low temperature (4.2 K) absorption spectrum of the 4 Chl *a*-RC complex (curve a). Curves b and c (multiplied  $\times 2.5$ ) correspond to the difference between the absorption spectrum of the 4 Chl *a*-RC and those of the 6 Chl *a*-RC and 5 Chl *a*-RC.



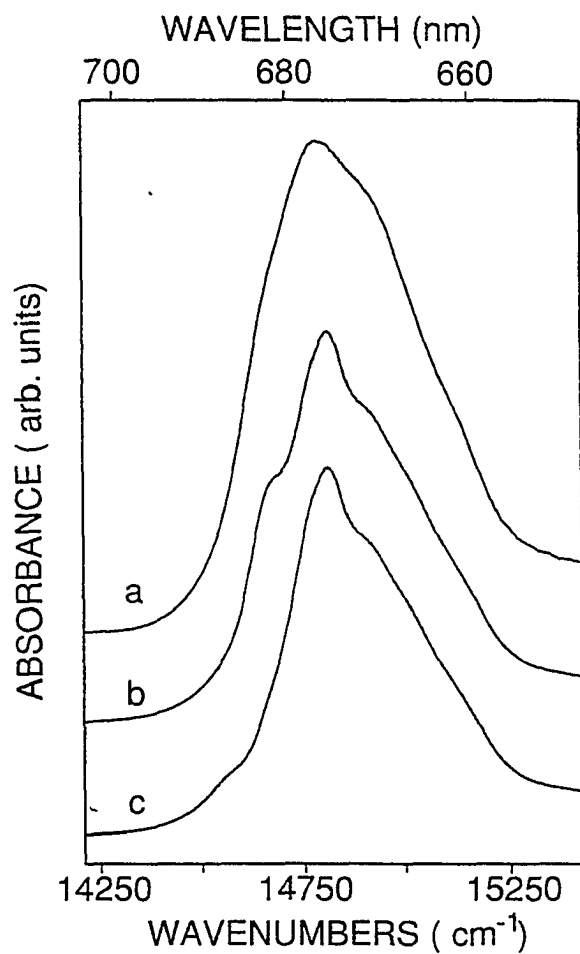


Figure 5. Low temperature (4.2 K) absorption spectrum of CP47 complex (curve a). Spectrum b corresponds to the difference between the absorption spectrum of CP47-RC complex (spectrum c in Figure 6) and that of 4 Chl *a*-RC. Spectrum c was obtained from spectrum by subtracting out the ~684 nm band (see text for discussion).

is the absorption of the CP47 sample which contains less absorption at 670 nm due to non-native Chl *a* than the CP47(I) sample reported on in the accompanying paper [14]. In that paper it was shown that the contribution to absorption at 670 nm due to non-native Chl *a* molecules varies significantly from preparation to preparation. It is reasonable to assume that some amount of non-native Chl *a* still contaminates the absorption at 670 nm in spectrum a of Fig. 5. With a slight reduction in the intensity at 670 nm, this spectrum would quite closely resemble spectrum b of Fig. 5, especially if allowance were to be made for larger inhomogeneous broadening of the spectral features for CP47 than for the CP47-RC minus 4 Chl *a*-RC difference spectrum. The suggestion of larger inhomogeneous broadening seems plausible given the additional step required to isolate CP47 from the CP47-RC complex and the fragility of the CP47 complex.

We turn next to the 4.2 K absorption spectra for the three CP47-RC preparations, Fig. 6. In the accompanying paper [14] spectrum c and that of the 4 Chl *a*-RC were used to determine a Chl *a*/CP47 content of  $14 \pm 2$ . The intensity of spectrum c in Fig. 6 relative to those of the spectra for the other two CP47-RC preparations (a and b) are set by the requirement that the intensities of their  $Q_x$ -Pheo *a* bands be equal, see inset in upper right hand corner. There are significant differences between the three absorption spectra of Fig. 6. In particular, spectra a and b possess considerably more absorption near 684 and 670 nm than spectrum c. The additional absorption near 684 nm for spectrum a relative to c is shown in the inset at the upper left hand corner. The major difference between spectra a and c at wavelengths shorter than 683 nm (not shown) can be assigned mainly to Chl *a* absorbing, relatively broadly, in the vicinity of 670 nm. Noting again that spectrum c led to a Chl *a*/CP47-RC content of  $18 \pm 2$  we determined, by integration of the three spectra in Fig. 6 out to 660 nm, that the corresponding number for the preparations corresponding to

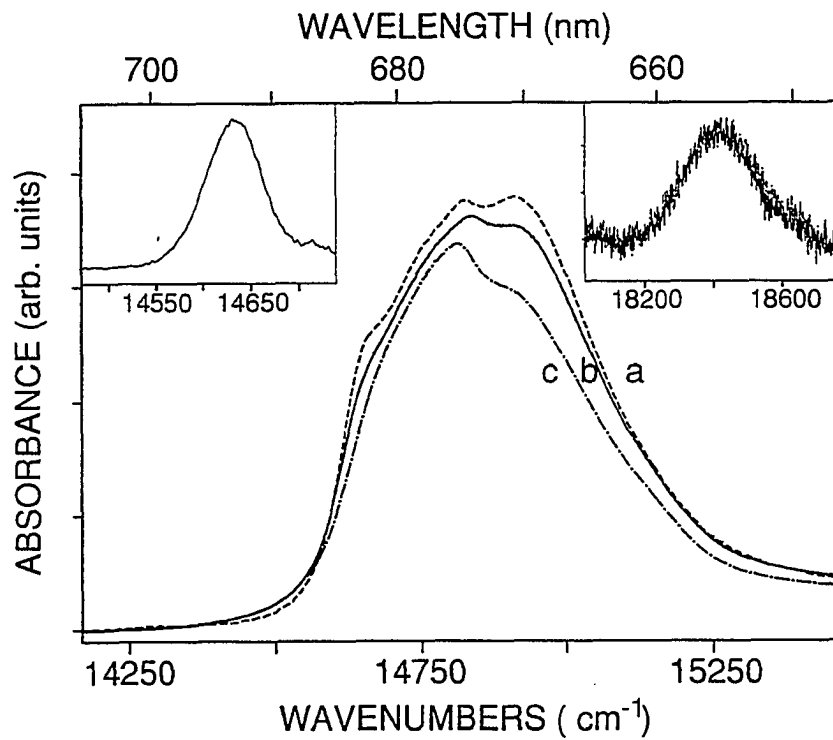


Figure 6. Low temperature (4.2 K) absorption spectrum (a, b and c) of three CP47-RC preparations normalized to same intensity of their  $Q_x$ -Pheo *a* bands (see upper right inset). The difference between spectra a and c (in the  $\sim 684$  nm region) is shown in the upper left inset.

spectra a and b is  $23 \pm 2$  and  $21 \pm 2$ , respectively. It is interesting that the variable contribution from the  $\sim 684$  nm absorbing Chl *a* molecules seen in CP47-RC preparations is observed for CP47 preparations [14] as well as RC preparations, *vide infra*. This is consistent with, but does not prove, the suggestion [3] that the 684 nm absorbing Chl *a* may be linker molecules associated with the core complex.

It is worthwhile, therefore, to explore the extent to which standard spectra for the 4 Chl *a*-RC, CP47 and the 684 nm absorbing Chl *a* can be used to simulate the spectra for RC samples with a Chl *a* content greater than 4. For the standard spectrum of the 684 nm Chl *a* we chose a Gaussian with a width of  $120 \text{ cm}^{-1}$  as determined in the preceding paper [14] on CP47. This is slightly wider than the apparent width of the 684 nm profile shown in the insert of Fig. 6. (It is shown later that higher energy absorption in the  $Q_y$ -region associated with the 684 nm absorbing Chl *a* is weak.) For the standard spectrum of a 4 Chl *a*-RC we used the experimental spectrum (a of Fig. 4) since the contribution to it from the 684 nm absorbing Chl *a* is small (equivalent to  $\sim 0.2$  Chl *a* molecules [55]). The spectrum used for CP47 is shown as curve c in Fig. 5. This spectrum was obtained from spectrum b of the same figure by subtracting out the  $\sim 684$  nm band. Note that in spectrum c there is weak feature near 687 nm. In the accompanying paper [14] hole burning was used to identify a 687 nm state of CP47 which is excitonically correlated with the lowest energy state at 690 nm. The three standard spectra were used to simulate the absorption spectra of the 5 Chl *a*- and 6 Chl *a*-RC samples, Fig. 7. The solid curves in frames A and B are the experimental spectra for the 5 and 6 Chl *a*-RC samples. The dashed curves are the simulated absorption spectra. The overall fits are quite reasonable. For the 5 Chl *a*-RC sample the simulation corresponds to an average composition of 4 Chl *a*-RC + 0.8 Chl *a* (CP47) + 0.2 Chl *a* (684 nm). The corresponding decomposition

for the 6 Chl *a*-RC is 4 Chl *a*-RC + 1.9 Chl *a* (CP47) + 0.4 Chl *a* (684 nm). Since the 4 Chl *a*-RC contains 0.2 Chl *a* (684 nm), *vide supra*, the 5 and 6 Chl *a*-RC sample would then contain, on average, 0.4 and 0.6 Chl *a* (684 nm), respectively. The %-contaminations (on a complex basis) by CP47 would be 6 and 13, respectively when the number of Chl *a* molecules per CP47 is taken to be 14, *vide supra*. Gel electrophoretic analysis of the 6 Chl *a*-RC preparation yielded an upper limit for the Chl *a* contamination from CP47 equal to 4% of the number of Chl *a*/CP47, cf. section II. A value of 14 for the latter number yields an average contamination of 0.6 Chl *a* per RC, substantially lower than the value of 1.9 determined above. Although it was shown, *vide supra*, that a Chl *a* content for CP47 as high as about 20 is possible, such a content leads only to an increase of 0.2 for the average number of contaminating Chl *a* per RC. The reason(s) for the discrepancy are unclear. It is worth noting, however, that one can simulate the 6 Chl *a*-RC absorption spectrum about as well as in Fig. 7 with a reduction in CP47 contamination of about a factor of 2 if the reduction is compensated for by the addition of a relatively broad ( $\sim 200 \text{ cm}^{-1}$ ) absorption at 670 nm from additional, perhaps non-native, Chl *a*.

The two transient triplet population bottleneck hole spectra for the 4 Chl *a*- and 6 Chl *a*-RC preparations shown in Fig. 8 confirm that the latter preparation has the greater contribution from the 684 nm absorbing Chl *a*. Spectra a and b correspond to the 4 and 6 Chl *a* preparations, respectively. Both were obtained under non-line narrowing conditions with  $\lambda_B = 665 \text{ nm}$ . In spectrum a (dashed line) the hole is dominated by a component with a maximum at 681 nm (i.e., P680), with a weaker feature due to the 684 nm state. The contribution from the 684 nm state in spectrum b is significantly greater. The inset of Fig. 8 shows the difference spectrum obtained by subtracting spectrum a from spectrum b. The profile of this spectrum, centered near 684 nm, is similar to that shown in the inset of

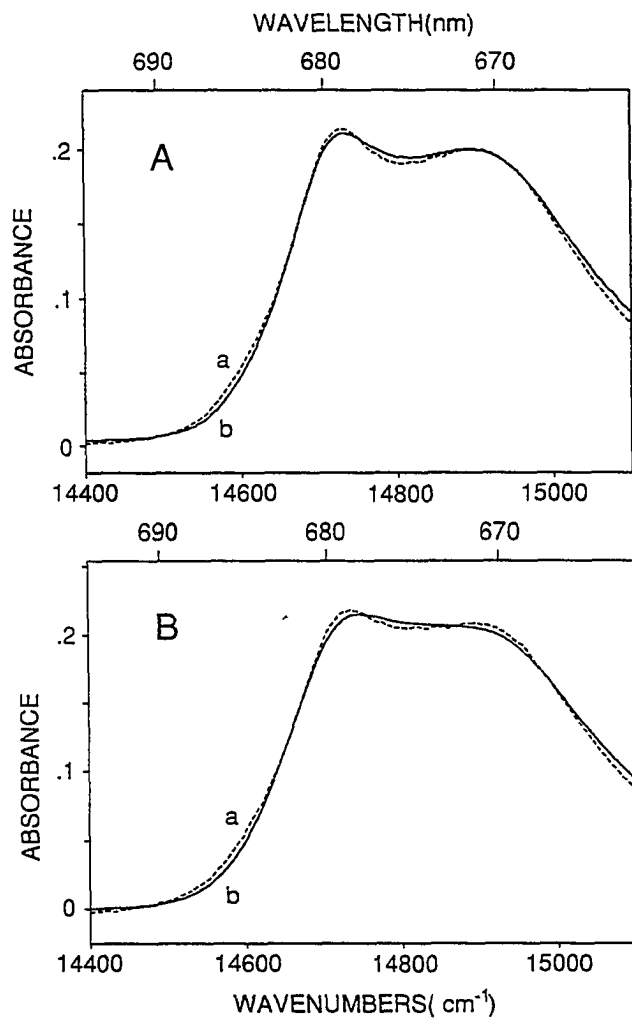


Figure 7. Low temperature (4.2 K) experimental (solid lines) and simulated (dashed lines) absorption spectra of the 5 Chl *a*-RC and 6 Chl *a*-RC are shown in frames A and B, respectively. See text for discussion.

Fig. 6 and, importantly, also spectrum B in Fig. 2 of CP47 given in the accompanying paper [14]. It is germane to note that the transient hole spectrum (non-line narrowed) of Kwa [34], for an RC sample assumed to contain 6 Chl *a* molecules, is quite similar to spectrum b of Fig. 8. This, together with a comparison of their 4.2 K absorption spectrum with those in Fig. 6, indicates that their RC preparation did possess a Chl *a* content much closer to 6 than 4. Our population bottleneck hole spectra for the 5 Chl *a*-RC preparation (not shown) also show that this preparation contains more 684 nm absorbing Chl *a* than the 4 Chl *a*-RC preparation. The difference absorption spectrum for these two preparations bears a strong resemblance to those shown in Fig. 4. Three additional preparations (~4.5, ~5.1 and ~5.7 Chl *a* per RC) were studied and yielded consistent results.

In the remainder of this section we present some additional, relevant results for the CP47-RC complex. Non-line narrowed, transient triplet-bottleneck hole spectra for the CP47-RC complex are shown in Fig. 9. Spectrum b is from the sample corresponding to absorption spectrum c of Fig. 6. Spectrum a was obtained following addition of a small amount of TX-100 detergent. The main effect is the narrowing and apparent shifting of the ~681 nm hole of spectrum b. The a – b difference spectrum (c) exhibits a feature at 684 nm. It is clear that P680 is the dominant contributor to the ~681 nm hole in spectrum b and that the smaller contribution from the 684 nm state is largely eliminated by TX-100. The same behavior from TX-100 is observed for the PS II RC [12]. Since spectrum b in Fig. 9 is from the sample with the smallest contribution from the 684 nm absorbing Chl *a* ( see spectrum c of Fig. 6), one would expect that the sample with the largest contribution (spectrum a of Fig. 8) should yield a transient hole spectrum that is more heavily contributed to by the 684 nm state. This spectrum is shown as curve d in Fig. 9 and is in accord with this expectation.

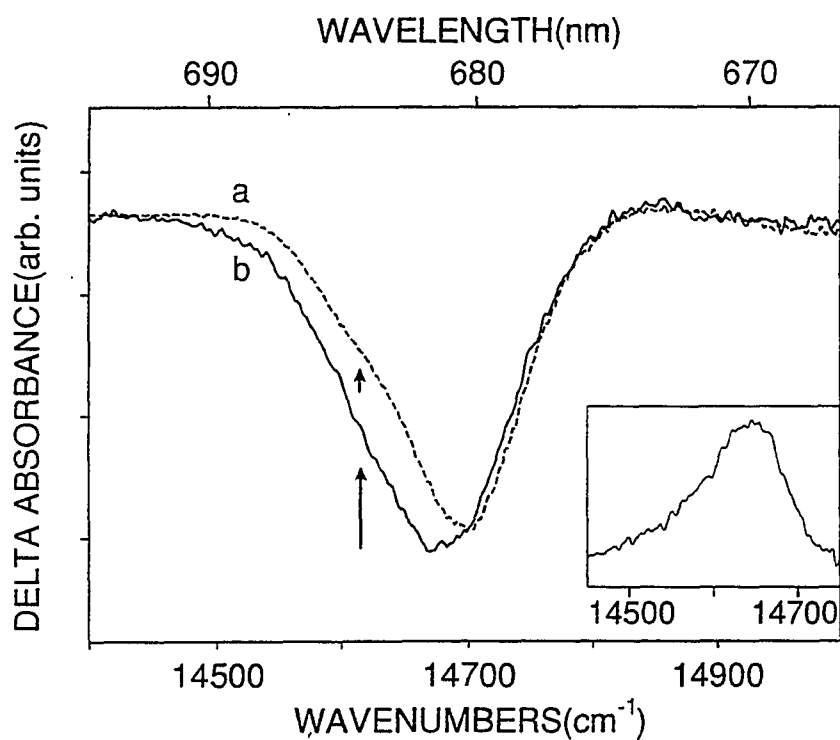


Figure 8. Transient triplet population bottleneck hole-burned spectra for the 4 Chl *a*-RC (a) and 6 Chl *a*-RC (b) preparations, respectively. Both spectra were obtained under non-line narrowing conditions with  $\lambda_B = 665$  nm.  $I_B \sim 200$  mW/cm<sup>2</sup>.  $\Delta OD$  changes at 680.4 nm in spectra a and b are 9.6% and 11%, respectively. The inset shows the difference spectrum between a and b in the 684 nm region.



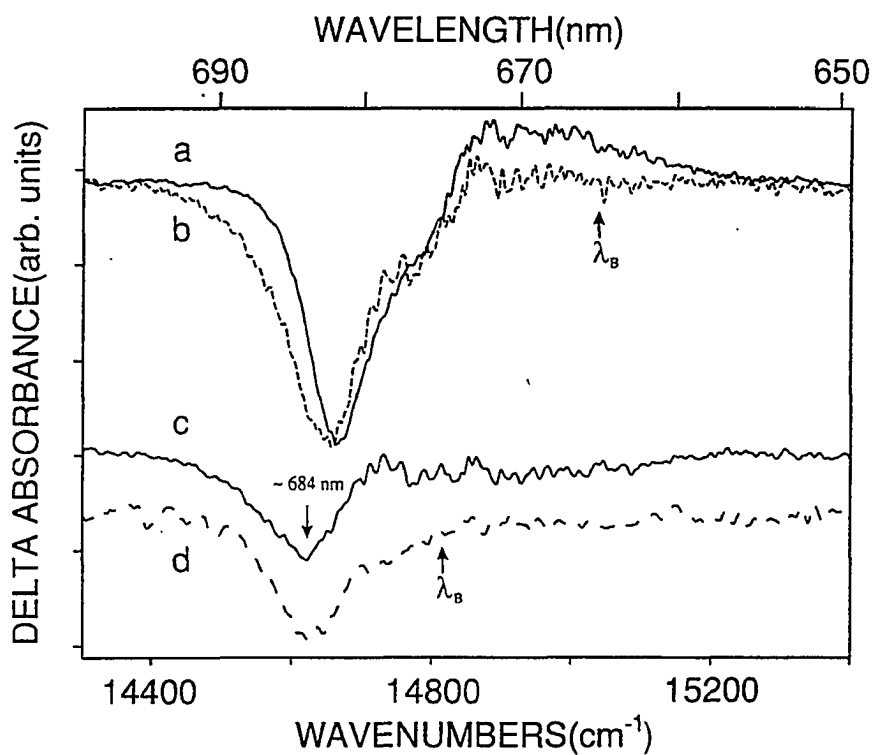


Figure 9. Transient (non-line narrowed) hole-burned spectra (4.2 K) of the CP47-RC complex in the absence (b) and presence of TX-100 detergent (a). Spectrum c corresponds to the difference b-a and curve d represents the transient hole-burned spectrum of the preparation with largest contribution from  $\sim 684$  nm state, see absorption spectrum a in Figure 6.

To conclude this section we present 4.2 K static fluorescence spectra of the CP47-RC complex which provide some support for the conclusions reached on the basis of the absorption and hole burned spectra. Fluorescence spectra for the sample whose absorption is least contaminated by disrupted Chl *a* and least contributed to by the 684 nm band (see spectrum c of Fig. 6) are shown as a and b in frame A of Fig. 10. Spectra a and b were obtained with  $\lambda_{\text{ex}} = 630$  and 400 nm, respectively. Both exhibit a dominant origin at  $\sim 690.3$  nm due to the lowest energy state of CP47 at 690 nm, see accompanying paper [14]. However, spectrum b exhibits relatively more fluorescence on the high energy side of 690 nm. The b – a difference spectrum (d) reveals a band at 684.5 nm. On the basis of the linear electron-phonon coupling analysis presented in the accompanying paper [14], this is precisely where one should expect the fluorescence origin of the 684 nm state to lie. Apparently, excitation at 400 nm produces relatively more 684.5 nm fluorescence, meaning that the 684 nm state is not totally efficient in transferring energy to the 687 and 690 nm states of CP47 [14].

Spectrum c of Fig. 10A ( $\lambda_{\text{ex}} = 400$  nm) is from the CP47-RC sample which yielded the absorption spectrum (a of Fig. 6) with the largest contribution from non-native Chl *a* molecules and the 684 nm absorbing Chl *a*. The spectrum is dominated by broad fluorescence from non-native Chl *a* molecules in the vicinity of 670 nm and fluorescence from the 684 nm state at  $\sim 684.5$  nm. The tailing to lower energy of 684.5 nm is probably due to fluorescence from the 690 nm state of CP47.

In refs. 13 and 14 it was shown that the 690 nm state of CP47 undergoes quite efficient persistent nonphotochemical hole burning. Burning into this state produces a large response (satellite hole) of its excitonically correlated (and non-fluorescent) 687 nm state. The anti-hole of the holes associated with these two states are very substantially

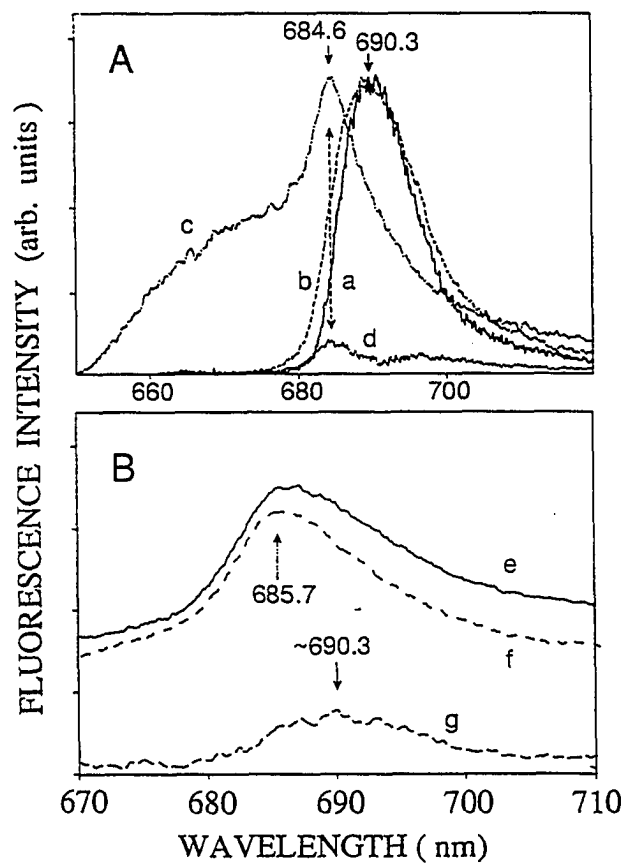


Figure 10. Low temperature (4.2 K) fluorescence spectra of two CP47-RC complexes obtained for  $\lambda_{\text{ex}} = 630$  nm (curve a) and  $\lambda_{\text{ex}} = 400$  nm (curves b and c), respectively. Curve d is the difference between spectra b and a (see text). Spectra e and f ( $\lambda_{\text{ex}} = 400$  nm) were obtained from the same sample as spectrum b after laser irradiation ( $\lambda_{\text{ex}} = 665$  nm) for  $t_{\text{B}} = 25$  min (e) and 40 min (f), respectively. Spectrum g is the e-f difference spectrum see text.

blue-shifted relative to the centroids of their respective holes, as has been observed for the  $Q_y$ -state of the active Pheo *a* of the PS II RC [9] and all of the many  $S_1(\pi\pi^*)$  states of molecules studied in amorphous hosts [56]. Thus, by burning to saturation, under non-linear narrowing conditions, one can grossly blue-shift all members of an inhomogeneous distribution of a particular state. Indeed, this is the essence of the approach used in our previous studies to produce line-narrowed triplet population bottleneck hole spectra of P680 free of contamination from a persistent hole burning contribution from the near-degenerate  $Q_y$ -state of a Pheo *a* molecule [38]. One should anticipate, therefore, that saturation hole burning might grossly affect the fluorescence spectrum. Spectra e and f of Fig. 10B establish that this is the case for the CP47-RC complex. Both spectra are for a sample from the same batch from which the sample used to acquire absorption spectrum c of Fig. 6 was obtained. The fluorescence spectrum ( $\lambda_{\text{ex}} = 400$  nm) which corresponds to the latter spectrum is curve b of Fig. 10A, peaked at 690.3 nm. Fluorescence spectra e and f were obtained ( $\lambda_{\text{ex}} = 400$  nm) following extended irradiation at 665 nm for 25 and 40 min, respectively. The fluorescence profiles of both spectra are peaked near 685 nm, over 5 nm to the blue of the fluorescence profile of spectrum b. Spectrum e still contains a contribution from the 690 nm state of CP47 as evidenced by the e-f difference spectrum (g). The fluorescence in spectra e and f is most likely due to the 684 nm state. The extent to which the extended irradiations, which lead to a markedly diminished fluorescence from the 690 nm state, are due to blue-shifting of the 690 nm state or the structural transformation associated with nonphotochemical hole burning is unclear.

#### IV. Further Discussion

The question of the Chl *a* content of the isolated D1-D2-cyt b<sub>559</sub> reaction center complex has been and continues to be of very considerable interest. Different isolation

procedures have led to preparations of RC with a Chl *a* content ranging between about 4 and 6. These procedures have been used to provide samples which have been used for time and frequency domain studies of the excited state electronic structure and transport properties of the RC. However in most of these studies the actual Chl *a* content of the RC sample(s) used was not determined (but often assumed on the basis of the isolation procedure employed). It was our difficulties with the interpretation of the low temperature absorption and hole burned spectra of RC samples of unknown Chl *a* content that led to the present paper in which results for 4, 5 and 6 Chl *a* content RC are reported. At the same time it was apparent that companion studies of the CP47 and CP47-RC complexes were also important for addressing the above question [13]. Taken as a whole, the results establish that 684 nm absorbing Chl *a* molecules and contamination of the RC by CP47 are important for understanding the differences between different RC samples.

The Chl *a* contents of 4, 5 and 6 molecules for the three RC preparations studied were determined by the biochemical procedure described in section II. It was shown that their  $Q_y$ -absorption spectra normalized to the same intensity of the  $Q_x$ -band of Pheo *a* are consistent with the relative Chl *a* contents. Even though the absorption spectrum of the 4 Chl *a*-RC (Fig. 3) is contributed to by the 684 nm band, its contribution relative to those for the 5-Chl *a* and 6 Chl *a*-RC is smaller (small enough so that the average number of associated Chl *a* molecules is within the uncertainty limits of the biochemical determination of the Chl *a* content of the 4 Chl *a*-RC preparation, see section II). It also follows that contamination of the 4 Chl *a*-RC by CP47 is small. Thus, the 4.2 K absorption spectrum of the 4 Chl *a* RC shown in Fig. 3(c) can serve as a fingerprint for a good (but probably not perfect) 4 Chl *a* RC preparation. Using this spectrum as a standard for the 4 Chl *a* RC and others for CP47 and the 684 nm absorbing Chl *a* (cf. section III), it proved possible to

simulate, quite well, the 4.2 K absorption spectra of RC samples containing more than 4 Chl *a* molecules (cf. Fig. 7 and discussion in section III) as superpositions of the three "standard" spectra. However, the value obtained from the simulation for the average number of CP47 Chl *a* molecules per RC should be viewed as an upper limit since the contribution to the absorption spectrum of high Chl *a* content RC from non-native Chl *a* absorbing at ~670 nm is ignored. For example, spectra a and b of Fig. 9 prove that the 684 nm absorbing Chl *a*, when disrupted, absorb at ~670 nm. There is also the question of the validity of our choice for the standard spectrum of CP47, cf. following subsection.

In what follows we consider first the nature of the 684 nm absorbing Chl *a* molecules of the PS II RC and the question of the Chl *a* content for the isolated RC. This is followed by discussion on the question of the nature of the primary electron-donor state, P680\*, of the D1-D2-cyt b559 RC of PS II.

#### **A. The 684 nm State (Band) Of The PS II Reaction Center**

The nature of this state of the D1-D2-cyt b559 RC has been previously considered. van Kan et al. [35] concluded that the weak 684 nm band (relative to P680) is the lower dimer component of the special pair of the RC, with the upper dimer component absorption of the special pair, P680, possessing a much higher absorption cross-section (a reversal of the situation in the bacterial RC). This group later argued against this assignment [36]. Certainly, the observation that the detergent TX-100 eliminates the 684 nm band but has little effect on P680 [13], coupled with the finding that there is a significant variation in the contribution of the 684 nm band to the low energy side of P680 for the 4, 5 and 6 Chl *a* RC preparations, cf. section III, disproves this hypothesis. Recently Kwa [34] reported on the results of triplet population bottleneck hole burning experiments on an RC preparation assumed to contain 6 Chl *a* molecules and explored the suggestion by van der Vos et al.

[20] and Otte et al. [36] that the 684 nm band is probably due to a second pool of P680. With this interpretation, P684 is a manifestation of gross heterogeneity; P684\*, like P680\*, serves as a primary donor state but for a different subset of RCs. There are difficulties with the heterogeneity-induced two-pool hypothesis. Why should P684 be so sensitive to TX-100 and P680 not be and why should the isolation procedure used to produce the 4 Chl *a* preparation reported on here be so selective against the subset of RC characterized by P684?

We explore, therefore, other interpretations. To this end we summarize the key findings of the present and accompanying paper [14] and earlier ones [13]:

1. A 684 nm band is observed for the D1-D2-cyt b<sub>559</sub> RC complex, and the isolated CP47 and CP47-RC complexes. For each complex the 684 nm state gives rise to transient population bottleneck hole burning. For the CP47 complex (minimally contaminated by non-native Chl *a* molecules) the transient spectrum is dominated by the 684 nm absorbing Chl *a* molecules (state). The transient hole spectra of the RC are dominated by P680 and a 684 nm state (see also Kwa [34]) with the intensity contribution from the latter being the weakest for the 4 Chl *a*-RC preparation.
2. The intensity contribution of the 684 nm band to the absorption and hole spectra of the RC, CP47 and CP47-RC complexes is highly variable. The addition of the detergent TX-100 to the glass-forming solvent eliminates the 684 nm band of the RC [13], of the CP47-RC complex (see Fig. 9) and of the CP47 complex (results not shown). This effect is accompanied by enhanced absorption at ~670 nm due to non-native Chl *a* molecules which undergo efficient persistent nonphotochemical hole burning (ref. 12 and unpublished

results).

3. Persistent nonphotochemical and transient population bottleneck hole burning data prove that the 684 nm band of CP47 is predominantly inhomogeneously broadened ( $\Gamma_{inh} \sim 120 \text{ cm}^{-1}$ ) and characterized by weak electron-phonon coupling ( $S \sim 0.2$ ,  $\omega_m \sim 20 \text{ cm}^{-1}$ ). The ZPH widths of the 684 nm state are  $\sim 1 \text{ cm}^{-1}$ , considerably sharper than the  $5\text{-}6 \text{ cm}^{-1}$  ZPH widths of P680 in the RC and CP47-RC complexes.

These results establish that the 684 nm Chl *a* molecule(s) bind to regions of the CP47 and RC protein subunits which are highly accessible to detergent molecules. This raises the possibility that they bind to the exterior of the protein. Affording support for this suggestion is our finding that the 684 nm Chl *a* content of RC preparations decreases with increasing time of washing on the anionic exchange column, cf. sections II and III. The results obtained thus far are consistent with, but do not prove, the suggestion [3] that the 684 nm Chl *a* are linker-type molecules associated with the PS II core complex rather than any particular subunit (e.g., CP47, RC) thereof. With this explanation one would not need to explain why both CP47 and the RC possess intrinsic Chl *a* absorbing at 684 nm with similar properties. However, that the 684 nm Chl *a* absorb  $\sim 90 \text{ cm}^{-1}$  to the red of P680 suggests that the 684 nm Chl *a* is either a dimer or a monomer with a special protein configuration. Either way, the linker concept would seem to demand that the 684 nm Chl *a* be associated with a low molecular weight protein (otherwise, the 684 nm Chl *a* would not survive the isolation of the RC from CP47). Although a 4.8 kDa protein of unknown function is observed by gel electrophoresis of PS II RC [57,58], we are not



aware of any works that have identified this protein by gel electrophoresis of CP47. This argues in favor of the interpretation that has both CP47 and the RC possessing 684 nm absorbing Chl *a*. Interestingly, our hole burning studies of the CP43 antenna complex have proven that its lowest energy state is at ~684 nm (unpublished results). Whichever of the two interpretations for the 684 nm Chl *a* observed for CP47 and the RC is correct, it is not unreasonable to view them as linker-type from the point of view of inter-complex energy transfer. The 684 nm state is within  $kT$  (room T) of the lowest energy 690 nm state of CP47 and P680\* of the RC is also thermally accessible from the 684 nm state. For *Rb. sphaeroides* the lowest energy state of the proximal antenna complex lies below the primary electron-donor state by  $\sim kT$  [59]. It is difficult to understand why the 684 nm Chl *a* would be superfluous to energy transfer within the core complex of PS II.

We consider next the approach used to simulate the absorption spectra of RC preparations with a high Chl *a* content, Fig. 7. With reference to the discussion in section III of this figure, it is clear that the approach is a reasonable one when the proper domicile of the 684 nm Chl *a* molecules is the CP47-RC complex. It would not be if both CP47 and the RC are characterized by intrinsic, 684 nm absorbing Chl *a*. Further work is required to ascertain whether this is the case. However, the fact that the 684 nm Chl *a* are so fragile promises to make the solution a difficult one. In any event, the simulation procedure is certainly valuable for estimating how much 684 nm Chl *a* and CP47 are present in RC preparations.

#### **B. The Chlorophyll a Content Of The PS II Reaction Center**

The present work establishes that RC preparations of high (>4) Chl *a* content are heterogeneous. A typical preparation must be considered to contain 4 Chl *a*-RC, 4 Chl *a*-RC bound to 684 nm Chl *a*, 4 Chl *a*-RC bound to CP47, etc. It is also possible

that RC preparations are generally contaminated by some non-native Chl *a* absorbing near 670 nm. On the basis of the results presented, we conclude that the number of Chl *a* molecules belonging to the interior (hydrophobic) region of the RC is 4 (as in the bacterial RC). If one assumes that the 684 nm absorbing Chl *a*, which have been identified in RC preparations, are of the linker-type (associated with the core complex), then the conclusion that the PS II RC possess 4 Chl *a* molecules is unavoidable. If one assumes that the 684 nm absorbing Chl *a* seen in RC preparations are intrinsic to the RC complex, then the number of Chl *a* molecules associated with the RC is six. But if the 684 nm Chl *a* are bound to the exterior region of the RC protein complex, as our results suggest, one could consider the 684 nm absorbing Chl *a* to be important only in energy transfer, but not in primary charge-separation. From this point of view the number of Chl *a* molecules in the interior of the RC is still four.

### C. Electron-Phonon Coupling And Nature Of P680

We had argued that P680 is probably a dimer because the electron-phonon (protein) coupling for the  $P680^* \leftarrow P680$  transition is as strong as that for the  $P^* \leftarrow P$  transitions of bacterial RC, cf. section I. The assumption made was that the primary donor state of a dimer is well suited and placed for mixing with charge-resonance and/or charge-transfer states of the RC. The results of electronic structure calculations [30,31] and dynamical simulations [60] for the bacterial RC provided support for this assumption. Furthermore, the dipole moment change for the  $P^* \leftarrow P$  transition in bacterial RC is very large [27-29]. Also important for our current reasoning is that the lowest energy exciton levels, B875 and B895, of, respectively, the B800-B850 and B870 antenna complexes of *Rb. sphaeroides* are characterized by weak coupling [59] even though the B850 and B870 bands are associated with an excitonically coupled tetramer of BChl *a* molecules. In fact,

all  $Q_y$ -states of antenna protein complexes studied thus far exhibit weak coupling [13]. This is also true of the active Pheo  $a$  and accessory Chl  $a$  molecules of the PS II RC and the  $Q_y$ -states of the accessory BChl and BPheo molecules of the bacterial RC [16,17]. However, although the coupling to low frequency protein phonons for  $P680^*$  is as strong as for  $P^*$  of the bacterial RC, the coupling to the special pair marker mode (pseudo-localized phonon) was not observed. For  $P870$  and  $P960$  of *Rb. sphaeroides* and *Rps. viridis* the marker mode frequency is 120 and 145  $\text{cm}^{-1}$  with Huang-Rhys S-factor values of 1.5 and 1.1, respectively [16,17]. Thus, a strict analogy between the coupling characteristics of  $P680^*$  and those of  $P870^*/P960^*$  was not established.

In this subsection  $\lambda_B$ -dependent hole spectra of the 4 Chl  $a$ -RC of PS II are presented which allow us to examine more closely the question of  $P680^*$  coupling to a "marker mode." The question of whether or not  $P680$  is a dimer is also addressed. We emphasize that we consider strong electron-phonon coupling, by itself, to only be a signature for the primary electron-donor state. That is, it is suggestive but not proof positive that the primary donor is a dimer.

Figure 11 shows triplet bottleneck hole spectra for the 4 Chl  $a$ -RC preparation obtained for five  $\lambda_B$ -values; 683.6, 682.6, 681.4, 680.5 and 679.6 nm. In each spectrum the zero-phonon hole (ZPH) is coincident with the burn wavelength. The ZPH is accompanied by the real- and pseudo-phonon sideband holes (PSBH) at  $\sim +20$  and  $\sim -20 \text{ cm}^{-1}$ , respectively, relative to the position of the ZPH. The PSBHs for spectra c and d are indicated by the short solid arrows. Given the optical density changes associated with the dominant hole profile in each spectrum, cf. figure caption, it is apparent that the spectra are characteristic of strong electron-phonon (protein) coupling. For the moment we focus only on the dominant hole profile in each spectrum. The weak features indicated by the

dashed and solid (long) arrows are considered later. Using the theory of hole profiles reviewed in refs. 13 and 61, we attempted to fit the P680 profiles shown in Fig. 11. The best overall agreement is shown in Fig. 12 and was obtained with  $S = 1.9$ ,  $\omega_m = 20 \text{ cm}^{-1}$ , a 1-phonon profile width of  $27.5 \text{ cm}^{-1}$  (cf. caption), an inhomogeneous width ( $\Gamma_{inh}$ ) for P680 of  $100 \text{ cm}^{-1}$ , a center frequency of  $14653 \text{ cm}^{-1}$  for the zero-phonon line (ZPL) Gaussian distribution and a width of  $3.5 \text{ cm}^{-1}$  for the ZPL width. The ZPL width used is larger than that expected ( $2.5 \text{ cm}^{-1}$ ) from the 2 ps lifetime of P680\* because the read resolution used for recording the spectra was  $4 \text{ cm}^{-1}$ , see inset spectrum of Fig. 11 and caption. Comparison of the spectra in Figs. 11 and 12 reveals that the theoretical fits account reasonably well for the dependencies of the ZPH, real- and pseudo-PSBH hole intensities on  $\lambda_B$ . However, they are by no means completely satisfactory. For example: (i) for spectra d and e the experimental profile falls off more rapidly than the theoretical profile to higher energy of the ZPH. The steepness of the drop-off in spectra d and e, of Fig. 11, suggests some type of interference; (ii) the intensity of the pseudo-PSBH relative to that of the real-PSBH in spectrum a of Fig. 11 is significantly higher than in spectrum a of Fig. 12; and (iii) the shoulder at 684 nm seen clearly in the c, d, and e experimental spectra is absent in the theoretical spectra. Despite these discrepancies we conclude, based on a large number of theoretical calculations, that the values given above for the variables used to generate the spectra in Fig. 12 are accurate. They are in good agreement with those we reported previously even though the  $\lambda_B$ -dependence of the hole profile shown in Fig. 11 is far more detailed.

Discrepancy (iii) is due to the fact that the theoretical fitting does not account for the contribution to the population bottleneck hole spectra from the 684 nm absorbing Chl *a*. Thus, it is not a real discrepancy. We have subtracted the non-line narrowed

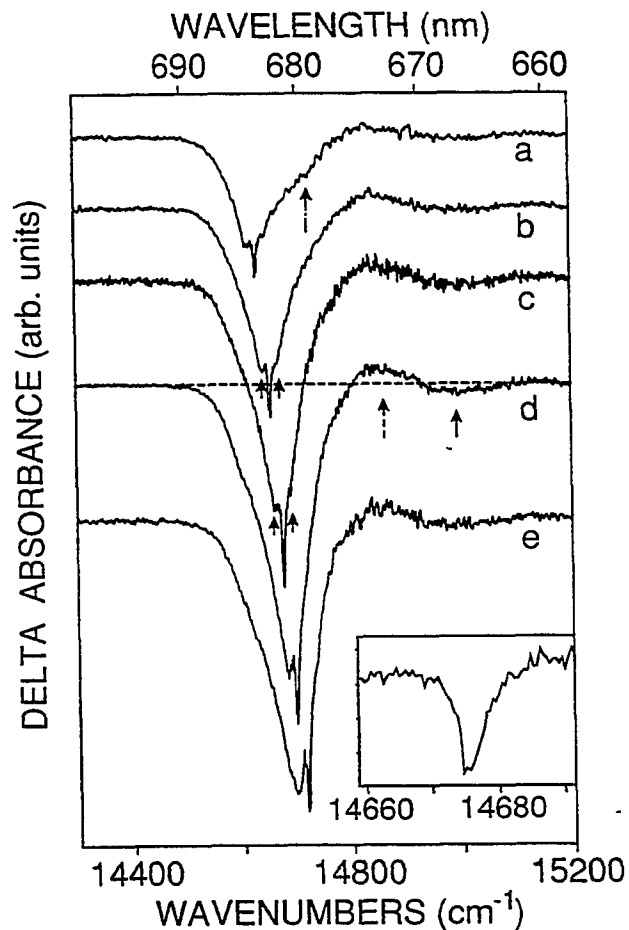


Figure 11. Low temperature (4.2 K) transient triplet bottleneck hole-burned spectra from the 4 Chl *a*-RC preparation. Burn intensity,  $\lambda_B$ , and  $\Delta OD$  change at the ZPH are (a) 330 mW/cm<sup>2</sup>, 683.6 nm, 20% (b) 370 mW/cm<sup>2</sup>, 682.6 nm, 15% (c) 400 mW/cm<sup>2</sup>, 681.4 nm, 23% (d) 400 mW/cm<sup>2</sup>, 680.5 nm, 22% (e) 360 mW/cm<sup>2</sup>, 679.6 nm, 17%, respectively. Read resolution is 4 cm<sup>-1</sup>. The inset shows the higher resolution (1 cm<sup>-1</sup>) scan of the zero-phonon hole at 681 nm. The ZPH width = 5.9 cm<sup>-1</sup>,  $T_B = 4.2$  K.

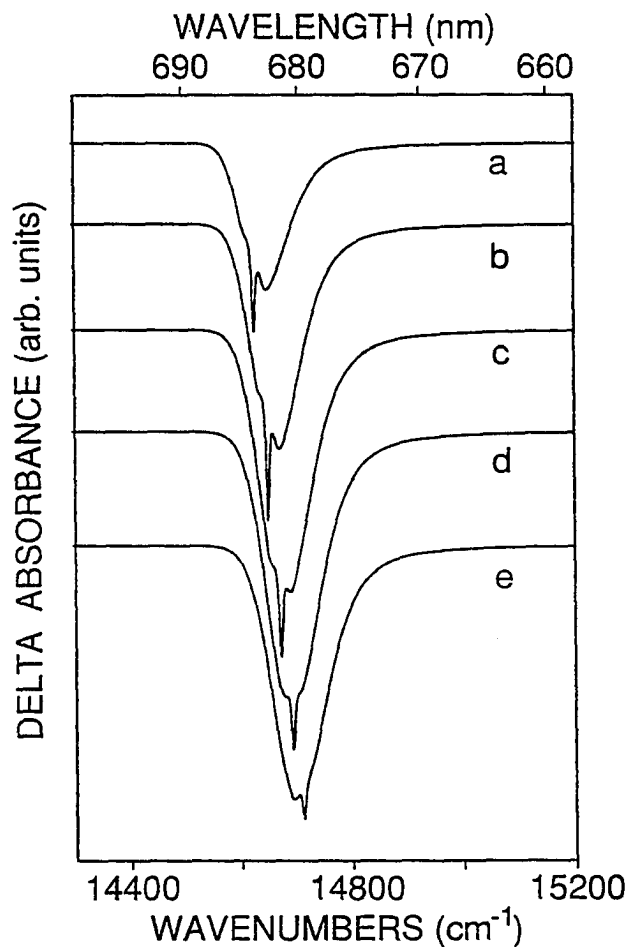


Figure 12. Simulated transient hole-burned spectra obtained for  $S = 1.9$ ,  $\omega_m = 20 \text{ cm}^{-1}$ ,  $\Gamma = 27.5 \text{ cm}^{-1}$ ,  $\Gamma_{inh} = 100 \text{ cm}^{-1}$ , and  $\gamma = 3.5 \text{ cm}^{-1}$ , with the center of the site distribution function at  $14653 \text{ cm}^{-1}$ . One-phonon profile ( $\Gamma$ ) on low and high energy sides is a Gaussian (half-width =  $10 \text{ cm}^{-1}$ ) and Lorentzian (half-width =  $17.5 \text{ cm}^{-1}$ ), respectively.

contribution from the 684 nm Chl *a* to the c, d and e spectra in Fig. 11 and refit the resulting spectra. The results (not shown) reveal that there is no significant change in the values of the theoretical variables used to generate the spectra in Fig. 12. Discrepancy (ii) is also attributed to the 684 nm absorbing Chl *a*. The burn-wavelength ( $\lambda_B$ ) used for spectrum a of Fig. 11, 683.6 nm, is close to the maximum of the absorption of the 684 nm Chl *a* and on the low energy tail of P680. Thus, we believe that this discrepancy is due to a line-narrowed interference from the 684 nm Chl *a*. Resolution of the first discrepancy, (i), is more difficult. This is because it depends on whether P680 is a monomer or a dimer.

On the basis of circular dichroism spectra, Braun et al. [62], Otte et al. [36] and Tetenkin et al. [63] concluded that P680 is a dimer with the upper component located near 666 nm. The hole spectra in Fig. 11 offer additional support because of the appearance of the weak satellite hole at 667 nm (long solid arrow). this hole lies  $\sim 300 \text{ cm}^{-1}$  to higher energy of the centroid of the P680 hole profile. The possibility that the  $\sim 300 \text{ cm}^{-1}$  hole is a vibronic feature building on the P680 origin hole can be dismissed because the hole spectra exhibit no higher energy satellite features (not shown). Although Chl *a* exhibits an excited state fundamental at  $340 \text{ cm}^{-1}$ , this mode is much weaker in the  $S_1(Q_y) \leftarrow S_0$  absorption spectrum than the most intense mode at  $\sim 720 \text{ cm}^{-1}$  [64]. The hole spectra of Kwa [34] also reveal a weak satellite feature near 667 nm. Importantly, Kwa determined that the 667 nm feature carries a polarization nearly opposite to that of the P680 hole. This and its weak absorption intensity are properties shared by the upper dimer component ( $P_+$ ) of the special pair of bacterial RC, e.g., *Rps. viridis* [65]. The above results suggest that two monomers contribute to P680. Since their excitonic interaction is only  $\sim 150 \text{ cm}^{-1}$  and the  $Q_y$ -absorption spectrum spans only  $\sim 500 \text{ cm}^{-1}$ , it is possible that more than two monomers make a significant contribution. An argument against this is given in section

IV.C. In any event, one should expect an interference to the hole spectra from the ground state absorption of a monomer since EPR [66] and absorbance detected magnetic resonance [20] measurements have shown that the triplet of the primary donor is localized on a single Chl *a* molecule. From Fig. 11 one observes that the only positive  $\Delta$ -absorbance is near 673 nm (dashed arrow). Its weakness suggests that it may be the high energy tail of a monomer band which interferes almost completely with the P680 hole.

We have followed up on this suggestion by correcting the hole spectra (b-e) for the interference and theoretically fitting the corrected spectra. The most satisfactory overall fitting was obtained with a monomer absorption profile centered at  $\sim 678$  nm and with a width of  $\sim 200$   $\text{cm}^{-1}$ . The integrated intensity of this profile was set equal to that of the P680 hole. The fits are not shown because they are not particularly noteworthy. For example, they do not lead to a much improved description of the PSBH regions of spectra d and e in Fig. 11. However, it is worthwhile showing some fits to the non-line narrowed hole spectrum. Figure 13 shows three sets (a, b, c) of spectra. The dot-dash spectrum of set a is the experimental spectrum. The solid spectrum in each set is the experimental spectrum corrected for the aforementioned monomer absorption and the contribution from the 684 nm Chl *a*. The dashed profiles are fits. The fit in set a was obtained with the values of the variables used for Fig. 12. Except for the fact that the fitted profile is shifted  $\sim 1$  nm to the red of the corrected experimental spectrum, it is quite good. The shift can be eliminated by moving the center of the ZPL frequency distribution to 682 nm. However, this results in a significant worsening of the theoretical fits to the line-narrowed spectra in Fig. 11. The fits in sets b and c of Fig. 13 were obtained by introducing a  $90$   $\text{cm}^{-1}$  mode which may be viewed as a potential analogue of the special pair marker mode of the bacterial RC. The Huang-Rhys factor used for this mode in set b and c is 0.3 and 0.5,



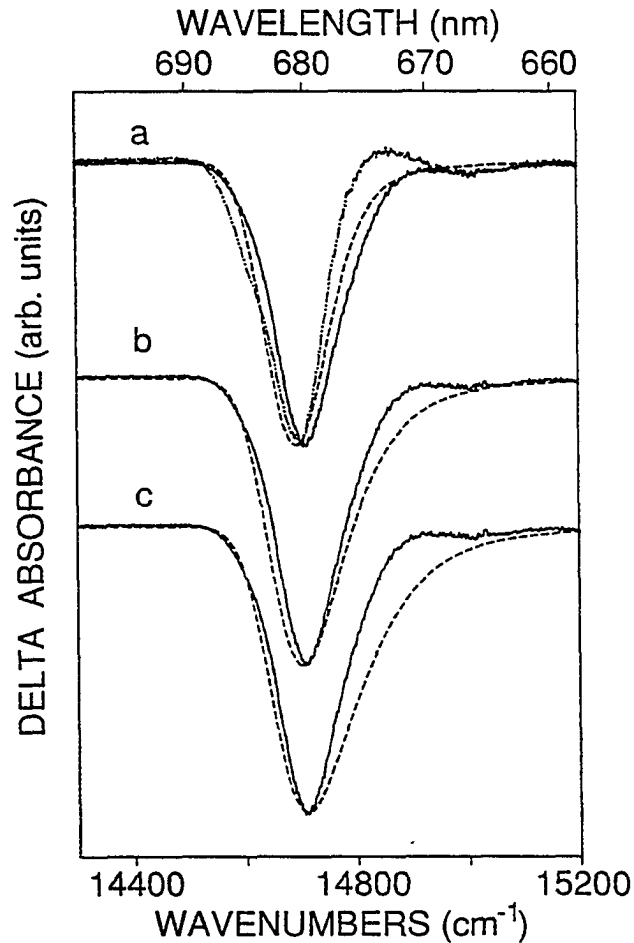


Figure 13. Experimental non-linear narrowed hole-burned ( $\lambda_B = 665$  nm,  $I_B \sim 200$  mW/cm<sup>2</sup>) spectrum of 4 Chl *a*-RC complex is shown in set a as the dashed-dotted line. The solid spectrum in each set is the experimental spectrum corrected for the monomer absorption (maximum at 678 nm, width = 200 cm<sup>-1</sup>) and the contribution from the 684 nm Chl *a* ( $\sim 0.15$  Chl *a*) (see text). The calculated spectrum (dashed line) in set a was obtained for the parameters given in the caption of Fig. 12. The calculated spectra in set b and c (dashed lines) were obtained by introducing a 90 cm<sup>-1</sup> mode with the Huang Rhys factor of 0.3 and 0.5, respectively (see text for details).

respectively. A homogeneous width of  $50 \text{ cm}^{-1}$  [16,17] was assigned to the  $90 \text{ cm}^{-1}$  mode. Although the maxima of these fits are close to that of the corrected spectrum, the widths are too large. We conclude that if a P680 "marker mode" exists, it is characterized by a small Huang-Rhys factor. The absorption spectrum (Fig. 2), itself, mandates a value considerably less than 1. We emphasize again that the values given above for the electron-phonon (protein) coupling parameters and  $\Gamma_{\text{inh}}$  for P680 are highly unlikely to be significantly changed in future theoretical fittings of the hole spectra from 4 Chl *a*-preparations.

The special pair marker mode (or, possibly, two closely spaced modes [17]) with its large Huang-Rhys factor is a unique signature of the special pair in the bacterial RC. It is an inter-monomer mode and, because of its low frequency, may be viewed as a pseudo-localized phonon. Its apparent absence in P680 offers additional support for the structure of the special pair in the PS II RC being significantly different than in the bacterial RC. We recall that the assignment of the state at 667 nm to the upper dimer component of P680 yields a dimer splitting,  $\sim 300 \text{ cm}^{-1}$ , that is much smaller than in the bacterial RC. In fact, the smallness of the splitting raises the possibility that the primary donor state,  $^1\text{P680}^*$ , cannot be understood simply in terms of the two monomers ( $\text{P}_1$ ,  $\text{P}_2$ ) of the special pair (analogous to  $\text{P}_L$  and  $\text{P}_M$  of the bacterial RC). With this in mind we explore a model in which  $^1\text{P680}^*$  is contributed to by two Chl *a* monomers and the 667 nm state is the upper dimer component. The possibility that the Pheo *a* molecule, which contributes to the 680 nm band, is one of the two monomers can be rejected. Previous nonphotochemical hole burning (NPHB) studies showed that this Pheo *a* band lies at 681.5 nm [9,25]. That the Pheo *a* band exhibits persistent NPHB, while P680 does not, and is characterized by weak electron-phonon coupling proves that the  $\text{Q}_y$ -state of Pheo *a* makes, at most, a small

contribution to the wavefunction of  $^1\text{P680}^*$ .

The fact that the upper dimer component of P680 located at 677 nm carries only about 3.5% of the absorption intensity of P680 deserves comment in the context of the above model. This percentage is based on the spectra of Fig. 11 with due account having been given to the previously discussed interference of the P680 hole by the monomer Chl *a* ground state absorption. Kwa [34] has determined a similar value. The percentage of 3.5 is smaller than the value of 10 for  $\text{P}_+$  of *Rps. viridis* [16]. Within the above model the smaller percentage would indicate that the  $\text{Q}_y$ -dipoles of the two P680 monomers are closer to anti-parallel than those in the bacterial RC which make an angle of  $139^\circ$  [67]. It is important to note that in the bacterial RC  $\text{P}_+$  and  $\text{P}_-$  are polarized nearly parallel and perpendicular to the membrane, i.e.,  $\text{C}_2$  symmetry is operative. Linear dichroism experiments [36,68] on oriented PS II RC samples have led to the conclusion that the  $\text{Q}_y$ -transition dipole of P680 is close to parallel to the membrane plane.

The question of whether the above model is consistent with the absorption spectrum of the 4 Chl *a*-RC, Fig. 2, must be considered. To this end we emphasize again that a Pheo *a* molecule contributes to the absorption band at 680 nm. For what follows one can consider that the oscillator strength of the Pheo *a* monomer is ~60-80% that of a Chl *a* molecule [16,69] although this value is not essential to the argument. The point is that the model predicts that both the 680 and 670 absorption bands for the 4 Chl *a*-RC should both have the absorption strength of slightly less than 3 Chl *a* molecules since the hole burning results prove that P680 carries most of the intensity of two Chl *a* molecules. Guided by the P680 absorption profile shown in Fig. 13 (a reflection of the corrected non-line narrowed P680 hole profile) we have deconvolved the absorption spectrum shown in Fig. 2. The combined P680 plus Pheo *a* profile was assigned a width of  $155\text{ cm}^{-1}$  with the

lower and higher sides being a Gaussian and Lorentzian, respectively. Utilization of a Lorentzian is more realistic than a Gaussian because of the high energy tailing of P680 due to strong electron-phonon coupling and the existence of very weak low frequency intramolecular modes. In addition, the Franck-Condon factors of ref. 64 were used to take into account the weak  $\sim 200\text{-}500\text{ cm}^{-1}$  vibronic bands which build on the 680 nm origin band(s). Allowance was also made for the weak upper dimer component of P680 at  $\sim 667\text{ nm}$ , *vide supra*. The result obtained is that the absorption at 680 nm represents 45% of the total  $Q_y$ -absorption, lower than the value of 50% expected from the above model. However, on the basis of our analysis of the absorption spectra of a large number of RC preparations, we are of the opinion that the absorption spectrum of Fig. 2 is not yet one of a perfect 4 Chl *a*-RC sample. By this is not inferred the presence of the small amount of 684 nm absorbing Chl *a*. Rather, we believe that some non-native Chl *a* still contribute to the absorption at 670 nm. One possible source of these Chl *a* molecules, which has not been mentioned, is P680 itself, i.e., the 4 Chl *a*-RC preparation could be contaminated by some denatured PS II RC. We propose that a perfect 4 Chl *a*-RC preparation would show enhanced absorption at 680 nm relative to that at 670 nm. Such a preparation would yield a percentage contribution from absorption centered at 680 nm closer to 50%. We conclude that the absorption spectrum of the 4 Chl *a*-RC cannot be said to be inconsistent with the model that has  $^1\text{P680}^*$ , the primary donor state, being the lowest allowed dimer state of two Chl *a* molecules.

To conclude this section we consider some possible scenarios for the two Chl *a* monomers of P680 which may be assigned to one of two classes; one in which the  $C_2$ -symmetry of the special pair is preserved and the other in which it is destroyed. The results discussed, thus far, are not inconsistent with the former class. For example,  $^1\text{P680}^*$  and its

dimer component could be the analogues of  $P_-$  and  $P_+$  of the bacterial RC provided the Mg...Mg distance between  $P_1$  and  $P_2$  of the PS II RC is  $\sim 10 \text{ \AA}$  (compared to  $7 \text{ \AA}$  between  $P_L$  and  $P_M$  of the bacterial RC) and there is a slight reorientation of  $P_1$  and  $P_2$  to yield a more anti-parallel configuration for their  $Q_y$ -transition dipoles. However, such a structure would appear to be at odds with the EPR results of van Mieghem et al. [66] from experiments on PS II enriched membranes and isolated RC oriented on mylar films. The results indicate that the triplet state of P680 is localized on a Chl *a* monomer whose plane makes an angle,  $30^\circ$ , with the membrane plane which is the same as those for the accessory BChl molecules of the bacterial RC (the planes of  $P_L$  and  $P_M$  make an angle of  $\sim 90^\circ$ ).

van Mieghem et al. favored the interpretation that has P680 being a Chl *a* monomer analogous to  $BChl_L$  or  $BChl_M$  of the bacterial RC. Of course, the observation that  $^3P^*$  is a monomer state is irrelevant to the question of whether  $^1P^*$  is a dimer state from the perspective of electronic structure and primary charge separation [70]. Nevertheless, the results of van Mieghem et al. would have one of the two monomers in the model being considered here being an accessory Chl monomer. Their analysis also revealed that the ring plane of the EPR-active Chl *a* monomer is rotated  $45^\circ$  compared to the accessory BChl of the bacterial RC. Following the work of van Mieghem et al., van der Vos et al. [20] reported on linear dichroism-ADMR experiments on RC preparations assumed to contain six Chl *a* molecules. Using the aforementioned  $30^\circ$  angle they concluded that the angle between the  $Q_y$ -transition dipole of the Chl *a* monomer and the membrane plane is  $36 \pm 8^\circ$ , a value significantly different from those of the special pair monomers and accessory BChl of the bacterial RC. For example, this angle for  $P_M$  and  $P_L$  of the special pair of the bacterial RC is  $\sim 14^\circ$  [20]. Because these workers did not detect an upper dimer component, they favored the interpretation that has  $^1P680^*$  being, functionally, a monomer

state. However, they did not conclude that the monomer Chl *a* is the analogue of one of the accessory BChl molecules of the bacterial RC. Rather, they left this as an open question.

Most recently, Noguchi et al. [71] have reported the results of triplet-singlet (ground state) FT-IR experiments on the PS II RC. They proposed that P680 is a dimer comprised of P<sub>1</sub> and P<sub>2</sub>, the analogues of P<sub>L</sub> and P<sub>M</sub> of the bacterial RC, but with the plane of P<sub>1</sub> being inclined at 30° with respect to the membrane plane. This pseudo-T-shaped structure is one in which the keto group of ring v of P<sub>1</sub> is directed away from the Mg of P<sub>2</sub>, i.e., it cannot serve as electron-donor ligand to its Mg. Only a qualitative argument, based on hydrogen-bonding, is provided for why such a structure is reasonable. The structural model of Noguchi et al. indicates that the Q<sub>y</sub>-transition dipoles of P<sub>1</sub> and P<sub>2</sub> of the PS II RC make an angle closer to 90° than the 140° angle in the bacterial RC. This would lead to a weakening of the excitonic interaction between P<sub>1</sub> and P<sub>2</sub>, relative to P<sub>L</sub> and P<sub>M</sub> of the bacterial RC. However, it would also lead to the absorption intensities for P<sub>+</sub> and P<sub>-</sub> of the PS II RC being closer in value, which is at odds with the hole burning results. Interestingly, the pseudo-T-shaped structure for the special pair would definitely render P<sub>1</sub> and P<sub>2</sub> energetically inequivalent, a consequence of the absence of C<sub>2</sub>-symmetry. One expects that the Q<sub>y</sub>-state of P<sub>2</sub> should lie higher in energy than that of P<sub>1</sub>, although not by as much as 350 cm<sup>-1</sup>, the value observed for the self-aggregated T-shaped dimer of Chl *a* at 4.2 K [72]. For this dimer the keto group of the donor Chl *a* is ligated to the Mg of the acceptor Chl *a*. However, a value of about 150 cm<sup>-1</sup> is not an unreasonable estimate given the inhomogeneous absorption widths of Chl *a* monomer absorption bands in solid matrices. Such a value would further diminish the state mixing between P<sub>1</sub> and P<sub>2</sub> (beyond that indicated by the structural model of Noguchi et al.).

In summary, the models of van Mieghem et al. and Noguchi et al. for  $^1P680^*$  are inconsistent with the results of hole burning, LD and CD experiments. The hole burning and absorption spectra for the 4 Chl *a*-RC are consistent with  $^1P680^*$  being a Chl *a* dimer state with its upper excitonic partner being  $\sim 300\text{ cm}^{-1}$  higher in energy, roughly oppositely polarized to P680 and very weakly absorbing. The sensitivity of the ADMR experiments of van der Vos et al. was not sufficient to detect the upper dimer component. Their conclusion that  $^1P680^*$  is functionally a monomer is untenable since the upper dimer component could be totally forbidden in absorption. The apparent weakness of the excitonic interaction of the dimer and the absence of the bacterial special pair marker mode in P680 strongly indicates that the bacterial special pair assumes a very different structure in the PS II RC. The notion that the structure difference is mainly due to an increase in the Mg...Mg distance by  $\sim 3\text{ \AA}$  and that this "weakened" special pair is still the primary donor is at odds with the EPR results of van Mieghem et al. The question of which two Chl *a* molecules in the PS II RC are associated with the primary donor state is unlikely to be settled until an x-ray structure is available. Nevertheless, we are currently exploring the possibility that the lowest energy  $Q_Y$ -state of a tilted and translationally displaced (relative to  $P_2$ )  $P_1$  together with a rotated ( $\sim 45^\circ$ ) or unrotated Chl *a*, might be reasonable candidates for the primary donor of the PS II RC. Of course, even if a cofactor-structure is found which is consistent with the available data the immensely difficult problem of proving that such a structure represents a global energy minimum still remains. Hopefully, an x-ray structure of the PS II RC will soon be available.

## V. Concluding Remarks

Considerable progress has recently been made towards an understanding of the excited electronic state structure and primary charge separation dynamics of the PS II RC.

This is less the case for the energy transfer dynamics. The present work establishes the importance of CP47 contamination and the 684 nm absorbing Chl *a* in preparations containing, on average, 5 and 6 Chl *a* molecules per RC complex. Our finding of CP47 contamination is not so surprising since our inspection of the gel profiles reported for most but not all of the preparations reviewed in ref. 3 show some contamination [73]. The 684 nm Chl *a* of the RC share similar properties with the 684 nm Chl *a* observed in CP47 preparations. If 684 nm Chl *a* are intrinsic to the RC, i.e. not linker-type, then their fragility (extreme sensitivity to TX-100) and variability indicate that they are located more towards the exterior of the RC complex. Our previous and present measurements of the  $^1\text{P680}^*$  lifetime, together with the time domain data, indicate that the 684 nm Chl *a* do not play a role in primary charge separation. However, both the 684 nm Chl *a* and CP47 contamination should be expected to complicate the interpretation of energy transfer data. Therefore, in our future studies of energy transfer dynamics and electron-phonon coupling, attention will be focused on 4 Chl *a*-RC preparations which contain negligibly low amounts of CP47, 684 nm Chl *a* and non-native Chl *a* absorbing near 670 nm.

### Acknowledgments

Research at the Ames Laboratory was supported by the Division of Chemical Sciences, Office of Basic Energy Sciences, U.S. Department of Energy. Ames Laboratory is operated for the U.S. Department of Energy by Iowa State University under Contract No. W-7405-Eng-82. Work at NREL was supported by the same division of USDOE under Contract No. DE-AC02-83 CH-10093. Raphael Picorel is grateful to DGICYT (Grant PB 89-0060 and CONCAI-DGA (Grant PCB 3-89) for financial support. The research of C.F.Y. was supported by NSF grant DCB 89-04075. We thank Steve Toon for his valuable assistance in sample preparation. We are grateful to S. L. S. Kwa for



providing us with his Ph.D. dissertation prior to publication of sections relevant to the present work.

## References

1. Nanba, O.; Satoh, K. *Proc. Natl. Acad. Sci. USA* 1987, 84, 109.
2. Renger, G. in *Topics in Photosynthesis*; Vol. 11; Barber, J., Ed.; Elsevier: 1992; p. 45.
3. Seibert, M. in *The Photosynthetic Reaction Center*; Vol. I; Deisenhofer, J.; Norris, J., Eds.; Academic Press: New York, 1993; p. 319.
4. Deisenhofer, J., Epp, O.; Mike, M.; Huber, R.; Michel, H. *J. Mol. Biol.* 1984, 180, 385.
5. Deisenhofer, J.; Epp, O.; Mike, K.; Huber, R.; Michel, H. *Nature* 1985, 318, 618.
6. Cramer, W. A.; Widger, W. R.; Herrmann, R. G.; Trebst, A. *Trends Biochem. Sci.* 1985, 10, 125. Kyle, D. J. *Photochem. Photobiol.* 1985, 41, 107.
7. Friesner, R.; Won, Y. *Biochim. Biophys. Acta* 1989, 777, 122. Parson, W. W. in *Chlorophylls*; Scheer, H., Ed.; CRC Press: Boca Rotan; 1991; p. 1153.
8. Reddy, N. R. S.; Kolaczowski, S. V.; Small, G. J. *Science* 1993, 260, 68.
9. Tang, D.; Jankowiak, R.; Seibert, M.; Yocum, C. F.; Small, G. J. *J. Phys. Chem.* 1990, 94, 6519.
10. McTavish, H.; Picorel, R.; Seibert, M. *Plant Physiol.* 1989, 98, 452.
11. Dekker, J. P.; Bowlby, N. R.; Yocum, C. F. *FEBS Lett.* 1989, 254, 150.
12. Tang, D.; Jankowiak, R.; Seibert, M.; Small, G. J. *Photosynth. Res.* 1990, 27, 19.
13. Jankowiak, R.; Small, G. J. in *The Photosynthetic Reaction Center*; Vol. II; Deisenhofer, J., Norris, J., Eds.; Academic Press: New York, 1993; p. 133.
14. Chang, H.-C.; Jankowiak, R.; Yocum, C. F.; Picorel, R.; Seibert, M.; Small, G. J. *J. Phys. Chem.*, 1994, 98, 7717.

15. Satoh, K. in *The Photosynthetic Reaction Center*; Vol. I; Deisenhofer, J., Norris, J., Eds.; Academic Press: New York, 1993; p. 289.
16. Reddy, N. R. S.; Kolaczowski, S. V.; Small, G. J. *J. Phys. Chem.* 1993, 97, 6934.
17. Lyle, P. A.; Kolaczowski, S. V.; Small, G. J. *J. Phys. Chem.* 1993, 97, 6926.
18. Hayes, J. M.; Gillie, J. K.; Tang, D.; Small, G. J. *Biochim. Biophys. Acta* 1988, 932, 287.
19. Breton, J. in *Perspectives in Photosynthesis*; Jortner, J., Pullman, B., Eds.; Kluwer Academic: Dordrecht, 1990, p. 23.
20. van der Vos, R.; van Leeuwen, P. J.; Braun, P.; Hoff, A. J. *Biochim. Biophys. Acta* 1992, 1140, 184.
21. Jankowiak, R.; Small, G. J. *Science* 1987, 237, 618. Hayes, J. M.; Jankowiak, R., Small, G. J. in *Persistent Spectral Hole Burning: Science and Applications*; Moerner, W. E., Ed.; Springer Verlag: New York, 1988, p. 151.
22. Rutherford, A. W. *Biochim. Biophys. Acta* 1985, 807, 189.
23. Vink, K. J.; de Boer, S.; Plijter, J. J.; Hoff, A. J.; Wiersma, D. A. *Chem. Phys. Lett.* 1987, 142, 433.
24. Jankowiak, R.; Hayes, J. M.; Small, G. J. *Chemical Reviews* 1993, 93(4), 1471.
25. Tang, D.; Johnson, S. G.; Jankowiak, R.; Hayes, J. M.; Small, G. J.; Tiede, D. M. in *Perspectives in Photosynthesis*; Jortner, J., Pullman, B., Eds.; Kluwer Academic: Dordrecht, 1990, p. 99.
26. Johnson, S. G.; Tang, D.; Jankowiak, R.; Hayes, J. M.; Small, G. J.; Tiede, D. M. *J. Phys. Chem.* 1990, 94, 5849.
27. Lockhart, D. J.; Boxer, S. G. *Biochemistry* 1987, 26, 664.
28. Lockhart, D. J.; Boxer, S. G. *Proc. Natl. Acad. Sci. U.S.A.* 1988, 85, 107.
29. Boxer, S. G. in *The Photosynthetic Reaction Center*; Vol. II; Deisenhofer, J., Norris, J., Eds.; Academic Press: New York, 1993; p. 177.

30. Parson, W. W.; Warshel, A. *J. Am. Chem. Soc.* 1987, 109, 6152.
31. Scherer, P. O. J.; Fischer, S. F. *Chem. Phys.* 1989, 131, 115.
32. Gillie, J. K.; Lyle, P. A.; Small, G. J.; Golbeck, J. H. *Photosynth. Res.* 1989, 22, 233.
33. Krauss, N.; Hinrichs, W.; Witt, I.; Fromme, P.; Pritzkow, W.; Dauter, Z.; Betzel, C.; Wilson, K. S.; Witt, H. T.; Saenger, W. *Nature* 1993, 361, 326.
34. Kwa, S. L. S.; Eijkelhoff, C.; van Grondelle, R.; Dekker, J. P. *J. Phys. Chem.*, submitted. Kwa, S. L. S., Ph.D. thesis, Department of Physics and Astronomy, Vrije University.
35. van Kan, P. J. M.; Otte, S. C. M.; Kleinherenbrink, A. M.; Nieveen, M. C.; Aartsma, T. J.; van Gorkom, H. J. *Biochim. Biophys. Acta* 1990, 1020, 146.
36. Otte, S. C. M.; van der Vos, R.; van Gorkom, H. J. *J. Photochem. Photobiol. B: Biol.* 1992, 15, 5.
37. Small, G. J.; Jankowiak, R.; Seibert, M.; Yocum, C. F.; Tang, D. in *Proceedings of Second Feldafing Workshop on the Structure and Function of Bacterial Reaction Centers*; Michel-Beyerle, Ed.; Springer Verlag: New York; 1991; p. 101.
38. Jankowiak, R.; Tang, D.; Small, G. J.; Seibert, J. *J. Phys. Chem.* 1989, 93, 1649.
39. Wasielewski, M. R.; Johnson, D. G.; Seibert, M.; Govindjee. *Proc. Natl. Acad. Sci. USA* 1989, 86, 524.
40. Wasielewski, M. R.; Johnson, D. G.; Seibert, M.; Govindjee; Preston, C.; Seibert, M. *Photosynthesis Res.* 1989, 22, 89.
41. Fleming, G. R.; Martin, J.-L.; Breton, J. *Nature* 1988, 333, 190.
42. Roelofs, T. A.; Gilbert, M.; Shuvalov, V. A.; Holtzwarth, A. R. *Biochim. Biophys. Acta* 1991, 1060, 237.
43. Gatzert, G.; Griebenow, K.; Muller, M. G.; Holtzwarth, A. R. in *Research in Photosynthesis*; Vol. II; Murata, N., Ed.; Kluwer Academic: Dordrecht, 1992; p. 69.

44. Roelofs, T. A.; Kwa, S. L. S.; van Grondelle, R.; Dekker, J.; Holtzwarth, A. R. *Biochim. Biophys. Acta* 1992, 1143, 147.
45. Fleming, G. R.; Martin, J. L.; Breton, J. *Nature* 1988, 85, 190.
46. Breton, J.; Martin, J.-L.; Fleming, G. R.; Lambry, J.-C. *Biochemistry* 1988, 27, 8276.
47. Durrant, J. R.; Hastings, G.; Joseph, D. M.; Barber, J.; Porter, G.; Klug, D. R. *Proc. Natl. Acad. Sci. USA* 1992, 89, 11632.
48. Durrant, J. R.; Hastings, G.; Hong, Q.; Barber, J.; Porter, G.; Klug, D. R. *Chem. Phys. Letts.* 1992, 188, 54.
49. Seibert, M.; Picorel, R.; Rubin, A. B.; Connolly, J. S. *Plant Physiol.* 1988, 87, 303.
50. Chumanov, G.; Picorel, R.; Toon, S.; Seibert, M.; Cotton, T. M. *Photochem. Photobiol.* in press.
51. Dunahay, T. G.; Staehelin, L. A.; Seibert, M.; Ogilvie, P. D.; Berg, S. P. *Biochim. Biophys. Acta* 1994, 764, 179.
52. Montoya, G.; Yruela, I.; Picorel, R. *FEBS Lett.* 1990, 283, 255.
53. Jankowiak, R.; Small, G. J. *Anal. Chem.* 1989, 61(18), 1023A.
54. The measured area ratios (a:b:c) are 6.0:4.9:4.0.
55. This value was determined by subtracting a 684 nm Gaussian with a width of  $120 \text{ cm}^{-1}$  and an intensity which resulted in the low energy side of P680 being a Gaussian.
56. Shu, L.; Small, G. J. *Chem. Phys.* 1990, 141, 447.
57. Ikeuchi, M.; Inoue, Y. *FEBS Letters* 1988, 241, 99.
58. Webber, A. N.; Packman, L.; Chapman, D. J.; Barber, J.; Gray, J. C. *FEBS Letters* 1989, 242(2), 259.
59. Reddy, N. R. S.; Picorel, R.; Small, G. J. *J. Phys. Chem.* 1992, 96, 6458.

60. For a review see Parson, W. W.; Warshel, A. in *The Photosynthetic Reaction Center*; Vol. II; Deisenhofer, J., Norris, J., Eds.; Academic Press: New York, 1993; p. 23.
61. Reddy, N. R. S., Lyle, P. A.; Small, G. J. *Photosyn. Res.* 1992, 31, 167.
62. Braun, P.; Greenberg, B. M.; Scherz, A. *Biochemistry* 1990, 29, 10376.
63. Tetenkin, V. L.; Gulyacv, B. A.; Seibert, M.; Rubin, A. B. *FEBS Lett.* 1989, 250, 459.
64. Gillie, J. K.; Small, G. J.; Golbeck, J. H. *J. Phys. Chem.* 1989, 93, 1620.
65. Ref. 16 and refs. therein.
66. van Mieghem, F. J. E.; Satoh, K.; Rutherford, A. W. *Biochim. Biophys. Acta* 1991, 1058, 379.
67. Won, Y.; Friesner, R. A. *J. Phys. Chem.* 1988, 2, 2208.
68. van Dorssen, R. J.; Breton, J.; Plijter, J. J.; Satoh, K.; van Gorkom, H. J.; Amesz, J. *Biochim. Biophys. Acta* 1987, 893, 267.
69. Vernon, L. P. *Photosyn. Res.* 1960, 9, 89.
70. Norris, J.; Budil, D. E.; Gast, P.; Chang, C.-H.; El-Kabbani; Schiffer, M. *Proc. Natl. Acad. Sci. U.S.A.* 1989, 86, 4335.
71. Noguchi, T.; Inoue, Y.; Satoh, K. *Biochemistry* 1993, 32, 7186.
72. Carter, T. P.; Small, G. J. *J. Phys. Chem.* 1986, 90, 199.
73. Picorel, R.; Seibert, M. To be published.

**CHAPTER 6 TEMPERATURE DEPENDENT HOLE BURNING  
OF THE 684 NM CHLOROPHYLL A OF THE ISOLATED  
REACTION CENTER OF PHOTOSYSTEM II: CONFIRMATION  
OF THE LINKER MODEL**

A paper published in *Chem. Phys.*, 1995, 194, 323

H.-C. Chang, G. J. Small, and R. Jankowiak

**ABSTRACT**

Currently the nature of the additional chlorophyll *a* (Chl *a*) molecules which take the number of Chl *a* per isolated D1-D2-cyt b559 complex beyond the value of four for the bacterial reaction center is a subject of much importance and interest. Chang et al. [*J. Phys. Chem.* 98 (1994), 7725], who studied preparations of this complex with significantly different Chl *a* contents, concluded that the 684 nm absorbing Chl *a* contribute to the additional Chl *a* and proposed that they are of the linker type, serving to shuttle energy from the proximal antenna complex to the reaction center. Implicit in this model is that the 684 nm Chl *a* communicate with the primary electron donor Chl *a* (P680) via energy transfer and that the resulting detrapping of the Q<sub>y</sub>-state of the 684 nm Chl *a* should depend strongly on temperature. Temperature dependent transient hole spectra are presented that are in complete accord with this prediction. Theoretical calculations on the kinetics and temperature dependence of the hole profile of the 680 nm absorption band are presented and provide convincing support for the linker model. The data are argued to be inconsistent with other models.

## I. Introduction

The D1-D2-cyt b559 reaction center (RC) complex of photosystem II (PS II) was first isolated and characterized by Nanba and Satoh in 1987 [1]. Their procedure led to preparations with 5 chlorophyll *a* (Chl *a*) per 2 pheophytin *a* (Pheo *a*) molecules per RC (plus 1  $\beta$  carotene and 1 cyt b559). The 2 quinone molecules were lost during isolation, which is also the case for all isolation procedures reported to date. Subsequent developments in isolation of the PS II RC have been recently reviewed [2,3]. Modifications [4-6] of the Nanba-Satoh procedure and the development of different procedures [7,8] led to improvements in stability of the RC which spawned a substantial number of time domain [9-13] and spectral hole burning studies [14-17] of its primary charge separation and energy transfer dynamics (for a review see ref. 2). Considerable evidence exists which indicates that the Chl *a* / Pheo *a* ratio depends on the isolation procedure and other factors [3]. Preparations with 4-6 Chl *a* per 2 Pheo *a* molecules have been reported [3]. For the present paper, the precise value of the Chl *a* / Pheo *a* ratio for the samples studied is unimportant since the paper is concerned only with characterization of the 684 nm Chl *a*.

Concerning primary charge separation, the first hole burning studies on P680\* by Vink and co-workers [18] led to the identification of only a broad hole, while subsequent studies revealed the zero-phonon hole [15-17] which led to a lifetime of  $1.9 \pm 0.2$  ps for P680\* (primary donor state) at 4.2 K. Pump-probe experiments on samples from the same batch led to a lifetime of  $3.0 \pm 0.6$  ps for primary charge separation at 277 K [9]. These workers later reported a time constant of  $1.4 \pm 0.2$  ps for this process (P680\* Pheo  $\rightarrow$  P680<sup>+</sup> Pheo<sup>-</sup>) at 15 K [10]. A number of other time domain studies followed [12,13] and there is now quite general agreement that primary charge separation in the PS II RC occurs

in  $\sim 3$  ps at biological temperatures and that it undergoes a slight acceleration with decreasing temperature [10,15]. There is, therefore, a striking analogy with the primary charge separation kinetics in bacterial RC [19-21] despite the fact that the monomers of the special pair of P680 are much more weakly coupled than in the *Rb. sphaeroides* and *Rps. viridis* RC [22]. It should be emphasized that, since the work of Jankowiak et al. [15], we have performed hole burning studies on several different PS II RC preparations [15-17] as well as the CP47-RC complex [14]. CP47 is a proximal antenna complex of PS II. In all cases, the zero-phonon holes burned into P680 yielded a P680\* lifetime of 1.9 ps at 4.2 K. Thus, it would appear that the primary charge separation kinetics are insensitive to the ensemble averaged Chl *a* / RC ratio. How one interprets this would depend on the interpretation given to the "additional" Chl *a* molecules which take the average Chl *a* content of the PS II RC beyond the value of 4 for the bacterial RC.

On the basis of the very recent papers by Kwa et al. [22] and Chang et al. [17] it would appear that there remain only two viable interpretations for the 684 nm Chl *a*. Chang et al. studied three PS II RC preparations with Chl *a* ratios of  $\sim 1:1.2:1.5$ . It was proven that an increase in the Chl *a* content was contributed to by an increase in the amount of 684 nm absorbing Chl *a* [17]. The existence of the 684 nm Chl *a* was already firmly established [14,23,24]. Chang et al. concluded that the 684 nm Chl *a* are "linker" molecules important to energy transfer from the CP47 proximal antenna complex to P680 and that they are located at the exterior of the RC protein complex. They also concluded that the correct number of Chl *a* belonging to the hydrophobic interior of the RC is 4, in analogy with the bacterial RC. The fragility of the 684 nm Chl *a* was demonstrated and it was asserted that in RC preparations with lower Chl *a* content one has a heterogeneous mixture comprised of RC which possess and RC which are devoid of the 684 nm Chl *a* (but



all RC possess P680). In addition, Chang et al. [17] pointed out the complications for stoichiometry associated with contamination of RC preparations by CP47 and dysfunctional Chl *a* (absorbing near 670 nm). Kwa et al. [22] placed a different interpretation on the 684 nm Chl *a*, one that has these Chl *a* being a second pool of *primary* electron donor (P684) with the other being P680. Given that P684\* lies lower in energy than P680\* and the fragility of the 684 nm Chl *a* (relative to the P680 Chl *a*), the model of Kwa et al. raises the interesting possibility that P684 is the remnant of the primary donor in the membrane bound RC, i.e., P680 of the isolated RC is a perturbed version of the membrane bound primary donor which, nevertheless, is still capable of triggering charge separation in 3 ps.

In the gross heterogeneity model of Kwa et al., RC which possess P684 as the primary donor cannot communicate with RC which possess P680 as the primary donor. In the model of Chang et al., all RC particles possess P680 as the one and only primary donor Chl *a* but only a fraction of RC particles possess 684 nm Chl *a*. This fraction depends on the isolation procedure and sample handling. For those particles which possess 684 nm Chl *a*, the 684 nm Chl *a* can communicate with the P680 Chl *a* via energy transfer. It is this difference between the two models that led to the temperature dependent hole burning studies reported on here. By way of review (see refs. 14, 25 and 26 for details), both P680\* and the Q<sub>y</sub>-state of the 684 nm Chl *a* can be studied by transient population bottleneck hole burning via their lowest triplet state. The contributions of P680 and the 684 nm Chl *a* to the hole profile of the prominent PS II RC 680 nm absorption band (see Fig. 1) are distinguishable at sufficiently low temperatures [17,22,27]. Given the close proximity ( $\sim 90 \text{ cm}^{-1}$ ) of the Q<sub>y</sub>-state of the 684 nm Chl *a* to P680\* and the rapid decay of P680\* due to charge separation, the model of Chang et al. predicts that the contribution of

the 684 nm Chl *a* to the hole profile of the 680 nm band should undergo a significant decrease with increasing temperature above 4.2 K due to thermally induced energy transfer from the Q<sub>Y</sub>-state of the 684 nm Chl *a* to P680\*. Furthermore, the contribution from the 684 nm Chl *a* should be recovered upon completion of the temperature cycle. The results presented are in accord with these predictions. Kinetic calculations, which take into account the intrinsic glass-like structural heterogeneity of the protein complex, are presented which support the application of the model of Chang et al. for temperature dependence of the hole profile for the 680 nm absorption band. Theoretical calculations (with no adjustable parameters) are presented which provide an accurate accounting of the temperature dependence of this hole profile.

## II. Experimental Section

The apparatus used for the absorption and hole burning measurements was as described recently in refs. 16 and 28. Briefly, hole burning employed a Coherent CR699-21 ring dye laser (linewidth of  $0.07 \text{ cm}^{-1}$ ) pumped by a 6-W Coherent Innova argon-ion laser. Hole and absorption spectra were read with a Bruker HR 120 Fourier transform spectrometer. All reported results were obtained in the temperature range of 4.2-77 K using a convection-cooled liquid helium cryostat. For the 77 K studies, helium was replaced with liquid nitrogen. Hole burning conditions and read resolution are given in the figure captions.

Samples from three separate preparations were generously provided by M. Seibert and R. Picorel. Preparations I (~4.1 Chl *a* / 2 Pheo *a*) and II (~4.2 Chl *a* / 2 Pheo *a*) of the D1-D2-cyt b559 complex were obtained with high yield from PS II membranes isolated from spinach leaves, according to the method of Yruela et al. [29]. Preparation III, with an

estimated  $\sim 4.5$  Chl *a* / Pheo *a*, was obtained from spinach according to the procedure of Nanba and Satoh [1] as described in [2]. The Chl *a* / Pheo *a* ratios were determined as described in Montoya et al. [30]. The relative ratios of the Chl *a* in the three preparations were determined using the 4.2 K absorption method described in ref. 17 and found to be consistent with those calculated from the above data. We note that the method of Montoya et al. [30] may underestimate the Chl *a* / Pheo *a* ratio [31] to an extent greater than the 10% estimate given in ref. 17. Again, the uncertainty in this ratio is irrelevant to the present paper. Results presented in the following section allow for an assessment of differences between the contributions from 684 nm Chl *a* and dysfunctional Chl *a* to the three preparations. All preparations were stored in the dark at  $-80^\circ$  C. For low temperature studies, glycerol was added (66% v/v) to sample aliquots to avoid glass cracking.

### III. Results And Discussion

#### A. Temperature Dependence of Absorption and Transient Hole Spectra

The 4.2 K absorption spectra of preparation I and II are shown in Fig. 1 as curves a and b, respectively. As in ref. 17, the spectra are normalized to the same intensity of the  $Q_x$ -band of Pheo *a*. Comparison of the two indicates that preparation II has the somewhat higher Chl *a* content, in agreement with the results of the preceding section. Based on the results of ref. 17, in which three RC preparations with Chl *a* ratios 1:1.25:1.50 were studied, we conclude that preparation II has more dysfunctional Chl *a* absorbing at  $\sim 670$  nm. The bulk of the intensity of the relatively broad 670 nm band is due to the two accessory Chl *a* and, perhaps, also to one of the two Pheo *a* molecules. The other Pheo *a* molecule absorbs at  $\sim 681$  nm [16,32,33]. Subtraction of spectra a and b reveals that the

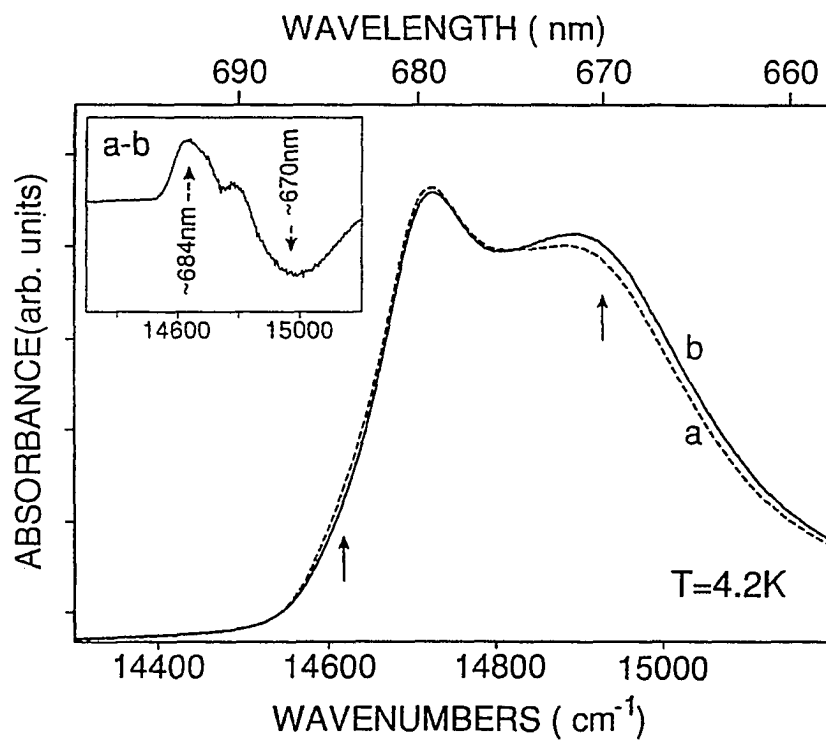


Figure 1. Absorption spectra of PS II RC for preparation I (curve a) and II (curve b), obtained at  $T = 4.2\text{ K}$ . The inset represents the difference spectrum between a and b.

inhomogeneous width of the  $Q_y$ -band for the dysfunctional Chl  $a$  is very large,  $\sim 300 \text{ cm}^{-1}$ , see inset. The band at 680 nm is heavily contributed to by P680. In both spectra there is a discernible shoulder near 684 nm (solid arrow). Subtraction of the two spectra reveals that preparation I has the larger contribution of 684 nm Chl  $a$ , see inset. We emphasize again [17] that the contributions from the 684 nm and dysfunctional Chl  $a$  depend on the isolation procedure employed. In addition, it is known that [14,17] the 684 nm Chl  $a$  is very fragile, e.g. easily disrupted by small amounts of Triton X-100 added to the glass forming solvent. It has been suggested that the relative concentration of 684 nm Chl  $a$  can be increased by carrying out the isolation in the dark [25]. Comparison of the 4.2 K absorption spectra for preparations I-III with those of ref. 17 revealed that contamination of the former by the proximal CP47 antenna complex is negligibly small.

Figure 2 shows the 4.2 K (a and b) and 77 K (c and d) transient hole burned spectra for preparations I and II obtained under non-line narrowing conditions ( $\lambda_B = 665 \text{ nm}$ ). Following the procedure of ref. 15 it was confirmed that these spectra are not contributed to by the  $Q_y$ -state of Pheo  $a$  near 681 nm. We note that previous hole burning studies led to the assignment of the broad hole feature near 667 nm as the upper dimer component of the P680 special pair [17,22]. Our interest here is in the hole centered near 680 nm. We consider first spectra a (preparation I) and b (preparation II),  $T = 4.2 \text{ K}$ . Both hole profiles are due primarily to P680 and both show the low energy shoulder at 684 nm (solid arrow) identified in previous work [14,17]. Spectrum b is very similar to that shown in Fig. 2 of ref. 17 for an RC preparation believed to have contained approximately 4 Chl  $a$  per RC (but see section II). The difference between spectra a and b of Fig. 2, see inset, confirms that preparation I contains more 684 nm Chl  $a$  than preparation II. Preparation III was found to contain more 684 nm Chl  $a$  than both I and II (results not shown). Turning next

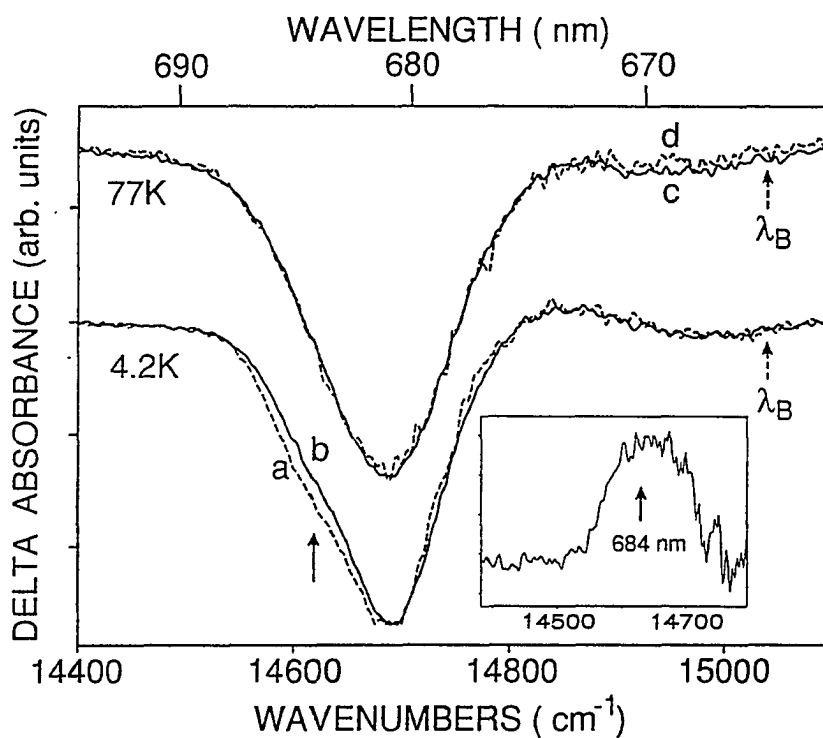


Figure 2. Non-linear narrowed transient hole spectra of PS II RC obtained at 77 K and 4.2 K, with laser excitation wavelength of  $\lambda = 665$  nm.  $\Delta OD$  changes (%) at 681-nm in spectra a, b, c, and d are 5, 6, 5 and 6, respectively. The inset shows the difference spectrum, between b and a, in the 684-nm region.

to the 77 K results (spectra c and d) it is seen that the 680 nm profiles are essentially indistinguishable. (This is also the case for preparation III, result not shown.) This indistinguishability at 77 K provides an important clue to the nature of the 684 nm Chl *a*.

It led to perform more detailed temperature-dependent studies and carry out theoretical analysis of the 680 nm hole profile as a function of temperature. For these studies we chose preparation III because of its higher average 684 nm Chl *a* content per RC. Transient hole burned spectra for preparation III are shown in Fig. 3A for 4.2, 15, 30 and 56 K. Attention is drawn to the temperature dependence of the low energy side of the hole profile. Intriguingly, it sharpens as the temperature is increased above 4.2 K, upto ~ 30 K. This is more easily seen by plotting the half-width (low energy side) of the 680 nm hole versus temperature, X's in Fig. 4. The half-width reaches a minimum value near 25 K. The open square data point for Fig. 4 is the half-width measured after cycling back to 4.2 K following the temperature excursion to 77 K. That is, the observed narrowing effect with increasing temperature is reversible. We return to this important observation in the following section. The origin of the narrowing becomes transparent by examining the difference between the 4.2 and 15 K hole profiles which is shown in the inset of Fig. 3A. The contribution of the 684 nm Chl *a* to the hole profile undergoes a significant reduction from 4.2 to 15 K. The implications of this and the aforementioned reversibility for the nature of the 684 nm Chl *a* are considered in section IV. An important comparison against the hole narrowing effect is the temperature dependence of the absorption profile centered near 680 nm. For the temperature range of interest, 4.2-77 K, the profile exhibits no narrowing, only normal thermal broadening. As an example, Fig. 5 shows the absorption profile for  $T = 4.2$  and 30 K. Normal thermal broadening of both the low and high energy

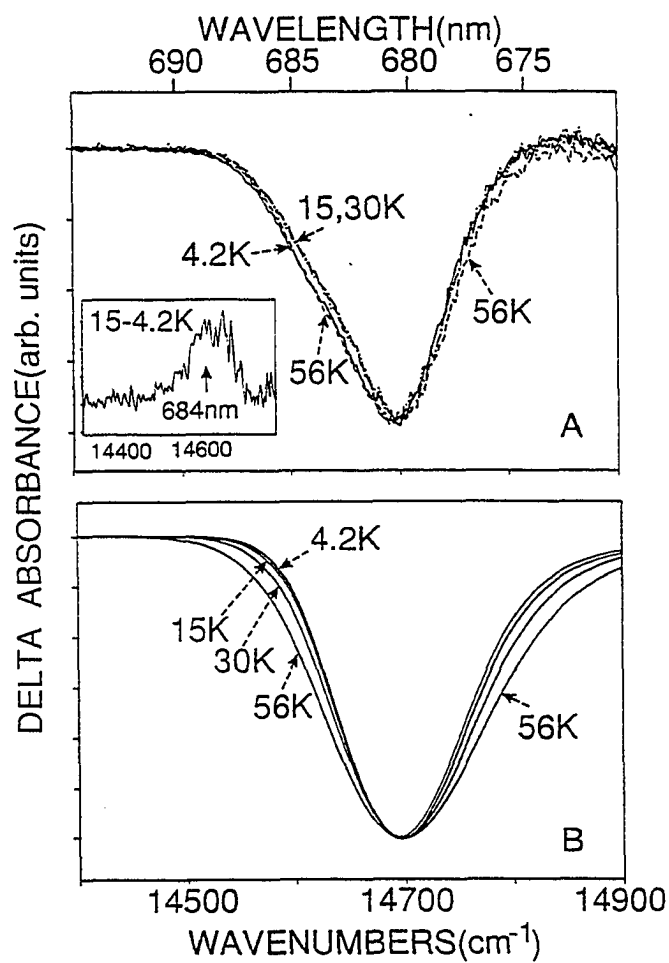


Figure 3. Transient triplet bottleneck hole spectra (Frame A) of preparation III obtained under non-linear narrowing conditions with  $\lambda_B = 665$  nm at  $T = 4.2, 15, 30$  and  $56$  K. The inset shows the difference spectrum between spectra obtained at  $T = 15$  K and  $4.2$  K, respectively. Frame B shows the calculated P680 hole profile for  $T = 4.2, 15, 30,$  and  $56$  K.



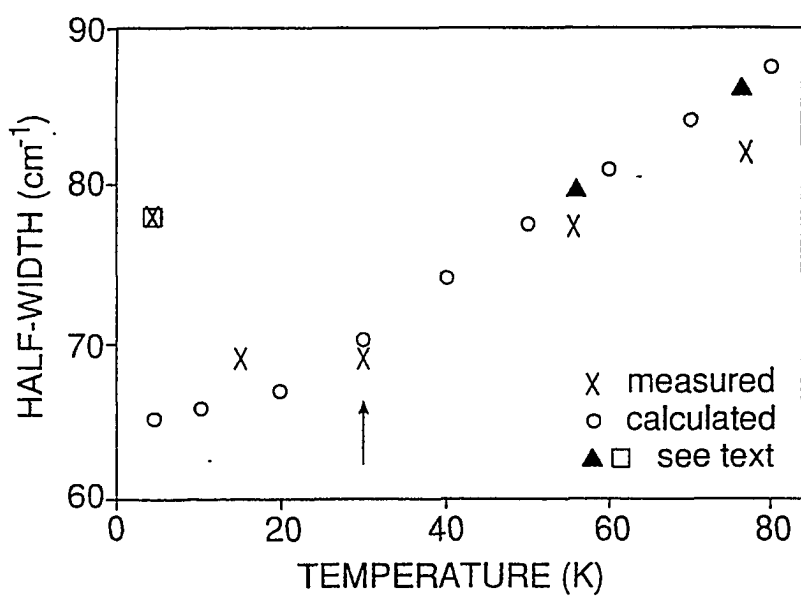


Figure 4. Temperature dependence of half-width (low energy side) of the experimental (crosses and rectangle) and calculated (circles) transient hole spectra for preparation III. The experimental half-width of the hole after temperature has been cycled back to 4.2 K is indicated by the rectangle. The triangles show the measured half-width at 56 K and 77 K corrected for the monomer absorption.

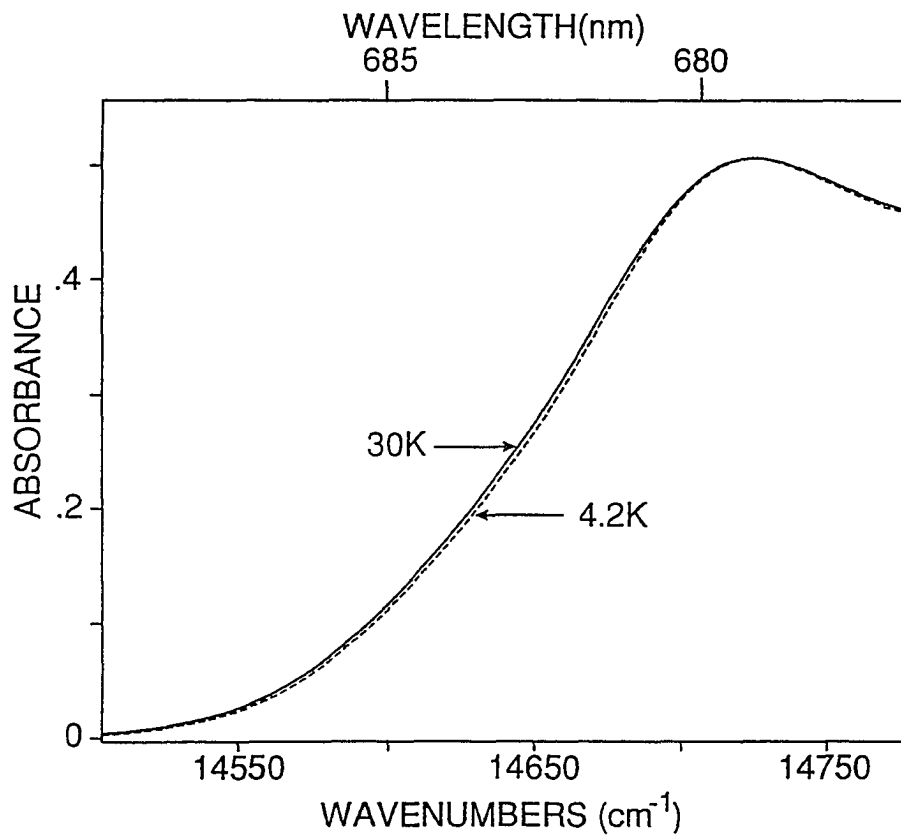


Figure 5. Absorption spectra of PS II RC, in the 680-684 nm region, obtained at  $T = 4.2$  K and  $T = 30$  K.

sides is observed. This finding proves that the diminution of the contribution of the 684 nm Chl *a* to the transient hole profile is an excited state phenomenon, cf. section IV.

We end this subsection by presenting calculated results on the temperature dependence of P680's non-line narrowed hole profile. These calculations were performed with the theory of Hayes et al. [34] which is a generalization of that of Hayes et al. [35] to arbitrary temperature. The input parameter values used are those from ref. 17, cf. Table I. The results are shown in Fig. 3B. As expected, both the low and high energy sides of the P680 broaden with increasing temperature. The results for the half-width of the low energy side of the profile are shown as the circles in Fig. 4. They should be compared with the experimental data points (X's). Comparison of the calculated P680 profiles (Fig. 3B) with the experimental profiles (Fig. 3A) reveals that the high energy sides of the latter are sharper than those of the former. This is due to the fact that the experimental profiles have not been corrected for the interference of the positive absorption from an effective ground state Chl *a* monomer associated with  $^3\text{P680}^*$  [17,18,22] (the bottleneck state for the transient hole burning). This problem is dealt with in the following subsection. Correction for this interference led to the triangular experimental half-widths in Fig. 4. The agreement between theory and experiment is then good for  $T \leq 30$  K.

In summary, the unusual temperature dependence of the low energy side of the 680 nm hole profile has a simple explanation, one that is based on the interplay between the diminution of the contribution of the 684 nm Chl *a* to the profile with increasing temperature and normal thermal broadening of P680 due to linear electron-phonon coupling.

Table I. Parameter values used to calculate hole-burned spectra for PS II RC.

	P680	Monomer Absorption Band	
S	1.9	(0,0)	678.5 nm
$\omega_m$	20 cm <sup>-1</sup>	fwhm <sup>4</sup>	210 cm <sup>-1</sup>
$\Gamma^1$	27.5 cm <sup>-1</sup>	$\Gamma_{inh}$	175 cm <sup>-1</sup>
$\Gamma_{inh}$	100 cm <sup>-1</sup>	$\omega_m$	20 cm <sup>-1</sup>
SDF <sup>2</sup>	682.45 nm	S	0.5
$\gamma^3$	3.5 cm <sup>-1</sup>		

<sup>1</sup>One-phonon profile width.

<sup>2</sup>Wavelength of maximum of the zero-phonon line distribution.

<sup>3</sup>Half-width of the zero phonon line. This value is unimportant for T d 15 K since the zero-phonon line intensity is essentially zero due to Franck-Condon forbiddenness.

<sup>4</sup>Full-width at half maximum; temperature broadening of the monomer band was calculated using the theory of Hayes et al. [33], with the parameters listed above. At 77 K, for example, this broadening equals ~25 cm<sup>-1</sup>.

## B. Theoretical Fits To Transient Hole Spectra

In other work [14,15,17] it was shown that the theory of Hayes et al. [35] provided reasonable but imperfect fits to the burn wavelength dependence of the line-narrowed hole profile of the 680 nm band at 4.2 K. The less than perfect fits were due to interference to the P680 hole profile from the effective Chl *a* monomer ground state absorption associated with  $^3\text{P680}^*$  as well as the 684 nm Chl *a*. Kwa et al. [22] experienced similar difficulties. Nevertheless, the values of the Huang-Rhys factor ( $S$ ), the mean phonon frequency ( $\omega_m$ ), one-phonon profile width ( $\Gamma$ ) and inhomogeneous broadening ( $\Gamma_{\text{inh}}$ ) and center frequency ( $\omega_c$ ) of the distribution of zero-phonon line frequencies for P680 could be determined [17], of Table I. The values of  $S = 1.9$ ,  $\omega_m = 20 \text{ cm}^{-1}$ ,  $\Gamma = 27.5 \text{ cm}^{-1}$  and  $\Gamma_{\text{inh}} = 100 \text{ cm}^{-1}$  were in gratifyingly close agreement with those determined earlier by Jankowiak et al. [15]. Also given in Table I are the values from ref. 17 for the band maximum (678.5 nm), and inhomogeneous broadening ( $175 \text{ cm}^{-1}$ ) for the  $^3\text{P680}^*$  ground state monomer absorption, 4.2 K. All of the above parameter values were used for the theoretical fitting to the high temperature 680 nm hole profiles presented below. The only adjustment made was to take into account the thermal broadening of the effective ground state monomer absorption band of  $^3\text{P680}^*$ , cf., caption to Table I for details.

As shown in the preceding subsection, the contribution to the hole profile of the 680 nm absorption band from the 684 nm Chl *a* appears to vanish for sufficiently high temperatures. In what follows we present transient hole spectra for  $T = 77$  and  $56 \text{ K}$ . For the fitting of these spectra (including burn wavelength dependence) we assumed that there is *no* contribution from the 684 nm Chl *a*. That is, the fits, with no adjustable parameters, are based on the 680 nm hole profile being due to P680 and the ground state monomer absorption of  $^3\text{P680}^*$ , of Table I. Again, the temperature and burn wavelength dependent hole profiles were fitted with the theory of Hayes et al. [34]. In the following section we

present a model for the 684 nm Chl *a* which is based on the 684 nm Chl *a* being of the linker type, cf. Introduction, and show that this model is entirely consistent with the just stated assumption.

Figure 6 shows the transient hole spectra obtained with  $\lambda_B = 665$  nm at 77 K (B) and 56 K (A). The dashed profiles are experimental while the solid curves are the calculated profiles. The experimental profiles have been corrected for the interference from the Chl *a* monomer absorption under the reasonable assumption that this absorption carries one-half the intensity of P680 [17,22]. The agreement between the calculated and experimental hole profiles is good. We also obtained hole spectra for  $\lambda_B$  located within the 680 nm band. The results for  $T = 77$  K and  $\lambda_B = 680, 681, 682$  and  $683$  nm are shown (noisy curves) in Fig. 7. In each frame the solid curve is the theoretical fit. The fits, obtained with no adjustable parameters, are gratifyingly good. Chang et al. [17] investigated the extent to which a special pair marker mode ( $\omega_{sp}$ ) with  $\omega_{sp} \sim 100$   $\text{cm}^{-1}$  might contribute to the high energy side of the P680 hole profile since such a mode with  $\omega_{sp} = 120/145$   $\text{cm}^{-1}$  and  $S_{sp} = 1.5/1.1$  is of primary importance in determining the  $P^* \leftarrow P$  absorption profile of *Rb. sphaeroides* / *Rps. viridis* [26]. They concluded that, if such a contribution exists, it must be weak, with  $S_{sp} \lesssim 0.3$ . To test this conclusion we extended the fitting of the results of Fig. 7 to include a contribution from the marker mode. The fits (not shown) confirm the conclusion of Chang et al. [17]. As discussed by Chang et al., the absence of a significant contribution of a marker mode to P680 is just another piece of evidence for the structure of the P680 special pair being significantly different from that of the special pair of bacterial RC.

The theory of Hayes et al. [34] also accounts for the dependence of the integrated hole intensity on burn frequency. To further test the values of the parameters given in

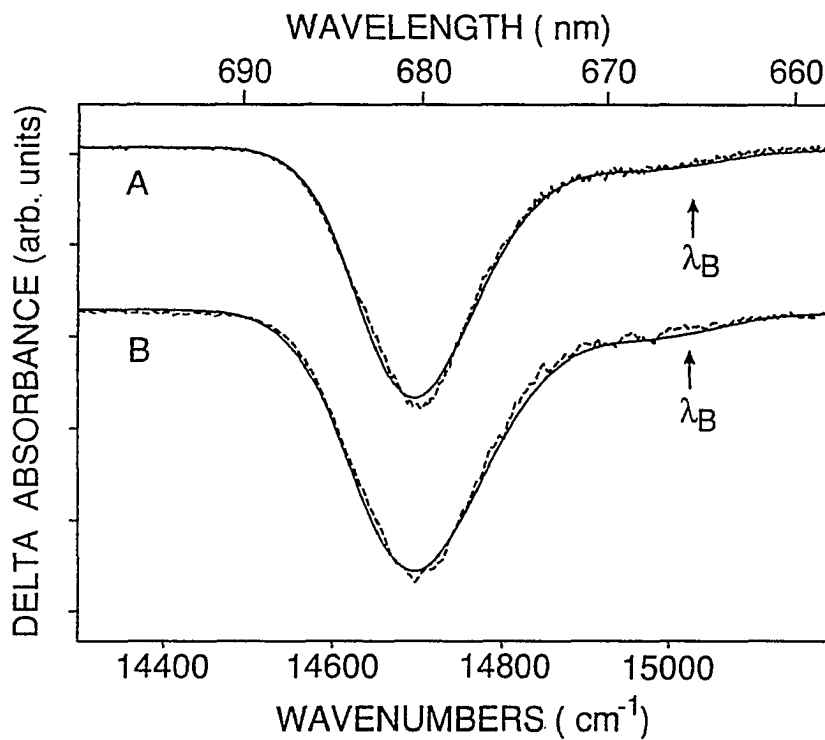


Figure 6. Frames A and B show calculated (solid lines) and experimental transient (dashed lines) hole spectra for preparation III obtained for  $\lambda_B = 665$  nm ( $I_B \sim 320$  mW/cm<sup>2</sup>) at 56 K and 77 K, respectively. The experimental spectra have been corrected for the monomer absorption, cf. text.

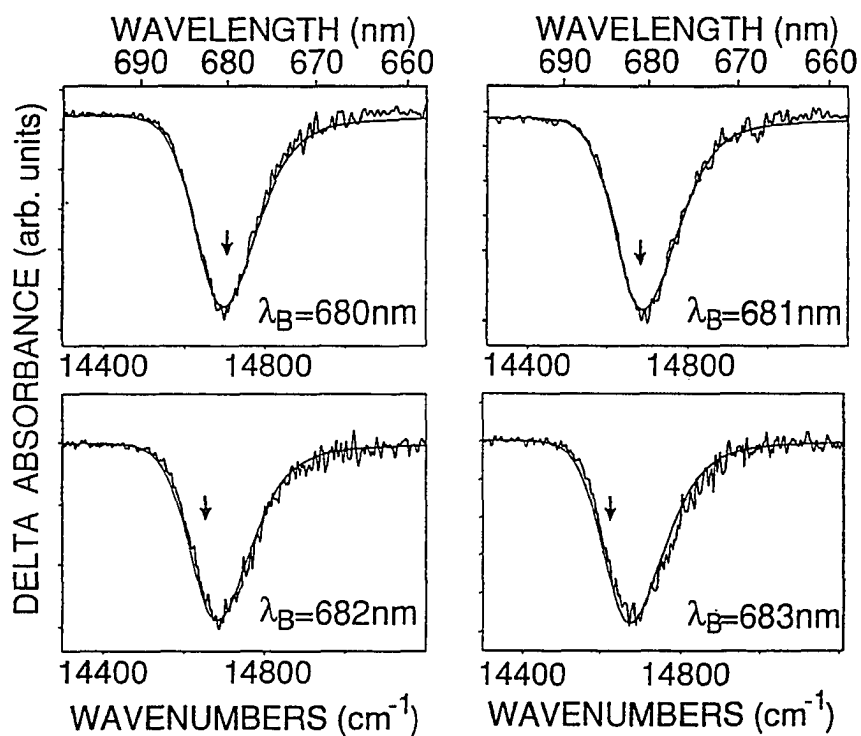


Figure 7. Experimental hole spectra (noisy solid lines), corrected for the monomer absorption, obtained at 77 K for different excitation wavelengths, i.e., 680, 681, 682, and 683 nm. Spectra were obtained with 4 cm<sup>-1</sup> resolution. The calculated (solid lines) profiles were obtained for the parameters given in Table I.



Table I we performed constant burn fluence experiments as a function of burn frequency. These experiments led to the experimental data points (X's) shown in Fig. 8. The diamonds in Fig. 8 correspond to the calculated hole areas. Again, the agreement between experiment and theory is good.

#### IV. Additional Results And Discussion

We discuss first, in the context of the results of the preceding section, the viability of the model that has 684 nm Chl *a* being a second pool of primary electron donor, i.e. P684. This model appears most reasonable when it is assumed that P680 is a manifestation of damage to P684 produced by the isolation and sample handling procedure, i.e., P684 of the isolated RC is the remnant of the true primary donor of the membrane bound RC [36,37]. The results of the preceding section prove that the contribution of the 684 nm Chl *a* to the 680 nm transient hole profile decreases with increasing temperature (above 4.2 K) and becomes negligibly small for  $T = 56$  K. Furthermore, the contribution to the low energy side of the 680 nm hole from the 684 nm Chl *a* is completely recovered by cycling back to 4.2 K. At the same time the absorption profile exhibits normal thermal broadening on both its low and high energy sides, Fig. 5. The spectra of Fig. 5 prove that the temperature-induced hole narrowing effect must be an excited state phenomenon since increasing temperature between 4.2 and 30 K does not perturb (eliminate) the 684 nm Chl *a* in the ground state. The P684 model could be argued to be consistent with the hole narrowing effect if it were to be assumed that the intersystem crossing yield of the  $Q_y$ -state of the 684 nm Chl *a* undergoes a very significant diminution with temperature between 4.2 and 30 K. We can conceive of no physical bases for this and, furthermore, the intersystem crossing yield for protochlorophylls in glasses has been shown to be independent of

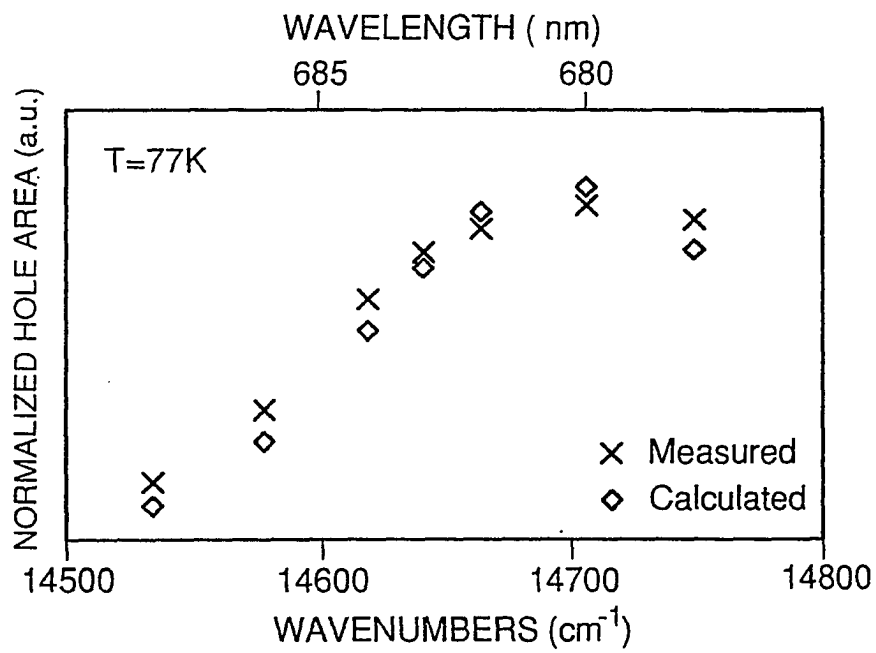
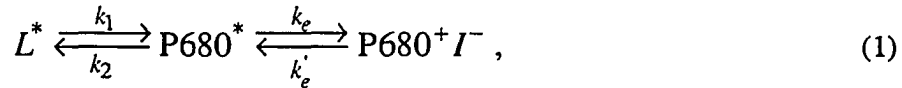


Figure 8. Normalized integrated transient hole areas plotted as a function of the excitation wavelength. Crosses and diamonds correspond to the experimental and calculated data, respectively.  $T = 77$  K and burn intensity  $\sim 100$  mW/cm<sup>2</sup>.

temperature [38]. We conclude, therefore, that the P684 model is untenable.

In what follows we present kinetic calculations which show that the model of Chang et al. [17], one that has the 684 nm Chl *a* being of the linker type important for energy transfer from the proximal antenna complexes to P680, is consistent with the results of the preceding section.

We denote the Q<sub>y</sub>-state of the 684 nm Chl *a* by L\*. Within the linker model of Chang et al. [17], L\* can serve as a trap state for P680\* since it lies lower in energy than P680\* by  $\Delta E \sim 90 \text{ cm}^{-1}$  (4 nm). For the experiments that led to the results of the previous section, it should be noted that L\* can also be directly populated by laser excitation and by energy transfer from the accessory Chl *a* (in this case where  $\lambda_B = 665 \text{ nm}$ ). We avoid this complexity by considering that at  $t = 0$  all the population is in L\*, i.e.,  $L^*(\Delta E, T, t = 0) = 1$ . For our purposes it suffices to consider the kinetic scheme



(where  $I \equiv$  electron acceptor) since our interest is in the temporal evolution of L\*, viewed as a population, due to thermally induced energy transfer to P680\*. That is, the decay of L\* to its ground state and triplet state (responsible for the hole burning of the 684 nm band) need not be included. We make the reasonable assumption that  $k_e \gg k_e'$ . The solution to (1) is then [39]

$$L^*(\Delta E, T, t) = L_0 [a_1 \exp(-\gamma_1 t) + a_2 \exp(-\gamma_2 t)] \quad (2)$$

where  $a_1 = k_1(\gamma_1 - k_e) / [\gamma_1(\gamma_1 - \gamma_2)]$  and  $a_2 = k_1(k_e - \gamma_2) / [\gamma_2(\gamma_1 - \gamma_2)]$ . The apparent rate constants  $\gamma_1$  and  $\gamma_2$  are given by:

$$\gamma_{1,2} = 1/2 \{k_1 + k_2 + k_e \pm [(k_1 + k_2 + k_e)^2 - 4k_1k_e]^{1/2}\}. \quad (3)$$

For the calculations which follow we assumed microscopic reversibility, i.e.  $k_1 = k_2 \exp(-\Delta E/kT)$ . It is well known that [40,41] structural heterogeneity of the protein leads to a distribution of values for  $\Delta E$ . Thus, one must average  $L^*$  of Eq. 2 over this distribution:

$$L^*(T, t) = \int_0^{\infty} d(\Delta E) g(\Delta E) L^*(\Delta E, T, t), \quad (4)$$

where we take  $g(\Delta E)$  to be a Gaussian with variance  $\sigma^2$  and a mean value for the energy gap of  $\Delta E_0$ .  $L^*(T, t)$  is now the population for the ensemble of RC. Again,  $\Delta E = E(\text{P680}^*) - E(L^*)$ . Hole burning has shown that [26] the site excitation energies of different electronic states of photosynthetic protein complexes are largely uncorrelated. In the absence of correlation,  $2.35 \sigma \sim 2^{1/2} \Gamma_{\text{inh}}$ , where, in this case,  $\Gamma_{\text{inh}}$  is the inhomogeneous broadening of both the P680 and 684 nm absorption bands. From Table I,  $\Gamma_{\text{inh}} \sim 100 \text{ cm}^{-1}$ . We allowed for some correlation by setting  $2\sigma = 60 \text{ cm}^{-1}$ .  $\Delta E_0$  was set equal to  $86 \text{ cm}^{-1}$  (4 nm). This choice of parameter values justifies the lower limit of the integral in Eq. 4. The calculation effectively takes into account  $\Delta E$ -values in the range of  $\sim 0$ -200  $\text{cm}^{-1}$  but ignores any dependence of  $k_2$  on  $\Delta E$ . That neglect should not affect the conclusions reached below.

The biexponential decay behavior of  $L^*$  for the single RC, Eq. 2, together with the distribution  $\Delta E$ -values leads to non-single exponential depopulation (detrapping) kinetics for  $L^*(T, t)$ , Eq. 2, of the RC ensemble. What was calculated, therefore, is the average lifetime,  $\langle \tau(T) \rangle$ , for  $L^*$  of the ensemble:

$$\begin{aligned}
\langle \tau(T) \rangle &= \int_0^{\infty} dt L^*(T, t) \\
&= \int_0^{\infty} dt \int_0^{\infty} d(\Delta E) L^*(\Delta E, T, t) \frac{1}{\sqrt{2\pi\sigma}} \exp[-(\Delta E - \Delta E_o)^2 / 2\sigma^2],
\end{aligned} \tag{5}$$

where  $L^*(\Delta E, T, t)$  is given by Eq. 2. It is known that the lifetime of P680\* is only weakly temperature dependent [9,10]; we chose  $k_e = (2.5 \text{ ps})^{-1}$  which is the average between the room temperature and 4.2 K values [9,15]. The rate constant  $k_2$  in scheme (1) is not known and, thus, calculations were performed for  $k_2 = (0.1 \text{ ps})^{-1}$  and  $(20 \text{ ps})^{-1}$ . Since in the linker model the 684 nm Chl *a* (L) are situated at the exterior of the RC complex, the former rate is viewed as being too fast. However, it seems likely that the true value lies somewhere between the two extremes.

The results for  $\langle \tau(T) \rangle$  are shown in Fig. 9, where the circles and squares correspond to  $k_2 = (0.1 \text{ ps})^{-1}$  and  $(20 \text{ ps})^{-1}$ , respectively. The solid arrow locates  $T = 30 \text{ K}$ . Values of  $\langle \tau(T) \rangle$ , the average detrapping time of  $L^*$ , are given in Table II. These values should be compared to the inverse of the intersystem crossing rate,  $(k_{IX})^{-1}$ , for  $L^*$  since the transient hole burning of the 684 nm Chl *a* reported on here is due to formation of  $^3L^*$ . The quantum yield for triplet formation is given by  $\phi_{IX}(T) \sim k_{IX} / (k_{IX} + k_{IC} + \langle \tau(T) \rangle^{-1})$ , where  $k_{IC}$  is the rate constant for internal conversion to the ground state. Since transient hole burning is readily observed for the 684 nm at 4.2 K, it is reasonable to take  $k_{IX} \sim k_{IC}$  with  $k_{IX} \sim (\text{lns})^{-1}$  [42]. From Table II it can be seen that  $\phi_{IX}(77 \text{ K}) \sim 0$  for both  $k_2$ -values used (and, therefore, any  $k_2$ -values in between), a result consistent with the data presented in the previous section. At 4.2 K,  $\langle \tau \rangle$  is extremely long, meaning that  $\phi_{IX}$  has a significant magnitude, consistent with experiment. Returning to Fig. 9 we note

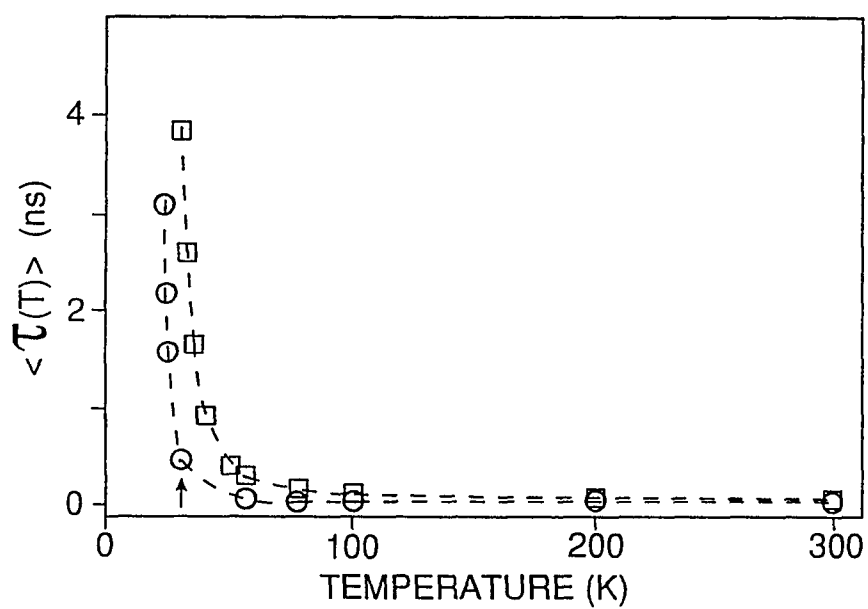


Figure 9. Temperature dependence of the average detrapping time  $\langle \tau(T) \rangle$  for the 684 nm  $Q_y$ -state. Results shown for two values of the  $P680^* \rightarrow L^*$  rate constant;  $k_2 = (20 \text{ ps})^{-1}$  [squares] and  $(0.1 \text{ ps})^{-1}$  [circles].

that  $\langle\tau(T)\rangle$  begins to increase rapidly at  $\sim 30$  and  $\sim 50$  K for  $k_2 = (0.1 \text{ ps})^{-1}$  and  $(20 \text{ ps})^{-1}$ , respectively. Again, this is in qualitative accord with the results of Fig. 3A and Fig. 4.

In summary, the linker model for the 684 nm Chl *a* of the PS II RC is entirely consistent with the temperature dependence of the 680 nm band hole profile. When  $k_2$  of scheme (1) is measured and more fine-grained temperature dependent hole spectra are available, we expect that even better agreement between experiment and theory will be achieved.

To conclude this section we consider one of the two  $k_2$ -values used in the calculations; namely  $k_2 = (0.1 \text{ ps})^{-1}$ . As mentioned, this rate seems too fast for energy transfer from P680\* to the  $Q_y$ -state of linker Chl *a*,  $L^*$ . If every RC of the ensemble possessed 684 nm Chl *a*, the width of the ZPH for P680 would reflect a lifetime of 0.1 ps. We have measured the width of this ZPH for several different RC preparations [15-17,28, unpublished results] and for the CP47-RC complex [14] and, in all cases, the hole width yielded a P680\* lifetime of  $\sim 1.9$  ps at 4.2 K, which is in close agreement with time domain measurements, cf. Introduction. These results, and, in particular, the result for the CP47-RC complex, suggest that  $k_2 \leq (1.8 \text{ ps})^{-1}$ .

Finally, a short comment on the nature of the 684 nm Chl *a* is in order. Brudvig et al. [43] showed that the PS II membranes possess a unique chlorophyll molecule(s), denoted as Chl<sub>Z</sub>, which is different from the accessory Chls, assuming structural analogy with the bacterial RC. They proposed that Chl<sub>Z</sub> (susceptible to photooxidation [43,44]) is located on the hydrophobic surface of the D1/D2 complex and suggested that the histidines-118 of the D1 and D2 proteins may serve as its potential ligands. Interestingly, an EPR signal similar to that of Chl<sub>Z</sub><sup>+</sup> in PS II membranes has also been observed in D1-D2-cyt b559 preparations [45] suggesting that indeed the Chl<sub>Z</sub> moiety, as a cofactor, might

Table II. Temperature dependence of the average detrapping time  $\langle\tau(T)\rangle$  for the 684-nm  $Q_y$ -state.

T [K]	$\langle\tau(T)\rangle$ (ps)	$\langle\tau(T)\rangle$ (ps)
	$k_2 = (0.1 \text{ ps})^{-1}$	$k_2 = (20 \text{ ps})^{-1}$
300	3.9	$3.4 \times 10^1$
200	4.9	$4.3 \times 10^1$
100	9.8	$8.5 \times 10^1$
77	$1.5 \times 10^1$	$1.3 \times 10^2$
40	$1.0 \times 10^2$	$8.8 \times 10^2$
35	$1.9 \times 10^2$	$1.6 \times 10^3$
30	$4.4 \times 10^2$	$3.8 \times 10^3$
25	$1.6 \times 10^3$	$1.4 \times 10^4$
20	$1.2 \times 10^4$	$1.0 \times 10^5$
4.2	$1.6 \times 10^{13}$	$1.4 \times 10^{15}$



be closely associated with the PS II RC. All the above, in agreement with our preliminary results (data not shown), raises the interesting question whether or not the ~684 nm Chl *a* and Chl<sub>z</sub> could be the same entity. Such a hypothesis seems to be very attractive; it would support the previous work of Brudvig et al. [43,44], indicating that some of the additional Chl *a* observed in the isolated PS II RC, in agreement with our linker model, could serve to link the antenna to the reaction center. Further experiments to test this working hypothesis are in progress.

### Acknowledgements

Research at the Ames Laboratory was supported by the Division of Chemical Sciences, Office of Basic Energy Sciences, U.S. Department of Energy. Ames Laboratory is operated for USDOE by Iowa State University under contract W-7405-Eng-82. We would like to thank R. Picorel and M. Seibert of the National Renewable Energy Laboratory for generously providing us with the reaction center preparations and J. M. Hayes of the Ames Laboratory for assistance at the early stages of the calculations of the temperature dependent hole profiles. We are grateful to Dow Chemical for supporting one of us (H-C. Chang) through a Research Fellowship.

### References

1. Nanba, O; Satoh, K. *Proc. Natl. Acad. Sci. USA* 1987, 84, 109.
2. Seibert, M. in: *The Photosynthetic Reaction Center*, Vol. I; Deisenhofer, J., Norris, J., Eds.; Academic Press: New York, 1993, p. 319.
3. Satoh, K. *ibid.* p. 289.
4. Chapman, D.J.; Goumans, K.; Barber, J. *Biochim. Biophys. Acta* 1988, 933, 423.
5. McTavish, H.; Picorel, R.; Seibert, M. *Plant Physiol.* 1989, 89, 452.

6. Satoh, K.; Nakane, H. in: *Current Research in Photosynthesis*; Baltscheffsky, M., Ed.; Kluwer Academic Publ.: Dordrecht; Vol. 1, 1989, p. 271.
7. Akabori, K.; Tsukamoto, H.; Tsukihata, J.; Motokawa, O.; Toyoshima, Y. *Biochim. Biophys. Acta* 1988, 932, 345.
8. Ghanotakis, D.F.; DePaula, J.C.; Demetris, D.M.; Bowlby, N.R.; Peterson, J.; Babcock, G.T.; Yocum, C.F. *Biochim. Biophys. Acta* 1989, 974, 44.
9. Wasielewski, M.R.; Johnson, D.G.; Seibert, M.; Govindjee *Proc. Natl. Acad. Sci.* 1989, 86, 524.
10. Wasielewski, M.R.; Johnson, D.G.; Seibert, M.; Govindjee; Preston, C.; Seibert, M. *Photosyn. Res.* 1989, 22, 89.
11. Durrant, J.R.; Hastings, G.; Joseph, D.M.; Barber, J.; Porter, G.; Klug, D.R. *Proc. Natl. Acad. Sci. USA* 1992, 89, 11632; *ibid. Biochemistry* 1993, 32, 8259.
12. Hastings, G.; Durrant, J.R.; Barber, J.; Porter, G.; Klug, D.R. *Biochemistry* 1992, 31, 7638.
13. Holzwarth, A.R.; Muller, M.G.; Gatzert, G.; Hucke, M.; Griebenow, K. *J. of Lumin.* 1994, 60 & 61, 497.
14. Jankowiak, R.; G. J. Small, G.J. in *The Photosynthetic Reaction Center*, Vol. 2; Deisenhofer, J., Norris, J., Eds.; Academic Press: New York, 1993, p.133.
15. Jankowiak, R.; Tang, D.; Small, G.J.; Seibert, M. *J. Phys. Chem.* 1989, 93, 1649.
16. Tang, D.; Jankowiak, R.; Seibert, M.; Yocum, C.F.; Small, G.J. *J. Phys. Chem.* 1990, 94, 6519.
17. Chang, H.-C.; Jankowiak, R.; Reddy, N.R.S.; Yocum, C.F.; Picorel, R.; Seibert, M.; Small, G.J. *J. Phys. Chem.* 1994, 98, 7725.
18. Vink, K.J.; de Boer, S.; Plijter, J.J.; Hoff, A.J.; Wiersma, D.A. *Chem. Phys. Lett.* 1987, 142, 433.
19. Kirmaier, C.; Holten, D. in *The Photosynthetic Reaction Center*, Vol. II; Deisenhofer, J., Norris, J.R., Eds.; Academic Press: New York, 1993, p. 49.

20. Parson, W.W. in *Chlorophylls*; Scheer, H., Ed.; CRC Press: Boca Raton, 1991, p. 1153.
21. Friesner, R.A.; Won, Y. *Biochim. Biophys. Acta* 1989, 977, 99.
22. Kwa, S.L.S.; Eijkelhoff, C.; van Grondelle, R.; Dekker, J.P. *J. Phys. Chem.* 1994, 98, 7702.
23. Van der Vos, R.; van Leeuwen, P.J.; Braun, P.; Hoff, A.J. *Biochim. Biophys. Acta* 1992, 1140, 184.
24. Otte, S.C.M.; van der Vos, R.; van Gorkom, H.J. *J. Photochem. Photobiol.* 1990, B15, 5.
25. Van Grondelle, R.; Dekker, J.P.; Gillbro, T.; Sundstrom, V. *Biochim. Biophys. Acta* 1994, 1187, 1.
26. Jankowiak, R.; Hayes, J.M.; Small, G.J. *Chem. Rev.* 1993, 93, 1471.
27. Van Kan, P.J.M.; Otte, S.C.M.; Kleinherenbrink, A.M.; Nieveen, M.C.; Aartsma, T.J.; van Gorkom, H.J. *Biochim. Biophys. Acta* 1990, 1020, 146.
28. Tang, D.; Jankowiak, R.; Seibert, M.; Small, G.J. *Photosynth. Res.* 1991, 27, 19.
29. Yruela, I.; van Kan, P.J.M.; Muller, M.G.; Holzwarth, A.R. *FEBS Letters* 1994, 339, 25.
30. Montoya, G.; Yruela, I.; Picorel, R. *FEBS Lett.* 1990, 283, 255.
31. Dekker, J.P. (private communication).
32. Breton, J. in: *Perspectives in Photosynthesis*; Jortner, J., Pullman, B., Eds.; Kluwer Academic: Dordrecht, 1990, p.23.
33. Van der Vos, R.; van Leeuwen, P.J.; Braun, P.; Hoff, A.J. *Biochim. Biophys. Acta* 1992, 1140, 184.
34. Hayes, J.M.; Lyle, P.A.; Small, G.J. *J. Phys. Chem.* 1994, 98, 7337.
35. Hayes, J.M.; Gillie, J.K.; Tang, D.; Small, G.J. *Biochim. Biophys. Acta* 1988, 932, 287.

36. Carbonera, D.; Valentin, M.D.; Giacometti, G.; Agostini, G. *Biochim. Biophys. Acta* 1994, 1185, 167.
37. Carbonera, D.; Giacometti, G.; Agostini, G. *FEBS Lett.* 1994, 343, 200.
38. Avarma, R.; Muring, K.; Suisalu, A. *Chem. Phys. Lett.* 1981, 77, 88.
39. Moore, J.W.; Pearson, R.G. in *Kinetics and Mechanism*; John Wiley & Sons: New York, 1981, p.313.
40. Frauenfelder, H.; Sligar, S.G.; Wolynes, P.G. *Science* 1993, 254, 1598.
41. Small, G.J.; Hayes, J.M.; Silbey, R.J. *J. Phys. Chem.* 1992, 96, 7499.
42. Karukstis, K.K. in: *Chlorophylls*; Scheer, H., Ed.; CRC Press: Boca Raton, Fla., 1991, chapter 3, p.769.
43. Koulougliotis, D.; Innes, J.B.; Brudvig, G.W. *Biochemistry* 1994, 33, 11814.
44. Buser, C.A.; Thompson, L.K.; Diner, B.A.; Brudvig, G.W. *Biochemistry* 1990, 29, 8977.
45. Nugent, J.A.H.; Telfer, A.; Demetriou, C.; Barber, L. *FEBS Lett.* 1989, 255, 53.

## CHAPTER 7 PRESSURE DEPENDENCE OF PRIMARY CHARGE SEPARATION IN A PHOTOSYNTHETIC REACTION CENTER

A paper to be published in *Chem. Phys.* 1995, in press

H.-C. Chang, R. Jankowiak, N. R. S. Reddy and G. J. Small

### Abstract

Spectral hole burning is used to study the pressure dependence of the  $Q_y^-$  absorption spectrum and primary charge separation kinetics of the D1-D2-cyt b<sub>559</sub> reaction center complex of photosystem II. The 4.2 K lifetime of P680\*, the primary donor state, lengthens from 2.0 ps at 0.1 MPa to 7.0 ps at 267 MPa. Importantly, this effect is irreversible (plastic), in sharp contrast with the elastic effects of pressure on the low temperature absorption and non-line narrowed hole spectrum of P680. These observations and data which show that the electron-phonon coupling is weakly dependent on pressure, suggest a model that has the plastic behavior of charge separation kinetics due mainly to the pressure dependence of the energy of the acceptor state and of the variance of the P680\*-acceptor energy gap stemming from structural heterogeneity. Nonadiabatic rate expressions, which take into account the distribution of energy gap values, are used to estimate the linear pressure shift of the acceptor state energy for both the superexchange and two-step mechanisms for primary charge separation. For both mechanisms shifts in the vicinity of  $1 \text{ cm}^{-1}/\text{MPa}$  are required to explain the data, a value which is not unreasonable based on pressure dependent studies of other systems. The results point to the marriage of hole burning (also ultra-fast spectroscopy) and high pressures as having considerable

potential for the study of primary transport dynamics in reaction center and antenna complexes.

## I. Introduction

The problem of primary charge separation in photosynthetic reaction centers (RC) remains as one of great interest and intense study. The bacterial RC of *Rhodobacter sphaeroides* and *Rhodospseudomonas viridis* have received the most attention since their crystal structures are known and their  $Q_y$ -absorption spectra particularly well resolved [for recent reviews see refs. 1-6]. However, primary charge separation in the D1-D2-cyt b559 RC of photosystem II has received increased attention [for reviews see refs. 7,8] since its isolation in 1987 by Nanba and Satoh [9]. There is significant sequence homology between the L and M proteins of the bacterial RC and the D1 and D2 proteins [10-13]. By analogy with the bacterial RC, the PS II RC possesses a special pair of chlorophyll *a* (Chl *a*) molecules which, however, are considerably less strongly exciton-coupled than in the bacterial RC [14,15], two pheophytin *a* (Pheo *a*) and two quinone molecules, which are lost during isolation of the RC. While the  $Q_y$ -absorption spectrum of the PS II RC spans a range of only about  $500\text{ cm}^{-1}$  (spectrum a of frame B in Fig. 1 is the spectrum at 1 atm and 4.2 K) the spectra of the bacterial RC span a range of about  $3000\text{ cm}^{-1}$ . Despite this and other differences, both the bacterial and PS II RC reduce the active BPheo (Pheo) molecule in 3 ps at room temperature following excitation of the primary donor state  $P^*$  ( $P_{\text{L}}$ ). Moreover, this reduction undergoes a slight acceleration in the low temperature limit (for the data on the PS II RC see refs. 14 and 16-18).

Both ultrafast and spectral hole burning spectroscopies have been extensively applied to the study of the bacterial and the PS II RC and, in the case of the bacterial RC,

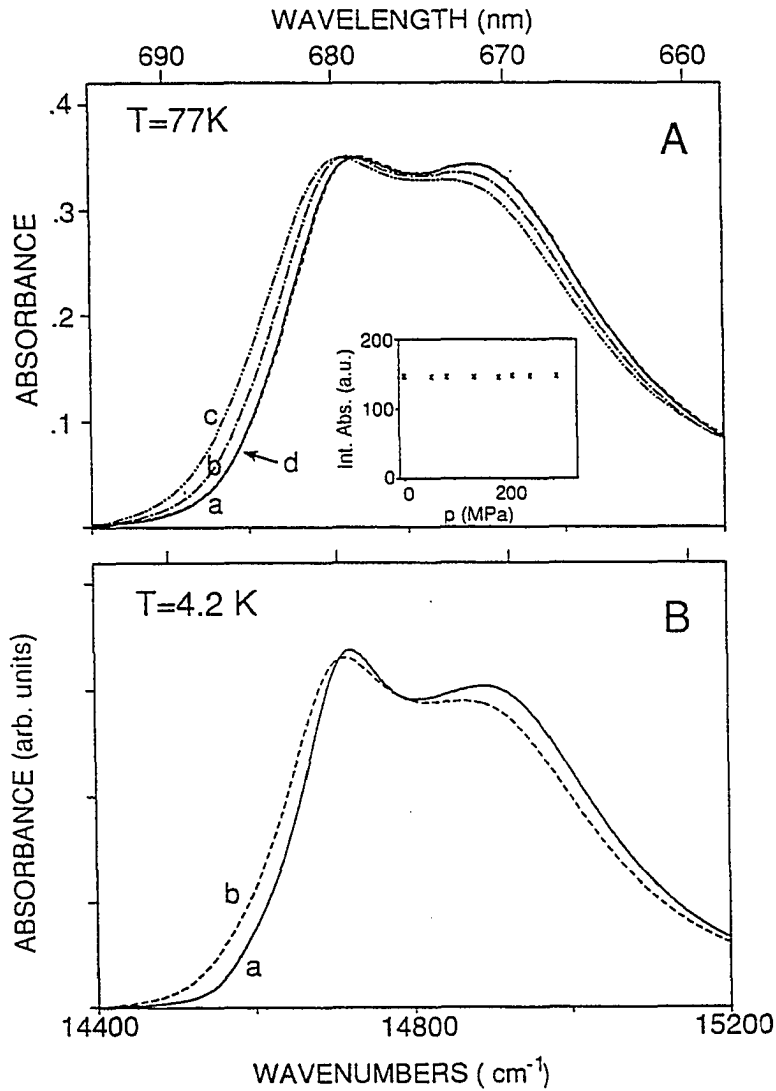


Figure 1. Frame A: absorption ( $Q_y$ -region) of PS II-RC obtained at  $T = 77$  K for  $p = 0.1$  MPa (curve a), 141 MPa (curve b), and 308 MPa, respectively. Spectrum d is the spectrum upon pressure release. The inset shows the absence of a pressure dependence of the integrated absorption intensity. Frame B: low-temperature ( $T = 4.2$  K) absorption spectra of PS II RC obtained at  $p = 0.1$  MPa (curve a) and  $p = 267$  MPa (curve b), respectively.

site directed mutagenesis has been used to investigate the effects of specific residues on the driving force of charge separation [19]. In addition, the Stark effect has been employed to probe the electronic structure of  $P^*$  [20] and to determine the dependence of the primary charge separation kinetics on applied field in the bacterial RC [21,22].

Recently, we initiated a program to study the effects of pressure on the excited electronic state structure and transport dynamics of photosynthetic protein complexes. Windsor and coworkers [23-25] had already demonstrated that pressures of  $\sim 350$  MPa have a significant effect on the kinetics of secondary charge separation in the RC of *Rb. sphaeroides* and *Rps. viridis*, cf. section IV. These works and those on the  $Q_y$ -absorption spectra of the *Rps. viridis* [26] and *Rb. sphaeroides* [27,28] RC, the B800-B850 antenna complex [29] of *Rb. sphaeroides* and of the FMO antenna complex of *Chlorobium tepidum* [30] have clearly demonstrated that the linear pressure shifts (to the red) of  $Q_y$ -states can be large ( $\sim 0.5 \text{ cm}^{-1}/\text{MPa}$  for P870 and P960 of *Rb. sphaeroides* and *Rps. viridis*). In addition, the pressure shifts for different  $Q_y$ -states of a given complex are generally not the same. This is important since one can alter the energy gap(s) associated with energy and electron transfer. In addition, however, pressure may affect other parameters important to transfer such as the reorganization energy (electron-phonon coupling), the electronic coupling and the structural heterogeneity which leads, for example, to a distribution of values for donor-acceptor energy gaps. Fortunately, spectral hole burning can be used to examine the pressure dependencies of these quantities.

In this paper we present the results of high pressure-hole burning studies of the electronic structure and primary charge separation kinetics ( $P680^*$  lifetime) of the PS II RC. To the best of our knowledge this is the first report of pressure having a significant effect on primary charge separation; at 4.2 K (low temperature limit) the  $P680^*$  lifetime of



2.0 ps at 0.1 MPa lengthens by a factor of 3.5 as the pressure is increased to 267 MPa. This pronounced effect is irreversible (plastic) in contrast with the elastic pressure dependence of the low temperature (4.2, 77 K) absorption and non-line narrowed P680 hole spectrum. This contrasting behavior, together with other observations, allow for a quite straightforward theoretical analysis of the pressure dependence of the primary charge separation kinetics.

By way of background on the PS II RC, we mention that the understanding of the excited state electronic structure and primary charge separation kinetics of the PS II RC is made more difficult than for the bacterial RC due to spectral congestion. Whereas all six  $Q_y$ -state absorption bands of the RC of *Rps. viridis* have been resolved at 4.2 K [31], only two bands at ~680 and ~670 nm are apparent in the spectra of Fig. 1. Although the special pair, P680, is the major contributor to the 680 nm band, there is also a contribution from the active Pheo *a* molecule [16,32,33]. Fortunately, spectral hole burning can isolate P680\* and the Pheo *a*  $Q_y$ -state. The latter gives rise to persistent nonphotochemical hole burning while P680\* does not [16]. Typical preparations of PS II particles contain additional Chl *a* which take the Chl *a* / Pheo *a* ratio beyond the value of 2 for the bacterial RC [10-11]. Contributing to the additional Chl *a* are the fragile 684 nm absorbing Chl *a* [14], which have very recently been proven to be "linker" Chl *a*, located near the periphery of the complex. These Chl *a* serve to shuttle energy from the proximal antenna complexes to P680 [34]. However, the contribution from the 684 nm Chl *a* to the triplet bottleneck hole profile associated with the 680 nm absorption band is eliminated at temperatures  $\geq 30$  K [34], cf. section III. Despite the apparent variability in the amount of the additional Chl *a* contributing to PS II RC, hole burning of many different preparations have shown that the P680\* lifetime at 4.2 K is invariant to the amount of additional Chl *a*,

$1.9 \pm 0.2$  ps [14]. Indeed, the P680\* lifetime has also been found to be the same for the PS II RC-CP47 complex [35], where CP47 is one of the two (CP43 being the other) proximal antenna complexes. Returning to the 670 nm absorption band, we note that it is contributed to by the two accessory Chl *a* of the hydrophobic core of the RC and, probably, also by the second Pheo *a* molecule. Based on the results of refs. 14 and 35 it appears certain that dysfunctional Chl *a* produced during isolation and sample handling also contribute. In this paper, however, the 670 nm band is of no concern.

## II. Experimental

High pressures were generated by a three-stage compressor (model U11, Unipress-equipment Division, Polish Academy of Sciences, Warsaw, Poland). Helium gas is used as the pressure transmitting medium. Gas flow between compressor stages is regulated by needle valves with the first stage connected to a helium gas cylinder. At the heart of the compressor is a pump capable of generating pressures of up to 80 MPa with manually controlled output. Compression ratios in the first and second stages are close to one and five, respectively. The multiplication ratio for the third stage is 79 so that the maximum pressure is 1.5 GPa. A flexible thick walled beryllium-copper capillary (od/id = 3 mm/0.3 mm) connects the third stage of the compressor with a specially designed high pressure optical cell (Unipressequipment) for variable temperatures which has a maximum pressure rating of 800 MPa. A manganin resistance gauge (model MPG10, Unipressequipment) was placed inside the third stage of the compressor to measure the gaseous helium pressure.

The main cylindrical body of the pressure cell was made of Be-Cu alloy (Brush alloy 25) with an outer diameter and height of 80 and 76 mm, respectively. A schematic of the cell is given in Fig.2. Samples contained in double walled gelatin capsule (sample

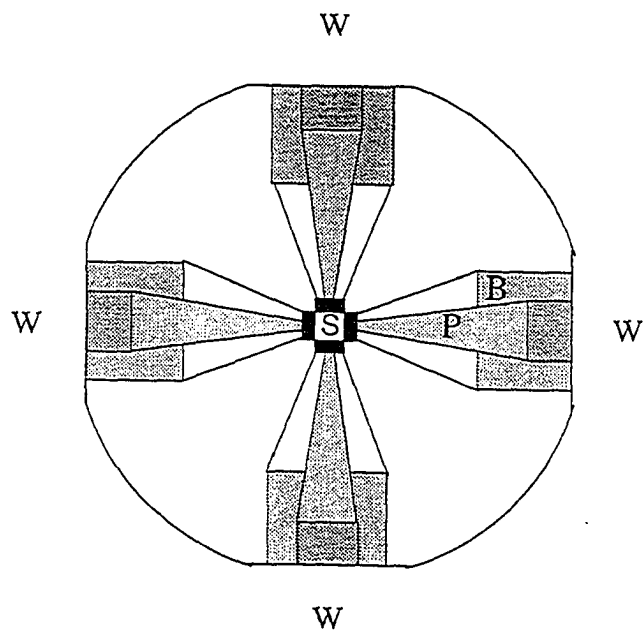


Figure 2. Top view of the high pressure cell showing the conical (P) and annular brass plug (B) holding the sapphire windows (dark rectangles) surrounding the sample (S). Optical access labeled by W.

volume of  $(7 \text{ mm})^3$ ) are placed in the cell cavity which has an outer diameter and height of 7 and 8 mm, respectively. Optical access to the sample is provided by four sapphire windows (thickness of 4 mm). Windows are supported by window plugs (Ni-Cr alloy) having a conical light port with 2.5 mm inner diameter aperture and a 14 degree opening angle. Each conical plug is held in place by an annular brass plug. Tightening of the brass plugs (using specially designed O-rings covered with a thin layer of indium) isolates the high pressure sample region from the outside. For low temperature measurements the pressure cell is placed in a custom made liquid helium cryostat with a 3.5 inch inner diameter tail section (model II DT supervaritemp, Janis Research Co., Wilmington, MA). Sample temperature was monitored using a calibrated (1.4-360 K) silicon diode thermometer (Lake Shore Cryogenic Model DT-470) mounted on top of the pressure cell. Performing high pressure experiments at low temperatures presents some difficulties since helium solidifies at a pressure of 18 MPa at 4.2 K and, e.g., at 800 MPa at 55 K. Thus, at 4.2 K the sample needs to be warmed to effect a pressure change at higher pressures. Furthermore, once the sample is cooled below the freezing point of helium there is a slight pressure drop from the third compressor stage to the pressure cell due to blockage of the capillary (prior to freezing of He in the cell). This pressure drop was corrected for using a calibration curve which was provided by Unipress. Calibration was obtained by comparison of pressures measured at the cell cavity with a silicon diode with those measured in the third stage of the compressor, *vide-supra*. Note: utilization of high pressures poses a potential danger to the operator. To minimize danger we employed safety shields (6 mm thick polycarbonate, Lexan<sup>tm</sup>) of suitable heights around the cryostat and compressor so as to block/redirect flying debris in the case of accidental decompression of either the pressure cell or the compressor. The Be-Cu high pressure line

(length of ~2 m) was encased in a tough flexible metal shroud and secured to the laboratory ceiling.

The hole burning setup used is described elsewhere [16,17]. Briefly, absorption and hole burned spectra were recorded with a Bruker HR120 Fourier transform spectrometer. A Coherent CR699-21 ring dye laser (linewidth of  $0.07\text{ cm}^{-1}$ ), pumped by a 6 W Coherent Innova argon ion laser, was used for hole burning. The spectrometer was used at a resolution of  $4\text{ cm}^{-1}$  except for high resolution scans of the zero-phonon holes.

Samples of the D1-D2-cyt b<sub>559</sub> RC complex from spinach leaves were generously provided by M. Seibert and R. Picorel. Details of the isolation procedure are given in ref. 14. The 4.2 K (0.1 MPa) absorption spectrum shown as a of frame B in Fig. 1 is similar to the absorption spectrum given in Fig. 2 (spectrum a) of ref. 14.

### III. Experimental Results

Illustrative  $Q_y$ -absorption spectra of the PS II RC obtained at different pressures are shown in Fig. 1 for 77 K (A) and 4.2 K (B). Spectra a, b and c of frame A correspond to pressures of 0.1, 141 and 308 MPa, respectively. These and several other spectra ( $p < 308\text{ MPa}$ ) yielded linear pressure shifts (77 K) of  $-0.08$  and  $-0.04\text{ cm}^{-1}/\text{MPa}$  for the 680 and 670 nm bands, respectively. Spectrum d was obtained at 77 K following release of pressure from 308 MPa to 0.1 MPa. This spectrum is indistinguishable from spectrum a of the "virgin" sample obtained at 0.1 MPa. As proven in ref. 16, the pheophytin band at ~681 nm can be isolated for study by nonphotochemical hole burning (P680\* does not undergo measurable nonphotochemical hole burning). The pressure dependence of the pheophytin hole at 77 K and 4.2 K burned under non-line narrowing conditions yielded a linear pressure shift of  $-0.04\text{ cm}^{-1}/\text{MPa}$  and its pressure behavior was observed to be elastic (results not shown). As discussed in section IV, the above pressure shifts are

considerably smaller than those of the bacterial RC. The absorption spectra of frame B obtained at 0.1 MPa (a) and 267 MPa (b) illustrate the extent to which the 680 and 670 nm bands are better resolved at 4.2 K. Not shown is the 4.2 K absorption spectrum obtained upon pressure release from 267 MPa to 0.1 MPa. It is identical to that of the virgin sample at 0.1 MPa, spectrum a. On the basis of the absorption spectrum it would appear that the pressure induced structural changes of the PS II RC are elastic at 4.2 and 77 K.

In what follows we will be concerned only with the 680 nm band and, in particular, P680. To this end we employed triplet bottleneck hole burning, cf. section I. Transient hole profiles obtained at 4.2 K under non-linear narrowing conditions ( $\lambda_B = 665$  nm) are shown in Fig. 2 for pressures of 0.1 MPa (a) and 267 MPa (b). The transient hole near 680 nm is dominated by P680 although there is a small contribution from the 684 nm linker Chl *a* [14], dashed arrow in spectrum a. From the data in the inset the linear pressure shift (at  $T = 4.2$  K) of the 680 nm hole is  $-0.07$   $\text{cm}^{-1}/\text{MPa}$ . There is also a significant pressure broadening effect, *vide infra*. The broad and relatively weak ( $\sim \times 10$ ) hole near 668 nm is the upper dimer component of the special pair [14,15]. By analogy with the special pair of the bacterial RC, the upper and lower components can be referred to as  $P_+$  and  $P_-$  (P680\*) [14,15]. The hole spectra obtained at pressures of 0.1, 141, and 267 MPa indicate that the linear pressure shift for  $P_+$  is the same as that for  $P_-$  within experimental uncertainty,  $\pm 0.01$   $\text{cm}^{-1}/\text{MPa}$ . By way of contrast, the shifts for  $P_-$  and  $P_+$  of *Rps. viridis* at 4.2 K are  $-0.42$  and  $-0.15$   $\text{cm}^{-1}/\text{MPa}$  [22,26].

It was recently proven that the contribution from the 684 nm Chl *a* to the triplet bottleneck hole profile at 680 nm is eliminated at temperatures  $\geq 30$  K [34]. This is a consequence of thermally induced energy transfer from the  $Q_y$ -state of the 684 nm "linker" Chl *a* to P680\* which undergoes electron transfer in 2 ps [14]. At 4.2 K this energy

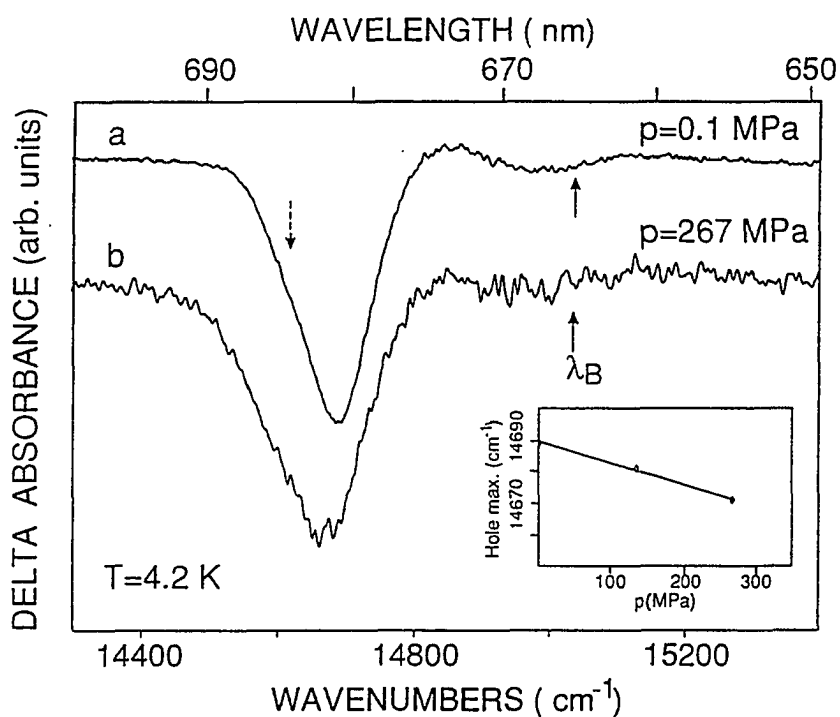


Figure 3. Transient triplet bottleneck hole spectra of PS II RC obtained under non-linear narrowing conditions with  $\lambda_B = 665$  nm at  $T = 4.2$  K and  $p = 0.1$  MPa (curve a) and  $p = 267$  MPa (curve b). The inset shows the pressure shift rate per MPa of the hole maximum ( $-0.07$  cm<sup>-1</sup>/MPa). Burn intensity at the sample  $\sim 200$  mW/cm<sup>2</sup>. Positions of the hole maxima were obtained by fitting the top one-third of the hole to a Gaussian. Estimated uncertainty in shift rate is  $\pm 0.005$  cm<sup>-1</sup>/MPa.

transfer process is negligible [34].

In view of this, the pressure dependence of the 680 nm hole was determined at 77 K ( $\lambda_B = 665$  nm) so as to better isolate P680. 680 nm hole profiles are shown in Fig. 4(A) for 25 and 308 MPa. The results obtained for twelve pressure values, frame B, yielded a linear pressure shift and broadening of  $-0.09$  and  $-0.10$   $\text{cm}^{-1}/\text{MPa}$ , respectively. The triangle and square data points in frame B of Fig. 4 were obtained following release of pressure from 308 MPa to 0.1 MPa and are equal to those obtained for the virgin sample at 0.1 MPa. Thus, the non-linear narrowed 680 nm hole profile also indicates that the pressure induced structural changes of the PS II RC are elastic. That is, there is no indication of denaturation or irreversible conformational drift (plasticity). We note that the 680 nm hole is determined by the P680 hole profile and an interference from the ground state absorption of a Chl *a* monomer associated with  $^3\text{P680}^*$  [14,15]. Correction for the interference led to a value of  $0.16$   $\text{cm}^{-1}/\text{MPa}$  for the linear broadening of P680, *vide infra*.

In order to determine whether the primary charge separation kinetics ( $\text{P680}^*$  lifetime) carries a pressure dependence, triplet bottleneck hole burning experiments were performed under line-narrowing conditions at 4.2 K. Such experiments at  $p = 1$  atm had led earlier to a  $\text{P680}^*$  lifetime of  $1.9 \pm 0.2$  ps at 4.2 K [14,16,35]. P680 profiles obtained with  $\lambda_B = 680.5$  nm are shown in Fig. 5 for a pressure of 0.1 MPa (a) and 267 MPa (b). The sharp feature in each spectrum is the zero-phonon hole (ZPH) which is coincident with the burn frequency. The broader underlying structure is due to the phonon sideband holes which have been thoroughly discussed [14,34] but will be considered again in section IV. The results of calculations presented in the same section indicate that the pressure dependence of the linear electron-phonon coupling is weak and that the pressure dependence of the entire P680 profile can be explained in terms of a narrowing of the ZPH



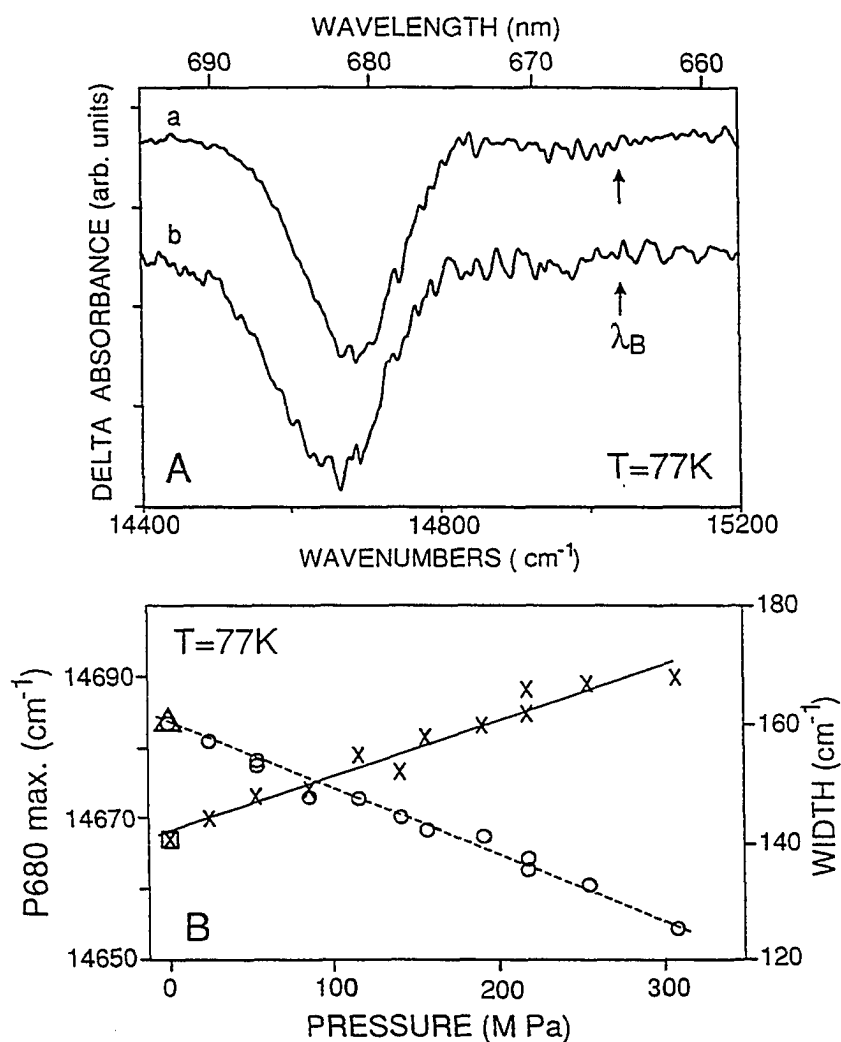


Figure 4. Frame A: non-line narrowed transient hole-burned spectra of PS II RC obtained at 77 K and  $p = 25$  MPa (curve a) and  $p = 308$  MPa (curve b), respectively. Frame B: pressure dependence of the hole width (crosses) and the frequency position of the P680 hole maximum (circles). The square and triangle denote the hole width and P680 maximum upon pressure release to  $p = 0.1$  MPa. Burn intensity at the sample estimated to be  $\sim 200$  mW/cm<sup>2</sup>. Uncertainty in cited values of pressure shift and broadening is  $\pm 0.003$  cm<sup>-1</sup>/MPa and  $\pm 0.01$  cm<sup>-1</sup>/MPa, respectively.

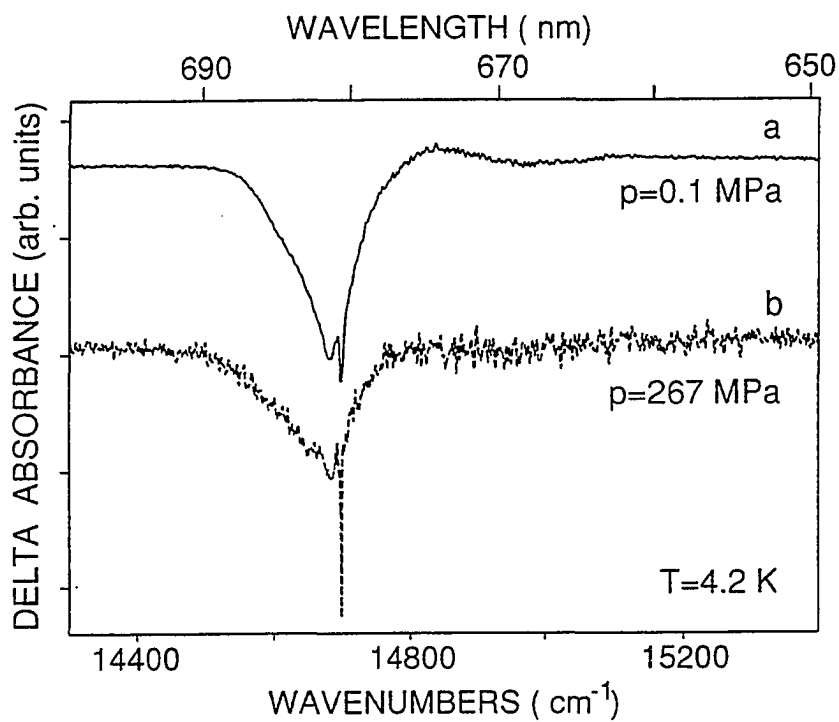


Figure 5. Line-narrowed transient triplet bottleneck hole spectra (4.2 K) obtained at two different pressures:  $p = 0.1$  MPa (curve a), and  $p = 267$  MPa (curve b), respectively ;  $\lambda_B = 680.4$  nm. The ZPH widths are  $5.2$   $\text{cm}^{-1}$  (at  $p = 0.1$  MPa) and  $1.5$   $\text{cm}^{-1}$  ( $p = 267$  MPa), respectively. Burn intensity at the sample  $\sim 100$   $\text{mW}/\text{cm}^2$ .

and an increase of the inhomogeneous broadening with increasing pressure. High resolution scans of the ZPH for 0.1 MPa and 267 MPa yielded ZPH widths of  $5.2 \text{ cm}^{-1}$  (0.1 MPa) and  $1.5 \text{ cm}^{-1}$  (267 MPa), see Fig. 5, which correspond to P680\* lifetimes of 2.0 and 7.0 ps, respectively. To the best of our knowledge this is the first demonstration that pressure can affect primary charge separation.

An important observation is presented in Fig. 6 (spectrum a). It is that upon release of pressure from 267 to 141 MPa and, subsequently, to 0.1 MPa, the 2.0 ps P680\* lifetime of the virgin sample at 0.1 MPa is not recovered. Rather, the 7.0 ps lifetime corresponding to a ZPH width of  $1.5 \text{ cm}^{-1}$  persists. Spectrum a of Fig. 6 should be compared with spectrum a of Fig. 5. Thus, unlike the absorption and non-line narrowed hole spectra of P680, the ZPH reveals a plastic response of the PS II RC to pressure. The persistence of the irreversibility of the pressure induced structural changes is conveyed by spectrum b of Fig. 6. This 0.1 MPa spectrum (4.2 K) was obtained after warming the sample (which yielded spectrum a of the same figure) to  $0^\circ \text{ C}$ , annealing for 3 h at  $0^\circ \text{ C}$  followed by cooling to 4.2 K. The depth of the ZPH in spectrum b has decreased by 30% while its width has increased to  $2.3 \text{ cm}^{-1}$ . It appears, therefore, that annealing at ice temperature can restore, at least partially, the PS II RC to its original "virgin" state.

Finally, Fig. 7 shows the pressure dependence of the P680 hole area obtained under non-line narrowing ( $\lambda_B = 665 \text{ nm}$ ) and constant burn intensity conditions at 77 K (X's). The open and solid square data points were obtained at 4.2 K with  $\lambda_B = 680.5 \text{ nm}$  for a pressure of 267 and 0.1 MPa, respectively. The data show that the steady state population of  $^3\text{P680}^*$  decreases at pressures greater than about 150 MPa which suggests that the yield for its formation from the  $\text{P680}^+\text{Pheo}^-$  radical pair state and/or its lifetime are affected by pressure. We note that a decrease in the lifetimes of singlet and triplet states of aromatic

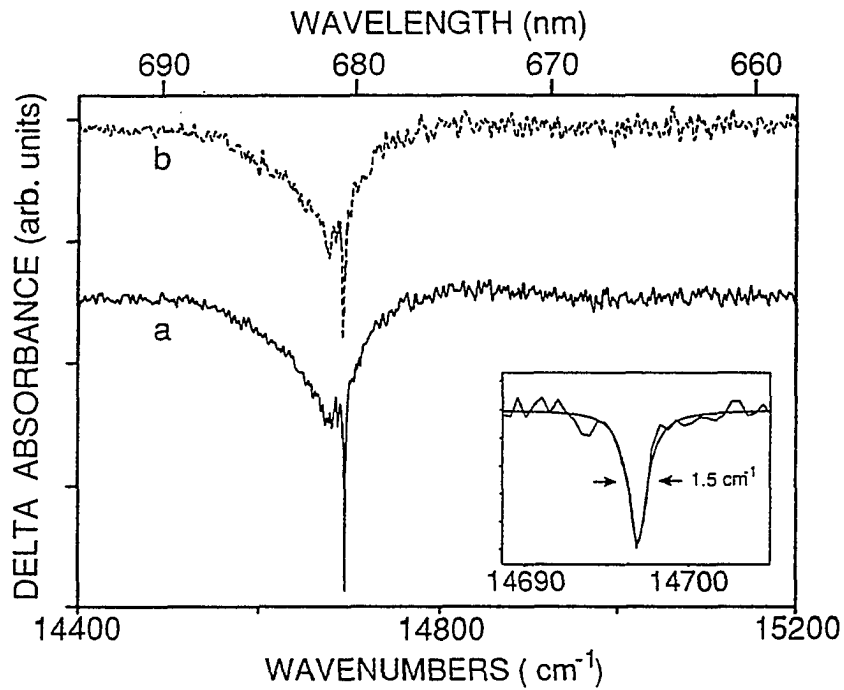


Figure 6. Line-narrowed transient hole spectra ( $T = 4.2$  K,  $\lambda_B = 680.5$  nm) obtained immediately upon pressure release to  $p = 0.1$  MPa (curve a) and after annealing (curve b) for 3 hrs. at ice temperature (see text for explanation). The inset shows the Lorentzian fit to the zero-phonon hole profile of spectrum a with  $2\gamma = 1.5$  cm<sup>-1</sup>. Burn intensity at the sample  $\sim 100$  mW/cm<sup>2</sup>.

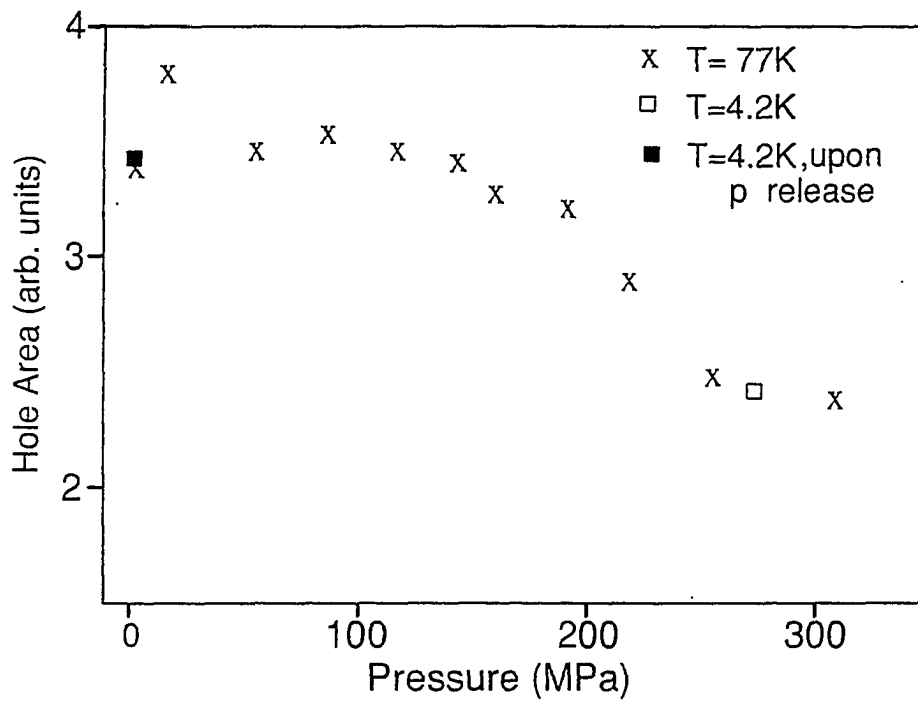


Figure 7. Pressure dependence of the normalized transient hole areas. Crosses and squares correspond to the integrated transient hole area obtained under non-line narrowing ( $T = 77\text{ K}$ ,  $\lambda_{\text{ex}} = 665\text{ nm}$ ) and line-narrowing ( $T = 4.2\text{ K}$ ; open black square  $\lambda_{\text{ex}} = 682.1\text{ nm}$ ; black square  $\lambda_{\text{ex}} = 680.5\text{ nm}$ ) conditions, respectively.

molecules have been reported [36] and that the triplet lifetime of BChl *a* in pyridine undergoes a decrease of 25% [25] over a pressure range comparable to ours. The data in Fig.7 also show that the pressure effect on the steady state population of  $^3P680^*$  is reversible (elastic), see solid square data point.

#### IV. Discussion And Calculations

##### A. Pressure Dependence Of The $Q_y$ -Spectra Of Other Photosynthetic Complexes

It is important to compare the linear pressure shifts of the 680 and 670 nm absorption bands, P680 and the active Pheo *a* at 681 nm against those reported for other photosynthetic protein complexes. Examples include the RC of *Rb. sphaeroides* [27] and *Rps. viridis* [22,26], the B800-B850 peripheral antenna complex of *Rb. sphaeroides* [29] and the proximal FMO antenna complex of *Chlorobium tepidum*. All these complexes are characterized, in part, by strong excitonic interactions. Comparison of the pressure dependences of their  $Q_y$ -band maxima against those for the PS II RC reveals that, overall, the linear shifts of the latter are considerably smaller. The results for the PS II RC are compared against those for five  $Q_y$ -bands of the RC of *Rps. viridis* in Table I. (It should be noted that the contribution from the internal charge transfer states of the special pair to the primary donor state of the bacterial RC may also be pressure dependent.) The linear pressure shift for B850 at 300 K is  $\sim -0.85 \text{ cm}^{-1}/\text{MPa}$  [29] while that for P870 of the *Rb. sphaeroides* RC at 300 K is  $-0.68 \text{ cm}^{-1}/\text{MPa}$  [27]. At  $T = 55 \text{ K}$ , the shift for the 824 and 814 nm bands of the FMO complex are both  $-0.12 \text{ cm}^{-1}/\text{MPa}$  [29]. It is also interesting to note that the linear pressure shift of the  $S_1$  state of chlorin in an *n*-octane matrix at 4.2 K is  $-0.05 \text{ cm}^{-1}/\text{MPa}$  [37]. Thus, the  $Q_y$ -states of the PS II RC exhibit

Table I. Comparison of the pressure shifts of the  $Q_y$ -states of the RC of PS II and *Rps. viridis* at 4.2 K.

PSII RC			RC of <i>Rps. viridis</i> <sup>a</sup>		
$\lambda$ (nm)	Assignment	dv/dp [cm <sup>-1</sup> /MPa] ( $\pm 0.01$ )	$\lambda$ (nm)	Assignment	dv/dp [cm <sup>-1</sup> /MPa] ( $\pm 0.01$ )
680.9	P680 (P <sub>-</sub> )	0.07	987.8	P960 (P <sub>-</sub> )	0.42
667.2	P <sub>+</sub>	0.07	833.4	P <sub>+</sub>	0.15
671.8	Chl <i>a</i>	0.04	835.3	BChl <sub>L,M</sub>	0.10
680.5	Pheo <i>a</i>	0.04	808.5	BPheo <sub>L</sub>	0.13
			794.0	BPheo <sub>M</sub>	0.05

<sup>a</sup>See ref. 22.

pressure dependences which are more similar to that of an  $S_1$  state of an isolated chromophore than states of an aggregate characterized by strong excitonic interactions. (Although microscopic theories have been developed for the interpretation of the pressure shift and broadening of the ZPH associated with isolated chromophores [38,39], no such theory exists for an aggregate of excitonically coupled chromophores). Returning to Table I, we point out that the 4.2 K linear pressure shifts for  $P_+$  and  $P_-$  of the PS II RC are both  $-0.07 \text{ cm}^{-1}/\text{MPa}$  while those for *Rps. viridis* are  $-0.42$  and  $-0.15 \text{ cm}^{-1}/\text{MPa}$ , respectively. The unequal shifts for  $P_+$  and  $P_-$  of *Rps. viridis* can be qualitatively understood [26] in terms of the simple dimer exciton model when the dispersion shift (D) of the dimer is pressure dependent or in terms of the differing contributions of the internal charge transfer states of the special pair to  $P_+$  and  $P_-$  [40]. For the special pair of *Rps. viridis*, the Mg...Mg and interplanar separation distance is 7.0 and 3.3 Å, respectively [10,11]. The smallness of the linear pressure shifts for  $P_+$  and  $P_-$  of the PS II RC provides additional evidence for the excitonic interaction between the monomers of the special pair being weak [14,15]. The small special pair splitting of  $\sim 300 \text{ cm}^{-1}$  for the PS II RC (the splitting for the *Rps. viridis* RC is  $1900 \text{ cm}^{-1}$  at 4.2 K [31,41]) was used to estimate a Mg...Mg distance of  $\sim 11 \text{ Å}$  [15]. Why the linear pressure shifts for the 670 nm absorption band and the 681 nm  $Q_y$ -band of the active Pheo *a* are so small is an interesting question but one that need await an X-ray structure of the PS II RC.

## B. Elastic And Plastic Structural Changes

On the basis only of the pressure dependences of the 4.2 and 77 K absorption spectra and the non-line narrowed transient hole spectra of P680 as well as the pressure dependence of the steady state population of  $^3\text{P680}^*$  (Fig. 7), the pressure induced



structural changes of the PS II RC would be classified as elastic (reversible). The observation, at high resolution, of an irreversible decrease in the width of the ZPH from  $5.2 \text{ cm}^{-1}$  at 0.1 MPa to  $1.5 \text{ cm}^{-1}$  at 267 MPa, which corresponds to an increase from 2.0 to 7.0 ps for the  $^1\text{P680}^*$  lifetime, establishes that there is a plastic component to the structural changes. Before considering possible explanations of these observations, we note that it is well established that the complexity of proteins can result in both elastic and conformational (plastic) pressure induced structural changes [42,43]. Conformational drift, which is essentially irreversible, can be qualitatively understood in terms of a hierarchy of configurational changes in a complex ("glass-like") solid [42,43]. Conformational drift has been observed in several small oligomeric proteins [44]. It has also been demonstrated that, although pressures of up to 100-200 MPa at physiological or ambient temperatures produce no significant changes in the optical spectra of heme proteins, subtle structural changes can be detected by NMR [45]. Windsor et al. [23,24] have reported a pressure dependence for the secondary charge separation process ( $\text{P}^+\text{H}_\text{L}^-\text{Q}_\text{A} \rightarrow \text{P}^+\text{H}_\text{L}\text{Q}_\text{A}^-$ ) of the *Rb. sphaeroides* and *Rps. viridis* RC at room temperature. A pressure of 120 MPa accelerated the electron transfer in *Rps. viridis* by a factor of 1.4 (127 versus 181 ps) [24]. This effect was reversible upon pressure release, but higher residual amounts of  $\text{P}^+$  ( $\times 2.5$ ) remained at 266 ms, indicating some long term changes that inhibited the  $\text{Q}_\text{A}^-$  or  $\text{Q}_\text{B}^-$  to  $\text{P}^+$  recombination reaction. Higher pressures of  $\sim 240$  MPa partially inhibited the secondary charge separation which was completely suppressed at  $\sim 350$  MPa with only the ns charge recombination reaction being observed. After release of pressure and resting at 0.1 MPa, gradual but only partial recovery of secondary charge separation occurred [24]. Windsor et al. suggested as a possible explanation that, at high pressures, the quinone molecule (Q) may leave its site in the RC and that annealing upon pressure release may

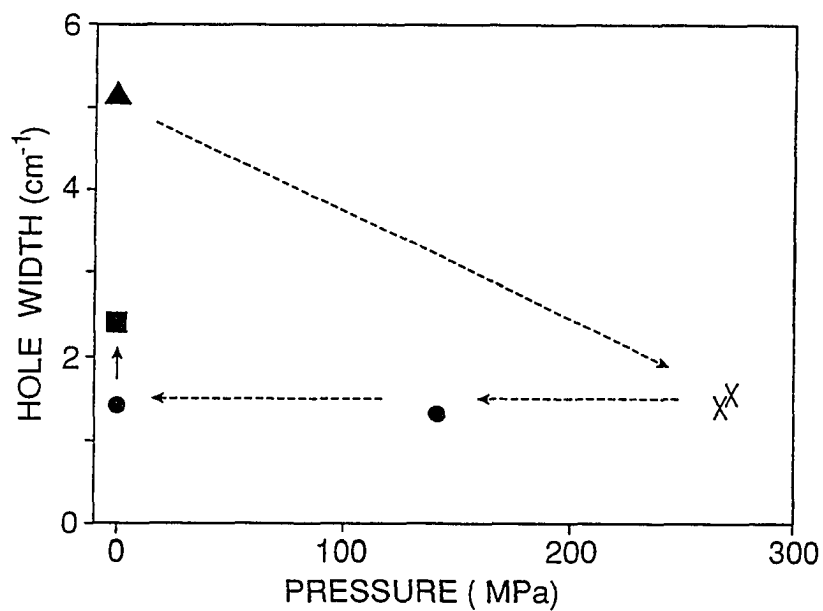


Figure 8. Pressure dependence of the zero-phonon hole width obtained from the transient hole spectra presented in Figs. 5 and 6. Triangle corresponds to ZPH width obtained at  $p = 0.1$  MPa; crosses correspond to the ZPH width obtained in two independent experiments at  $p = 267$  MPa and  $p = 278$  MPa, circles correspond to the ZPH width measured upon release of pressure from 267 to 141 MPa and subsequently to 0.1 MPa. The square corresponds to the hole width obtained after annealing (see Figure 5, curve b).

allow return to its native pocket. (We note that in the isolation of the PS II RC both of the quinone molecules are lost).

For clarity, the results for the pressure dependence of the P680 ZPH are summarized in Fig. 8. The triangular data point is for the virgin sample at 0.1 MPa. The crosses at ~270 MPa are data from two different experiments. The solid circle data points prove that the pressure induced diminution in the primary charge separation rate is irreversible. We note that to obtain the transient hole spectrum at 0.1 MPa, following the measurement at 270 MPa, required increasing the temperature from 4.2 to ~30 K, at which temperature the pressure was reduced to 0.1 MPa, followed by cooling to 4.2 K. The entire procedure took several hours with the sample being held at 30 K for about one hour. The rectangular data point was obtained following pressure release, warming and annealing at ice temperature for 3 h and subsequent cooling to 4.2 K. That annealing (resting) for a much longer period of time would return the RC to its virgin state is a possibility that cannot be excluded.

The observation that the pressure induced changes of the low temperature  $Q_y$ -absorption spectrum and non-line narrowed P680 hole profile are elastic suggests that the energy of the dark charge transfer state(s) involved in primary charge separation is of utmost importance in understanding the results of Fig.8. It is certain that the plasticity associated with charge separation is not due to P680\* or the electron-phonon coupling. One can reasonably assert that the absorption spectrum and non-line narrowed hole profile of P680 should be determined primarily by the structure of the cofactors and immediate protein environment. On the other hand, the energy of the dark charge transfer state can also be expected [46,47] to be sensitive to the structure of the more hydrophilic exterior of the protein where a larger number of potentially ionizable residues exist. (We remind the

reader that the PS II RC studied are isolated particles, i.e. not membrane bound.) What is being proposed is that the pressure induced structural changes near the exterior of the RC are characterized by a significant degree of plasticity while those of the core are mainly elastic.

### C. Simulation Of The Pressure Dependence Of The P680 Hole Profile

A theory of the overall hole profile in the low temperature limit which is valid for arbitrarily strong electron-phonon coupling and large inhomogeneous broadening ( $\Gamma_{inh}$ ) has been available for several years [48] and has been discussed in several review articles [25,49,50]. It has been successfully applied to P870 and P960 of *Rb. sphaeroides* and *Rps. viridis*, respectively [41,51]. Recently, the theory was generalized for arbitrary temperature [52] and used to accurately account for the temperature and burn frequency dependence of the P680 hole profile at 1 atm [34]. For the sake of brevity we do not review the theory here. The values of the parameters from refs. 14 and 34, which characterize the P680 absorption band, are given in the first column of Table II.  $S$  and  $\omega_m$  are the protein phonon Huang-Rhys factor and mean phonon frequency, respectively. Twice  $\sigma$  is approximately the width of the one-phonon profile. For P870 and P960, a special pair marker mode ( $\omega_{sp}$ ) is also important to the description of the absorption and hole profiles;  $S_{sp}/\omega_{sp} = 1.5/120$  and  $1.1/145$ , respectively [51]. Such a mode is only of minor importance for P680 as evidenced by a value for  $S_{sp}$  of  $\lesssim 0.3$  [14]. Continuing,  $\nu_m$  is the frequency of the maximum of the distribution of zero-phonon line frequencies for P680 and FWHM is the width of P680 at 4.2 K.

Consideration of pressure dependence of the P680 hole profile is simplified by the observation that the average phonon frequency ( $\omega_m$ ) and Huang-Rhys factor  $S$  are

Table II. Parameters used to calculate pressure dependence of PS II RC hole spectra at  $T = 77$  K.

	P680 Absorption Band	Monomer Absorption Band
$S$	1.9	0.5
$\omega_m$	$20 \text{ cm}^{-1}$	$20 \text{ cm}^{-1}$
$\sigma^a$	$13.8 \text{ cm}^{-1}$	$13.8 \text{ cm}^{-1}$
$\Gamma_{inh}$	$100 \text{ cm}^{-1}$	$175 \text{ cm}^{-1}$
$\nu_{max}^b$	680.5 nm	678.5 nm
FWHM <sup>c</sup>	$190 \text{ cm}^{-1}$	$210 \text{ cm}^{-1}$
$\nu_m^d$	682.5 nm	678.9 nm
$d\Gamma_{inh}/dp$	$0.16 \text{ cm}^{-1}/\text{MPa}$	$0.16 \text{ cm}^{-1}/\text{MPa}$
$d\nu_{max}/dp$	$-0.09 \text{ cm}^{-1}/\text{MPa}$	$-0.09 \text{ cm}^{-1}/\text{MPa}$

<sup>a</sup> Twice  $\sigma$  is approximately the width of the one-phonon profile.

<sup>b</sup> Maximum of the (0,0) absorption band.

<sup>c</sup> Full-width at half maximum; temperature broadening of the monomer band at 0.1 MPa was calculated using the theory of Hayes et al. [52] with  $\omega_m = 20 \text{ cm}^{-1}$ ,  $S = 0.5$  and  $\Gamma_{inh} = 175 \text{ cm}^{-1}$ .

<sup>d</sup> Maximum of the zero-phonon line distribution function.

independent of pressure up to the maximum value used. Based on simulation of hole profiles for various parameters we find that the pressure dependence of the 4.2 K line-narrowed P680 hole profile is well accounted for by a pressure dependence for  $\Gamma_{\text{inh}}$  and  $\gamma$ , where  $\gamma$  is the homogeneous width of the zero-phonon line. The effect of a pressure dependence for  $\gamma$  on the 4.2 K P680 profile is demonstrated in Fig. 9. Hole profiles were calculated with the parameter values listed in the first column of Table II for  $p = 1$  atm. Spectra a-d correspond to  $\gamma$ -values of 2.5, 1.0, 0.75 and 0.5  $\text{cm}^{-1}$ . The homogeneous width of the ZPH is  $2\gamma$  [53]. The intensity of the ZPH relative to the broad hole is very weak, i.e.,  $\sim 2\%$ , since the electron-phonon coupling is strong ( $S=1.9$ ). The calculations provide good agreement with the experimentally observed increase in depth of the ZPH (and its narrowing) but do not account for the broadening of the broad underlying structure. To account for this effect, keeping in mind that  $S$  and  $\omega_m$  are pressure independent, one has to take into account the increase of  $\Gamma_{\text{inh}}$  with increasing pressure. To this end we turned to the 77 K non-line narrowed P680 hole profiles. The calculated (solid smooth curves) and measured P680 hole profiles are compared in Fig. 10. The experimental spectra have been corrected for interference from the ground state of 1 Chl *a* monomer associated with the bottleneck state  $^3\text{P680}^*$  as described in refs. 14 and 34. The P680 and monomer values listed in Table II for the first seven parameters ( $S$ - $\nu_m$ ) are from ref. 34. We find that the pressure dependence of the 77 K non-line narrowed P680 hole profile is well accounted for by setting  $d\nu_{\text{max}}/dp$  equal to the experimental linear pressure shift for P680 ( $-0.09 \text{ cm}^{-1}/\text{MPa}$ ) and with  $d\Gamma_{\text{inh}}/dp = 0.16 \text{ cm}^{-1}/\text{MPa}$ . The same values were used for the monomer absorption band, see Table II. The agreement between the calculated and experimental hole profiles is excellent.

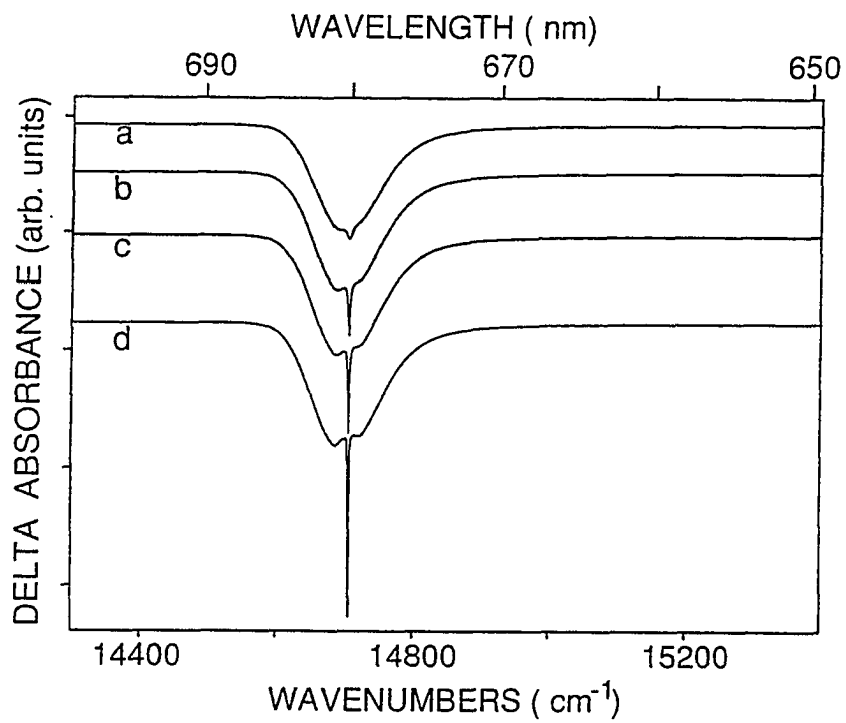


Figure 9. Calculated 4.2 K P680 transient hole profiles obtained for  $S = 1.9$ ,  $\omega_m = 20 \text{ cm}^{-1}$ ,  $\sigma = 13.8 \text{ cm}^{-1}$ ,  $\Gamma_{\text{inh}} = 100 \text{ cm}^{-1}$ , and  $\gamma = 2.5 \text{ cm}^{-1}$ (a),  $1 \text{ cm}^{-1}$ (b),  $0.75 \text{ cm}^{-1}$ (c), and  $0.5 \text{ cm}^{-1}$ (d), respectively.

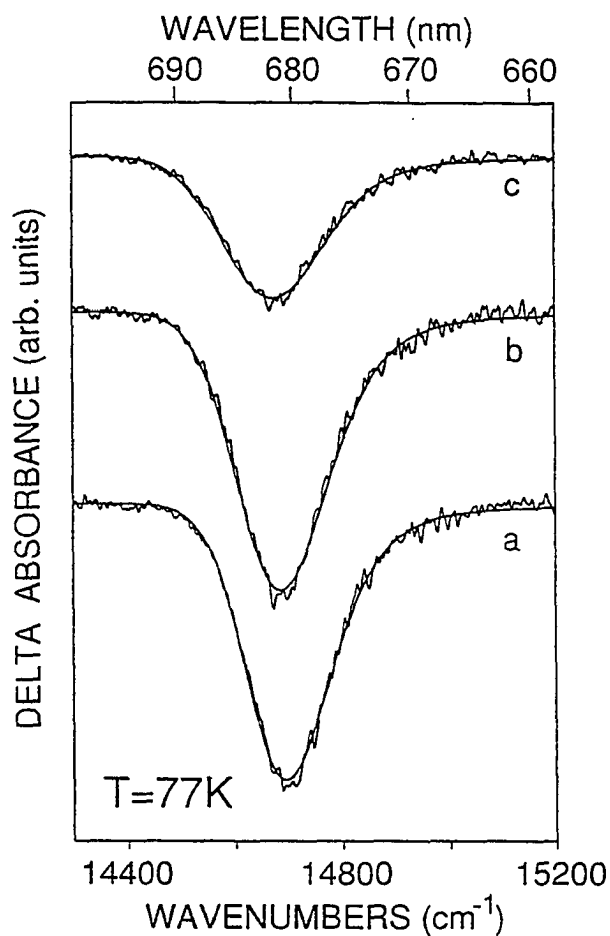


Figure 10. Experimental (noisy lines) and calculated (solid lines) non-linear narrowed transient hole-burned ( $\lambda_B = 665$  nm,  $T = 77$  K) spectra of PS II RC complex (corrected for the monomer absorption) and obtained for three different pressures:  $p = 25$  MPa (curve a),  $p = 141$  MPa (curve b), and  $p = 308$  MPa (curve c), respectively.



#### D. Pressure Dependence Of Primary Charge Separation

Our data show that the lifetime of P680\* in the low temperature limit increases from 2.0 to 7.0 ps as pressure increases from 0.1 to 267 MPa. This effect is irreversible while the pressure induced effect on the absorption and non-line narrowed P680 hole spectra are reversible (elastic). These contrasting elastic and conformational drift behaviors suggest that the plastic structural changes affect mainly the dark charge transfer state(s) involved in primary charge separation. As mentioned earlier, such structural changes might be mainly located at the more hydrophilic exterior of the protein where a larger number of potentially ionizable residues reside. Molecular dynamics simulations have demonstrated the sensitivity of the energetics of charge transfer states to such charged residues in the bacterial RC [46,47]. In what follows we explore the consequences of the assumption that the plastic pressure effect on P680\*'s lifetime is due to an irreversible pressure effect on the charge separated state. (The data prove that the effect of pressure on P680\*'s energy and inhomogeneous broadening is elastic.)

We take the reorganization energy and electronic coupling matrix element  $V$  to be independent of pressure, the justification being that the linear electron-phonon coupling ( $S, \omega_m$ ) for the P680\*  $\leftarrow$  P680 transition is independent of pressure and that the pressure induced changes in the absorption and non-line narrowed P680 hole spectra are reversible. The former finding is consistent with our pressure data for P960 of *Rps. viridis* [26] and the lowest  $Q_y$ -state of the FMO antenna complex of *Chlorobium tepidum* [30]. By analogy with the bacterial RC, both the two-step and superexchange mechanisms will be considered. We hasten to add that it is not our intent to distinguish between the two. For analysis we use nonadiabatic Golden rule rate expressions based on the work of Small et al. [54] which takes into account the distribution of donor-acceptor energy gap ( $\Omega$ ) values

which stems from the glass-like structural heterogeneity of proteins. A distribution of values for  $V$  will be ignored, which appears to be reasonable in view of the results of burn frequency dependent hole burning studies of P870 of *Rb. sphaeroides* [51,55]. We denote P680\* by D and P<sup>+</sup>Chl<sup>-</sup> (two-step) and P<sup>+</sup>Pheo<sup>-</sup> (superexchange) by A. For the former mechanism the average value of  $k_{DA}$  is

$$\langle k_{DA} \rangle = 2\pi V^2 \left[ 2\pi (\Gamma^2 + \Sigma(T)^2) \right]^{-1/2} \exp \left[ -(\Omega_0 - S\omega_m)^2 / 2(\Gamma^2 + \Sigma(T)^2) \right], \quad (1)$$

where  $\Omega_0$  is the mean value of the D-A adiabatic electronic energy gap,  $\Gamma^2$  the variance of the  $\Omega$ -distribution and  $S$  and  $\omega_m$  the Huang-Rhys factor and mean frequency of the protein phonons which mediate charge separation. As will be apparent, the  $\Omega_0$ -value to be used is sufficiently small to justify the assumption that low frequency phonons alone are responsible for the reorganization energy. Twice  $\Sigma(T)$  is approximately the homogeneous width of the nuclear factor associated with the Golden rule:

$$\Sigma(T)^2 = \tilde{S} (\sigma^2 + \omega_m^2), \quad (2)$$

where

$$\tilde{S}(T) = S \operatorname{ctnh}(\hbar\omega_m / 2kT) \quad (3)$$

with  $2\sigma \approx$  the width of the one-phonon profile. For the superexchange mechanism we consider that both phonons and a localized intramolecular Chl/Pheo mode of frequency  $\omega_{loc}$  contribute to the reorganization energy. To this end we define  $\Omega_0' = \Omega_0 - \omega_{loc}$ . The

average value of the rate constant is then

$$\begin{aligned} \langle k_{DA} \rangle = & 2\pi V^2 (2 FC_{loc}) \left[ 2\pi(\Gamma^2 + \Sigma(T)^2) \right]^{-1/2} \\ & \times \exp \left[ -(\Omega'_0 - S\omega_m)^2 / 2(\Gamma^2 + \Sigma(T)^2) \right], \end{aligned} \quad (4)$$

where  $V$  is now the superexchange electronic coupling [54] and  $FC_{loc}$  is the Franck-Condon factor for the high frequency localized mode. The factor of 2 in front of  $FC_{loc}$  allows for this mode to reside on a Chl of the special pair or on the active Pheo. Equation (4) is valid for small values of  $FC_{loc}$  ( $\lesssim 0.2$ ) and strong electron-phonon coupling, both of which conditions are satisfied in our model calculations. Utilization of average value expressions for  $k_{DA}$  is appropriate when  $\Gamma^2 \lesssim \Sigma(T)^2$  [53], a condition which guarantees that the decay of  $P680^*$  is essentially single-exponential, i.e. not significantly dispersive. This condition is also met.

In the calculations we used for  $\Omega_0$  the average 277 K value of  $890 \text{ cm}^{-1}$  reported for the free energy gap between  $P680^*$  and  $P680^+Pheo^-$  by Booth et al. [56]. There is some uncertainty in this value; a value as high as  $1000 \text{ cm}^{-1}$  has been reported [57]. However, this is of no consequence since our intent is mainly to estimate the pressure shift for the acceptor state which is consistent with the observed pressure dependence of the primary charge separation kinetics. The parameter values used are listed in Table III. The values of 20 and  $13.8 \text{ cm}^{-1}$  for  $\omega_m$  and  $\sigma$  are those determined by hole burning of the  $P680^* \leftarrow P680$  transition. For analysis of the pressure dependence it suffices at this time to consider only the case where the reorganization energy,  $S\omega_m$ , due to phonons equals  $\Omega_0$  (two-step mechanism) or  $\Omega_0^{\phi}$  (superexchange mechanism) for  $p = 1 \text{ atm}$  and  $T = 4.2 \text{ K}$ .

For the superexchange mechanism we chose  $\omega_{\text{loc}} = 710 \text{ cm}^{-1}$  so that  $\Omega_0' = 180 \text{ cm}^{-1}$ . The choice of  $710 \text{ cm}^{-1}$  was based on the fact that the most intense Franck-Condon mode in the  $Q_y \leftarrow S_0$  transition of Chl *a* is near this frequency [58]. The FC factor is 0.05 [58] but several weaker nearby modes are observed [58-60]. The situation for Pheo *a* is similar [59,60]. Although we are concerned with the FC factors for Chl *a*  $\rightarrow$  Chl *a*<sup>+</sup> and Pheo *a*  $\rightarrow$  Pheo *a*<sup>-</sup>, simple  $\pi$ -MO arguments indicate that the choice of  $\text{FC}_{\text{loc}} = 0.2$ , Table III, is reasonable, especially when several modes in the vicinity of  $710 \text{ cm}^{-1}$  are lumped together. For the two-step mechanism we used the value of  $360 \text{ cm}^{-1}$  from ref. 54 for the reorganization energy of the first step so that, with  $S\omega_m = \Omega_0$ ,  $\Omega_0 = 360 \text{ cm}^{-1}$ . We hasten to add that calculations were performed for  $S\omega_m \neq \Omega_0(\Omega_0')$  under the constraint that the weak temperature dependence of the primary charge separation must be accounted for. The qualitative aspects of the pressure dependence analysis reported on below are not altered by modest energy gap-reorganization energy mismatches. Turning next to the values of 100 and  $200 \text{ cm}^{-1}$  used for  $\Gamma$ , we note that the zero-phonon line distributions for different states of a photosynthetic complex are largely uncorrelated so that  $2.35\Gamma \approx (\Gamma_{\text{inh,D}}^2 + \Gamma_{\text{inh,A}}^2)^{1/2}$  [54], where  $\Gamma_{\text{inh,D}}$  and  $\Gamma_{\text{inh,A}}$  are the inhomogeneous broadenings associated with the ground state to donor and acceptor state absorption transitions. The latter is forbidden. Under the assumption that  $\Gamma_{\text{inh,D}} \approx \Gamma_{\text{inh,A}}$ , one has  $2.35\Gamma \approx 2^{1/2} \Gamma_{\text{inh,D}}$ . For  $D = \text{P680}^*$  (Table II), one obtains  $\Gamma \sim 60 \text{ cm}^{-1}$ , which is close to the value of  $100 \text{ cm}^{-1}$ . Recently, Bixon et al. [60] have presented data which indicate that  $\Gamma_{\text{inh}}$  for a charge separated state could be significantly larger than assumed above; thus, our use also of  $\Gamma = 200 \text{ cm}^{-1}$ .

Before presenting the results on the pressure dependence of charge separation, we show the Marcus curves ( Figure 10) for the two-step (frame A) and superexchange

Table III. Parameters used for calculation of pressure dependence of primary charge separation.

Parameters	Superexchange Mechanism	Two-Step Mechanism
$\omega_m$ (cm <sup>-1</sup> )	20	20
$\sigma$ (cm <sup>-1</sup> )	13.8	13.8
S	9	18
$\omega_{loc}$ (cm <sup>-1</sup> )	710	–
FC <sub>loc</sub>	0.2	–
$\Omega_0'$ (cm <sup>-1</sup> )	180	–
$\Omega_0$ (cm <sup>-1</sup> )	890	360

(frame B) mechanisms for  $p = 1$  atm (low T limit). The solid and dashed curves correspond to  $\Gamma = 100$  and  $200 \text{ cm}^{-1}$ , respectively. As expected, the dependence of the rate on the energy gap weakens as  $\Gamma$  is increased. In frames A and B, the value of  $\log \langle k_{DA} \rangle$  at  $\Omega_0 - S\omega_m = 0$  and  $\Omega_0' - S\omega_m$ , respectively, corresponds to the experimental P680\* lifetime of 2.0 ps (4.2 K). The values of the electronic coupling  $V$  are given in the caption. For example, for frame A,  $V = 12.3$  and  $15.4 \text{ cm}^{-1}$  for  $\Gamma = 100$  and  $200 \text{ cm}^{-1}$ , respectively. The increase in  $V$  (for a fixed lifetime) with increasing  $\Gamma$  is expected on the basis of Eqs. (1) and (4). The calculated 300 K lifetimes of P680\* are given in the caption and can be compared with the measured value of  $3.0 \pm 0.6$  ps [62]. The important point is that the temperature dependence weakens with increasing  $\Gamma$  [54].

Finally, we turn to the pressure dependence of the primary charge separation kinetics at 4.2 K. On the basis of the experimental data and arguments given above, we believe that the model which has the pressure dependence due, primarily, to the effects of irreversible pressure induced structural changes on the A state (P680<sup>+</sup>Chl<sup>-</sup> or P680<sup>+</sup>Pheo<sup>-</sup>) is a reasonable starting point. There are two effects: the pressure dependence of  $\Gamma_{inh,A}$  and of the energy of the A state. We fix the former by increasing  $\Gamma$  (0.1 MPa) by a factor 1.5 for  $P = 267$  MPa (this is somewhat larger than the value determined by assuming that the pressure dependence of  $\Gamma_{inh,P680^*}$ , Table II, is equal to that of  $\Gamma_{inh,A}$ ). Thus, the only adjustable parameter is  $\Omega_0$  for the two-step mechanism and  $\Omega_0'$  for the superexchange mechanism. Again, we present results only for the case  $\Omega_0, \Omega_0' = S\omega_m$  at 0.1 MPa. For the two-step mechanism we find that  $|\Omega_0(0.1 \text{ MPa}) - \Omega_0(267 \text{ MPa})| \equiv |\Delta\Omega_0| = 259$  and  $427 \text{ cm}^{-1}$  for  $\Gamma(0.1 \text{ MPa}) = 100$  and  $200 \text{ cm}^{-1}$ , respectively. For the superexchange mechanism we find that  $|\Omega_0'(0.1 \text{ MPa}) - \Omega_0'(217 \text{ MPa})| \equiv |\Delta\Omega_0'| = 231$  and  $410 \text{ cm}^{-1}$  for  $\Gamma(0.1 \text{ MPa}) = 100$  and  $200 \text{ cm}^{-1}$ , respectively. Thus, explanation of the pressure

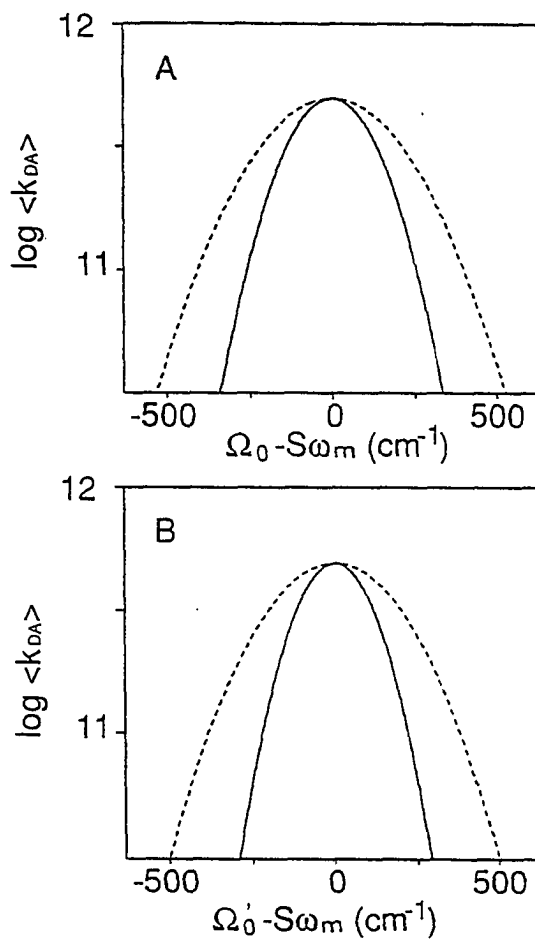


Figure 11. A plot of the dependence of  $\log \langle k_{DA} \rangle$  on  $(\Omega_0 - S\omega_m)$  (frame A; two step mechanism) and  $\Omega_0' - S\omega_m$  (frame B; superexchange mechanism), respectively. The solid and dashed curves in frames A and B were obtained with  $V = 12.3, 18.1 \text{ cm}^{-1}$  and  $V = 15.4, 23.7 \text{ cm}^{-1}$  for  $\Gamma = 100$  and  $200 \text{ cm}^{-1}$ , respectively. The calculated 300 K lifetimes of P680\* (using Eq. 1) for both two-step and superexchange mechanisms are 6.7 and 5.6 ps and 4.6 and 3.7 ps for  $\Gamma = 100$  and  $200 \text{ cm}^{-1}$ , respectively.

dependence requires a (linear) pressure shift for the acceptor (A) state energy of about  $1 \text{ cm}^{-1}/\text{MPa}$  in magnitude. This is a factor of 2 greater than the shifts (negative) for P960\* and P870\* which, although mainly excitonic, do have significant charge transfer character. Unfortunately, there is a dearth of pressure data for charge transfer states of suitable model systems. We are aware only of the work of Rollinson and Drickamer [63] on the intramolecular charge transfer state ( $S_1$ ) of several compounds including 9-anthryl-dimethylaniline and 6-propionyl-2-dimethylamino-naphthalene. For pressures  $\leq 400 \text{ MPa}$ , the shifts are negative and close to linear at room temperature and in the vicinity of  $\approx 1 \text{ cm}^{-1}/\text{MPa}$  (solvent dependent). Because we are not able to directly observe the acceptor state, it is not possible to determine the sign of  $\Delta\Omega_0$  ( $\Delta\Omega_0'$ ). For positive sign the system would move into the inverted regime of the Marcus curve. In future work it will be important to study the pressure dependence of the charge transfer states of a wider variety of model systems.

## V. Final Remarks

It has demonstrated, for the first time, that pressure can have a pronounced effect on primary charge separation of a reaction center. At 270 MPa the P680\* lifetime is a factor of 3.5 longer than its 1 atm value of 2 ps in the low temperature limit. While this effect is plastic, the pressure induced effects on the  $Q_y$ -absorption and non-linear narrowed P680 hole profile are elastic. The latter observation, together with the observation that the linear electron-phonon coupling of the P680\*  $\leftarrow$  P680 transition is, at most, weakly dependent on pressure, allowed us to eliminate P680\* and the electronic coupling  $V$  as sources for the plastic pressure dependence of the primary charge separation kinetics. Within the standard model of primary charge separation [22], it was then possible to focus



on the acceptor state ( $P680^+Pheo^-$  and  $P680^+Chl^-$  for the superexchange and two-step mechanisms, respectively). Since the pressure dependence of the inhomogeneous broadening of the  $P680^* \leftarrow P680$  transition was measured, we were able to come up with reasonable estimates for the pressure dependence of  $\Gamma^2$ , the variance of the distribution of donor-acceptor energy gap values. This left the pressure dependence of the acceptor state energy as the only variable in our model calculations. It was found that the pressure dependence could be explained with a linear pressure shift of  $\approx 1 \text{ cm}^{-1}/\text{MPa}$  in magnitude for the acceptor state. (The data and calculations do not permit a distinction between the superexchange and two-step mechanisms.) At this time such a shift cannot be considered to be unreasonable. On the basis of the results of Rollinson and Drickamer [63], we are of the opinion that the effect of increasing pressure (for values used in this work) is to red shift the acceptor state, but this remains to be proven. We emphasize that the model used for the analysis is just that but one that can be scrutinized since the PS II RC would appear to be an ideal candidate for more detailed studies of the pressure dependence of primary charge separation. Such studies of the PS II RC as well as of the bacterial RC, whose structure is known, are planned.

### **Acknowledgment**

Research at the Ames Laboratory was supported by the Division of Chemical Sciences, Office of Basic Energy Sciences, U.S. Department of Energy. Ames Laboratory is operated for USDOE by Iowa State University under contract W-7405-Eng-82. We would like to thank M. Seibert and R. Picorel of the National Renewable Energy Laboratory for generously providing us with the RC preparations. We would like to thank H. G. Drickamer for drawing our attention to ref. 63. H.-C. Chang is indebted to Dow

Chemical for support through a Research Fellowship.

## References

1. Kirmaier, C.; Holten, D. *Photosyn. Res.* 1987, 13, 225.
2. Feher, G.; Allen, J.P.; Okamura, M.Y.; Rees, D.C. *Nature* 1989, 339, 111.
3. Parson, W.W. in *Chlorophylls*; Scheer, H., Ed.; CRC Press: Boca Raton, 1991, p.1153.
4. Kirmaier, C.; Holten, D. in *The Photosynthetic Reaction Center*, Vol. II; Deisenhofer, J., Norris, J., Eds.; Academic Press: New York, 1993, p. 49.
5. Shuvalov, V.A., *ibid.*, p. 71.
6. Friesner, R.A.; Won, Y. *Biochim. Biophys. Acta* 1989, 977, 99.
7. Seibert, M. in *The Photosynthetic Reaction Center*, Vol. I; Deisenhofer, J., Norris, J., Eds.; Academic Press: New York, 1993, p. 319.
8. Renger, G. in *Topics in Photosynthesis*, Vol. 11; Barber, J., Ed.; Elsevier, 1992, p. 45.
9. Nanba, O.; Satoh, K. *Proc. Natl. Acad. Sci. USA* 1987, 84, 109.
10. Deisenhofer, J.; Epp, O.; Miki, K.; Huber, R.; Michel, H. *J. Mol. Biol.* 1984, 180, 385.
11. Deisenhofer, J.; Epp, O.; Miki, K.; Huber, R.; Michel, H. *Nature* 1985, 318, 618.
12. Cramer, W.A.; Widger, W.R.; Herrmann, R.G.; Trebst, A. *Trends Biochem. Sci.* 1985, 10, 125.
13. Kyle, D.J. *Photochem. Photobiol.* 1985, 41, 107.
14. Chang, H.-C.; Jankowiak, R.; Reddy, N.R.S.; Yocum, C.F.; Picorel, R.; Seibert, M.; Small, G.J. *J. Phys. Chem.* 1994, 98, 7725.
15. Kwa, S.L.S.; Eijkelhoff, C.; van Grondelle, R.; Dekker, J.P. *J. Phys. Chem.* 1994, 98, 7702.

16. Jankowiak, R.; Tang, D.; Small, G.J.; Seibert, M. *J. Phys. Chem.* 1989, 93, 1649.
17. Tang, D.; Jankowiak, R.; Seibert, M.; Yocum, C.F.; Small, G.J. *J. Phys. Chem.* 1990, 94, 6519.
18. Wasielewski, M.R.; Johnson, D.G.; Govindjee; Preston, C.; and Seibert, M. *Photosyn. Res.* 1989, 22, 89.
19. Woodbury, N.W.; Peloquin, J.M.; Alden, R.G.; Lin, X.; Lin, S.; Taguchi, A.K.W.; Williams, J.C.; Allen, J.P. *Biochem.* 1994, 33, 8101.
20. Boxer, S.G. in *The Photosynthetic Reaction Center*, Vol. II; Deisenhofer, J., Norris, J., Eds.; Academic Press: New York, 1993, p. 177.
21. Lockhart, D.J.; Kirmaier, C.; Holten, D.; Boxer, S.G. *J. Phys. Chem.* 1990, 94, 6987.
22. Small, G.J. *Chem. Phys.*, this issue.
23. Redline, N.L.; Windsor, M.W. *Chem. Phys. Lett.* 1991, 186, 204.
24. Redline, N.L.; Windsor, M.W. *Chem. Phys. Lett.* 1992, 198, 334.
25. Hoganson, C.W.; Windsor, M.W.; Farkas, D.I.; Parson, W.W. *Biochim. Biophys. Acta* 1987, 892, 275.
26. Reddy, N.R.S.; Small, G.J. *Advances in Photosynthesis*, submitted.
27. Clayton, R.K.; DeVault, D. *Photochem. Photobiol.* 1972, 15, 165.
28. Freiberg, A.; Ellervee, A.; Kukk, P.; Laisaar, A.; Tars, M.; Timpmann, K. *Chem. Phys. Lett.* 1993, 214, 10.
29. Tars, M.; Ellervee, A.; Kukk, P.; Laisaar, A.; Saarnak, A.; Freiberg, A. *Lithuanian J. of Physics* (in press).
30. Reddy, N.R.S.; Jankowiak, R.; Small, G.J. to be submitted.
31. Reddy, N.R.S.; Kolaczowski, S.V.; Small, G.J. *Science* 1993, 260, 68.

32. Breton, J. in *Perspectives in Photosynthesis*; Jornter, J., Pullman, B., Eds.; Kluwer Academic: Dordrecht, 1990, p. 23.
33. Van der Vos, R.; van Leeuwen, P.J.; Braun, P.; Hoff, A.J. *Biochim. Biophys. Acta* 1992, 1140, 184.
34. Chang, H.-C.; Small, G.J.; Jankowiak, R. *Chem. Phys.*, in press.
35. Jankowiak, R.; Small, G.J. in *the Photosynthetic Reaction Center*, Vol. II; Deisenhofer, J., Norris, J., Eds.; Academic Press: New York, 1993, p. 133.
36. Milinchuk, V.K.; Kovarskii, A.L. in *High-Pressure Chemistry and Physics of Polymers*; Kovarskii, A.L., Ed.; CRC Press: Boca Raton, 1994, Chapter 5, p. 155.
37. Ellervee, A.; Jaaniso, R.; Kikas, J.; Laisaar, A.; Suisalu, A.; Shcherbakov, V. *Chem. Phys. Lett.* 1991, 176, 472.
38. Laird, B.B.; Skinner, J.L. *J. Chem. Phys.* 1989, 90, 3274.
39. Sesselmann, Th.; Richter, W.; Haarer, D.; Morawitz, H. *Phys. Rev. B* 1987, 36, 7601.
40. Thompson, M.A.; Fajer, J. *J. Phys. Chem.* 1992, 96, 2933.
41. Reddy, N.R.S.; Kolaczowski, S.V.; Small, G.J. *J. Phys. Chem.* 1993, 97, 6934.
42. Frauenfelder, H. etc. *J. Phys. Chem.* 1990, 94, 1024.
43. Noguti, T.; Go, N. *Proteins* 1989, 5, 97.
44. Weber, G. in *Protein Interactions*; Chapman-Hall: New York, 1992.
45. Jonas, J.; Jonas, A. *Annu. Rev. Biophys. Biomol. Struct.* 1994, 23, 287.
46. Gehlen, J.N.; Marchi, M.; Chandler, D. *Science* 1994, 263, 499.
47. Warshel, A.; Chu, Z.T.; Parson, W.W. *Photochem. Photobiol.* 1994, A82, 123.
48. Hayes, J.M.; Gillie, J.K.; Tang, D.; Small, G.J. *Biochim. Biophys. Acta* 1988, 932, 287.
49. Jankowiak, R.; Hayes, J.M.; Small, G.J. *Chem. Rev.* 1993, 93 1471.

50. Reddy, N.R.S.; Lyle, P.A.; Small, G.J. *Photosyn. Res.* 1992, 31, 167.
51. Lyle, P.A.; Kolaczowski, S.V.; Small, G.J. *J. Phys. Chem.* 1993, 97, 6926.
52. Hayes, J.M.; Lyle, P.A.; Small, G.J. *J. Phys. Chem.* 1994, 98, 7337.
53. Völker, S. in *Relaxation Processes in Molecular Excited States*; Fünfschilling, J., Ed.; Kluwer Academic Publisher: The Netherlands, 1989, p. 113.
54. Small, G.J.; Hayes, J.M.; Silbey, R.J. *J. Phys. Chem.* 1992, 96, 7499.
55. Kolaczowski, S.V.; Lyle, P.A.; Small, G.J. in *The Photosynthetic Bacterial Reaction Center II*; Breton, J.; Vermeglio, A., Eds.; NATO ASI Series 237; Plenum Press: New York, 1992, p. 173.
56. Booth, P.J.; Crystall, B.; Ahmad, I.; Barber, J.; Porter, G.; Klug, D.R. *Biochem.* 1991, 30, 7573.
57. Roelof, T.A.; Gilbert, M.; Shuvalov, V.A.; Holzwarth, A.R. *Biochim. Biophys. Acta* 1991, 1060, 237.
58. Gillie, J.K.; Small, G.J.; Golbeck, J.H. *J. Phys. Chem.* 1989, 93, 1620.
59. Avarmaa, R.A.; Rebane, K.K. *Chem. Phys.* 1982, 68, 191.
60. Avarmaa, R.A.; Rebane, K.K. *Spectrochimica Acta* 1985, 41A, 1365.
61. Bixon, M.; Jortner, J.; Michel-Beyerle, M.E. *Chem. Phys.* (in this issue).
62. Wasielewski, M.R.; Johnson, D.G.; Seibert, M.; Govindjee, *Proc. Natl. Acad. Sci.* 1989, 86, 524.
63. Rollinson, A.M.; Drickamer, H.G. *J. Chem. Phys.* 1980, 73, 5981.
64. Moser, C.C.; Jension, R.J.; Szarka, A.Z.; Repinec, S.T.; Hochstrasser, R.M.; Dutton, P.L. *Chem. Phys.*, this issue.

## CHAPTER 8 GENERAL CONCLUSIONS

Considerable progress has been made towards an understanding of the excited electronic state structure and primary charge separation dynamics of the PS II RC. The present work establishes the importance of CP47 contamination and the 684 nm absorbing Chl *a* in preparations containing, on average, 5 and 6 Chl *a* molecules per RC complex. Our previous and present measurements of the  $^1\text{P680}^*$  lifetime, together with the time domain data, indicate that the 684 nm Chl *a* do not play a role in primary charge separation. However, both the 684 nm Chl *a* and CP47 contamination should be expected to complicate the interpretation of energy transfer data. Therefore, in future studies of energy transfer dynamics and electron-phonon coupling, attention should be focused on 4 Chl *a*-RC preparations which contain negligibly low amounts of CP47, 684 nm Chl *a* and non-native Chl *a* absorbing near 670 nm.

The 684 nm absorbing Chl *a* contribute to the additional Chl *a* are of the linker type, serving to shuttle energy from the proximal antenna complex to the reaction center. Implicit in this model is that the 684 nm Chl *a* communicate with the primary electron donor Chl *a* (P680) via energy transfer and that the resulting detrapping of the  $\text{Q}_y$ -state of the 684 nm Chl *a* should depend strongly on temperature. Temperature dependent transient hole spectra are presented that are in complete accord with this prediction. Theoretical calculations on the kinetics and temperature dependence of the hole profile of the 680 nm absorption band are presented and provide convincing support for the linker model. The data are argued to be inconsistent with other models.

In the CP47 protein complex, attention is focused on the lower energy chlorophyll *a*  $\text{Q}_y$ -states. On the basis of the analysis of the hole and static fluorescence spectra at

4.2K, the lowest energy state of CP47 was found to be at 690 nm. The 690 nm and 687 nm states are excitonically correlated and correspond to an excitonically coupled dimer.

It has demonstrated, for the first time, that pressure can have a pronounced effect on primary charge separation of a reaction center. The 4.2K lifetime of P680\*, the primary donor state, increases from 2.0 ps to 7.0 ps as pressure increases from 0.1 to 267 MPa. While this effect is plastic, the pressure induced effects on the Q<sub>y</sub>-absorption and non-linear narrowed P680 hole profile are elastic. The latter observation, together with the observation that the linear electron-phonon coupling of the P680\* ← P680 transition is, at most, weakly dependent on pressure, allowed us to eliminate P680\* and the electronic coupling V as sources for the plastic pressure dependence of the primary charge separation kinetics. Within the standard model of primary charge separation, it was then possible to focus on the acceptor state (P680<sup>+</sup>Pheo<sup>-</sup> and P680<sup>+</sup>Chl<sup>-</sup> for the superexchange and two-step mechanisms, respectively). It was found that the pressure dependence could be explained with a linear pressure shift of  $\approx 1 \text{ cm}^{-1}/\text{MPa}$  in magnitude for the acceptor state. (The data and calculations do not permit a distinction between the superexchange and two-step mechanisms.) We emphasize that the PS II RC appears to be an ideal candidate for more detailed studies of the pressure dependence of primary charge separation.

## ACKNOWLEDGEMENTS

It is a pleasure rather than a duty to record my thanks to my advisors, many friends, and organizations for their guidance, help, encouragement, and financial assistance during my years of research. In particular I want to mention Professor Small whose steady advice and rigorous criticism prevented me from making many mistakes. The work contained here is certainly more a product of his efforts than of mine. I am grateful to Professor Struve who allows me to choose him as one of the coadvisors. A large thank you goes to Dr. Ryszard Jankowiak and Dr. N.Raja.S. Reddy for discussions and experimental guidance in my research projects of Photosystem II. Thanks must go to Dr. John M. Hayes for the use of the hole simulation programs.

Life in Ames was enriched not only by the facilities of the University, but also by many friendships. First in Prof. Small's group I would like to thank Dr. Freek Ariese, Dr. Tonu Reinot, Myungkoo Suh, Wook-Hyun Kim, Hsing-Mei Wu, Nick Milanovich for their help and keeping the research atmosphere a good one to work in. In Prof. Struve's group I would like to thank Dr. Herbert van Amerongen, Dr. Su Lin, Dr. Sergei Savikhin, and Chuck Smith for their assistance.

I am indebted to several organizations for their financial support. In particular I want to mention Ames Laboratory, Department of Chemistry, and Dow Chemicals.

Above all I am grateful to my parents, not only for their sacrificial assistance but also for their steady encouragement and unflinching love.



## APPENDIX A. A HOLE BURNING STUDY OF THE CP43 COMPLEX

### I. Introduction

CP43 protein complex is one of the interior Chl *a* light-harvesting antenna protein complexes for Photosystem II (PSII) [1]. The inner antenna of PSII of higher plants consists of two chlorophyll-protein complexes denoted as CP43 and CP47 according to their apparent molecular weights. It is generally assumed that the inner antenna, both CP47 and CP43, accept the excitation energy from the light-harvesting complex (LHC) and transfer it further to the reaction center [1]. The CP43 antenna can be easily detached from the PSII reaction center by increasing the detergent (dodecyl maltoside) concentration to over 1% [2]. Detachment of CP43 can also be observed in the PSII particles after treatment with strong reductant dithionite at a concentration of 2 mg(mg Chl)<sup>-1</sup> [2]. It was not possible to detach the antenna CP47 under similar conditions. Therefore, it has been suggested that the CP43 antenna is less closely associated with the D1-D2-Cyt b559 reaction center than is CP47.

The absolute structure of CP43 is not known [1]. As in CP47, hydropathy plots of CP43 can be interpreted by six membrane-spanning helices. Six helices are connected by five hydrophilic loops. The total number of histidyl residues, the possible Chl *a* binding site, in CP43 is 12 [1]. There is a considerable debate in literature about the Chl *a* content in CP43 complex [1,3,4]. For example, de Vitry et al. suggested that both CP47 and CP43 bound 20-25 chlorophylls/ protein [3], while Barbato et al. [4] found 9-12 Chl *a* per CP47 and CP43 complexes.

CP43 and CP47 were previously thought to be only Chl *a* and  $\beta$ -carotene binding

proteins [1,5]. Photoprotective energy dissipation is one of the important functions of  $\beta$ -carotene, due to a lower triplet energy level than those of chlorophyll. Recently, xanthophyll lutein, which also functions as dissipating excess of excitation energy into heat, was found in CP43 and CP47 [5]. So the regulation of energy transfer to the reaction center could be one of the important functions for CP43 and CP47.

The low temperature (8K) absorption and emission spectra of CP43 were reported by Carbonera et al.[6]. The absorption maxima of CP43 complex are at 437, 668, 681 nm, while the fluorescence maximum is located at about 682nm [6]. Picorel et al. [7] showed that the  $Q_y$  absorption bands of CP43 at  $T=48$  K could be resolved into four spectroscopic transitions of Chl *a* peaking at 682.3, 678.4, 671.5, and 661.4 nm. At 77 K fluorescence maximum was measured at  $\sim 685$  nm [1]. At 8 K, ODMR spectra revealed two triplet states peaking at 683 and 668 nm, respectively [6]. The former (683 nm) was assigned as the lowest energy component of the antenna funnel in CP43 [6].

## II. Results

### A. Absorption Spectra

The absorption spectra of CP43 protein complex from two different preparations were obtained at low temperature (4.2 K). Figure 1 shows the low temperature absorption and its fourth derivative spectrum (4.2 K) of the first preparation denoted as CP43(I). The fourth derivative (dashed line) reveals one major band located at 682.8 nm associated with four additional higher energy bands located at 678.5, 672.2, 668.1, 664.7 nm, respectively.

In contrast to the pronounced  $\sim 683$  nm absorption band revealed in the CP43(I) complex, the second preparation (CP43(II)) shows less intensity in that region, as illustrated in Figure 2a. Although the contribution from the  $\sim 683$  nm band depends on

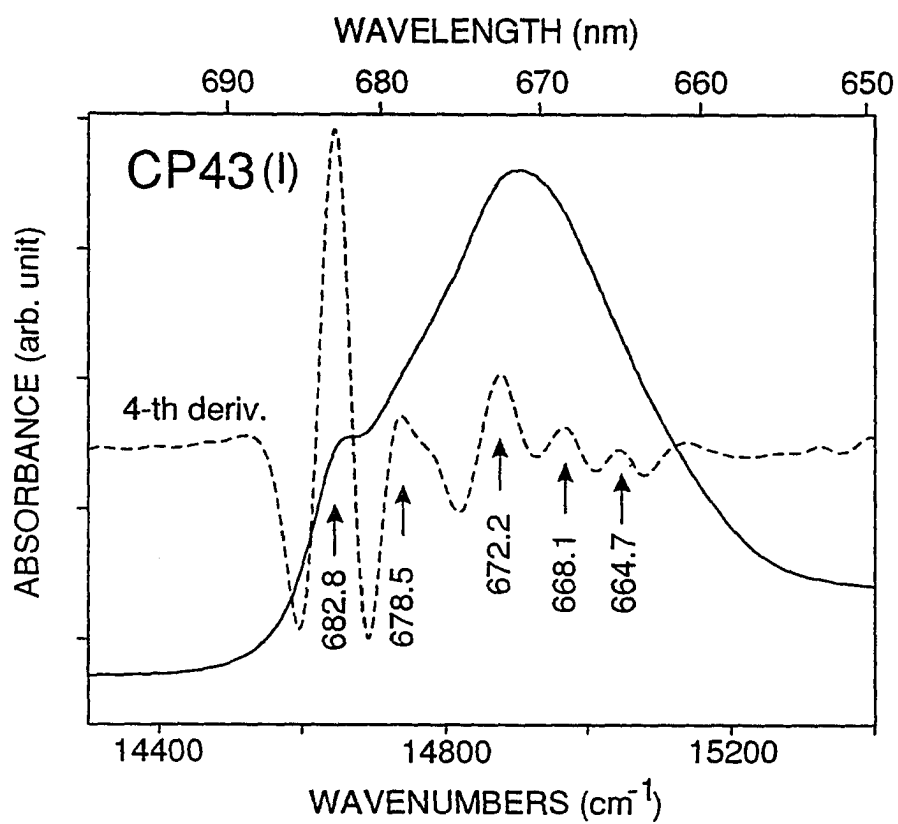


Figure 1. Absorption ( $Q_y$ -region) of CP43 (I) protein complex obtained at 4.2 K (solid line). Positions of the peaks revealed in fourth derivative (dashed line) are labeled.

preparation, the absorption spectra and their fourth derivatives are quite similar.

The difference between the above discussed preparations (i.e., CP43(I)-CP43(II)) is shown in Figure 3 (curve c) revealing the contribution of pigments absorbing at ~683 and 670 nm, respectively. In addition, the major absorption maximum at ~670 nm in CP43(I) (Figure 3a) is 2-3 nm blue shifted when compared with CP43(II) (Figure 3b).

### **B Persistent Hole Burned Spectra**

Several nonphotochemical hole burned spectra obtained at various burn wavelengths at 4.2 K are shown as Figure 4 and 5 for CP43(I) and CP43(II), respectively. Persistent hole-burning spectra in Figure 4 were obtained with  $\lambda_B = 675$  nm (a), 670 nm (b), and 655 nm (c) respectively. The broad hole (FWHM~90  $\text{cm}^{-1}$ ) located at 682.8 nm is invariant to  $\lambda_B$  as indicated by solid arrows. Thus, these ~683 nm Chls serve as the lowest energy trap. An additional satellite hole located at ~670 nm can be identified in curve a, although the interference from an antihole make the observation of the ~670 nm satellite hole difficult. Vibronic holes are revealed when  $\lambda_B = 655$  nm is utilized. The numbers correspond to the vibrational frequencies in the excited state of Chl *a* absorbing in ~678 nm region. These low-frequency modes are compared in Table I with the data obtained from Chl *a* in PSI [8].

Two persistent hole burned spectra of CP43(II), shown in Figure 5, were obtained with  $\lambda_B = 659.8$  nm (curve a), 658.8 nm (curve b), respectively. Similar vibronic hole-burned spectra were obtained. Due to a small difference in excitation energy (~20  $\text{cm}^{-1}$ ) between curves a and b, all of the low energy fine features keep track of laser frequency and are blue-shifted about 20  $\text{cm}^{-1}$  in curve b in comparison with curve a. The key observation is that the intensity of the invariant broad hole at ~683 nm is drastically reduced in CP43(II).

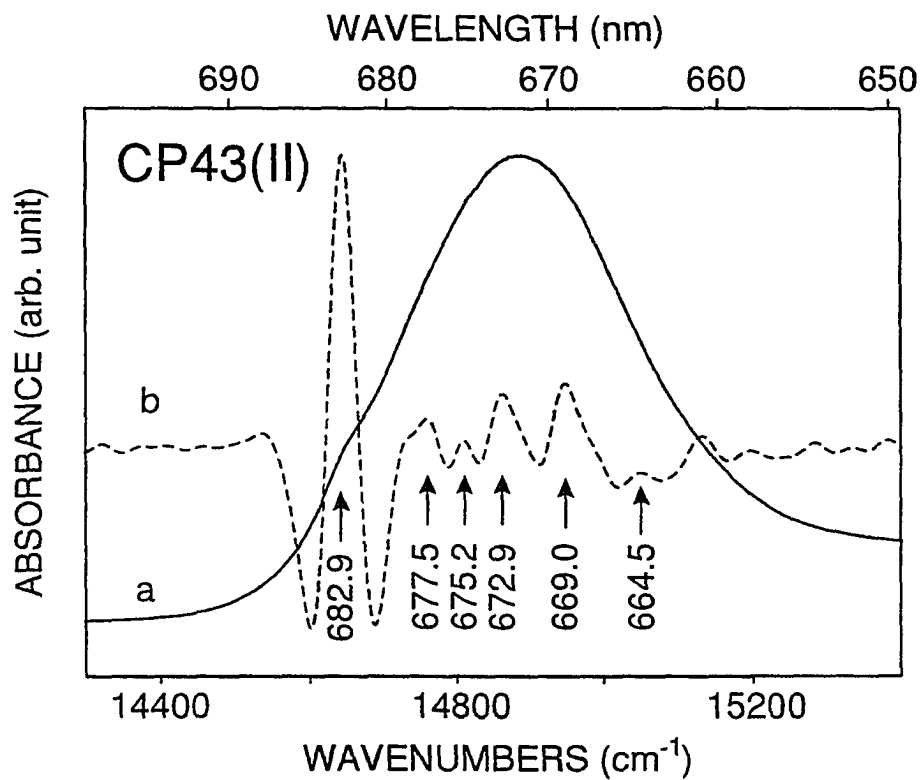


Figure 2. Absorption ( $Q_y$ -region) of CP43 (II) protein complex obtained at 4.2 K (solid line). Positions of the peaks revealed in fourth derivative (dashed line) are labeled.

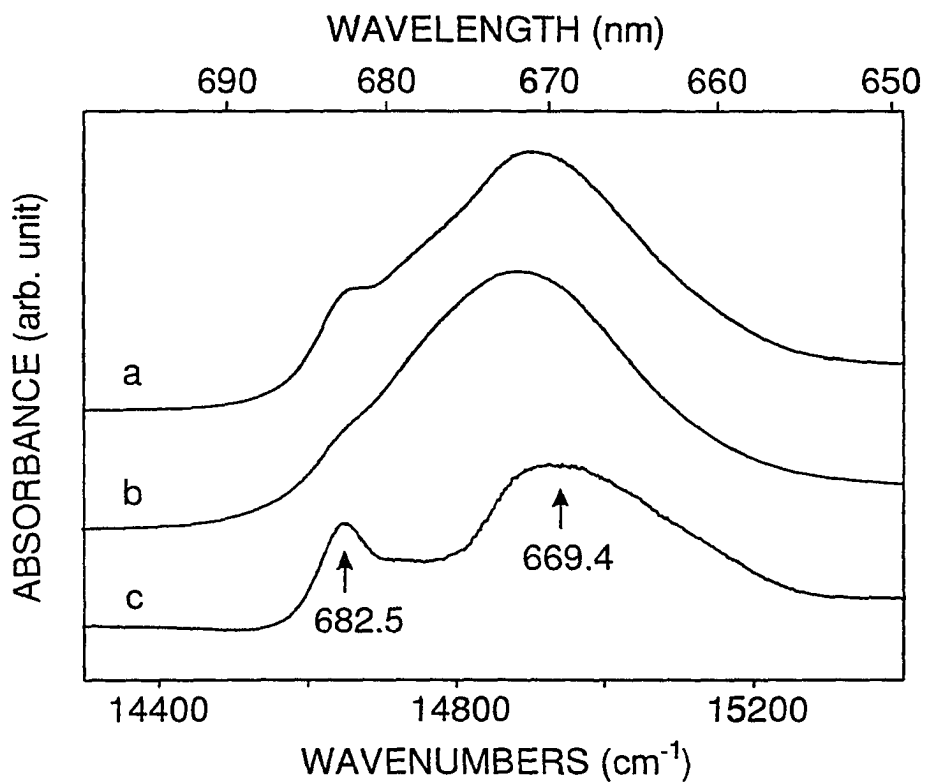


Figure 3. Low temperature (4.2 K) absorption ( $Q_y$ -region) of CP43 (I) (curve a) and CP43 (II) (curve b). The difference (curve c) between curve a and b reveals two maxima located at 682.5 and 669.4 nm, respectively.

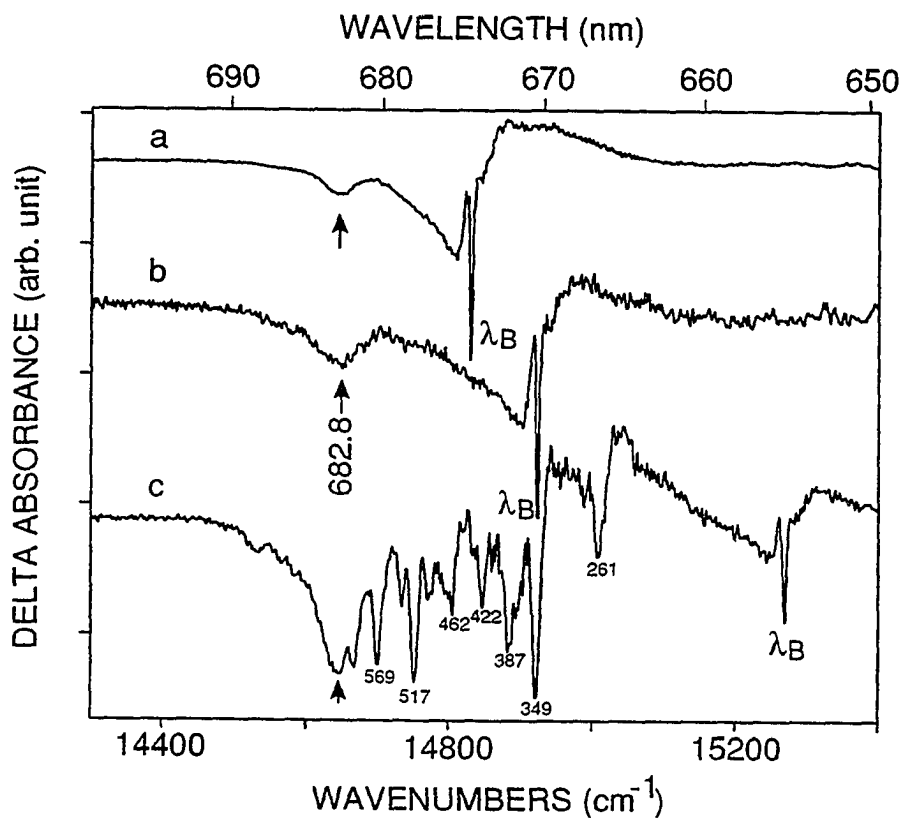


Figure 4. Persistent nonphotochemical hole burned spectra of CP43 (I) obtained at 4.2 K with  $\lambda_B = 675$  nm (curve a), 670 nm (curve b), and 655 nm (curve c), respectively. The vibrational frequencies of vibronic holes are labeled in curve c.

Table 1. Vibrational frequency ( $\text{cm}^{-1}$ ) obtained by nonphotochemical hole burning.

CP43	PSI
261	262
----	283
349	----
387	390
422	425
462	469
495	501
517	521
535	541
569	574
----	588



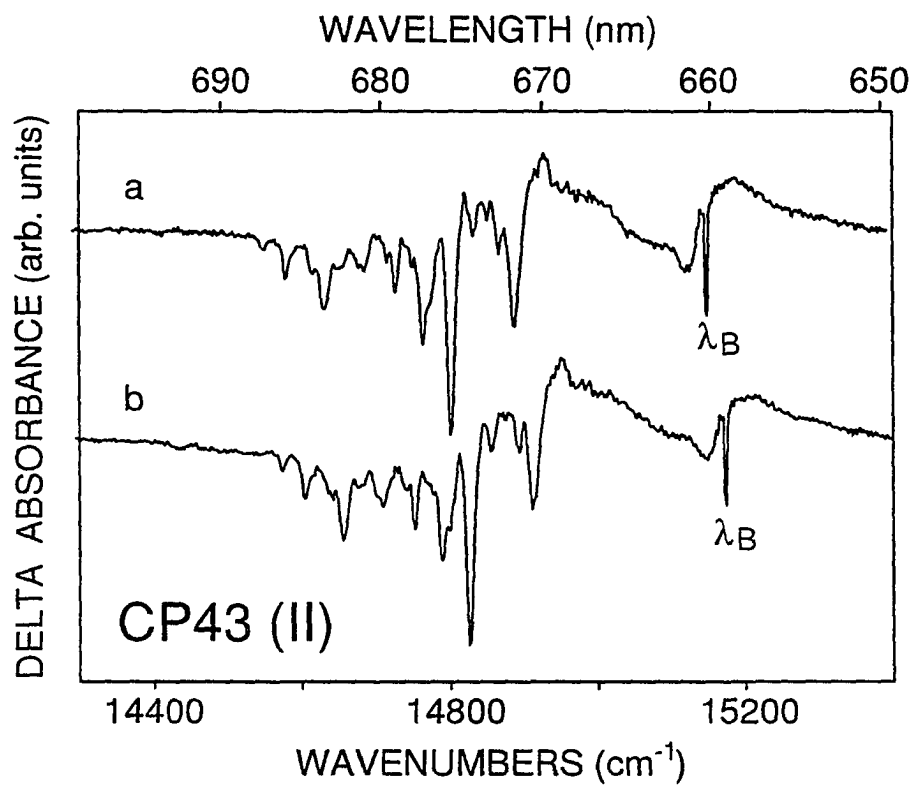


Figure 5. Persistent nonphotochemical hole burned spectra of CP43 (II) obtained at 4.2 K with  $\lambda_B = 660$  nm (curve a) and 659 nm (curve b), respectively.

Hole burning data of CP43(I) obtained with burn wavelength of  $\lambda_B = 675, 680.5,$  and 682 nm are shown as Figure 6. Two shallow holes located at  $\sim 671$  and  $\sim 678$  nm are identified as indicated by dashed arrows. Interestingly, the position of these two satellite holes is invariant to  $\lambda_B$  (dashed arrows).

Hole burned spectra of CP43(II) are shown in Figure 7. Again two satellite holes located at  $\sim 671$  and  $\sim 678$  nm are also revealed in the antihole region. The observed cusp-like features just to the right of the ZPH are yielded by the interference between the real-phonon sideband hole and the anti-hole.

### C Transient Hole Burned Spectra

The population-bottleneck hole burned spectra of CP43(I) (see Figure 8) revealed two broad features at  $\sim 683$  nm and  $\sim 670$  nm. As expected, the 683 nm band is greatly reduced in the population-bottleneck hole burned spectra of CP43(II) (data not shown). In curve a and b of Figure 8, the 683 nm hole feature exhibited abrupt termination at  $\lambda_B$ . It is possible that the 683 nm band is inhomogeneously broadened. The  $\sim 670$  nm hole (curve c) has a much larger bandwidth than the 683 nm hole. It is interesting to note that the difference between CP43(I) and CP43(II) (shown in Figure 3c) also reveals a component at  $\sim 670$  nm. This 670 nm band also exists in the population-bottleneck hole burned spectra of CP43(II) (data not shown).

## III. Discussion

### A. Absorption Spectra

The 4.2K absorption spectra, i.e., Figure 1 and 2, exhibit one band at  $\sim 683$  nm associated with several partially resolved bands at a higher energy side. Interestingly, a 684 nm band with  $\Gamma_{inh} = 110 \text{ cm}^{-1}$  was recently found in CP47 and D1-D2-cyt b559 protein complexes. The question arises, do these two bands show similar hole burning

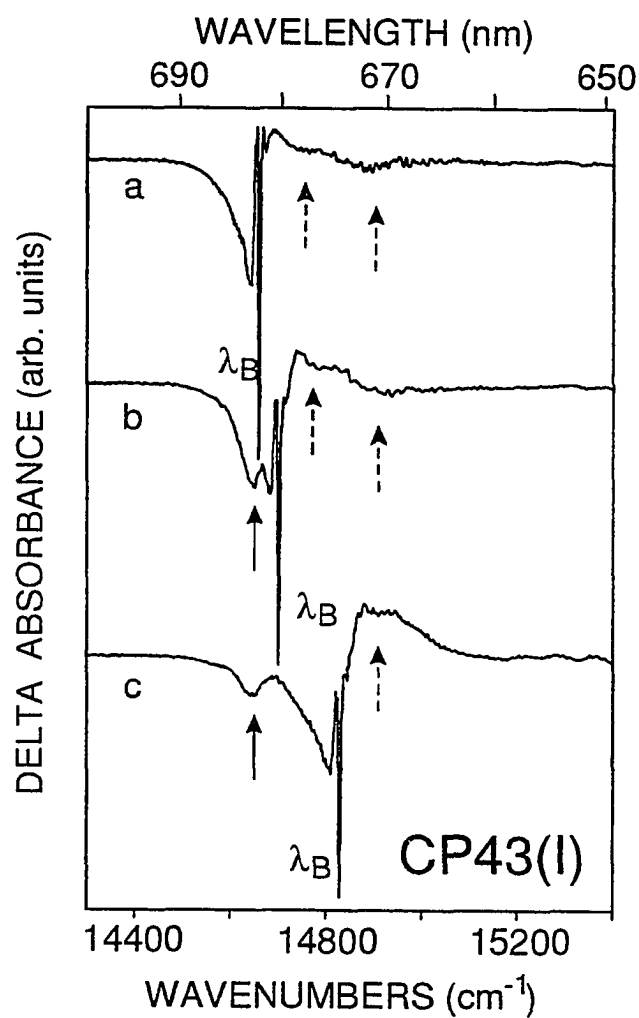


Figure 6. Persistent holes of CP43 (I) obtained with  $\lambda_B=682$  nm (curve a), 680 nm (curve b), and 675 nm (curve c), respectively. Satellite holes located at high energy side are indicated by dashed arrows.

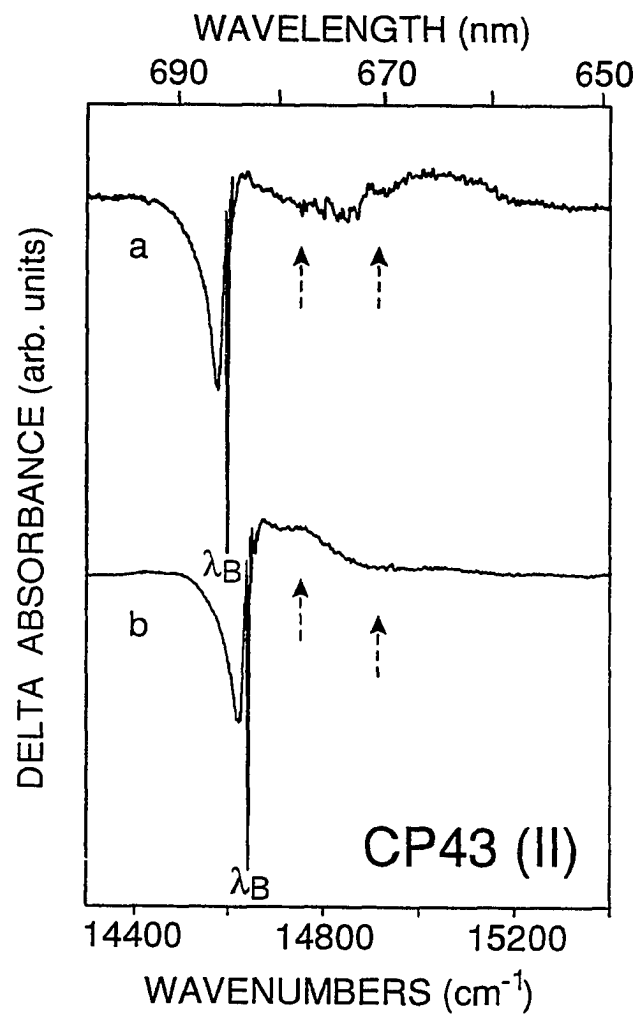


Figure 7. Persistent holes of CP43 (II) obtained with  $\lambda_B = 685$  nm (curve a), and 682.5 nm (curve b), respectively. Satellite holes located at high energy side are indicated by dashed arrows.

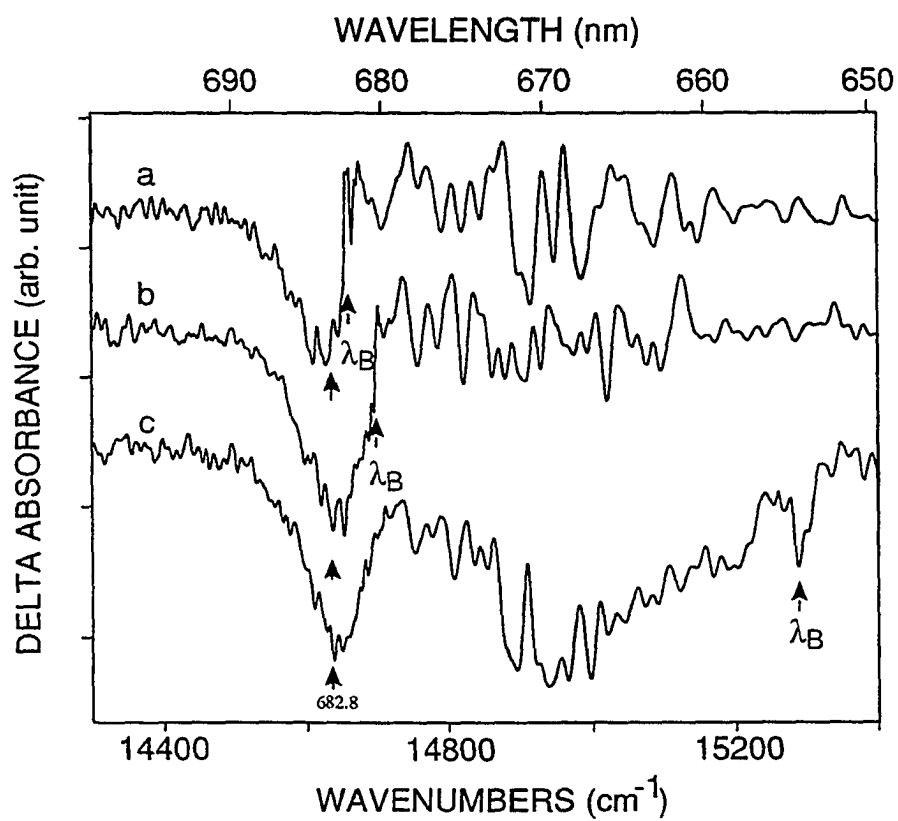


Figure 8. Low temperature (4.2 K) transient triplet bottleneck hole-burned spectra from CP43 (I) with  $\lambda_B = 682$  nm (curve a), 680 nm (curve b), and 655 nm (curve c), respectively.

patterns? This will be addressed below. The 670 nm broad feature revealed in the difference spectrum (Figure 3c) is also observed in transient hole spectra (two holes located at 670 and 683 nm, respectively). One should notice that these two transient holes (at 670 and 684 nm) are not connected, i.e., they originate from two different triplet bottlenecks (*vide infra*). We notice that ODMR experiments [6] also observed a ~670 nm band. It has been demonstrated that all preparations may contain some contribution from the dysfunctional Chls [8-10]. In contrast to the suggestion of disrupted Chl *a*, this band is assigned to an upper exciton band of a possible Chl *a* dimer or, simply showed an interaction with a different chlorophyll population absorbing at higher energy [6].

### **B. Persistent Hole Burned Spectra**

The Stokes shift between the absorption and fluorescence origin bands is given by  $2S\omega_m$ , where  $\omega_m$  is the mean phonon frequency. Persistent hole burned spectra indicated that a sharp zero-phonon hole can be observed at  $\lambda_B = 682$  nm (see Figure 6 and 7). Carbonera et al. [2] also reported ~682 nm to be the fluorescence maximum at 8K. All the observations given above indicate that the linear electron-phonon coupling of the 683 nm state is weak ( $S < 1$ ).

We note that the spectra of both Figure 6 and 7 show that hole burning of the low energy bands elicits weak responses from the higher energy absorption bands at ~671 and ~678 nm. It is interesting to note that these weak responses do not drastically diminish in CP43(II), which has much less 683 nm band, as revealed in Figure 5. This observation strongly suggests the satellite hole at 683 nm is not excitonically correlated with the higher energy holes at ~671 and ~678 nm. That is, the 683 nm band does not belong to a part of the CP43 exciton-interacting pigments. It is possible that another lower energy state, which is revealed in the low energy tail of CP43(II) (see Figure 2), serves as a shuttle state

for energy downward transfer between the higher energy state and the 683 nm band. In summary, based on the satellite hole structure observed in Figure 6 and 7, two states at 671 and 678 nm are identified as being excitonically correlated with the shuttle state which is located at the low energy side of CP43 absorption spectrum. The constant fluence action spectrum may provide further confirmation. The 683 nm hole, which can be further washed out, may not be one of the exciton states in CP43 protein complex. Similar behavior was revealed in the CP47 protein complex.

The pseudo-vibronic structures revealed with high energy excitation (Figure 4 and 5) provide the evidence for the existence of some disrupted Chl *a* in both CP43(I) and CP43(II). That is, the high resolution ZPH measurements may not accurately reflect the dynamics of fully functional energy transfer time in both CP43(I) and CP43(II).

### C. Transient Hole-Burning Spectra

The broad feature located at 670 nm appears in both the difference absorption spectrum (Figure 3c) and the population bottleneck hole burned spectra (Figure 8c). The key observation is that this 670 nm hole is diminished with lower excitation energy (Figure 8a and b). This observation invalidates the suggestion of Carbonera et al. that the 670 nm band may be due to an upper exciton band. Van Kan et al. [11] also reported an intense feature at 670 nm in the population bottleneck hole burned spectra in the CP47 protein complex. They concluded that it is most likely due to non-native Chl molecules produced by the isolation and/or sample handling procedures.

The 683 nm feature exhibited abrupt termination at  $\lambda_B$  (shown in Fig.8a and b). This result indicates the 683 nm band is inhomogeneously broadened. Similar behavior was reported for the 684 nm band in CP47. See Chapter 4 for more explanations.

**References**

1. Bricker, T.M. *Photosyn. Res.* 1990, 24, 1.
2. Giardi, M.T. *Planta* 1993, 190, 107.
3. De Vitry, C.; Wollmann, F-A.; Delepelaire, P. *Biochim. Biophys. Acta* 1984, 767, 415.
4. Barbato, R.E.; Rigoni, F.; Giardi, M.T.; Giacometti, G.M. *FEBS Lett.* 1989, 251, 147
5. Bassi, R.; Pineau, B.; Dainese, P.; Marquardt, J. *Eur. J. Biochem.* 1993, 212, 297.
6. Carbonera, D.; Giacometti, G.; Agostini, G.; Angerhofer, A.; Aust, V. *Chemical Physics Letters* 1992, 194, 275.
7. Picorel, R. private communication
8. Gillie, J.K.; Small, G.J.; Golbeck, J.H. *J. Phys. Chem.* 1989, 93, 1620
9. Chang, H-C.; Jankowiak, R.; Yocum, C.F.; Picorel, R.; Alfonso, M.; Seibert, M.; Small, G.J. *J. Phys. Chem.* 1994, 98, 7717.
10. Chang, H-C.; Jankowiak, R.; Reddy, N.R.S.; Yocum, C.F.; Picorel, R.; Seibert, M.; Small, G.J. *J. Phys. Chem.* 1994, 98, 7725
11. Van Kan, P.J.M.; Groot, M.L.; van Stokkum, I.H.M.; Kwa, S.L.S.; van Grondelle, R.; and Dekker, J.P. in *Research in Photosynthesis*, Vol. 1; Murata, N., Ed.; Kluwer: Netherlands, 1992, 271



## APPENDIX B: COMPARISON OF THE ABSORPTION SPECTRA OF THE PHOTOSYSTEM II D1-D2-CYT B<sub>559</sub> REACTION CENTER FROM TWO DIFFERENT PREPARATIONS

It is informative to examine the difference between absorption spectrum of D1-D2-cyt b<sub>559</sub> protein complexes prepared by two groups, i.e. Seibert (socalled 4 Chl *a* preparation) and Dekker, respectively. In earlier work [1], samples prepared by the procedures of McTarish et and Dekker et al. were studied utilizing hole burning technique. It was shown that the charge separation and energy transfer dynamics of the two preparations are very similar. Recently it was found that the relative Chl *a* content of the sample can be determined by normalizing the intensities of the Q<sub>x</sub>-band of Pheo *a* at 543 nm [2,3]. It is assumed that the absorption from Chl *a* and carotenoid only contribute to the broad background absorption which underlies the sharp Pheo *a* band at 543 nm. Low temperature (4.2 K) absorption spectra of preparations from Seibert (dashed line) and Dekker (solid line) are normalized to the same intensity of the Q<sub>x</sub>-band of Pheo *a* as shown in Figure 1. The extent to which the Pheo *a* Q<sub>x</sub>-band is resolved is illustrated by the inset spectra of Figure 1. A straight line obtained by the subtraction of Q<sub>x</sub>-band of Pheo *a* ensures that the normalization procedure is performed correctly (see inset). The normalized absorption spectra at the Q<sub>y</sub>-region from Seibert's (curve a) and Dekker's (curve b) preparations are shown in Figure 2. Comparison of the two indicates that Dekker's preparation has a higher Chl *a* content. Assuming that the Dekker preparation has ~6.4 Chl *a*/ 2 Pheo, as recently measured by HPLC method [4], the integration of the absorption spectrum of the Seibert preparation estimates the number of Chl *a*/ 2 Pheo as 5.3. Subtraction of spectra a and b, i.e. curve c, reveals that Dekker's preparation has less

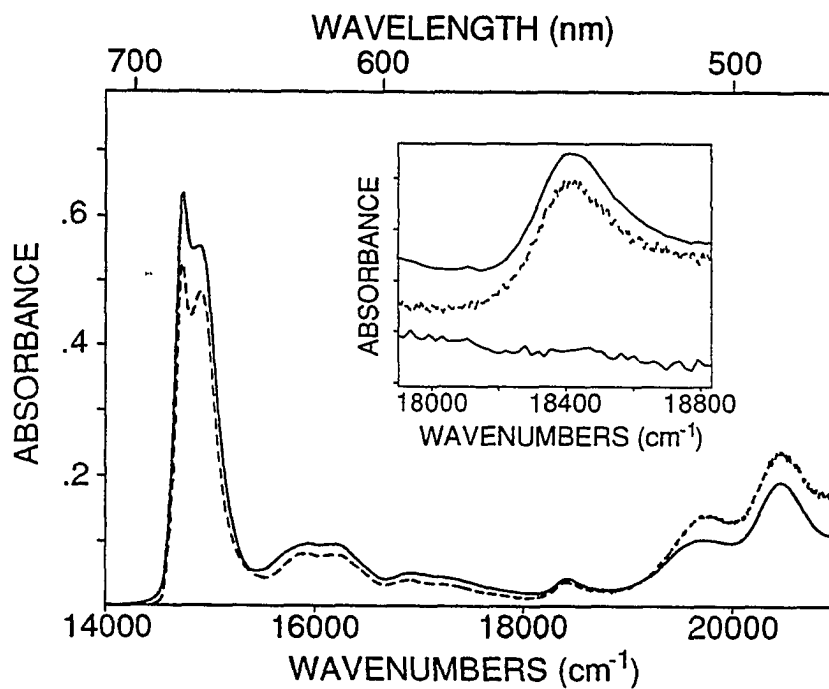


Figure 1 Low temperature (4.2 K) absorption spectra of D1-D2-cyt  $b_{559}$  protein complexes prepared by Seibert (dashed line) and Dekker (solid line), respectively. The spectra were normalized to the same intensity of the  $Q_x$  band of Pheo  $a$  (see inset). The difference between these two preparations in  $Q_x$  region is shown as the lower trace (see inset also).

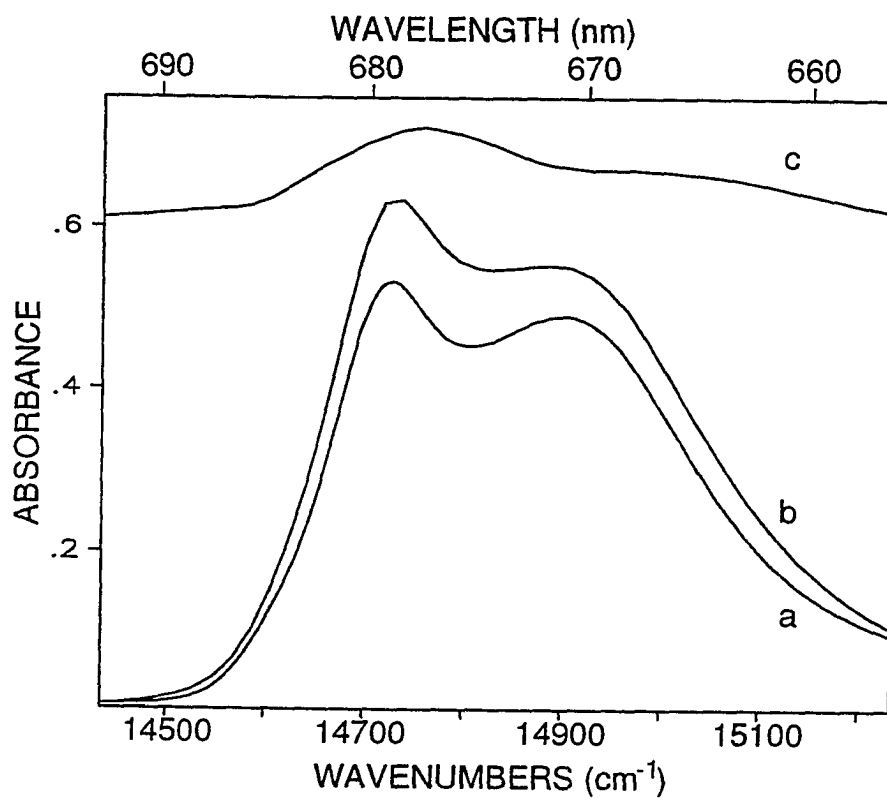


Figure 2. Absorption ( $Q_y$ -region) of D1-D2-cyt b559 complexes prepared by Seibert (curve a) and Dekker (curve b), respectively. Curve c corresponds to the difference between the absorption spectra of Dekker's and Seibert's preparations.

contribution from dysfunctional Chl *a* absorbing at ~670 nm, but may contain some contribution from the 684 nm band and/or CP47-D1-D2-cyt b<sub>559</sub>. Chang et al. [3] discussed the complications associated with proper stoichiometry assignment when the preparation is contaminated with CP47 and/or dysfunctional Chl *a*. Considerable evidence exists [5] which indicates that the Chl *a*/ Pheo *a* ratio depends on the isolation procedure and other factors. Holzwarth's group studied the picosecond fluorescence kinetics of long-term (samples from Shuvalov) [6] and short-term (from Dekker) [7] Triton-exposed RC particles. An ultrashort component of 1-6 ps, which has been resolved in samples from Shuvalov, was not resolved in Dekker's samples. The absence of the ultrashort component, assigned to the primary charge separation time, was attributed to the larger chlorophyll content of Dekker's preparation [7]. It is known that the maximum position of P680 transient holes is dependent on the purity of the RC preparations [3,8]. One should notice that the maximum position of the P680 hole of Dekker's preparation [9] lies between that of the 4 and 6 Chl *a*/ RC preparations [3].

#### References

1. Tang, D.; Jankowiak, R.; Seibert, M.; Yocum, C.F.; Small, G.J. *J. Phys. Chem.* 1990, 94, 6519
2. Chang, H.-C.; Jankowiak, R.; Yocum, C.F.; Picorel, R.; Alfonso, M.; Seibert, M.; Small, G.J. *J. Phys. Chem.* 1994, 98, 7717
3. Chang, H.-C.; Jankowiak, R.; Reddy, N.R.S.; Yocum, C.F.; Picorel, R.; Seibert, M.; Small, G.J. *J. Phys. Chem.* 1994, 98, 7725
4. Dekker, J.P. Private communication
5. Seibert, M. in *The Photosynthetic Reaction Center*; Vol.I; Deisenhofer, J., Norris, J., Eds.; Academic Press: New York, 1993, p.319

6. Roelofs, T.A.; Gilbert, M.; Shuvalov, V.A.; Holzwarth, A.R. *Biochim. Biophys. Acta* 1991, 1060, 237
7. Roelofs, T.A.; Kwa, S.L.S.; van Grondelle, R.; Dekker, J.P.; Holzwarth, A.R. *Biochim. Biophys. Acta* 1993, 1143, 147
8. Jankowiak, R.; Small, G.J. in *The Photosynthetic Reaction Center; Vol.II*; Deisenhofer, J., Norris, J., Eds.; Academic Press: New York, 1993, p.133
9. Kwa, S.L.S.; Eijkelhoff, C.; van Grondelle, R.; Dekker, J.P. *J. Phys. Chem.* 1994, 98, 7702